A COUPLED ROTOR-FUSELAGE AEROELASTIC ANALYSIS

USING

COMPLEX ROTOR MODES

by

WAYLAND YICK-FU CHAN, B.Sc., C.Eng., M.RAeS.

Thesis Submitted for The Degree of Doctor of Philosophy

DEPARTMENT OF MECHANICAL ENGINEERING AND AERONAUTICS
CITY UNIVERSITY
NORTHAMPTON SQUARE
LONDON EC1V 0HB

AUGUST 1996

TO: MY WIFE, KIT

AND OUR SON, THE LATE CHEUNG-LAM,

WHOM I LOVE AND OWE SO MUCH.

ACKNOWLEDGEMENTS

I would like to express my sincere gratitude to my colleague and industrial supervisor, Mr R E Hansford, of GKN Westland Helicopters Limited for the invaluable discussions and support throughout this research.

I am also deeply grateful to my supervisor, Professor G T S Done, of Department of Mechanical Engineering and Aeronautics, The City University for his guidance and encouragement.

Special thanks are also due to my colleague, Mr S A Holton, for his inspiration and constructive suggestions throughout the study. Acknowledgements also go to my colleagues in the Aeromechanics Department of GKN Westland Helicopters Limited, especially Mr N Griffiths, Mr P T W Juggins, Mr C J Auger and Dr C P Sotiriou for the numerous fruitful discussions.

I would also like to thank my colleagues at the Defence Research Agency (Farnborough), Mr W R Walker for the number of discussions and helpful suggestions and Mr C Young for furnishing most of the software.

Thanks also go to Professor A Simpson (ex Bristol University) and Professor B Noble (ex Wisconsin University) for the discussion and helpful suggestions on the treatment of complex modes orthogonality.

Last but not least, thanks are due to GKN Westland Helicopters Limited for allowing the use of facilities and also to the Defence Research Agency (Farnborough) for funding part of this research.

DECLARATION

I hereby grant powers of discretion to the University Librarian to allow this thesis to be copied in whole or in part without further reference to me. This permission covers only single copies made for study purposes, subject to the normal condition of acknowledgement.

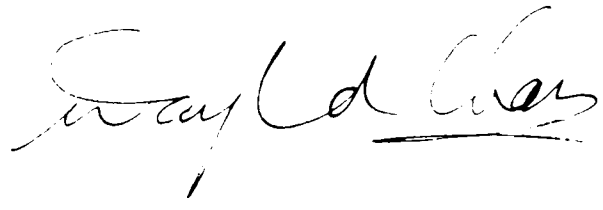

ABSTRACT

A new modal method capable of analysing the aeroelastic response of rotorcraft in both steady and manoeuvring flight is developed. Particular emphasis is given to the correct modelling of the dynamic interactions between the rotor and the fuselage. This is achieved via the use of complex rotor modes, which allows the effects of hub motion to be incorporated.

The modal Lagrangian equation for a single rotating blade using real modes as state variables is first derived. The important non-linear terms based on an ordering scheme are retained. This aeroelastic model is then extended to adopt the complex rotor modes as state variables. This concept, which is both new and analytically demanding, is furnished with minimum algebra.

A generalised proof of complex modes orthogonality and its application to the coupled rotor-fuselage dynamic system are provided. Important conclusions drawn from this proof include:

. A set of complex left-hand eigenvectors are required, together with the right-hand set, in order to reduce the system response equations to an uncoupled modal form suitable for a solution; and
. It is necessary for the modes analysis to be re-formulated as an eigenvalue problem replacing the transfer matrix solution procedure.

An orthogonalisation procedure is employed to reduce the complex system response equations to the uncoupled modal form. The procedure not only simplifies the algebraic process, but also identifies exactly the forcing functions present in the dynamic system modelled. However, for consistency with the dynamic model, it is necessary to restrict the blade model to a straight beam with small pre-deformed angles.

The need to treat both the complex coupled and reactionless mode sets simultaneously, when they are defined in different reference frames, requires special attention to the solution of the modal responses. A numerical technique is developed for filtering the applied forces and hence identifying the forcing for the respective mode types.

The fundamental issue regarding the true definition of angle of attack used for aerodynamic calculation is also addressed. The second order pseudo-torsion term must be removed from the incidence expression to ensure the aerodynamic loads are calculated correctly.

The determination of the blade structural loads using both Modal Summation and Force Integration methods is discussed and described. A novel numerical technique, based on curve fitting using Chebyshev polynomials coupled with analytical integration, is devised and shown for the first time to minimise the inherent numerical problems associated with Force Integration.

Finally, applications of the analytical model to include the effects of hub motion on vibratory loads calculation and to determine loads in an extreme manoeuvre are successfully demonstrated. The use of rotor modes by including transmission flexibility in a rotor dynamic model in loads calculation is also provided. These correlations establish the important milestone on the ability of this model to improve vibration prediction and to simulate manoeuvring flight. They also demonstrate the potential applications of this model. Recommendations for future research are also made.

CONTENTS

LIST OF FIGURES

LIST OF TABLES

NOTATION

A's,B's	Coefficient matrices of CRFD system equations (*Eqn.* 3.48);
A,B,C	Coefficient matrices (*Eqn.* 3.71);
$\frac{dA}{dr}$	Lift & drag loads resolvent in the axial direction (+ve out);
c	Blade chord;
C_r	Complex normalising factor (*Eqn.* 3.89);
C_T	Thrust coefficient, $\frac{T}{\frac{1}{2}\rho(\pi R^2)(\Omega R)^2}$;
$\frac{dD}{dr}$	Blade section aerodynamic drag (+ve lag back);
e_1, e_2	Flatwise and edgewise c.g. offset from the elastic axis (e.a.) (+ve above and forward);
e_{A1}, e_{A2}	Flatwise and edgewise tension axis offset from the e.a. (+ve above and forward);
E	Young's modulus;
EA	Spanwise stiffness, $\int\int E d\eta d\xi$, about the e.a,;
EB_1	First flatwise moment of area, $\int\int E\xi d\eta d\xi$, about the e.a.;
EB_2	First edgewise moment of area, $\int\int E\eta d\eta d\xi$, about the e.a.;
EC_1	Section elastic integral, $\int\int E(\eta^2+\xi^2)\xi d\eta d\xi$ about the e.a.;
EC_2	Section elastic integral, $\int\int E(\eta^2+\xi^2)\eta d\eta d\xi$ about the e.a.;
EC_1^*	Section elastic integral, $\int\int E(\eta^2+\xi^2)(\xi-e_{A1}) d\eta d\xi$, about the tension axis;
EC_2^*	Section elastic integral, $\int\int E(\eta^2+\xi^2)(\eta-e_{A2}) d\eta d\xi$, about the tension axis;
EI_{11}	Flatwise stiffness, $\int\int E\xi^2 d\eta d\xi$, about the e.a.;
EI_{22}	Edgewise stiffness, $\int\int E\eta^2 d\eta d\xi$, about the e.a.;
EI_{12}	Cross stiffness, $\int\int E\eta\xi d\eta d\xi$, about the e.a.;
EI_{11}^*	Flatwise stiffness, $\int\int E(\xi-e_{A1})^2 d\eta d\xi$, about the tension axis;
EI_{22}^*	Edgewise stiffness, $\int\int E(\eta-e_{A2})^2 d\eta d\xi$, about the tension axis;
EI_{12}^*	Cross stiffness, $\int\int E(\eta-e_{A2})(\xi-e_{A1}) d\eta d\xi$, about the tension axis;
FO,FC,FS	Coefficient matrices of the blade root forces (*Eqn.* 3.54);
$\underline{F}_k$	Vector of forces and moments on the k^{th} blade;
$\underline{F}_s$	Vector of spring forces;
F_D	Lag damper load (+ve compression);
$F_{x_H}, F_{y_H}, F_{z_H}$	Modal hub shear: longitudinal, lateral and vertical (+ve aft, starboard and up);
f_i	Modal forcing of the i^{th} real blade mode (*Eqn.* 3.89a);
$\underline{f}_1, \underline{f}_2$	RHS forcing vector (direct and indirect terms) (*Appendix* I);
$\underline{F}_1, \underline{F}_2$	Vector of coefficients of generalised coordinates (direct and indirect terms) (*Appendix* H6);

$\underline{f}$ RHS forcing vector n long (*Eqn.* 3.89a);

f Strain energy function;

g_i Modal forcing of the i^{th} complex rotor mode (*Eqn.* 3.89b);

$\underline{g}$ RHS forcing vector 2n long (*Eqn.* 3.89b);

g Kinetic energy function;

G Shear modulus;

GA Shear stiffness integral, $\int\int G d\eta d\xi$, about the e.a.;

GB_1 Shear elastic integral, $\int\int G\xi d\eta d\xi$, about the e.a.;

GB_2 Shear elastic integral, $\int\int G\eta d\eta d\xi$, about the e.a.;

GJ Torsional stiffness, $\int\int G(\eta^2+\xi^2)\, d\eta d\xi$;

$\underline{H}$ Vector of hub motion variables;

h_i Hub generalised variables;

$\underline{h}_i$ Modal hub motion vector of the i^{th} mode;

I_i Modal inertia for the i^{th} mode;

I_{ij} Modal inertia coefficient (*Appendix* H6);

$k_i's$ Coefficients in the 4^{th} Runge-Kutta solution algorithm;

k_A Radius of gyration about the tension centre;

km_1 Section flatwise radius of gyration, $\frac{\int\int \rho\xi d\eta d\xi}{\int\int \rho d\eta d\xi}$;

km_2 Section edgewise radius of gyration, $\frac{\int\int \rho\eta d\eta d\xi}{\int\int \rho d\eta d\xi}$;

km_{12} Cross section integral, $\frac{\int\int \rho\eta\xi d\eta d\xi}{\int\int \rho d\eta d\xi}$;

K Kinetic energy of the dynamical system;

K_L Matrix of linear spring rates;

K_R Matrix of rotational spring rates;

L_i, L_j, L_k Components of aerodynamic loads in the undeformed axis system;

L_x, L_y, L_z Linear spring rates;

l_u, L_v, L_w Coordinates of rigid rod attachment in the local deformed axis system (*Appendix* B);

$l_{r_s}, l_{\eta_s}, l_{\zeta_s}$ Position vector of the fixed end (F_s) of the spring relative to the local axis system (*Appendix* B);

l_D Lag damper arm length;

$\frac{dL}{dr}$ Blade section aerodynamic lift (+ve up);

m Blade mass distribution, $\int\int \rho d\eta d\xi$;

$\frac{dM}{dr}$ Blade section pitching moment (+ve leading edge up);

$M_{x_H}, M_{y_H}, M_{z_H}$ Modal hub moments: roll, pitch and yaw (+ve starboard up, pitch up and with rotation);

M_x, M_y, M_z Modal moments: torque, flap and lag (+ve leading edge up, flap down, lag forward);

$\mathbb{M},\mathbb{C},\mathbb{K}$	Coefficient matrices (*Eqn.*3.88);
M,C,K	Inertia, damping and stiffness matrices of a dynamical system equation in classical form;
$\underline{M}_s$	Vector of moments in the secondary load path (spring);
n	Harmonic index;
N	Number of modes; Number of blades;
N_S	Number of secondary load paths;
p_F,q_F,r_F	Aircraft roll, pitch and yaw rate in the body-axes;
p_H,q_H,r_H	Hub roll, pitch and yaw rate in the $HX_GY_GZ_G$-system;
p_{ij},q_{ij}	Components of strain tensor, i,j=1,2,3;
q_i	Generalised coordinate of the i^{th} real blade mode;
Q_i	Generalised force of the i^{th} mode;
r	Curvilinear radial coordinate;
$\underline{r}_A$	Position vector of the aerodynamic centre after deformation;
$\underline{r}_0,\underline{r}_1$	Position vector of the undeformed and deformed blade point in the local blade axis system;
$\underline{r}$	Position vector of blade point in the global undisturbed shaft axis system;
$\underline{r}_D$	Vector of linear elastic displacement of the elastic axis;
$\underline{r}_H$	Vector of linear elastic displacement at the hub;
$\underline{r}_S$	Position vector of point in the blade section axis system;
$\underline{r}_P$	Position vector of pre-deformed position of the elastic axis;
$\underline{r}_{Fs}$	Position vector of load path attachment point;
$\delta\underline{R}_L$	Vector of virtual translations in the local blade system;
$\delta\underline{\Gamma}_L$	Vector of virtual rotations in the local blade system;
R	Curvilinear length of rotor blades;
R_x,R_y,R_z	Rotational spring rates;
$\dot{\underline{R}}$	Vector of blade absolute velocities in the $HX_GY_GZ_G$-system;
$\underline{R}_H$	Vector of rotational velocities at the hub;
$\underline{R}_S$	Position vector of blade point in the global $HX_GY_GZ_G$-system;
s	Rotor solidity, $\frac{Nc}{\pi R}$;
S	Matrix containing steady blade root forces;
S_{ij}	Modal stiffness coefficient (*Appendix* H6);
s_1,s_2	Undeformed and deformed spring root attachment;
$\underline{SA}$	Vector of non-linear strain terms;
$\underline{SB}$	Vector of constants containing gravitational forces and steady aerodynamics;
t	Time parameter; Aerofoil thickness;
t_x,t_y,t_z	Control stiffness spring orientations;
T	Axial tension, EAu'; Rotor thrust;

U Strain energy of the dynamical system;

$\underline{U}$ Total velocity vector of the blade point

$\underline{U}_H$ Vector of linear velocities at the hub $\underline{U}_H=\{u_S, v_S, w_S\}$;

$\underline{U}_k$ Vector of k^{th} blade deformation variables;

$\underline{U}_0, \underline{U}_C, \underline{U}_S$ Vector of collective, cyclic cosine and sine components of blade deformation variables;

U_p, V_p, W_p Pre-deformed coordinates of blade elastic axis in the $H'X_pY_pZ_p$-system;

U_R, U_T, U_P Radial, tangential and perpendicular air velocity components in the Oxyz-system (+ve outward, l.e. to t.e. and up);

U_s Strain energy contribution due to secondary load paths;

u, v, w Blade axial, lag and flap displacements;

u_F, v_F, w_F Aircraft forward, sideslip and heave velocity in the body-axes;

u_S, v_S, w_S Hub velocity components in the undisturbed shaft axis system;

$\underline{V}$ Air velocity vector; Modal vector;

V_x, V_y, V_z Blade radial, lag and flap Shear (+ve outboard, fwd and up);

δW Virtual Work;

x Non-dimensional radial coordinate: $U_p=x+O(\varepsilon^2)$;

x_j Blade generalised variables;

x_G, y_G, z_G Hub coordinate in the fuselage body axis system;

x_H, y_H, z_H Hub elastic displacement (+ve aft, starboard and up);

y_A, z_A Aerodynamic centre offset from e.a.;

Z Hub impedance matrix;

Axis Systems

$OX_FY_FZ_F$ Fuselage body axis system (Unit vectors: $\underline{I}_F, \underline{J}_F, \underline{K}_F$);

$HX_GY_GZ_G$ Non-rotating global undisturbed shaft axis system ($\underline{I}_G, \underline{J}_G, \underline{K}_G$);

$H'XYZ$ Non-rotating disturbed shaft axis system ($\underline{I}, \underline{J}, \underline{K}$);

$H'X_PY_PZ_P$ Rotating blade pre-deformed axis system ($\underline{I}_P, \underline{J}_P, \underline{K}_P$);

$Oxyz$ Rotating blade section axis system ($\underline{i}, \underline{j}, \underline{k}$);

$O'r\eta\xi$ Deformed blade section principal axis system ($\underline{i}', \underline{j}', \underline{k}'$);

$F_sX_sY_sZ_s$ Spring axis system ($\underline{i}_s, \underline{j}_s, \underline{k}_s$);

$\mathbb{B}, \mathbb{H}, \mathbb{R}$ Rotor reference, hub and inertia frames;

Greek

α Blade angle of attack;

α_D Inclination of lag damper load path;

γ_s Shaft tilt (+ve aft);

δ Variational operator; Damping factor;

ε_{ij} Strain tensor components: Classical $(i,j=1,2,3)$;
Eulerian $(i,j=r,\eta,\xi)$;

ζ, β, ϕ Blade lag, flap and twist angle (+ve lag forward, flap up,

leading edge up);

ζ_p, β_p Blade pre-sweep and pre-cone angles;

μ_x, μ_y, μ_z Normalised shaft velocity components (+ve forward, starboard, and down the shaft) ($\mu_x \equiv \mu$, the advance ratio);

$\underline{\lambda}$ Vector of normalised induced velocity;

λ_i Eigenvalue or complex natural frequency for the i^{th} mode;

η_i Generalised coordinate for the i^{th} complex mode;

η_0, ξ_0 Blade principal chordwise and flatwise axis;

η, ξ Blade chordwise and flatwise coordinate;

A_0, A_1, B_1 Collective, lateral cyclic and longitudinal cyclic pitch;

$\bar{\vartheta}$ Total blade pitch angle: $\bar{\vartheta} = \vartheta_p + \vartheta(\psi) + \phi - \vartheta_b$;

$\vartheta(\psi)$ Blade control pitch angle: $\vartheta(\psi) = A_0 - A_1\cos\psi - B_1\sin\psi$;

ϑ_p Blade pre-twist or built-in twist;

ϑ_b Pseudo-torsion parameter;

ϑ_M Blade pitch used in modes calculation;

$\hat{\vartheta}$ Blade pitch angle: $\hat{\vartheta} = \vartheta_p + \vartheta(\psi) + \phi$;

$H(r-r_s)$ Heaviside function : $H(x-y) = 1$ for $x \geq y$;
$= 0$ for $x < y$;

$\delta(r-r_s)$ Dirac Delta function: $\delta(x-y) = 1$ for $x = y$;
$= 0$ for $x \neq y$;

ξ Pedal input;

ρ Blade density;

σ_{ij} Stress tensor components;

ψ_k Azimuth position of the k^{th} blade ($=\psi_1+\Omega t$);

Ω Rotor speed;

ω_i Blade natural frequency for the i^{th} mode: $\lambda_i = i\omega_i$;

$[\omega_H]$ Matrix of hub angular velocities (*Eqn.* 3.18);

φ Inflow angle;

ϕ Elastic twist;

χ Non-dimensional scaling parameter, $\chi = \frac{m\Omega^2R^2}{EA}$;

$\phi_H, \vartheta_H, \psi_H$ Hub elastic roll, pitch and yaw angles;

Φ, Γ Modal matrix comprising of RH and LH modal vectors 2n long;

$\underline{\varphi}, \underline{\gamma}$ RH and LH-modal vector n long;

$\underline{\Phi}, \underline{\Gamma}$ RH and LH-modal vector 2n long;

Subscripts

A Aeroelastics;

C, c Coupled components;

def. Deformed;

D Dynamics or damper;

F	Fuselage;
H	Hub;
m	Modal parameter;
o,c,s	Collective, cyclic (cosine) and cyclic (sine) components;
P	Pre-deformed coordinate;
ℝ,r	Reactionless components;
ST	Steady state;
T	Total;

Miscellaneous

$\dot{()}$	$\partial()/\partial t$;
$()'$	$\partial()/\partial x$;
{},$\underline{()}$	Vector notation;
[]	Matrix notation;
$[]^T$	Matrix transpose;
$()^*$	Conjugate;
$[]^H$	Hermitian = $[]^{*T}$
$\overline{()}$	Sum of pre-deformed and elastic components;

Abbreviations

AHS	American Helicopter Society;
BERP	British Experimental Rotor Program;
c.g.	Centre of gravity;
CMRB	Composite Main Rotor Blade;
CPI	Chebyshev Polynomial Integration;
CRFA	Coupled Rotor-Fuselage Aeroelastics;
CRFD	Coupled Rotor-Fuselage Dynamics;
CRFM	Coupled Rotor-Fuselage Model;
DRA	Defence Research Agency; (Formerly RAE: Royal Aerospace Establishment);
Eqn(s).	Equation(s);
ERF	European Rotorcraft Forum;
KTAS	True air speed (knots);
LH,LHS	Left-hand, left-hand side;
RAeS	Royal Aeronautical Society;
RH,RHS	Right-hand, right-hand side;
WHL	GKN Westland Helicopters Limited.

CHAPTER 1 - INTRODUCTION

1.1 Background

The need to predict helicopter rotor loads, aeroelastic stability and airframe vibration accurately has always been a challenging and formidable task for the designers. The history of helicopter development is marked by their continuous efforts to overcome problems of unpleasant vibration and dynamic instabilities inherent in this type of aircraft.

The advancement of rotorcraft technology in recent years has furnished a basis for designers to expand the flight envelope and manoeuvre capability but without increasing airframe vibration or piloting difficulties. In order to ensure that helicopters meet the various demanding tasks in military applications and also to improve passenger and crew comfort for civil transportation, analysts must have a clear understanding of the rotorcraft behaviour in flight.

The lift and propulsive power of conventional helicopters are derived primarily from the main rotor. This feature provides its capability in performing both hovering and axial flight. However, in forward and manoeuvring flight, the rotor is being forced to operate in a flow environment which is continuously changing. Because of such complexity, many aspects of helicopter behaviour are still not fully understood. Also there is a lack of insight into the physics of rotor and fuselage interactions in both dynamics and aerodynamics. This lack of understanding does not always guarantee the best helicopter design.

Helicopter engineering involves many disciplines, as is amply illustrated in the textbooks by Bramwell [1.1] and Johnson [1.2]. The complexity and highly coupled nature of rotorcraft behaviour stems from various sources. In terms of aerodynamics, the rotor is subjected to a variety of complex flow regimes such as reverse, transonic and unsteady flow as well as the flow field emerging from the fuselage. Also in the blade tip region where high speed is evident, 3-dimensional effects become important. In terms of dynamics, couplings arise from both the structural and inertial properties of the blades and also between the rotor and the fuselage. These are further complicated by the non-linear dynamics of the blade pitch control mechanism.

To improve helicopter controllability and agility and to reduce maintenance cost, new hub configurations are increasingly used *eg.* hingeless and bearingless hubs. These rotor types eliminate the hinges used in a conventional articulated rotor but they give a new dimension of structural coupling behaviour. In the assessment of flying qualities, complexity also arises from the modelling of control linkages between the pilot and the rotor and the implementation of various control laws.

All of these technical disciplines must be correctly combined in order that the helicopter behaviour can be analysed accurately. The challenge now confronting helicopter analysts is the ability to predict rotorcraft behaviour in all flight regimes accurately.

1.2 The Research Objectives

The main purpose of this study is to develop an analytical model capable of analysing the aeroelastic response of the rotorcraft in both steady and manoeuvring flight. Two primary objectives are identified. First, the model must be capable of including the effects of elastic hub motions, *ie.* the fuselage response, in the loads analysis such that the dynamic interactions between the rotor and fuselage are correctly incorporated. Secondly, the model must also be capable of determining the rotor loads and airframe vibration during manoeuvring flight. This is the first time in which both of these issues are being addressed together in a rotorcraft aeroelastic analysis.

In order to accomplish these objectives, the analysis is necessarily complex. This study also aims to ensure the method is practical but yet the important aspects of the modelling philosophy are captured. The rotorcraft configuration to be examined is limited to the conventional helicopter with main/tail rotor configuration. However, the analysis is developed in such a way that extension to provide modelling flexibility can be achieved with ease.

In addition to the said objectives, some of the more fundamental issues of rotor modelling are also addressed. These issues include the true definition of angle of attack used in the aerodynamic calculation - an issue which has cast doubt for many years. It also aims to address the

numerical deficiencies inherent in the force integration method - a preferred blade loads determination procedure.

In order to couple the dynamics of rotor and fuselage, complex rotor modes are needed. The concept of complex modes, not furnished before, is introduced. A rigorous mathematical proof of the complex modes orthogonality by way of a generalised relationship is provided. Its application to the helicopter analysis is both new and analytically demanding.

Development of aerodynamic models for the loads calculation is not part of this study but description of the various models adopted is provided for completeness.

Let us first review the existing modelling philosophies and examine some of the more current aeroelastic analysis tools in order to understand the approach taken in this study.

1.3 Scope and Modelling Philosophy of Helicopter Analysis

A number of helicopter aeroelastic analyses have been developed with varying degrees of sophistication. However, the complexity in rotary-wing systems imposes stringent demands on the level of modelling in any analysis, and aeroelastic modelling is far from mature. This has been concluded in a number of thorough reviews on rotorcraft aeroelasticity published in the past twenty-five years.

The first significant review provided by Loewy [1.3] in 1969 highlighted a wide range of specific dynamic and aeroelastic problems even when the technology was still fairly basic. For example, one of his conclusions was that the effect of the azimuthal variation of swash-plate stiffness as experienced by the blade pitch control rod could no longer be ignored. A systematic study of rotor load prediction capabilities based on a hypothetical rotor model, was carried out by Ormiston [1.4] after the AGARD conference held in 1973. He concluded that large differences in the rotor load prediction capability between various analyses was attributable to differences at the fundamental levels, namely the solution method used and the modelling of structural dynamics and aerodynamics. In 1982, Arcidiacono and Sopher [1.5] conducted a similar survey and they concluded that a

good deal of fundamental work had been done since Ormiston's review. These included improvement in aerodynamic modelling in a number of key areas such as dynamic stall, blade-vortex interactions and the inclusion of 3-dimensional flow effects and also the inclusion of structural coupling and control system in the dynamic modelling.

In the study by Bousman and Mantay [1.6] in 1987, it was concluded that although the prediction of mean and oscillatory loads was acceptable for design purposes, the physical phenomena were still not completely understood. The comprehensive survey by Friedmann [1.7] in 1990 on the principal developments in various modelling aspects also concluded that the capability in rotor loads prediction has not been significantly improved and there is still much to be done. A close scrutiny of these reviews has led to the conclusion that the modelling in rotor aerodynamics and dynamics is still far from satisfactory.

For reasons of simplicity, most existing analytical methods treat the rotor and the fuselage separately and their limitations are well recognised. The underlying philosophies are;

(1) The distribution of loads on the rotor blade and control system can be calculated with reasonable accuracy without considering the finite hub impedance. This is based on the assumption that most in-service helicopters do not exhibit significant hub motion; and

(2) The fuselage vibration can be reasonably estimated using the hub loads calculated on a hub-fixed condition even when the vibratory sources in the rotor are not fully understood.

Although these analyses have been successfully used in the design and analysis of helicopters, some important aspects of rotor behaviour and rotor-fuselage interaction are not adequately modelled. The applications of these analyses to flight conditions other than level flight are often limited and are treated in an *ad hoc* fashion. For example, WHL's coupled modes analysis: Program R150 [1.8], calculates the rotor loads using hub-fixed blade modes. The hub loads are then used to assess airframe vibration by treating the rotor as a lumped mass. The effect of manoeuvre motion is accounted for by including the aircraft steady pitch and roll motion only.

The dynamic characteristics of the rotor system depend not only on the distribution of blade structural and inertial properties and the hub

configurations, but also on the dynamics of the systems to which the rotor is attached. These systems are principally the fuselage, the transmission and the control linkage. The assumption of isolating the treatment of rotor and fuselage can no longer be justified. In order to describe the rotor behaviour adequately, it is important that the dynamic interaction between these systems is taken into consideration.

The advancement of computer technology equips analysts with a powerful tool allowing them to model rotorcraft problem with added complexity. However, simply introducing more details into the modelling does not necessarily provide a better understanding of the complex behaviour of the rotorcraft. Johnson [1.9] has highlighted some of the key issues which should be included in any rotorcraft aeroelastic analysis. These issues include the fully non-linear aeroelastic solution, improved aerodynamics and the modelling of configurational dependent dynamics. In the next section, the various ways of dealing with these issues by some of the current comprehensive analyses is examined.

1.4 Overview of Current Comprehensive Analyses

Comprehensiveness is a term now widely used in the rotary-wing industry. It defines the ability to combine the modelling of various rotorcraft disciplines and to simulate manoeuvring flight. It also provides the flexibility to model different rotorcraft and hub configurations, blade planform geometry and control system dynamics.

A number of comprehensive rotorcraft aeroelastic analyses are being developed, usually by teams of engineers and scientists. Some of the modelling philosophies are briefly reviewed. This is a vast subject, which is already backed by a considerable volume of existing literature. The purpose of this review is to highlight some of the important features encapsulated in these analyses. A chart is compiled in *Table* 1 to provide a framework for subsequent discussions.

One of the more noticeable comprehensive analyses is marked by the development of the 2GCHAS suite [1.10A], owned by the US Army. It is a large computer software system designed to analyse a wide spectrum of rotorcraft problems, to provide resources for basic research and to be used as a design tool in the various phases of engineering activity. Its method lies in the assembly procedure and is finite element method

based. The structural model is founded on a building block approach where the coupling procedure makes use of constraints applied at the boundary between individual components. The solution is obtained by solving the complete system equation. This system provides the modelling flexibility and ability to analyse large motion manoeuvres. Despite extensive development since 1979, very little correlation on manoeuvres has been published [1.10B] and the software system is not available outside the USA.

Program CAMRAD/JA of Johnson Aeronautics [1.11A] is another comprehensive model based on the modal method. Its modelling strategy lies in the integration of recent technology uniformly to avoid limitations presented by the older analyses. Rotor shaft motion effects are included by allowing relative motion from one frame of reference to another. A selection of wake and dynamic inflow models is also available. The analysis is applicable to a twin-rotor aircraft and to various hub configurations but its true manoeuvre capability is yet to be demonstrated. An updated version, CAMRAD/II [1.11B], is now available. The main differences are the use of finite element methods and the extended capability to model more complex configurations. This program is gradually gaining popularity and is likely to be used as a bench-mark for other comprehensive analyses of the same generation.

Program RDYNE of Sikorsky Aircraft [1.12], based on the sub-structure synthesis method developed by Hurty [1.13], assembles a dynamic model of the helicopter from physical components contained in the base and external modules. These modules, which contain geometrical and aerodynamic non-linearities, are assembled to form the complete dynamic equation. The coupled system response is obtained by integrating the differential equation with respect to time. The structural modelling in RDYNE is versatile but its manoeuvre capability is limited.

The approach adopted by Eurocopter Deutschland (formerly MBB) [1.14] is based on multi-body system dynamics, where a number of rigid and flexible bodies are inter-connected. This is achieved by considering the motion of a typical body in an arbitrarily moving reference frame, thus allowing large motions to take place between these elements. The central theme is to develop a general set of dynamic equations of motion from each of these bodies. In this manner, the arbitrary connection between different bodies can be modelled and leads to a

model with a high degree of flexibility. However it treats the structure as an assemblage of rigid body components and does not possess the capability of modelling the true aeroelastic and non-linear behaviour.

Program GRASP [1.15] is an analytical tool used principally to investigate the aeromechanical stability problem of a bearingless rotor with homogeneous isotropic beams. It combines the finite element method for its modelling flexibility and the multi-body approach for its ability to handle large motions. It differs from standard finite element programs by allowing sub-structures to move relative to each other with no small angle assumption. This capability facilitates the modelling of rotorcraft structures including rotating and non-rotating interfaces and details of blade/root kinematics for various rotor types. It also differs from the standard multi-body approach by including aeroelastic effects, inflow dynamics and non-linear aerodynamics. The approach is to treat the non-linear static and linearised dynamic behaviour of rotorcraft represented by arbitrarily connected rigid body and beam elements. It thus removes the restrictions introduced by the linear small displacement approximation on beam elastic deformation and application to a fixed number of configurations. Despite its attractive features, the program is currently limited to the analysis of aeroelastic stability only.

General observations of these comprehensive tools are that they provide solutions to a wide range of rotorcraft problems with emphases being placed on modelling flexibility. They are more complex but do not necessarily provide the insight into the rotorcraft behaviour. There is also a lack of verification on their true manoeuvre capability.

1.5 Methods of Aeroelastic Analysis

Various methods: modal, finite element, multi-body dynamics and numerical, are all being used for rotorcraft aeroelastic analysis. The modal approach assumes that the system dynamics can be described by a selected number of degrees of freedom *eg.* Program R150 [1.8]. The finite element method assembles the equations governing the individual elements into the global system equation by imposing boundary constraints from which the solution is obtained *eg.* Friedmann [1.16]. The multi-body dynamics approach combines the flexibility of the finite

element method with that of multi-bodies for dealing with large motion for rotorcraft *eg.* Program GRASP [1.15]. Last but not least, in a numerical approach, both the formulation and solution of the equations of motion are carried out numerically *eg.* AGEM by Done *et al* [1.17]. This avoids the need of invoking ordering assumptions and the laborious algebraic derivation of the aeroelastic equations.

In order to strive for physical insight, a modal method is adopted in this study. The modal approach provides a greater analytical flexibility than that of the finite element method or the multi-body hybrid approach since the number of degrees of freedom used in the solution is much less, hence reduced computation time. Although for an exact treatment an infinite number of modes is needed, in recognising that the dominant vibration modes are confined to the lower frequency spectrum, the rotor dynamic behaviour can be modelled with sufficient accuracy using only a finite number of lower order modes. The deficiency associated with the modal method is that it does not treat the forcings of higher order modes due to the inherent truncation of the number of modes. However, a method does exist to alleviate such a deficiency [1.18].

Whilst the finite element or the multi-body methods offer modelling flexibility, they have their disadvantages. A shortcoming of finite element methods is that excessive computation time is needed to perform the assembly and solution procedures. In addition, traditional finite elements cannot accommodate large rotations and special finite elements are needed for modelling centrifugal and Coriolis loads. In the hybrid multi-body approach, large rigid body motions are included by using moving reference frames, and the body is assumed to undergo small or moderate rotations relative to the reference. This approach permits the use of standard finite elements but requires a more complicated assembly and solution procedure. Despite the simplicity offered by the numerical approach, post-processing of the results in terms of the modal contents would be needed to gain insight.

1.6 Structure of The Thesis

In this chapter, a background on the complex nature of helicopter is provided. The objectives of this study are then defined. The modelling philosophies and limitations of existing methods are reviewed

and are followed by an overview of some of the current comprehensive analyses. Both of which provide a framework for this study. The chapter was concluded by the discussion of various methods applicable to this type of analysis and the reasons for adopting the modal method.

In Chapter 2, the important aspects in the modelling of rotor structural dynamics and aeroelastics are considered. The assumptions adopted for the beam kinematics are discussed and the basic dynamic principles used in the analysis are reviewed. The chapter is concluded by discussing the application of REDUCE, a symbolic algebra software system, to alleviate the manual effort for deriving the algebraic equations but its limitation is also recorded.

Chapter 3 details the development of the analysis method. Particular emphasis is given to the various coordinate transformations and the ordering scheme adopted. The concept of complex rotor modes is introduced, followed by the description of the dynamic analysis and its solution method. A rigorous mathematical proof of the classical orthogonality for the complex rotor modes is provided and its influence on the dynamic modelling is discussed. An orthogonalisation procedure, applicable to all mode types, is introduced. It allows the system response equations to be reduced to a modal form, suitable for a solution, without reverting to laborious algebra. The method of solution employing complex rotor modes is described, with due consideration given to the simultaneous treatment of different mode types. The various techniques used to determine the blade structural loads are discussed. A novel technique for alleviating the inherent numerical problems with the force integration method is also introduced.

Chapter 4 first describes the main analysis procedure of the software - Program CRFA, developed for this analysis. Applications of this method to determine rotor loads during a manoeuvre and to include the effect of elastic hub motions on rotor vibratory loads are demonstrated. Finally the application of rotor modes by including the transmission flexibility in the loads calculation is also provided.

Finally, Chapter 5 draws conclusions from this study and recommends topics for future research.

Company Code	BELL COPTER	BOEING C60	SIKORSKY RDYNE	NASA CAMRAD	US ARMY 2GCHAS	AGUSTA ...	MBB Multi-body	AEROSPATIALE ...	WESTLAND CRFM
Application	Performance Loads Vibration Aero.stability	Vibration Loads Vibration	Time History S.S.Response Aero.stability	Performance Loads & Vibration Flight Dynamics Aero.Stability Transient Analysis	Performance Loads & Vibration Aero.stability Control Acoustics	Non-linear Behaviour of rotor/complete helicopter	Aero.stability Forced response	S.S.Response Forced Response Loads & Vibration Aero stability Blade stall flutter	Performance Loads & Vibration Airloads Aero.stability
Method of Solution	Runge-kutta	Harmonic Response	Newton-Beta	Num.Integration	Newton-Raphson	?	Shooting method with Floquet	Newton-beta	Z-transform Runge-kutta
STRUCTURAL DYNAMICS									
Blade	Straight	Straight	Straight	Straight	N.L.beam elements	Rigid elements	N.L. continuum beam	Straight	Straight or curved
Eqn.of Motion	Modal	Finite Element	Modal	Modal	FE and Modal	FE	FE	Modal	Modal
Modes	Rotor Modes (12 Max)	25+ flex beam	30 blade modes	Blade 10B,5T	?	——	——	Blade modes with hub motion	Rotor Modes (upto 50)
Load Cal'n Method	M.S. & U.F.	——	?	?		?	?	?	MS,FI plus UF for single blade
Modelling Capability	Modal data update M.B.C. Various roots	Redundant L.P. Tip Effect	Aeroelastic Rotor Elastic fuselage Rot.-Fixed Vib.Abs. Transmission Iso.	Multi-rotor conf. Various Hub conf Engine Drive Train	Multi-rotor conf. Various hub conf. N.L.spring/damper	Modelling complex structure incl. rotating element spring/damper	Various root conf Pitch control	Aeroelastic rotor Elastic fuselage Control System Vibration absorber	Multiple L.P. Various hub conf. Control Systems
Elastic hub motion	No	Harmonic Displ.	Yes	Yes	Yes	?	Yes	Yes	Yes
Rotor/Body Int'ion	No	Yes	Yes	Yes	Yes	Yes	Yes	?	Yes
Coupling Systems	No	?	Fuselage Transmission	Fuselage Transmission	Fuselage Transmission Control	Fuselage Transmission Control	Multi-body using sub-structuring	Multi-body using branch modes	Fuselage Transmission
Ordering	Yes	?	?	?	?	?	?	?	
AERODYNAMICS									
Gen.Aerodynamics	Compressibility Unsteady Aerodyn Yawed flow effect	Tip effect Fuselage upwash	Quasi-steady	Lifting line Steady,2D aerofoil data with 3D & uns. corrections	Linear Quasi-steady	Compressibility Stall Reversed flow	?	Quasi-steady (2D) Unsteady aero (3D) N.L. 2D theory	Compressibility Unsteady aerodyn
Dynamics Stall	Lift(Tarzania) Drag(Harris) Moment(Carta)	Lift(Tarzania) Drag(Harris) Moment(Tarzanin)	Simplified Aero & Look-up Tables	Johnson Gormel	Finite difference aero model	Steady aero data (2D aero+3D corr) Unsteady aero data (empirical)	Section aerodyn	3D stall model	Indicial Model for L,D,M below stall Time delay for dyn stall (Beddoes)
Ind Vel.Model	Uniform Inflow Dress Inflow L.V.Table Mod.Momentum Prescribed Far Wake Free wake	Deformed Near Wake Prescribed Far Wake Variable Inflow Lifting Line Vortex Rigid Wake	Influence coeff Momentum Inflow Variable Inflow Annulus Inf.(hover) Glauert Inflow	Prescribed Wake Freewake (Scully) Uniform Inflow Non-uniform inflow with rigid wake	Dyn.Inflow element Freewake	Glauert-Coleman Mangler-Squire Uniform	Simple vortex disc for lifting screw in oblique flow	?	Glauert Vortex Ring (Young) In'active Near Wake Far Wake (Beddoes) Fuselage Upwash
Manoeuvre Capability	Yes	No	Limited	Yes	Yes	Yes (using gust field defn)	Yes	?	Yes
Remarks	Elastic Fuselage	No inter-harmonic coupling; No struct effects of twist/pitch	Sub-structuring	Future bench-mark		Modelling generality			

Some abbreviations: MS - Modal Summation; FI - Force Integration; UF - Unified Formulation; FE - Finite Element.

CHAPTER 2 - MODELLING CONSIDERATIONS AND BASIC ASSUMPTIONS

2.1 Introduction

An accurate prediction of rotor aeroelastic behaviour requires accurate modelling of the structural dynamics of the rotor system, the aerodynamic derivatives of the blade aerofoil sections and a detailed description of the aerodynamic environment in which the rotor operates. The advent of composite materials in the construction of rotor blades and hubs has also brought along additional complexity to blade structural modelling. As the analysis of rotorcraft becomes ever more complex, due consideration must be given to ensure that the modelling is sufficiently accurate and yet computationally feasible. In this chapter, the modelling of the rotor dynamics and the assumptions on beam kinematics, with particular emphasis on practical application, are discussed and described.

2.2 Considerations for the Modelling of Rotorcraft Dynamics and Aeroelastics

One of the main contributors of complexity in rotorcraft dynamic coupling arises from the presence of the rotating and non-rotating components. The first analytical study to deal with such a system was attributed to Coleman & Feingold [2.1], who described the well-known ground resonance phenomenon by considering a rotor with rigid blades having flap-lag freedoms on a rigid fuselage with undercarriage flexibility. They made use of the multi-blade coordinate to describe the transformation between the coordinate system fixed in the blade and that fixed in the body. A useful description and an application of these coordinates in coupling the rotor/fuselage were made by Hohenemser and Yin [2.2] and also by Done [2.3] in a simplified approach to the ground resonance study. However, for most practical applications, the use of multi-blade coordinates is still primitive in rotorcraft analysis.

Attempts to couple the rotor with the fuselage are done differently. For instance, the fuselage vibration is assessed by treating the rotor as a lumped mass and using the loads calculated using hub-fixed modes as in Program R150. Conversely, the fuselage has been incorporated as a set of hub impedances, prescribed as a harmonic variation, into the

rotor loads calculation, *eg.* the work carried out by Sopher & Kottapalli [2.4] on a wind tunnel helicopter model. Further evidence has also identified the need for a better representation of the coupled rotor-fuselage system. It is the purpose of this study to address some of these issues.

2.2.1 Effects of Transmission System Flexibility on Rotor Dynamics

The inclusion of the transmission flexibility allows the shaft to rotate, which cannot at present be accommodated in the hub-fixed modes calculation. The mechanism of this shaft rotation effectively reduces the in-plane stiffness of the rotor when a net yaw moment is applied to the shaft. An example calculation by Griffiths [2.5] has detected a shift of the blade second lead-lag frequency from 4.31R to 3.48R (1R = once per revolution) for a 4-bladed Lynx main rotor when transmission flexibility, using an impedance representation, was included in the analysis. This frequency shift only occurs for the collective motion of the blades, *ie.* when being forced at 0R,4R,8R.. *etc.*

Flight test results [2.6] have shown that the 4R mast stresses actually decrease with increasing rotor speed, which suggests that the effective value of the blade second lead-lag frequency is actually below 4R, since the natural frequency reduces as rotor speed increases. Griffiths [2.5] also showed that the inclusion of transmission flexibility has improved the phase correlation of 4R edgewise bending moments with flight test data. Thus the transmission flexibility can no longer be ignored and must be included in the dynamic analysis in order to improve the loads calculation.

2.2.2 Hub Motion Effects on Rotor Loads and Fuselage Dynamics

In a modal approach, the rotating blade modes used in the response analysis are normally defined at a hub-fixed condition. The hub-fixed assumption for rotor dynamic analyses does not strictly hold because perturbatory hub elastic motions exist. The effect of hub motion on the oscillatory blade loads, as well as the vibratory hub loads, are well recognised as highlighted in [2.4]. This is particularly true near the blade passing frequency (NR) and is very sensitive to the fuselage dynamic response.

The loads on a rotor include both steady and oscillatory components, described by 1R,2R.. *etc.* In general, the rotor loads are dominated by the steady component and the first few harmonics. These are the loads that determine the fatigue life and ultimate strength of blades and control circuit linkages, and are of prime interest to rotor designers. At harmonics above two, the loads generally become progressively smaller and often have little influence on the fatigue life for blades of good structural design with natural frequencies well separated from the forcing harmonics. However, it is these higher harmonic loads that are the main sources of vibration in the fuselage. An understanding of the origins of these loads is fundamental in order to predict the airframe vibration accurately.

In addition, the approximation of applying head forces and moments, calculated for a rigidly supported rotor, to the flexible airframe can lead to errors in vibration calculation. For example, Gabel and Sankewitsch [2.7] introduced hub motions as harmonic excitations in the assessment of helicopter vibration. Using this approach, they showed that when the rotor impedance is used to correct the rotor forces and moments input to the airframe, the fuselage vibrations are better predicted.

In this analysis, the effects of hub motion will be considered both as external inertia forcings at the hub and included in the modes calculation. In the former approach, the blade dynamics can be modelled as hub-fixed rotating blade modes with the hub motion being calculated from measured or predicted fuselage responses. The latter approach implies that the modes are complex.

2.2.3 Coupled Rotor-Fuselage Responses

An assessment of the importance of rotor-fuselage coupling on airframe vibration response using a simplified finite element fuselage structural model was made by Rutkowski [2.8]. Forced responses of coupled and uncoupled rotor fuselage configurations were studied. The results showed that the qualitative behaviour of the responses appeared to be similar in the two cases, but that the magnitude of the uncoupled (approximate) response was considerably larger than the coupled (near exact) response. Also it was found that the magnitude of the fuselage response at the natural frequencies was highly dependent on their

proximity to the blade frequencies. Rutkowski's study has illustrated the significance of coupled system characteristics on fuselage modes.

2.2.4 Effects of Multiple Torsion Frequencies and Control Circuit Stiffness on Rotor Dynamics

An examination of the Lynx main rotor control circuit load paths reveals that the value of control circuit stiffness experienced by a single blade depends on the motion of all the blades, since the upper part of the swash-plate experiences different stiffnesses around the azimuth due to the positioning of the fixed system jacks.

Multiple torsion frequencies, described as collective, lateral and longitudinal cyclic, and reactionless frequencies, ranging from 3.8R to 6.2R have been identified both analytically and experimentally (using spectral analysis of blade torsion moment and spider arm bending moment) on the Lynx aircraft. However, in a conventional single blade analysis, only one of these frequencies can be used in the calculation of blade responses. In the study by Griffiths [2.5], it was shown that the prediction of airframe vibration and rotor loads could be significantly altered depending on which mode was used. The modes used for the response analysis must adequately reflect the true placement of torsional frequencies.

In addition, the calculation on a Sea King tail rotor by Holton [2.9] has shown large effects on the blade stability margins when the transmission system and control circuit impedance are included in the single blade analysis. The control circuit model for both hydraulics on and off cases is represented by two mass-spring-damper systems, where the parameters are obtained from measured dynamic characteristics based on collective rotor motion. The transmission dynamic model is represented using ten transmission system modes obtained from a dynamic model of the gear-train system. The large differences in the blade stability margins for the two cases, with and without coupling to the control circuit and transmission system, highlight the need to include the latter in the stability calculation.

2.2.5 Modelling of Lag Damper

Lag dampers are introduced primarily to suppress the ground resonance

instability in rotorcraft but they pose significant modelling problems to the analysts. The lag damper characteristics, which are highly non-linear and frequency dependent, must be modelled adequately in order that the rotor loads be predicted accurately.

Correlations of measured and predicted blade root edgewise bending moment have shown large discrepancies. This is due mainly to the differences found in the fundamental lag frequencies between the predicted (based on a single blade mode analysis program) and the measured (based on a cyclic stir on the ground run). For instance, these frequencies are found to be 0.66R and 0.73R respectively for a Lynx main rotor [2.10]. This shift of frequency is primarily attributed to the increased stiffness due to the lag damper. Unless it is included in the modes calculation, the blade dynamics cannot be modelled accurately.

In this analysis, the effects of a lag damper will be modelled as external discrete loads in the main blade load path. Also the linear lag damper load can be included as a main constituent in the modes calculation. The latter approach implies the modes are complex and that the linear lag damper load must be subtracted from the total loads in the response calculation.

2.2.6 Modelling of The Effects due to Variation of Rotor Speed and Blade Pitch Angle

The dynamic characteristics of a rotor blade are normally calculated at a constant rotor speed and a representative blade collective pitch. The application of time-varying cyclic pitch implies that the blade mode shapes vary around the azimuth. Because of the excessive computation required, such time dependent mode shapes cannot yet be accommodated. Bell Helicopters of the USA has included an option into Program COPTER [2.11] to enable the rotor dynamics to be numerically interpolated for different pitch applications. This has shown some improvement in the prediction of oscillatory loads. In this analysis, although there is a potential to include cyclic pitch in the modes calculation when complex modes are introduced, this will not be done for some time yet. In order to account for the time varying pitch, the perturbations in pitch will be treated as forcing functions in the response analysis.

The variation of rotor speed is also of equal importance in rotor dynamics. During a manoeuvre, the rotor can operate over a range of speed, *eg.* 85%NR to 105%NR (NR=Nominal rotor speed) in a flyaway. This means that the modes must be calculated for each rotor speed and this is clearly not practical. In this analysis, we consider only the kinematic effect of the rotor speed variation to allow transitional flight and engine torque perturbation. It will be treated as forcing functions and will not be considered in the modes calculation.

2.3 Blade Structural Modelling

Rotor blades are effectively slender beams where the aspect ratio is an order higher than the lifting surface of a fixed wing aircraft. This feature has an important implication in that the rotor blade analysis reduces effectively to a 1-dimensional *ie.* beam problem. Advanced section and planform geometry rotor blades are introduced to improve aerodynamic efficiency, and for structural simplicity, bearingless hub configurations are also used. Both of these can only be accomplished by the application of composite materials in the blade and hub construction. It is therefore necessary to examine the basic assumptions for the practical application of this analysis to composite rotor blades.

2.3.1 Composite Materials and Bearingless Rotor

The introduction of composite materials in rotor blade construction are primarily to increase the blade fatigue strength and damage tolerance. Composite materials are anisotropic and their non-homogeneity introduces various deformation couplings which are absent in isotropic materials. The advantage is that they allow the designers to select fibre lay-ups for optimal structural coupling to reduce vibration - a topic which has received attention in recent years under the heading of aeroelastic tailoring as surveyed by Shirk *et al* [2.12]. Its introduction has also led to substantial research efforts to develop dynamic models which are suitable for structural dynamic and aeroelastic analysis for these types of blade construction.

Hodges [2.13] presented an excellent review of composite beam modelling in 1990 and he concluded that a structural theory that is sufficiently

general to treat such complicated structures with their variation of cross-section, spanwise non-uniformity and potentially large deflection, does not yet exist. However, many of such composite beam theories *eg.* the anisotropic theory developed by Bauchau and Hong [2.14] have been successfully applied to a thin-walled section blade with large displacements. They also highlighted some of the non-classical behaviour, such as sectional warping and shear deformations in composite blades. Although the importance of these non-classical effects is recognised, in order to prevent amplification of the problem and detraction from the set objectives, certain assumptions on composite blade modelling are made in this analysis.

One of the main difficulties of modelling composite beams is to extract the stiffness properties of arbitrary cross-sections and then structurally reduce them to a beam problem. Although the 3-dimensional anisotropic behaviour in composite blades is recognised, providing the geometric variations of the blade are "moderate", the blade can be considered uniform at any particular cross-section. Thus the analysis can be done once for each cross-section and is independent of the non-linear global deformation. This partial de-coupling is assumed to be possible without rigorous proof as concluded by Hodges [2.13] and is adopted in this study.

The bearingless rotor systems eliminate conventional blade root hinges and bearings by using structural elements that are sufficiently soft in torsion to accommodate all the blade pitch control. The flexible structure makes the dynamic modelling of the systems much more complicated and difficult to analyse.

In order to account for the softer torsional flexibility, a quantitative argument is used. The structural torsional moment along a deformed blade is defined principally as the product of torsional rigidity (GJ) and the rate of twist (ϕ'). For rotor blades made of conventional materials, GJ is of the same order as the bending stiffness, hence the twist ϕ will be small. For flexible structural elements, the converse is true. In this analysis, an ordering scheme is defined to retain the magnitude on the torsional moment such that a balance of rigidity and deformation can be maintained.

2.3.2 Assumptions of Small Strains and Uniaxial Stress - Moderate Deformation

Essential to the derivation of non-linear aeroelastic equations is the development of a non-linear strain-displacement relationship. The use of this relationship, together with the Hooke's Law, permits the strain energy to be expressed in terms of the deformation quantities.

One of the most notable treatments of the non-linear strain-displacement relationship for rotor blades was due to Dowell & Hodges [2.15] in 1974. They derived the relationship from a general standpoint and then reduced it to a second order problem on the assumption that the strain components are small. The small strain assumption is justified by the fact that massive bodies in which strain components are small can only be subject to small elastic displacements and rotations. Conversely, thin bodies such as beams can undergo moderate elastic deformations even when the strains are small.

The small strain assumption has important implications in that the higher order non-linear strain terms can be neglected. Thus the definition of strain based on the deformed length increment (Eulerian) and on the original length increment (Lagrangian) become identical. By adopting this small strain assumption, the usual stress-strain relationship of the material can be applied in this analysis.

Similarly, the assumption of uniaxial stress is also invoked in this study. This implies that the stress components in the other directions are at least an order of magnitude smaller than the axial stress. Hence the strain energy resulting from products of stress and strain components in the direction normal to the axial orientation can be neglected. This assumption reduces the magnitude of analysis by, at least, an order [2.13].

2.3.3 Effects of Sectional Warping and Shear Deformation

The Euler-Bernoulli beam bending theory assumes that a cross-section remains plane after deformation. However, when composite materials are used, several non-classical effects, such as torsional related warping and transverse shear deformation can become important. Their effects are essentially non-linear and, when included, the computational effort

will be substantially increased as shown by Bauchau & Liu [2.16].

Shear deformations describe shearing of the cross-section and are of the same order as the bending slopes. The difference between the shearing and the bending of a cross section represents a reduction of bending slope. For conventional rotor blades, including those of composite material construction, shear deformations are very small. This is also true for most bearingless rotors. Shear deformation is noticeable only if unconventional materials *eg.* rubber based, are used in the blade construction.

In general beam deformation, in- and out-of-plane warping as well as torsional warping can occur. The uniaxial stress assumption requires only the torsional warping to be considered as shown by Hodges & Dowell [2.15]. However, this effect is small for applications involving closed sections. It can be safely disregarded without loss of accuracy.

In order to contain this analysis to a manageable size, both sectional warping and shear deformation are excluded *ie.* Euler-Bernoulli beam theory applies and there is no distinction between section rotation angles and bending slopes. However, it should be noted that by making such assumptions, the important coupling effects *eg.* those induced by biased ply lay-ups for aeroelastic tailoring cannot be treated in this analysis. Extension to deal with these issues is required in the future.

2.3.4 Exact vs Approximate Analysis

In the derivation of the non-linear aeroelastic equations in an explicit manner, a large number of higher order terms will appear and simplifying assumptions are essential to reduce its complexity. Although an exact treatment of load-strain relationship based on a complicated vector approach has been postulated [2.17A], and later refined [2.17B] by Hodges, such an approach is highly mathematical and does not necessarily provide the insight required. Furthermore, its applications are yet to be proven. Exact formulation of the displacement-transformation was also initiated by Simpson [2.18] but an ordering scheme was eventually invoked in order to simplify his analysis.

A simpler derivation can result if an approximation is assumed at the outset. The approach adopted here belongs to the class of explicitly-ordered beam theories described in [2.13] in which each of the parameters is assigned a value relative to an ordering parameter whose magnitude is assigned *a priori*. This provides a systematic process for discarding the higher order terms. Furthermore with the use of REDUCE (*Section* 2.5), higher order terms can be included with ease if they are found to be important in certain applications. The choice of such an ordering scheme is the subject of *Section* 3.2.

2.4 Basic Dynamic Principles

Whilst in principle, it is always possible to obtain the equations of motion of any mechanical system, whether continuous or discrete, by Newton's Second Law and D'Alembert's Principle, the practical task may be rendered extremely difficult by the presence of internal forces. Also one has to consider very carefully the signs of various forces, as mistakes often arise because an action has been confused with a reaction. Such difficulties can be avoided by using energy methods, *eg.* Hamilton's Principle, which is based on elementary mathematical operation such as differentiation of the energy functions. The prime task is that of writing down the energy expressions for the idealised system, in terms of a suitable set of coordinates referenced to a convenient frame.

Application of both Hamilton's Principle and the Newtonian method to developing the rotor aeroelastic equations was made by Hodges & Dowell [2.15]. They concluded that the former method is more mathematically rigorous and systematic, while the latter provides more physical insight.

Other important advantages associated with Hamilton's Principle are:

a) It is independent of the coordinates chosen to define the motion of the system;
b) A consistent set of equations will result if the energy expressions are accurate to the desired order of magnitude; and
c) The appropriate boundary conditions will be a by-product of the derivation.

Thus the energy approach is the most appropriate for this analysis and the two energy formulations, namely the Lagrangian equation and the Hamilton's Principle, are employed.

2.4.1 Lagrangian Equation

The modal response equation for the coupled rotor-fuselage system is obtained by applying the Lagrangian equation to the kinetic energy, potential energy and virtual work expressed in terms of the generalised coordinates. In its general form, the Lagrangian equation is given by

$$\frac{d}{dt}\left\{ \frac{\partial K}{\partial \dot{q}_i} \right\} - \frac{\partial K}{\partial q_i} + \frac{\partial U}{\partial q_i} = \frac{\delta W}{\delta q_i} = Q_i \; ; \quad i = 1,2,.....,n$$

where K is the kinetic energy of the system;

U is the potential energy of the system;

W is the virtual work due to external forces;

q_i is a suitably defined i^{th} generalised coordinate;

Q_i is the generalised force;

n is the number of coordinates chosen; and

δ is the variational parameter.

The dissipation function $\mathbb{F}$ (power), which is dimensionally inconsistent with K,U & W (energy and work), is purposely excluded from the formulation. Such dissipative actions within the system arise from viscous or frictional effects and are non-conservative. They will be included in the virtual work. The generalised force consists of all external aerodynamic loads.

The above equation presents a complete formulation of the equations of motion of a dynamic system with n degrees of freedom, all constraints being assumed holonomic. In general, these equations will not be linear in q_i's, and their time derivatives *ie.* q_iq_j, $\dot{q}_i\dot{q}_j, \dot{q}_iq_j, ..,$ *etc.* will occur. However, for studies of small oscillation about an equilibrium state, the q_i's and their time derivatives may be assumed to be small, hence higher product terms can be ignored.

2.4.2 Hamilton's Principle

The expressions for blade structural loads are obtained by applying the Hamilton's Principle. By considering the variation of energy due to variation in each degree of freedom, the load components are derived. The virtual displacements may be arbitrarily assigned at time t provided that geometric constraints are not violated.

The Hamilton Principle, given in its most general form, is

$$\int_{t_1}^{t_2} [\delta(U-K) - \delta W]\, dt = 0$$

where the variables are defined as before and t_1, t_2 are the arbitrary time limits. Suitable expressions for U,K and W can then be determined and combined within the variational statement to give the desired equations.

2.5 Application of REDUCE

The derivation of non-linear aeroelastic equations, a process which is conceptually very straight forward but immensely tedious to perform, is carried out using the algebraic computing software system, REDUCE [2.19]. An example application to a wind turbine problem was made by Garrad & Quarton [2.20].

The use of REDUCE provides the basic mechanism for deriving the non-linear equations, avoiding the laborious and error prone process of derivation by hand. REDUCE allows individual variables to be weighted, then an overall weight level is applied. Products of variables exceeding the specified weight level are discarded. Algebraic differentiation in accordance with Hamilton's Principle and the Lagrangian equation can then be carried out.

Initial attempts to retain terms of higher order had led to substantial time and effort being wasted. Although the effectiveness of REDUCE is less than originally envisaged, it remains an indispensable tool in the formulation and manipulation of lengthy equations. This is especially true when fundamental revisions are needed to the modelling assumption or when the ordering of a parameter is changed. In such cases, the modified equations can be obtained relatively quickly.

CHAPTER 3 - METHOD OF ANALYSIS

3.1 Introduction

The important ingredients which a rotorcraft aeroelastic analysis must possess were described in *Chapter* 2 where the emphasis was placed on practical applications. In this chapter, the development of an analytical model suitable for the coupled rotor-fuselage system is discussed and described.

In keeping with a striving for insight, a modal approach is adopted for this analysis. The formulation of the modal Lagrangian equation appropriate for a single blade is presented here in detail. The modes adopted are initially assumed real such that only the kinematic effects of elastic hub motion, as well as aircraft motion, are considered. Appropriate explanation to extend the Lagrangian equation to use rotor modes as state vectors is furnished. The approach adopted here provides the necessary insight into the analytical development and the application of complex modes in rotor response analysis.

In the general case, the rotor modes, as developed by Juggins [3.1], are appropriate to the coupled rotor-fuselage dynamic (CRFD) system. These rotor modes, including hub motion effects, are complex and they enable the dynamic interactions between the rotor and the fuselage to be correctly modelled. The concept of rotor modes, not given before, is furnished here to provide an understanding of its application in rotor response analysis.

The modal approach assumes the modes are small linearised perturbations about a steady state, whereby higher order products of these quantities can be eliminated systematically using an ordering scheme. The choice of such a scheme based on physical reasoning is discussed.

The various aerodynamic models adopted in this analysis are described to provide completeness in aeroelastic modelling. A rigorous approach in defining the true angle of attack expression for the aerodynamic calculation is presented to clarify the doubt cast for many years.

A pre-requisite for the successful application of modal analysis is to ensure that the modes possess the orthogonality relationship. This

ensures that they indeed provide an independent set of state vectors to uncouple the system response equations. However, no such proof was furnished before. This has proved to be one of the most formidable tasks during this study. The proof is finally accomplished using the bi-orthogonality relationship, employing both the left-hand (LH) and right-hand (RH) eigenvectors. Owing to the algebraic complexity, the relationship is available only in numerical form.

This orthogonality proof is applicable to all linearised dynamic systems, but it requires that the dynamic system equations be described by a set of second order differential equations in terms of displacements only. However, the system equations originally derived for the CRFD, configured to use the transfer matrix solution method, do not automatically result in the required form. Conversion of the system equations is demonstrated to ensure that the LH-eigenvectors can be obtained and the important conclusions it has led to in the formulation of dynamic equations are discussed.

Because the complex modes orthogonality obtained is available only in numerical form, the concept of an orthogonalisation procedure to uncouple the system response equation into a form suitable for a solution is introduced. The procedure is applicable to all system modes used.

Two sets of complex rotor modes: coupled and reactionless, are needed to define the total rotor response. The need to solve the responses of the two mode sets simultaneously, when they are defined in different frames of reference, requires special attention to the solution method. A numerical process for filtering the applied forces is introduced. This novel method is practical and provides an integrity check on the analytical model. This is then followed by the discussion of the solution algorithms adopted for this analysis.

The determination of structural loads on the blade and hub, in order to assess the blade stresses and airframe vibration level, is addressed. Formulations of the blade structural loads, based on Modal Summation and Force Integration methods, are described. The numerical problems inherent in Force Integration are discussed and a novel analytical integration technique for minimising such errors is introduced.

3.2 Formulation of the Modal Lagrangian Equation for a Single Blade using Real Modes

3.2.1 General Considerations

The formulation of the modal Lagrangian equation described in the following sections is valid for a single blade using real modes as state vectors initially. Extension and treatment to complex modes are described in *Section* 3.5.

a. Description of The Rotor Blade Model

The rotor blade is modelled as a continuous curved beam, which defines the locus of shear centres of a typical (k^{th}) blade of an N-bladed rotor. The position vector of a point in a cross-section is derived relative to an axis system fixed in the rotor. The cross-section, which can be non-symmetrical, is given freedoms to translate along and to rotate about the 3-directions relative to its local sectional axis system. The assumptions of zero warping and zero shear deformation of the cross-section are invoked (*Section* 2.3.3). However, the latter is included at the outset in order to provide a compatibility check with the dynamic analysis. That is, shear deformations are removed after the equations have been derived.

The fuselage response is included by allowing the hub to undergo (perturbatory) elastic deformations comprising 3 translations and 3 rotations with respect to a non-rotating frame of reference. The blade motions are defined relative to the disturbed hub such that the total displacement of the blade point referenced to the global axis system is the sum of blade and hub displacements.

We assume the system is holonomic such that the blade elastic deformations can be expressed in terms of a set of generalised coordinates $q_i(t)$, $(i=1,..,N)$, where q_i are real quantities. Let the blade deflection vector be denoted by $\underline{x}=\{u,v,w,\phi,\beta,\zeta\}^T$, then;

$$\underline{x}(r,t) = \underline{x}_{ST}(r) + \sum_{i=1}^{N} q_i(t)\underline{x}_i(r) \qquad (3.1)$$

where $\underline{x}_{ST}(r)$ are the steady state values at position r;

$\underline{x}_i(r)$ is the i^{th} mode shape values at position r;

and N is the number of modes considered.

It is noted here that only the kinematic effects of hub motion are included in this formulation valid for a single blade. However, when the elastic hub motions are included in the modes, they are also expressible in terms of the generalised coordinates as those in the blade *ie.*

$$\underline{H}(t) = \sum_{i=1}^{N} q_i(t)\underline{h}_i \qquad (3.2)$$

where $\underline{H}=\{x_H, y_H, z_H, \phi_H, \vartheta_H, \psi_H\}^T$ and h_i is the hub component in the modes. In this case, both the mode shapes and the generalised coordinates become complex quantities. At present, we are concerned only with the modal representation appropriate to *Eqn.* 3.1.

Substituting the relationships defined in *Eqn.* 3.1 in the kinetic energy (K), strain energy (U) and virtual work (δW), and differentiating with respect to $q_i(t)$, $\dot{q}_i(t)$ and t in accordance with the Lagrangian equation;

$$\frac{d}{dt}\left\{\frac{\partial K}{\partial \dot{q}_i}\right\} - \frac{\partial K}{\partial q_i} + \frac{\partial U}{\partial q_i} = \frac{\delta W}{\delta q_i} = Q_i \qquad i=1,2,..,N \qquad (3.3)$$

the modal Lagrangian equation for a single blade using real modes as state vectors is obtained.

The control circuit stiffness is modelled as a secondary load path to earth represented by a set of linear and rotational springs attached to the main blade. The springs, which provide additional strain energy, are included in the formulation of the modal Lagrangian equation. A non-linear lag damper, generating discrete loads in the main load path, is also included.

b. Modelling of Aircraft Motion

In order to determine the rotor response and loads through a manoeuvre, the rigid body fuselage (aircraft) motion has to be included. However, it needs only to be considered as kinematic and is included in the kinetic energy formulation. The aircraft motion is defined as a set of instantaneous hub rates comprising 3 linear velocities: forward, sideslip and heave and 3 angular rates: roll, pitch and yaw.

Manoeuvres are, by definition, any flight condition departing from its straight and level flight path, *eg.* a symmetric pull-up or a complex barrel roll. They are generally non-prescribed and involve large aircraft motion. The manoeuvre which the pilot wants to perform is limited by many factors, the most important being the control power and aerodynamic damping available. The control power depends on the rotor thrust and hub moment, which are governed by the pilot input using his main rotor controls and/or pedal input. The head moment then determines the maximum acceleration at which the aircraft can enter into the desired manoeuvre.

During a manoeuvre the rotor state is changing rapidly and the aircraft no longer has only one trim state. However, the aircraft motion through a manoeuvre can be modelled as a sequence of snap-shots, each having its own state. In this manner, the airframe can be modelled as a rigid body. The fuselage attitudes, rates and accelerations during a manoeuvre are determined by solving the body equilibrium equations. These are then fed back into the loads calculation.

The pilot controls required to maintain the aircraft flight path can then be uniquely determined at each time step during the manoeuvre. The aircraft motion is thus included in the analysis by effectively having a pilot model in the loop interacting with the aircraft responses through the manoeuvre. One such pilot model can be found in [3.2] developed by Hamm.

This forms the basis of aeroelastic modelling in this analysis and the derivation of the forced response equation can proceed.

3.2.2 Coordinate Systems and Transformations

In the formulation of the equations of motion of a rotor blade, various coordinate systems are used. As a result of the work on coordinate transformation by Peters & Ormiston [3.3], the derivation of the non-linear equations for rotor blades has been systemised to a high degree.

Consider an initially curved, closed section, rotor blade of curvilinear length R, mass per unit length m. The position of a typical (k^{th}) rotor blade with respect to an axis system fixed in the rotor, can be defined. A curved blade segment, in both its undeformed

and deformed states, is shown in *Figure* 3.1 below

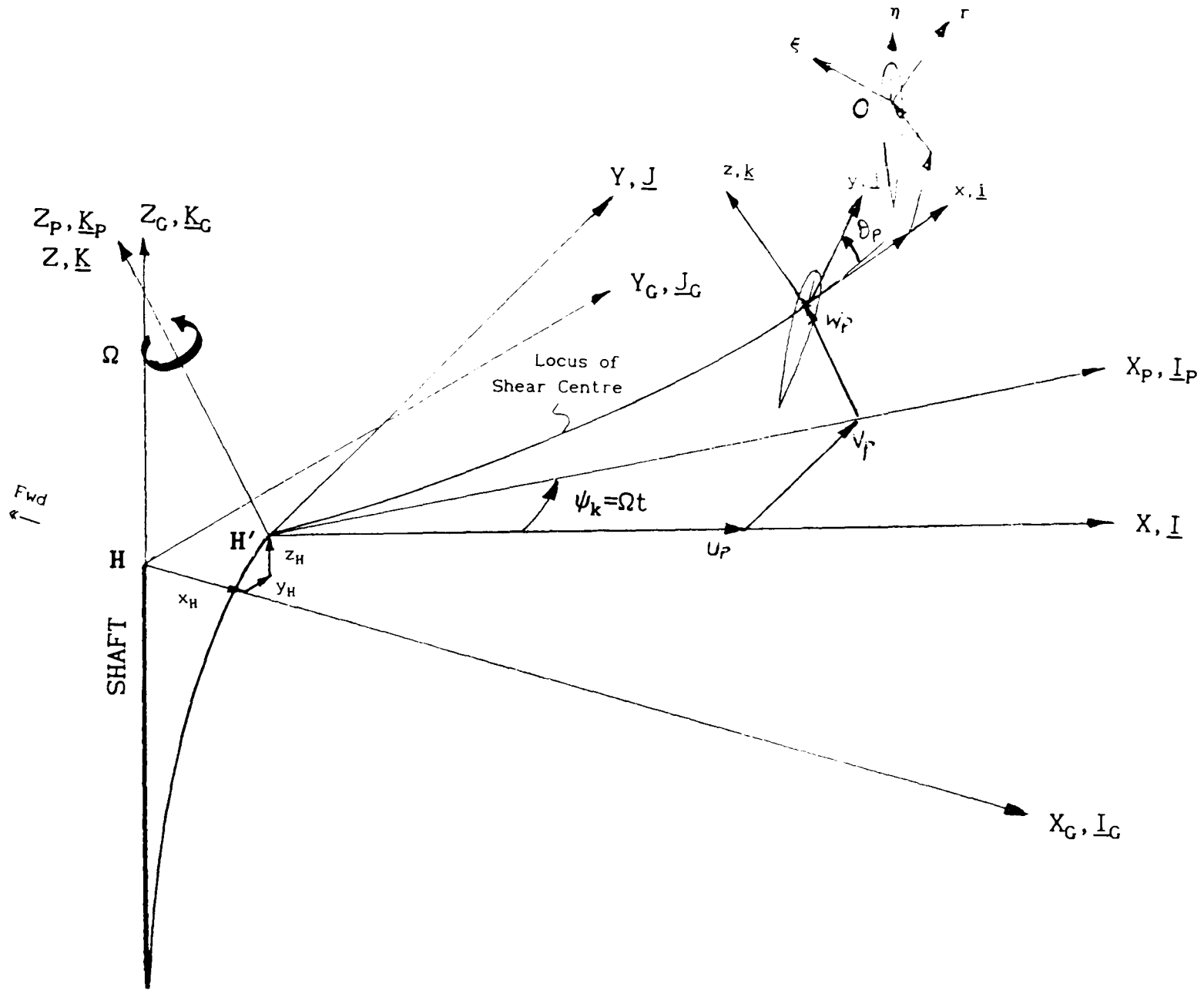

Figure 3.1: Blade Coordinate Systems and Deformations

The orthogonal global undeflected shaft $HX_GY_GZ_G$-axis system, with unit vectors $\underline{I}_G, \underline{J}_G, \underline{K}_G$, are fixed in the inertial frame $\mathbb{R}$ with the origin defined at the undisturbed hub position H. The HZ_G-axis is defined positive up along the rotor shaft and the HX_G, HY_G-axes are defined positive aft and to the starboard respectively, consistent with the right-handed system. The hub, which originally occupies position H, is allowed to undergo linear elastic deformation x_H, y_H, z_H parallel to the HX_G, HY_G, HZ_G-axes and Eulerian rotations taken in the order $\phi_H, \vartheta_H, \psi_H$ (roll, pitch then yaw) and is displaced to the new position H'. The rigid body fuselage motion, not yet included, is treated in *Section* 3.2.6.

The disturbed shaft H'XYZ-axis system with unit vectors $\underline{I}, \underline{J}, \underline{K}$ is defined in the hub frame $\mathbb{H}$. The blade pre-deformed $H'X_pY_pZ_p$-axis system, with unit vectors $\underline{I}_P, \underline{J}_P, \underline{K}_P$, is fixed in the reference frame $\mathbb{B}$ and rotates with respect to $\mathbb{H}$ at an constant angular velocity $\Omega\underline{K}_P$ and

occupies position $\psi_k=\Omega t+\psi_1$ at time t, where ψ_1 is an arbitrary reference position of the first blade. Point H', which is common to both $\mathbb{H}$ and $\mathbb{B}$, is located at the disturbed hub centre-line. The plane containing X,X_P and Y,Y_P is called the reference plane.

Let the undeformed beam be described by a curvilinear coordinate r which is measured from the origin H' along the beam elastic axis *ie.* the locus of shear centres. If r locates a point O, along the elastic axis, then point O is uniquely determined by the Cartesian coordinates (U_p,V_p,W_p), in the $H'X_PY_PZ_P$-axis system. The orientation of the cross-section at point O in its pre-deformed state is described uniquely by the local pre-sweep (ζ_p) and pre-cone (β_p) angles. Note that the pre-deformed coordinates are functions of not only space (r), but also time (t), since the blade portion outboard of the pitch bearing varies with cyclic pitch.

The orthogonal blade section Oxyz-axis system with unit vectors $\underline{i},\underline{j},\underline{k}$ and origin O is also fixed in $\mathbb{H}$. Bending deflections of the beam are accomplished by the displacements u,v,w of the elastic axis parallel to Ox,Oy,Oz-axes. After deformation, the origin O moves to O' and a blade fixed O'r$\eta\xi$-system with unit vectors $\underline{i}',\underline{j}',\underline{k}'$, is defined in the cross-section. The axes O'η,O'ξ are parallel to the section principal axes O'η_0,O'ξ_0 with origin defined at the displaced shear centre O'.

The Oxyz-system moves with the blade as the blade undergoes bending deformations and pitch angle $\vartheta(=\vartheta_p+\vartheta(\psi))$ rotations, including the built-in twist (ϑ_p) and the control pitch $\vartheta(\psi)(=A_0-A_1\cos\psi-B_1\sin\psi)$. The cross-section also undergoes ordered rotations; $\zeta,-\beta,\phi$, to occupy a new orientation. Although the deformed O'η,O'ξ axes do not lie exactly in the η_0,ξ_0-plane, the projection of the blade cross-section in the yz-plane before and after deformation is shown in *Figure* 3.2 below.

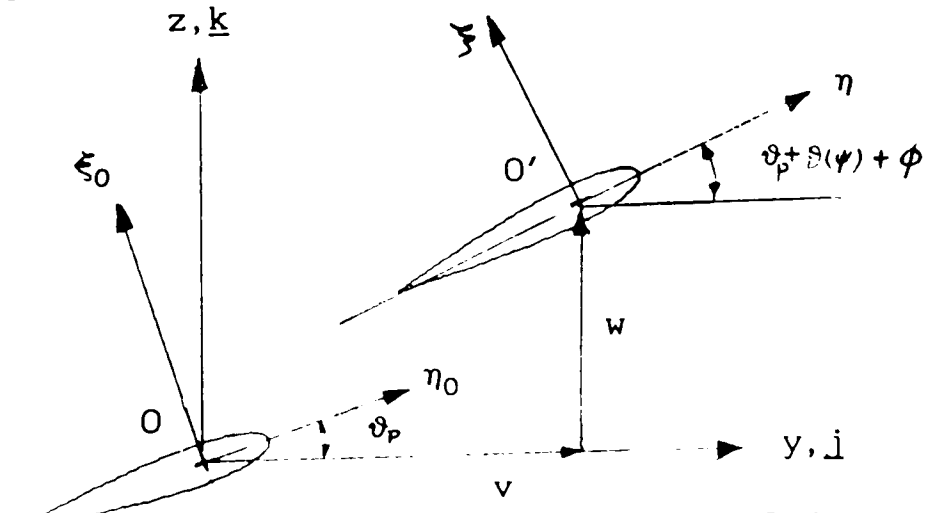

Figure 3.2: Blade Cross-Section Before and After Deformation

Before deformation, it is assumed that the blade section principal axes $O\eta_0, O\xi_0$ are rotated with respect to the undeformed coordinate by the pre-twist angle $\vartheta_p(r)$. After deformation, the elastic axis is displaced by u,v,w and the blade twisted through an angle ϕ, plus any control pitch angle $\vartheta(\psi)$.

3.2.3 Position Vector of A Blade Point

By considering the various coordinate transformations described above, the position vector of a point on the blade can be defined. Consider a point $P(0,\eta,\xi)$ defined in the blade section $Or\eta\xi$-axis system. The position vector of P in the blade elastic Oxyz-axis system, after deformation, is given by

$$\underline{r}_1 = \begin{Bmatrix} u \\ v \\ w \end{Bmatrix} + \begin{bmatrix} \cos\zeta & -\sin\zeta & 0 \\ \sin\zeta & \cos\zeta & 0 \\ 0 & 0 & 1 \end{bmatrix} \begin{bmatrix} \cos\beta & 0 & -\sin\beta \\ 0 & 1 & 0 \\ \sin\beta & 0 & \cos\beta \end{bmatrix} \begin{bmatrix} 1 & 0 & 0 \\ 0 & \cos\bar{\vartheta} & -\sin\bar{\vartheta} \\ 0 & \sin\bar{\vartheta} & \cos\bar{\vartheta} \end{bmatrix} \begin{Bmatrix} 0 \\ \eta \\ \xi \end{Bmatrix}$$

$$= \underline{r}_D + T_\zeta T_\beta T_{\bar{\vartheta}} \underline{r}_S \qquad (3.4)$$

where $\bar{\vartheta}=\vartheta_P+\vartheta(\psi)+\phi$. If the undeflected blade state is described by the pre-deformed coordinates such that $\underline{r}_P=(U_p,V_p,W_p)$, normalised by the rotor radius, R, then the position vector of P in the $H'X_PY_PZ_P$-axis system is given by

$$\underline{r}_2 = \begin{Bmatrix} U_p \\ V_p \\ W_p \end{Bmatrix} + \begin{bmatrix} \cos\zeta_p & -\sin\zeta_p & 0 \\ \sin\zeta_p & \cos\zeta_p & 0 \\ 0 & 0 & 1 \end{bmatrix} \begin{bmatrix} \cos\beta_p & 0 & -\sin\beta_p \\ 0 & 1 & 0 \\ \sin\beta_p & 0 & \cos\beta_p \end{bmatrix} \underline{r}_1$$

$$= \underline{r}_P + T_{\zeta_p} T_{\beta_p} \underline{r}_1 \qquad (3.5)$$

Further, it is assumed that the point P lies on a chosen (k^{th}) blade occupying azimuth position ψ_k with respect to the H'X-axis (+ve towards the rear of the disk). Then let the hub elastic deflection be described by $\underline{r}_H=\{x_H,y_H,z_H\}^T$ and rotations taken in the order of roll, pitch then yaw; $\phi_H,\vartheta_H,\psi_H$, the final position vector $\underline{R}_S$ of P in the global $HX_GY_GZ_G$-axis system is given by

$$\underline{R}_S = \begin{Bmatrix} x_H \\ y_H \\ z_H \end{Bmatrix} + \begin{bmatrix} 1 & 0 & 0 \\ 0 & \cos\phi_H & \sin\phi_H \\ 0 & -\sin\phi_H & \cos\phi_H \end{bmatrix} \begin{bmatrix} \cos\vartheta_H & 0 & \sin\vartheta_H \\ 0 & 1 & 0 \\ -\sin\vartheta_H & 0 & \cos\vartheta_H \end{bmatrix} \begin{bmatrix} \cos\psi_H & -\sin\psi_H & 0 \\ \sin\psi_H & \cos\psi_H & 0 \\ 0 & 0 & 1 \end{bmatrix} \begin{bmatrix} \cos\psi_k & -\sin\psi_k & 0 \\ \sin\psi_k & \cos\psi_k & 0 \\ 0 & 0 & 1 \end{bmatrix} \cdot \underline{r}_2$$

$$= \underline{r}_H + T_{\phi_H} T_{\vartheta_H} T_{\psi_H} T_{\psi_k} \underline{r}_2 \qquad (3.6)$$

Hence,

$$\underline{R}_S = \underline{r}_H + T_{\phi_H} T_{\vartheta_H} T_{\psi_H} T_{\psi_k} \left\{ \underline{r}_P + T_{\zeta_p} T_{\beta_p} \left\{ \underline{r}_D + T_{\zeta} T_{\beta} T_{\bar{\vartheta}} \underline{r}_S \right\} \right\} \tag{3.7}$$

where $\underline{r}_H = \begin{Bmatrix} x_H \\ y_H \\ z_H \end{Bmatrix}$; $\underline{r}_P = \begin{Bmatrix} U_p \\ V_p \\ W_p \end{Bmatrix}$; $\underline{r}_D = \begin{Bmatrix} u \\ v \\ w \end{Bmatrix}$; $\underline{r}_S = \begin{Bmatrix} 0 \\ \eta \\ \xi \end{Bmatrix}$, and the transformation matrices are defined as above. Thus the position vector of a point on the k^{th} blade before and after deformation is uniquely defined, and from which the energy expressions are obtained.

3.2.4 Effects of Coordinate Transformations on Blade Deformation

The blade deformation is described by a series of transformations and it is necessary to examine their implications. Let T denote the transformation between the systems $\underline{i},\underline{j},\underline{k}$ and $\underline{i}',\underline{j}',\underline{k}'$ before and after rotational deformations such that

$$\begin{Bmatrix} \underline{i}' \\ \underline{j}' \\ \underline{k}' \end{Bmatrix} = T^T \begin{Bmatrix} \underline{i} \\ \underline{j} \\ \underline{k} \end{Bmatrix} \quad \text{or} \quad \begin{Bmatrix} \underline{i} \\ \underline{j} \\ \underline{k} \end{Bmatrix} = T \begin{Bmatrix} \underline{i}' \\ \underline{j}' \\ \underline{k}' \end{Bmatrix} \tag{3.8}$$

The ordered Euler angles, $\zeta,-\beta,\bar{\vartheta}$, uniquely define the orientation of the local blade system $(\underline{i},\underline{j},\underline{k})$ and are shown in *Figure* 3.3 below;

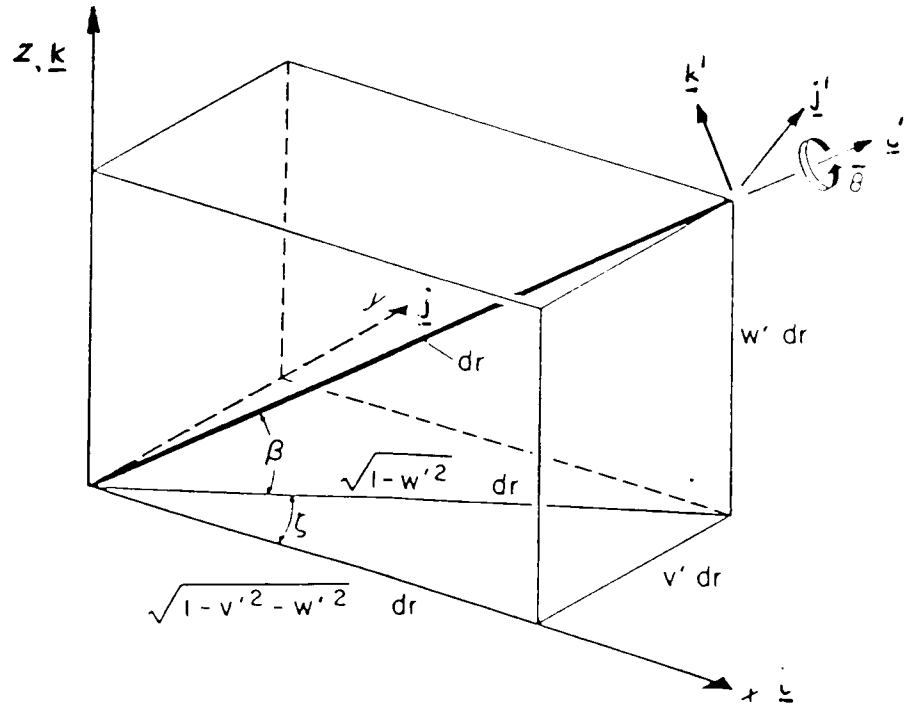

Figure 3.3: Blade Deformations and Euler Angles

T can be easily expressed in terms of these Euler angles as

$$T = T_{\zeta} T_{\beta} T_{\bar{\vartheta}} \tag{3.9}$$

$$= \begin{pmatrix} \cos\zeta & -\sin\zeta & 0 \\ \sin\zeta & \cos\zeta & 0 \\ 0 & 0 & 1 \end{pmatrix} \begin{pmatrix} \cos\beta & 0 & -\sin\beta \\ 0 & 1 & 0 \\ \sin\beta & 0 & \cos\beta \end{pmatrix} \begin{pmatrix} 1 & 0 & 0 \\ 0 & \cos\bar{\vartheta} & -\sin\bar{\vartheta} \\ 0 & \sin\bar{\vartheta} & \cos\bar{\vartheta} \end{pmatrix}$$

$$= \begin{pmatrix} \cos\zeta\cos\beta & -\sin\zeta & -\cos\zeta\sin\beta \\ \sin\zeta\cos\beta & \cos\zeta & -\sin\zeta\sin\beta \\ \sin\beta & 0 & \cos\beta \end{pmatrix} \begin{pmatrix} 1 & 0 & 0 \\ 0 & \cos\bar{\vartheta} & -\sin\bar{\vartheta} \\ 0 & \sin\bar{\vartheta} & \cos\bar{\vartheta} \end{pmatrix}$$

$$= \begin{pmatrix} \cos\zeta\cos\beta & -\sin\zeta\cos\bar{\vartheta}-\cos\zeta\sin\beta\sin\bar{\vartheta} & \sin\zeta\sin\bar{\vartheta}-\cos\zeta\sin\beta\cos\bar{\vartheta} \\ \sin\zeta\cos\beta & \cos\zeta\cos\bar{\vartheta}-\sin\zeta\sin\beta\sin\bar{\vartheta} & -\cos\zeta\sin\bar{\vartheta}-\sin\zeta\sin\beta\cos\bar{\vartheta} \\ \sin\beta & \cos\beta\sin\bar{\vartheta} & \cos\beta\cos\bar{\vartheta} \end{pmatrix}$$

The rotational sequence of the Eulerian angles, taken in the order ζ $-\beta,\bar{\vartheta}$, is arbitrary, other forms of transformations may also be used. Hodges *et al* [3.4] provided a detailed study on the effects using different orders of rotations. They concluded that the use of a different rotational sequence only results in a different definition of torsional variable, but the physics of the problem remains unaltered. It is the variables used to describe the position that are not unique.

Since rotor blade equations are normally written in terms of the bending and torsion deformations, it is convenient to express T in terms of the bending slopes, v',w'. From *Figure* 3.3, the following *exact* relationships are obtained;

$$\sin\beta=w',\ \cos\beta=\sqrt{1-w'^2},\ \sin\zeta=\frac{v'}{\sqrt{1-w'^2}},\ \cos\zeta=\frac{\sqrt{1-v'^2-w'^2}}{\sqrt{1-w'^2}} \qquad (3.10)$$

where $()'=\frac{\partial()}{\partial x}$, yielding T as

$$T = \begin{pmatrix} \sqrt{1-v'^2-w'^2} & \frac{-v'}{\sqrt{1-w'^2}} & \frac{-w'\sqrt{1-v'^2-w'^2}}{\sqrt{1-w'^2}} \\ v' & \frac{\sqrt{1-v'^2-w'^2}}{\sqrt{1-w'^2}} & \frac{-v'w'}{\sqrt{1-w'^2}} \\ w' & 0 & \sqrt{1-w'^2} \end{pmatrix} \begin{pmatrix} 1 & 0 & 0 \\ 0 & \cos\bar{\vartheta} & -\sin\bar{\vartheta} \\ 0 & \sin\bar{\vartheta} & \cos\bar{\vartheta} \end{pmatrix}$$

$$= \begin{bmatrix} & & \\ \sqrt{1-v'^2-w'^2} & \dfrac{-v'\cos\bar{\vartheta}-w'\sin\bar{\vartheta}\sqrt{1-v'^2-w'^2}}{\sqrt{1-w'^2}} & \dfrac{v'\sin\bar{\vartheta}-w'\cos\bar{\vartheta}\sqrt{1-v'^2-w'^2}}{\sqrt{1-w'^2}} \\ & & \\ v' & \dfrac{\cos\bar{\vartheta}\sqrt{1-v'^2-w'^2}-v'w'\sin\bar{\vartheta}}{\sqrt{1-w'^2}} & \dfrac{-\sin\bar{\vartheta}\sqrt{1-v'^2-w'^2}-v'w'\cos\bar{\vartheta}}{\sqrt{1-w'^2}} \\ & & \\ w' & \sin\bar{\vartheta}\sqrt{1-w'^2} & \cos\bar{\vartheta}\sqrt{1-w'^2} \end{bmatrix} \tag{3.11}$$

T is *exact* in *Eqn.*3.11. However, the determination of the third Euler angle, $\bar{\vartheta}$, requires either the formulation and solution of a differential equation for T by considering a small rotation $\underline{\omega}dr$ of the blade-fixed system as shown in [3.5], or more visibly, by considering the variation of $[T]^T[T] = I$ in stages as shown in *Appendix* A. Both approaches will result in an *exact* solution of the blade pitch angle $\bar{\vartheta}$

$$\bar{\vartheta} = \vartheta_p + \vartheta(\psi) + \phi - \int_0^r \left\{ \frac{v''w'}{\sqrt{1-v'^2-w'^2}} + \frac{w'^2w''v'}{(1-w'^2)\sqrt{1-v'^2-w'^2}} \right\} dr$$

$$= \underbrace{\vartheta_p + \vartheta(\psi) + \phi}_{\hat{\vartheta}} - \vartheta_b \tag{3.12}$$

where the built-in twist, ϑ_p, control pitch, $\vartheta(\psi)$, and elastic torsional deformation, ϕ, are taken to be zero inboard of the feathering bearing. It is clear that $\bar{\vartheta}$ is due not only to ϑ_p, $\vartheta(\psi)$ and ϕ alone, but second order contributions ϑ_b also arise. The latter is induced by pure lag and flap bending whilst the blade remains untwisted. This integral term, ϑ_b, is often referred to as "pseudo torsion" or "quasi-twist". To $O(\varepsilon^2)$,

$$\bar{\vartheta} = \hat{\vartheta} - \int_0^r v''w'dr + O(\varepsilon^3) \tag{3.13}$$

and hence T becomes:-

$$T = \begin{pmatrix} 1-\frac{(v'^2+w'^2)}{2} & -v'\cos\hat{\vartheta}-w'\sin\hat{\vartheta} & v'\sin\hat{\vartheta}-w'\cos\hat{\vartheta} \\ v' & (1-\frac{v'^2}{2})\cos\hat{\vartheta} & -(1-\frac{v'^2}{2})\sin\hat{\vartheta} \\ & +(\int v''w'dr-v'w')\sin\hat{\vartheta} & +(\int v''w'dr-v'w')\cos\hat{\vartheta} \\ w' & (1-\frac{w'^2}{2})\sin\hat{\vartheta} & (1-\frac{w'^2}{2})\cos\hat{\vartheta} \\ & -\cos\hat{\vartheta}\int v''w'dr & -\sin\hat{\vartheta}\int v''w'dr \end{pmatrix} + O(\varepsilon^3) \quad (3.14)$$

The transformation matrix T is orthogonal and is correct to $O(\varepsilon^2)$ but is by no means unique. Different $\bar{\vartheta}$, *eg.* [3.4,3.6 & 3.7], have also been derived by generating matrix orthogonality using different second order bending terms. It should only be regarded as the definition of the pitch parameter $\bar{\vartheta}$, which contains the built-in, applied, elastic and kinematic pitch components. The presence of ϑ_b has for some years cast doubt on the definition of angle of attack used in the aerodynamic loads calculation. Its implication will be discussed in *Section* 3.4.

3.2.5 An Ordering Scheme

In deriving the aeroelastic equations for the rotor blades, it is essential to retain non-linear terms. As a result, the algebraic equations can become extremely complex and contain a large number of terms. Over-complication in the equations can be avoided by neglecting the higher order product terms. This requires a scaling process to measure the magnitude of individual parameters, and hence their importance in a given context. The principle is that each parameter is assigned a relative magnitude based on physical reasonings and the assumptions made, then terms of higher order are systematically rejected. This provides an effective way for neglecting terms of least significance in a consistent manner, reducing the algebraic complexity, while retaining the essential features of the equations.

A scaling parameter ε is assigned a typical value of 0.1, the same order of magnitude as the (normalised) blade deformation v or w, such that $\varepsilon^2 \ll 1.0$ can be assumed. Non-linear terms, which have a magnitude of ε^3 *ie.* 0.1%, in the forced response and structural load equations, can be safely discarded. Essentially, the energy and virtual work expressions need only be derived to $O(\varepsilon^3)$ accuracy, where the generalised coordinate $q_i(t)$ is being assumed to be $O(\varepsilon)$, in line with the small perturbation theory.

For dynamical systems, the kinetic and strain energies are governed respectively by the inertial and structural properties which are then combined into one variational statement in accordance with the Hamilton's Principle. These properties are of different quantities and their relative magnitudes must first be considered.

To ensure that both energy expressions are derived to a consistent order, a non-dimensional parameter $\chi=\frac{m\Omega^2R^2}{EA}$ is used. χ was first introduced by Dowell & Hodges [3.5]. The physical significance of χ is that it relates the inertial and the structural properties via the blade tension, expressed as $T=m\Omega^2R^2=EAu'$ and is assigned to be $O(1)=O(\varepsilon^0)$. The fore-shortening term u is taken to be the order of the square of the bending slope v',w' *ie* $O(\varepsilon^2)$ and upon re-arranging, it is clear that $\chi=O(\varepsilon^2)$. Further discussion of the axial motion u will be given in *Section* 3.1.13.

The introduction of χ requires that the strain energy be derived to an order $O(\varepsilon^2)$ higher than the kinetic energy. However this can be dealt with more easily by choosing an ordering scheme which defines the magnitude of individual parameters, while the condition $\chi=O(\varepsilon^2)$ is maintained. The advantage of using a comparative ordering scheme is that for application to other blade structures, the magnitude of χ can be modified accordingly.

Depending upon the application, *eg.* for stability or vibration calculation, the emphasis can vary and a different ordering scheme can be used. Since the main concern here is on rotor load prediction, the magnitude for displacements and forces are defined relative to the rotor radius (R) and the axial tension (T), both of which are considered as O(1) quantities, consistent with χ. In addition, the radial coordinate x is of the order R *ie.* O(1) and the sectional coordinates η,ξ are of the same order as the blade chord (c) and thickness (t) *ie.* $O(\varepsilon)$. The relative magnitudes of the other variables are obtained on this basis. A list of the normalising factors is given in the *Table* 3.1 below;

Parameters	Normalising Factor
Linear Displacement	R
Linear Velocity	ΩR
Linear Acceleration	$\Omega^2 R$
Angular Displacement	1
Angular Velocity	Ω
Angular Acceleration	Ω^2
Blade Forces	$T(=m\Omega^2R^2)$
Blade Moments	TR

Table 3.1 - Normalising Factors used for The Blade and Hub Parameters

The appropriate magnitude of the ordered parameters are summarised in the following table;

Variables	Ordering
Blade	
$v, w, \phi, \zeta, \beta, v', w', \phi', \zeta', \beta', , \dot{v}, \dot{w}, \dot{\phi}, \dot{\zeta}, \dot{\beta}, \ddot{v}, \ddot{w}, \ddot{\phi}, \ddot{\zeta}, \ddot{\beta}$	ε
$u, \dot{u}, \ddot{u}, u'$	ε^2
Hub	
$x_H, y_H, z_H, \phi_H, \vartheta_H, \psi_H, \dot{x}_H, \dot{y}_H, \dot{z}_H, \dot{\phi}_H, \dot{\vartheta}_H, \dot{\psi}_H, \ddot{x}_H, \ddot{y}_H, \ddot{z}_H, \ddot{\phi}_H, \ddot{\vartheta}_H, \ddot{\psi}_H$	ε^2
Aircraft Motion	
μ_x	1
$\mu_y, \mu_z, p_H, q_H, r_H$	ε
$\dot{\mu}_x, \dot{\mu}_y, \dot{\mu}_z, \dot{p}_H, \dot{q}_H, \dot{r}_H$	ε^3
Pre-deformed Coordinates	
U_p	1
$V_p, W_p, \dot{V}_p, \dot{W}_p, \ddot{V}_p, \ddot{W}_p, \zeta_p(=V_p'), \beta_p(=W_p'), \dot{\zeta}_p, \dot{\beta}_p, \zeta_p', \beta_p'$	ε
Blade Loads	
V_x	1
V_y, V_z, M_y, M_z	ε
M_x	ε^2
Miscellaneous	
E, G	ε^{-4}
$m, \Omega, \vartheta, \dot{\vartheta}, \ddot{\vartheta}, T, R$	1
$\dot{\Omega}, \gamma_s, x_G, y_G, z_G, \eta, \xi$	ε
$\zeta - v', \beta - w', \zeta_p - V_p', \beta_p - W_p'$	ε^4

Table 3.2 - Ordering Scheme used for The Blade and Hub Parameters

The choice of this ordering scheme is based on physical considerations and the main assumptions invoked. The main implication of this ordering scheme is that, to $O(\varepsilon^3)$ there is no distinction between the section rotation angles and bending slopes *ie.* $\zeta=v'$, $\beta=w'$, $\zeta_p=V_p'$, $\beta_p=W_p'$,...*etc.* Although it is recognised that for advanced planform blades *eg.* Westland CMRB blade, large sweep and anhedral in the tip exist. Typical values are 30° sweep and 20° anhedral, with the extreme tip portion of sweep angle reaching 60°, shown in *Figure* 3.4 below;

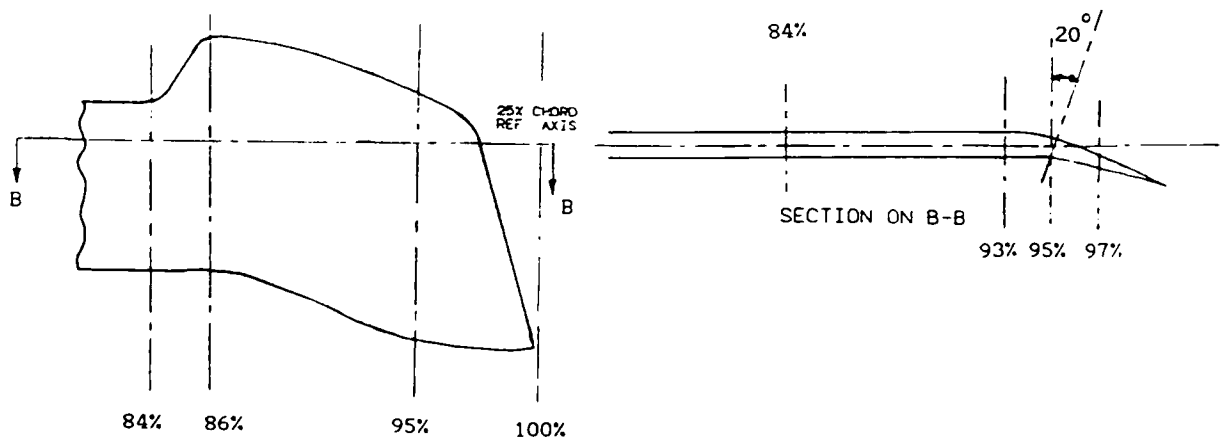

Figure 3.4: Example CMRB Blade Tip Sweep and Anhedral

While these angles are large, they exist only over small span in the tip region. For example, on the production CMRB main rotor blade, the 30° sweep is over 14%R and the 20° anhedral is over 5%R at the tip, and hence the pre-deformed coordinates are globally small. It is reasonable, and without loss of accuracy, to treat these quantities as $O(\varepsilon)$. Using this assumption, the initial problem of having to derive the energy expressions of enormous size, when they were assumed to be O(1) quantities, was avoided.

3.2.6 Velocity Vector of The Blade Point

The kinetic energy of a single blade is given by

$$K = \int_0^R \frac{1}{2} \iint_{\eta\xi} \rho \, \underline{\dot{R}} \cdot \underline{\dot{R}} \, d\eta \, d\xi \, dr \qquad (3.15)$$

where ρ is the blade density and $\underline{\dot{R}}$ is the vector of absolute velocities of the blade point. The velocities at the hub are obtained by transforming the body velocities. Consider the following schematic diagram *Figure* 3.5

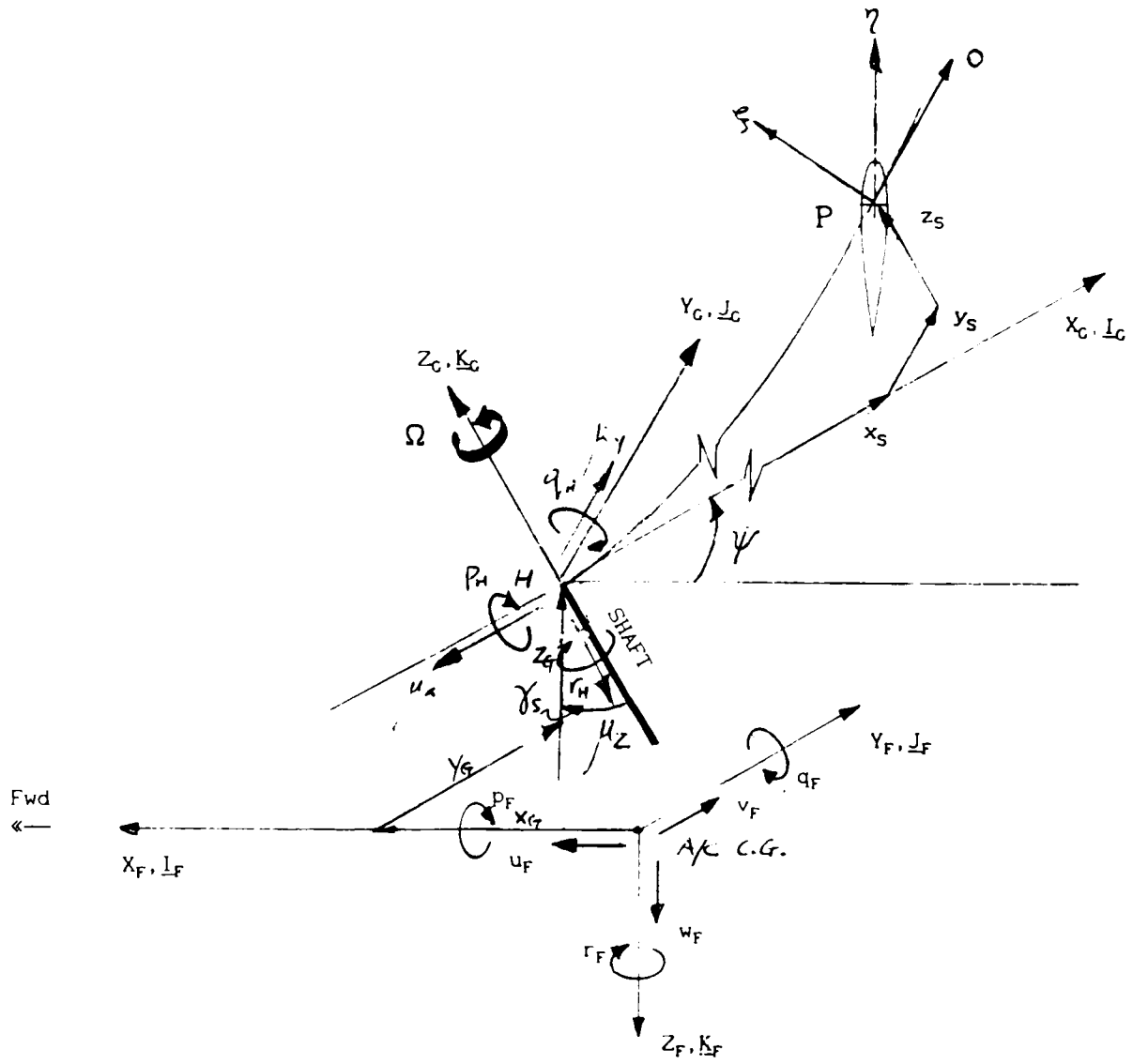

Figure 3.5: Aircraft Motion Kinematics

The vectors of linear and rotational velocities at the hub are related to the velocities at the aircraft c.g. as

$$\begin{Bmatrix}\mu_x\\ \mu_y\\ \mu_z\end{Bmatrix} = \begin{bmatrix}\cos\gamma_s & 0 & \sin\gamma_s\\ 0 & 1 & 0\\ -\sin\gamma_s & 0 & \cos\gamma_s\end{bmatrix} \cdot \begin{Bmatrix}u_F - z_G q_F - y_G r_F\\ v_F + z_G p_F + x_G r_F\\ w_F + y_G p_F - x_G q_F\end{Bmatrix} \qquad (3.16)$$

and

$$\begin{Bmatrix}p_H\\ q_H\\ r_H\end{Bmatrix} = \begin{bmatrix}\cos\gamma_s & 0 & \sin\gamma_s\\ 0 & 1 & 0\\ -\sin\gamma_s & 0 & \cos\gamma_s\end{bmatrix} \cdot \begin{Bmatrix}p_F\\ q_F\\ r_F\end{Bmatrix} \qquad (3.17)$$

where μ_x, μ_y, μ_z are the aircraft velocities with μ_x being the advance ratio and p_H, q_H, r_H are the aircraft rates. x_G, y_G, z_G are the hub offsets from the aircraft c.g. All the quantities are normalised appropriately.

In the shaft axis system,

$$\underline{U}_H = \begin{Bmatrix}u_S\\ v_S\\ w_S\end{Bmatrix} = \begin{Bmatrix}-\mu_x\\ \mu_y\\ -\mu_z\end{Bmatrix} \quad \text{and} \quad \underline{R}_H = \begin{Bmatrix}p_S\\ q_S\\ r_S\end{Bmatrix} = \begin{Bmatrix}-p_H\\ q_H\\ -r_H\end{Bmatrix}$$

The absolute velocity of the blade point is then given by

$$\dot{\underline{R}} = \dot{\underline{R}}_S + \underline{U}_H + \omega_H \cdot \underline{R}_S \tag{3.18}$$

where $\omega_H = \begin{pmatrix} 0 & -r_S & q_S \\ r_S & 0 & -p_S \\ -q_S & p_S & 0 \end{pmatrix} = \begin{pmatrix} 0 & r_H & q_H \\ -r_H & 0 & p_H \\ -q_H & -p_H & 0 \end{pmatrix}$ is the skew-symmetric matrix of hub angular velocities and $\underline{R}_S$ is the vector position of a blade point, defined in *Eqn*.3.7.

3.2.7 Kinetic Energy Consideration

The manner in which the kinetic energy of the blade is to be formulated is such that only the strain energy contribution to the total potential energy needs to be considered. The potential energy due to centrifugal stiffening effects, is implicit in the kinetic energy formulation.

The blade kinetic energy K can be written in the integral form as;

$$\begin{aligned} K &= \int_0^R \frac{1}{2} \iint_{\eta\xi} \rho \, \dot{\underline{R}} \cdot \dot{\underline{R}} \, d\eta \, d\xi \\ &= \int_0^R \frac{1}{2} \iint_{\eta\xi} \rho \, (\dot{\underline{R}}_s^T + \underline{U}_H^T - \underline{R}_s^T \cdot \omega_H)(\dot{\underline{R}}_s + \underline{U}_H + \omega_H \cdot \underline{R}_s) \, d\eta \, d\xi \, dr \\ &= \int_0^R g(u, v, w, \phi, \zeta, \beta, \dot{u}, \dot{v}, \dot{w}, \dot{\phi}, \dot{\zeta}, \dot{\beta}, \\ &\qquad x_H, y_H, z_H, \phi_H, \vartheta_H, \psi_H, \dot{x}_H, \dot{y}_H, \dot{z}_H, \dot{\phi}_H, \dot{\vartheta}_H, \dot{\psi}_H, \\ &\qquad \mu_x, \mu_y, \mu_z, p_H, q_H, r_H, r, V_p, W_p, \zeta_p, \beta_p, \dot{V}_p, \dot{W}_p, \dot{\zeta}_p, \dot{\beta}_p, \vartheta, \dot{\vartheta}, \Omega, t) \, dr \end{aligned} \tag{3.19}$$

where g is the kinetic energy function.

The explicit derivation of the kinetic energy to $O(\varepsilon^3)$ accuracy is not entirely straightforward even with the use of REDUCE. It can be made simpler by deriving the terms $\frac{d}{dt}\left\{ \frac{\partial K}{\partial \dot{q}_i} \right\} - \frac{\partial K}{\partial q_i}$ in the Lagrangian equation directly using the differential operators defined as

$$\frac{\partial}{\partial \dot{q}_i} = \sum_x \frac{\partial}{\partial \dot{x}} \frac{\partial \dot{x}}{\partial \dot{q}_i} \tag{3.20a}$$

$$\frac{\partial}{\partial q_i} = \sum_x \frac{\partial}{\partial x} \frac{\partial x}{\partial q_i} \tag{3.20b}$$

where x denotes u, v, w, ϕ, β or ζ, and from *Eqn* 3.1,

$$\frac{\partial x}{\partial q_i} = \frac{\partial \dot{x}}{\partial \dot{q}_i} = x_i(r) \tag{3.21}$$

The section inertial constants are defined in the blade principal axis system with the origin at the shear centre, coincidental with the quarter chord, as

$$m = \iint_{\eta\xi} \rho d\eta d\xi; \qquad me_1 = \iint_{\eta\xi} \rho\xi d\eta d\xi; \qquad me_2 = \iint_{\eta\xi} \rho\eta d\eta d\xi;$$

$$mk_1^2 = \iint_{\eta\xi} \rho\xi^2 d\eta d\xi; \quad mk_2^2 = \iint_{\eta\xi} \rho\eta^2 d\eta d\xi. \quad mk_{12} = \iint_{\eta\xi} \rho\eta\xi d\eta d\xi; \tag{3.22}$$

where ρ is the blade density and m is the mass per unit length at the blade section, e_1, e_2 are the c.g. offsets from the elastic axis and km_1, km_2 are the radii of gyration about the two principal axes.

3.2.8 Strain Energy Consideration

The strain energy is obtained by considering the blade deformation. Let $\underline{r}_1$ and $\underline{r}_0$ denote the position vectors of the same point P in the deformed and undeformed state respectively in the H'XYZ, then,

$$\underline{r}_1 = \begin{Bmatrix} U_p \\ V_p \\ W_p \end{Bmatrix} + \underbrace{T_{\zeta_p} T_{\beta_p}} \left\{ \begin{Bmatrix} u \\ v \\ w \end{Bmatrix} + \underbrace{T_\zeta T_\beta} T_{\bar{\vartheta}} \begin{Bmatrix} 0 \\ \eta \\ \xi \end{Bmatrix} \right\}$$

$$= \underline{r}_P + P \left\{ \underline{r}_D + T_1 \, T_{\bar{\vartheta}} \, \underline{r}_S \right\} \tag{3.23}$$

where $P = T_{\zeta_P} T_{\beta_P}$; $T_1 = T_\zeta T_\beta$; and

$$\underline{r}_0 = \underline{r}_1 \big|_{u=v=w=\phi=\beta=\zeta=0}$$

$$= \begin{Bmatrix} U_p \\ V_p \\ W_p \end{Bmatrix} + \underbrace{T_{\zeta_p} T_{\beta_p}} T_\vartheta \begin{Bmatrix} 0 \\ \eta_0 \\ \xi_0 \end{Bmatrix}$$

$$= \underline{r}_P + P \; T_\vartheta \; \underline{r}_{S_0} \tag{3.24}$$

where $\eta_0 = \eta \big|_{u=v=w=\phi=\beta=\zeta=0}$; $\xi_0 = \xi \big|_{u=v=w=\phi=\beta=\zeta=0}$

The classical strain tensor components ε_{ij} (i,j=1,2,3) can be written in terms of the differentials of $\underline{r}_1$ and $\underline{r}_0$ as

$$\underline{dr}_1 \cdot \underline{dr}_1 - \underline{dr}_0 \cdot \underline{dr}_0 = 2\{dr \; d\eta \; d\xi\} \begin{bmatrix} \varepsilon_{11} & \varepsilon_{12} & \varepsilon_{13} \\ & \varepsilon_{22} & \varepsilon_{23} \\ \text{Sym.} & & \varepsilon_{33} \end{bmatrix} \begin{Bmatrix} dr \\ d\eta \\ d\xi \end{Bmatrix} \tag{3.25}$$

where $dr, d\eta, d\xi$ are the increments along the deformed elastic axis, and the two cross-sectional axes respectively. The differentials $\underline{dr}_1$ and $\underline{dr}_0$ are obtained by differentiating $\underline{r}_1$ and $\underline{r}_0$ with respect to r, η, ξ as

$$\underline{dr}_1 = \frac{\partial \underline{r}_1}{\partial x}\frac{\partial x}{\partial r}\,dr + \frac{\partial \underline{r}_1}{\partial \eta}\,d\eta + \frac{\partial \underline{r}_1}{\partial \xi}\,d\xi \qquad (3.26a)$$

$$\underline{dr}_0 = \frac{\partial \underline{r}_0}{\partial x}\frac{\partial x}{\partial r}\,dr + \frac{\partial \underline{r}_0}{\partial \eta_0}\frac{\partial \eta_0}{\partial \eta}\,d\eta + \frac{\partial \underline{r}_0}{\partial \xi_0}\frac{\partial \xi_0}{\partial \xi}\,d\xi \qquad (3.26b)$$

The assumption of zero warping implies that

$$\frac{\partial \eta_0}{\partial \eta} = \frac{\partial \xi_0}{\partial \xi} = 1 \quad \Rightarrow \quad \frac{\partial}{\partial \eta_0} \equiv \frac{\partial}{\partial \eta} \text{ and } \frac{\partial}{\partial \xi_0} \equiv \frac{\partial}{\partial \xi} \qquad (3.27)$$

ie. to $O(\varepsilon^2)$, η, ξ are equivalent to η_0, ξ_0 and $\frac{\partial}{\partial r} \cong \frac{\partial}{\partial x} = ()'$ such that $\frac{\partial x}{\partial r} = 1$.

Hence, the differentials $\underline{dr}_1$ and $\underline{dr}_0$ become;

$$\underline{dr}_1 = \left\{ \underline{r}_P' + P'\underline{r}_D + P\underline{r}_D' + (P'T_1T_{\bar{\vartheta}} + PT_1'T_{\bar{\vartheta}} + PT_1T_{\bar{\vartheta}}')\underline{r}_S \right\} dr + PT_1T_{\bar{\vartheta}} \begin{Bmatrix} 0 \\ d\eta \\ d\xi \end{Bmatrix}$$

$$\underline{dr}_0 = \left\{ \underline{r}_P' + (P'T_{\vartheta} + PT_{\vartheta}')\,\underline{r}_S \right\} dr + PT_{\vartheta} \begin{Bmatrix} 0 \\ d\eta \\ d\xi \end{Bmatrix}$$

For ease of evaluation, they are written in component forms as

$$\underline{dr}_1 = \begin{bmatrix} p_{11} & p_{12} & p_{13} \\ p_{21} & p_{22} & p_{23} \\ p_{31} & p_{32} & p_{33} \end{bmatrix} \cdot \begin{Bmatrix} dr \\ d\eta \\ d\xi \end{Bmatrix} \qquad (3.28a)$$

$$\underline{dr}_0 = \begin{bmatrix} q_{11} & q_{12} & q_{13} \\ q_{21} & q_{22} & q_{23} \\ q_{31} & q_{32} & q_{33} \end{bmatrix} \cdot \begin{Bmatrix} dr \\ d\eta \\ d\xi \end{Bmatrix} \qquad (3.28b)$$

such that the strain tensor components ε_{ij} $(i,j=1,2,3)$ are expressed as

$$\varepsilon_{ij} = \frac{1}{2}\sum_{k=1}^{3} (p_{ki}p_{kj} - q_{ki}q_{kj}) \qquad i,j=1,2,3 \qquad (3.29)$$

Although the shear strain ε_{23} is usually non-zero, its magnitude is two orders smaller than those of ε_{12} & ε_{13}, and can therefore be neglected [3.5]. Also the assumption of uniaxial stress for a slender beam *ie.* $\sigma_{\eta\eta}=\sigma_{\xi\xi}=\sigma_{\eta\xi}=0$, implies that it is only necessary to evaluate the 3 strain components, $\varepsilon_{11}, \varepsilon_{12}, \varepsilon_{13}$. From REDUCE and to $O(\varepsilon^3)$ accuracy with $\zeta_p=V_p'$, $\beta_p=W_p'$, ..*etc*, they are,

CRFA Strain Tensor Components

$$
\begin{aligned}
\varepsilon_{11} &= (\eta^2+\xi^2)\vartheta'\phi' + u' + \frac{v'^2}{2} + \frac{w'^2}{2} - vV_p'' - wW_p'' + u(v'V_p'' + w'W_p'') \\
&+ 2\eta\vartheta'\left\{ \phi(\zeta-v')\cos\vartheta + \phi(\beta-w')\sin\vartheta - u(V_p''\sin\vartheta - W_p''\cos\vartheta) + (\zeta-v')\sin\vartheta - (\beta-w')\cos\vartheta \right\} \\
&+ 2\xi\vartheta'\left\{ -\phi(\zeta-v')\sin\vartheta + \phi(\beta-w')\sin\vartheta - u(V_p''\cos\vartheta - W_p''\sin\vartheta) + (\zeta-v')\cos\vartheta + (\beta-w')\sin\vartheta \right\} \\
&+ 2\eta\left\{ \phi'(\zeta-v')\sin\vartheta - \phi'(\beta-w')\cos\vartheta - \zeta'(\cos\vartheta-\phi\sin\vartheta) - \beta'(\sin\vartheta+\phi\cos\vartheta) + \phi V_p''\sin\vartheta - \phi W_p''\cos\vartheta \right\} \\
&+ 2\xi\left\{ \phi'(\zeta-v')\cos\vartheta + \phi'(\beta-w')\sin\vartheta + \zeta'(\sin\vartheta+\phi\cos\vartheta) - \beta'(\cos\vartheta-\phi\sin\vartheta) + \phi V_p''\cos\vartheta + \phi W_p''\sin\vartheta \right\} + O(\varepsilon^4)
\end{aligned}
$$

$$
\begin{aligned}
\varepsilon_{12} &= \frac{1}{2}\left\{ \xi(-\phi' - \beta\zeta' + \zeta W_p'' - \beta V_p'') \right. \\
&+ \frac{1}{2}\phi^2(\zeta-v')\cos\vartheta + \frac{1}{2}\phi^2(\beta-w')\sin\vartheta - \phi u(V_p''\sin\vartheta - W_p''\cos\vartheta) + u(V_p''\cos\vartheta + W_p''\sin\vartheta) \\
&+ \phi(\zeta-v')\sin\vartheta - \phi(\beta-w')\cos\vartheta + \zeta(vV_p'' + wW_p'')\cos\vartheta + \beta(vV_p'' + wW_p'')\sin\vartheta \\
&- W_p'(wV_p''\cos\vartheta - vV_p''\sin\vartheta) - u'(v'\cos\vartheta + w'\sin\vartheta) \\
&+ \zeta^2(\zeta-v')\cos\vartheta + \beta^2(\beta-w')\sin\vartheta + \beta\zeta(\zeta-v')\sin\vartheta + \frac{1}{2}\beta^2(\zeta-v')\cos\vartheta - \frac{1}{2}w'\zeta^2\sin\vartheta \\
&\left. - \frac{1}{3}\zeta^3\cos\vartheta - \frac{1}{3}\beta^3\sin\vartheta - (\zeta-v')\cos\vartheta - (\beta-w')\sin\vartheta \right\} + O(\varepsilon^4)
\end{aligned}
$$

$$
\begin{aligned}
\varepsilon_{13} &= \frac{1}{2}\left\{ \eta(\phi' + \beta\zeta' - \zeta W_p'' + \beta V_p'') \right. \\
&- \frac{1}{2}\phi^2(\zeta-v')\sin\vartheta + \frac{1}{2}\phi^2(\beta-w')\cos\vartheta - \phi u(V_p''\cos\vartheta + W_p''\sin\vartheta) - u(V_p''\sin\vartheta - W_p''\cos\vartheta) \\
&+ \phi(\zeta-v')\cos\vartheta + \phi(\beta-w')\sin\vartheta - \zeta(vV_p'' + wW_p'')\sin\vartheta + \beta(vV_p'' + wW_p'')\cos\vartheta \\
&+ W_p'(wV_p''\sin\vartheta - vV_p''\cos\vartheta) + u'(v'\sin\vartheta - w'\cos\vartheta) \\
&- \zeta^2(\zeta-v')\sin\vartheta - \beta^2(\beta-w')\cos\vartheta + \beta\zeta(\zeta-v')\cos\vartheta - \frac{1}{2}\beta^2(\zeta-v')\sin\vartheta - \frac{1}{2}w'\zeta^2\cos\vartheta \\
&\left. + \frac{1}{3}\zeta^3\sin\vartheta - \frac{1}{3}\beta^3\cos\vartheta + (\zeta-v')\sin\vartheta - (\beta-w')\cos\vartheta \right\} + O(\varepsilon^4)
\end{aligned}
\tag{3.30}
$$

It should be noted here that many of the terms in *Eqns.*3.30 will disappear if the zero shear flexibility is assumed. They are retained here in order that a check with the dynamic analysis can be made. Then by applying Hooke's Law, the stress tensor components σ_{ij} can be written in terms of the Eulerian strain tensors ε_{ij} $(i,j=r,\eta,\xi)$ as

$$
\begin{aligned}
\sigma_{rr} &= E\ \varepsilon_{rr} \\
\sigma_{r\eta} &= G\ \varepsilon_{r\eta} \\
\sigma_{r\xi} &= G\ \varepsilon_{r\xi}
\end{aligned}
\tag{3.31}
$$

where E and G are the Young's and shear modulus of the cross-section. The Eulerian strain tensors are related to the classical strain tensors [3.8] via

$$
\begin{aligned}
\varepsilon_{rr} &= \varepsilon_{11} \\
\varepsilon_{r\eta} &= 2\varepsilon_{12} \\
\varepsilon_{r\xi} &= 2\varepsilon_{13}
\end{aligned}
\tag{3.32}
$$

The blade strain energy U can be written in the integral form as;

$$
\begin{aligned}
U &= \int_0^R \frac{1}{2} \iint_{\eta\xi} \left\{ \sigma_{rr}\varepsilon_{rr} + \sigma_{r\eta}\varepsilon_{r\eta} + \sigma_{r\xi}\varepsilon_{r\xi} \right\} d\eta\ d\xi\ dr \\
&= \int_0^R \frac{1}{2} \iint_{\eta\xi} \left\{ E\varepsilon_{11}^2 + 4G(\varepsilon_{12}^2 + \varepsilon_{13}^2) \right\} d\eta\ d\xi\ dr
\end{aligned}
$$

$$= \int_0^R f(u,v,w,\phi,\zeta,\beta,u',v',w',\phi',\zeta',\beta',U_p,V_p,W_p,\zeta_p,\beta_p,\zeta_p',\beta_p')\ dr$$

(3.33)

where f is the strain energy function. Similarly, the formulation can be made simpler by deriving $\frac{\partial U}{\partial q_i}$ using

$$\frac{\partial U}{\partial q_i} = \int_0^R \iint_{\eta\xi} \left\{ E\varepsilon_{11}\frac{\partial \varepsilon_{11}}{\partial q_i} + 4G(\varepsilon_{12}\frac{\partial \varepsilon_{12}}{\partial q_i} + \varepsilon_{13}\frac{\partial \varepsilon_{13}}{\partial q_i}) \right\} d\eta\ d\xi\ dr \qquad (3.34)$$

where the differential operator is defined as

$$\frac{\partial}{\partial q_i} = \sum_x \frac{\partial x}{\partial q_i}\frac{\partial}{\partial x} = \sum_x x_i \frac{\partial}{\partial x} \qquad (3.35)$$

with $x = u,v,w,\phi,\beta,\zeta,u',v',w',\phi',\beta',\zeta'$. The section elastic constants are defined in the blade principal axis system as

$$EA = \iint_{\eta\xi} E d\eta d\xi; \qquad EB_1 = \iint_{\eta\xi} E\xi d\eta d\xi; \qquad EB_2 = \iint_{\eta\xi} E\eta d\eta d\xi;$$

$$EI_{11} = \iint_{\eta\xi} E\xi^2 d\eta d\xi; \quad EI_{22} = \iint_{\eta\xi} E\eta^2 d\eta d\xi; \quad EI_{12} = \iint_{\eta\xi} E\eta\xi d\eta d\xi;$$

$$GA = \iint_{\eta\xi} G d\eta d\xi; \qquad GB_1 = \iint_{\eta\xi} G\xi d\eta d\xi; \qquad GB_2 = \iint_{\eta\xi} G\eta d\eta d\xi; \quad GJ = \iint_{\eta\xi} G(\eta^2+\xi^2) d\eta d\xi$$

(3.36)

3.2.9 Virtual Work and Generalised Force

The blade generalised force Q_i is obtained by first determining the virtual work δW due to all external applied (non-conservative) forces *ie.* aerodynamics only. Consider the blade element, which is acted upon by the distributed aerodynamic lift, drag and moment, defined in the deformed axis system $\frac{dM}{dr}\underline{i}' - \frac{dD}{dr}\underline{j}' + \frac{dL}{dr}\underline{k}'$ as shown in *Figure* 3.6 below,

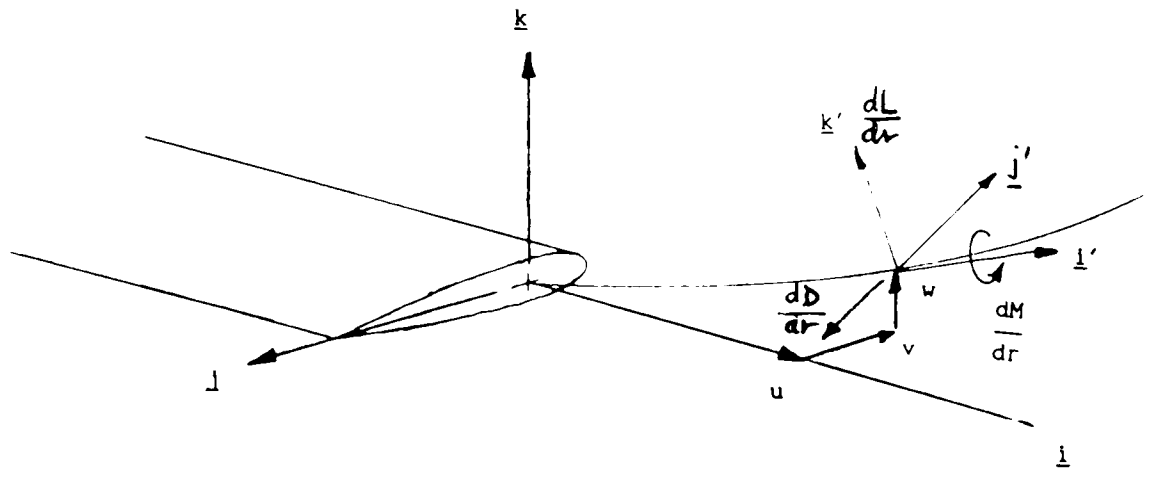

Figure 3.6: Aerodynamic Loadings on An Aerofoil Section

To obtain the virtual work, we first need to define the aerodynamic load components in the undeformed axis system, which is

$$\begin{Bmatrix} L_i \\ L_j \\ L_k \end{Bmatrix} = T \begin{Bmatrix} 0 \\ -\frac{dD}{dr} \\ \frac{dL}{dr} \end{Bmatrix} = \begin{bmatrix} \cos\zeta\cos\beta & -\sin\zeta & -\cos\zeta\sin\beta \\ \sin\zeta\cos\beta & \cos\zeta & -\sin\zeta\sin\beta \\ \sin\beta & 0 & \cos\beta \end{bmatrix} \begin{Bmatrix} 0 \\ -\frac{dD}{dr} \\ \frac{dL}{dr} \end{Bmatrix} = \begin{bmatrix} 1 & -v' & -w' \\ v' & 1 & 0 \\ w' & 0 & 1 \end{bmatrix} \begin{Bmatrix} 0 \\ -\frac{dD}{dr} \\ \frac{dL}{dr} \end{Bmatrix} + O(\varepsilon^3)$$

where T is for the bent blade (*Eqn.*3.11). Using the small angle assumption and assume $\frac{dL}{dr}, \frac{dD}{dr}$ are $O(\varepsilon)$ quantities, then to $O(\varepsilon^2)$ accuracy,

$$L_i = \frac{dD}{dr}v' - \frac{dL}{dr}w' + O(\varepsilon^3); \quad L_j = -\frac{dD}{dr} + O(\varepsilon^3); \quad L_k = \frac{dL}{dr} + O(\varepsilon^3)$$

Hence the virtual work due to aerodynamic loadings is

$$\delta W_{AERO} = \int_0^R \left\{ \left[\left(\frac{dD}{dr}v' - \frac{dL}{dr}w'\right)\underline{i} - \frac{dD}{dr}\underline{j} + \frac{dL}{dr}\underline{k} \right] \cdot \left[\delta u\underline{i} + \delta v\underline{j} + \delta w\underline{k}\right] + \frac{dM}{dr}\underline{i}' \cdot \delta\psi_i \underline{i}' \right\} dr + O(\varepsilon^4)$$

Since $\delta u = O(\varepsilon^2)$, then

$$\delta W_{AERO} = \int_0^R \left\{ -\frac{dD}{dr}\cdot\delta v + \frac{dL}{dr}\cdot\delta w + \frac{dM}{dr}\cdot\delta\psi_i \right\} dr + O(\varepsilon^4)$$

Consider the virtual rotation $\delta\psi_1$, which from *Appendix* A, is given by

$$\delta\psi_1 = \delta\vartheta + \delta\zeta\sin\beta$$
$$= \delta\vartheta + w'\delta v' + O(\varepsilon^3)$$

and $\vartheta = \vartheta_p + \phi - \int w'v''dr + O(\varepsilon^3)$

$$\therefore \delta\psi_1 = \delta\phi - \int \left[\delta w'v'' + \underline{w'\delta v''}\right]dr + w'\delta v' + O(\varepsilon^3)$$

Integrate the underlined term by parts,

$$= \delta\phi - w'\delta v' + \int \left[w''\delta v' - \delta w'v''\right]dr + w'\delta v' + O(\varepsilon^3)$$
$$= \delta\phi + \int \left[w''\delta v' - \delta w'v''\right]dr + O(\varepsilon^3)$$

Since the aerodynamic pitching moment is $O(\varepsilon^2)$, δW_{AERO} reduces to

$$\delta W_{AERO} = \int_0^R \left\{ -\frac{dD}{dr}\cdot\delta v + \frac{dL}{dr}\cdot\delta w + \frac{dM}{dr}\cdot\delta\phi \right\} dr + O(\varepsilon^4) \qquad (3.37)$$

The exercise above is used to illustrate the more thorough treatment of the pseudo-torsion and axial motion terms, should they not be neglected because of the ordering imposed on the pitching moment and axial displacement. The assumption made here is valid for most rotor applications. It should be noted that the simple appearance of this integral of aerodynamic terms (*Eqn.*3.37) is deceptive. The determination of blade section aerodynamic coefficients will be addressed in *Section* 3.3.

3.2.10 Modelling of Control Circuit System Stiffness

The control circuit system stiffness is modelled as a set of springs as shown in *Figure* 3.7 below,

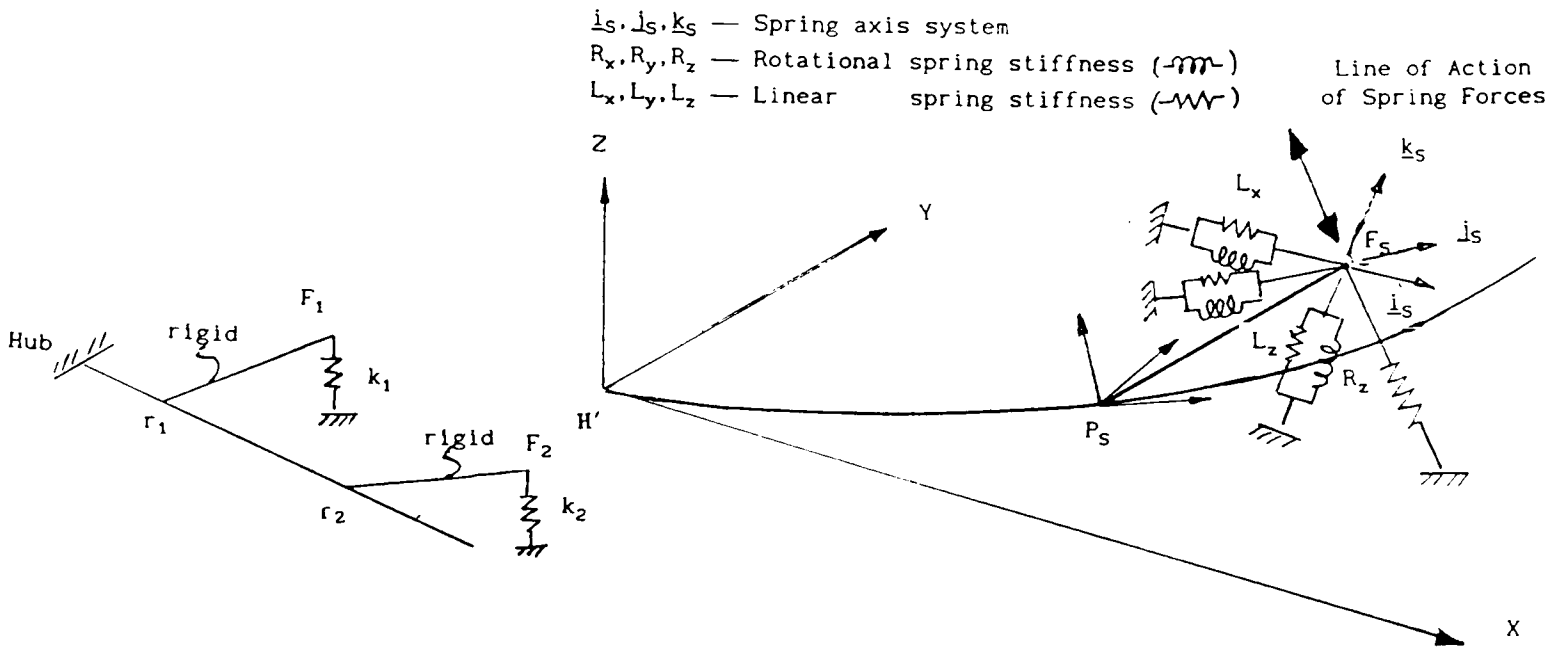

Figure 3.7: Modelling of Control Circuit System Stiffness

These spring forces and moments give rise to an additional strain energy U_s, which is included in the formulation of Lagrangian equation. U_s is obtained by considering the linear and rotational deformations of N_s such spring sets (*Appendix* B) and is given by

$$U_s = \frac{1}{2}\int_0^R \sum_{s=1}^{N_s} \delta(r_s)\Big\{\{u-\zeta l_v-\beta l_w, v+\zeta l_u-\phi l_w, w+\beta l_u-\phi l_w\}\ [L]\ \begin{Bmatrix} u-\zeta l_v-\phi l_w \\ v+\zeta l_u-\phi l_w \\ w+\beta l_u+\phi l_v \end{Bmatrix}$$

$$\{\phi+\beta\zeta, -\beta+\phi\zeta, \zeta+\phi\beta\}\ [R]\ \begin{Bmatrix} \phi & +\beta\zeta \\ -\beta & +\phi\zeta \\ \zeta & +\phi\beta \end{Bmatrix}\Big\}\ dr + O(\varepsilon^4) \qquad (3.38)$$

where $\begin{Bmatrix} l_u \\ l_v \\ l_w \end{Bmatrix} = \begin{Bmatrix} l_{r_s} \\ l_{\eta_s}\cos\vartheta - l_{\zeta_s}\sin\vartheta \\ l_{\eta_s}\sin\vartheta + l_{\zeta_s}\cos\vartheta \end{Bmatrix}$ are the coordinates of the rigid rod attachment F_s in the local deformed axis system, origin at r_s, $(l_{r_s}, l_{\eta_s}, l_{\zeta_s})$ is the position vector of F_s before deformation and

$[L] = P^T S \cdot \mathrm{Diag}(L_x, L_y, L_z) \cdot S^T P$; $[R] = P^T S \cdot \mathrm{Diag}(R_x, R_y, R_z) \cdot S^T P$;

where $P = T_{\zeta_P} T_{\beta_P}$, S is the transformation matrix between the spring and blade axis systems. L_x, L_y, L_z and R_x, R_y, R_z are the linear and rotational spring rates representing the control circuit and are defined in *Appendix* B. The variation of U_s is

$$\frac{\partial U_s}{\partial q_1} = \sum_x \frac{\partial U_s}{\partial x}\frac{\partial x}{\partial q_1} \qquad (3.39)$$

3.2.11 Modelling of Lag Damper

The lag damper is modelled as an external load path attached to the main blade via massless rigid rods. It generates discrete loads at the damper attachment points and is included in the Lagrangian equation as discrete forcings. For the EH101 aircraft, the inner arm of the lag damper is assumed to be earthed at the hub and for the Lynx aircraft, the damper is parallel to blade with both inboard and outboard attachment points. The EH101 lag damper geometry is shown in *Figure* 3.8 below,

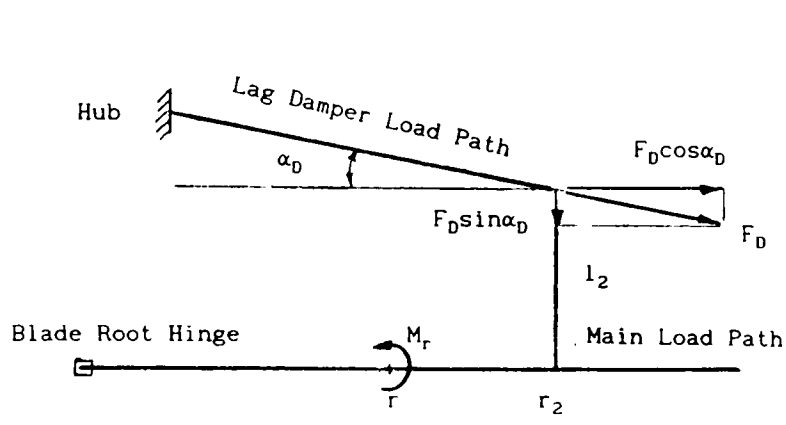

Lag Damper Geometry

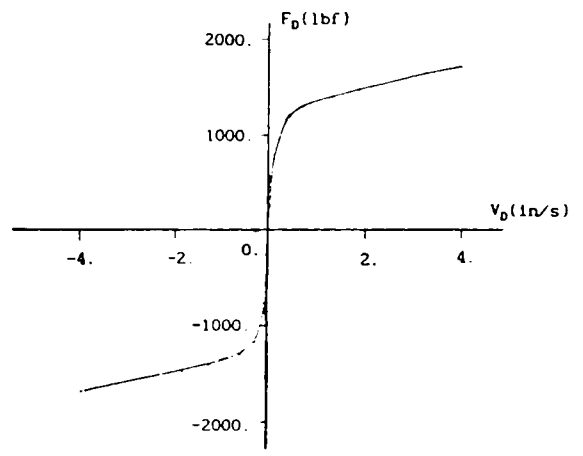

Lag Damper Characteristics.(Typical)

Figure 3.8: EH101 Lag Damper Geometry and Characteristics (Typical)

The non-linear damper characteristics, input in a table of force *vs* velocity, are shown typically above. The damper velocity is first determined from the modal contribution as;

$$v_D = -l_2\dot{v}'_2\cos\alpha_D - \dot{v}_2\sin\alpha_D \text{ at } r_2 \qquad (3.40)$$

where $\dot{v}'_2=\Omega\sum_i \dot{q}_i v'_i$, $\dot{v}_2=\Omega\sum_i \dot{q}_i v_i$ and the damper force F_D is interpolated from the damper characteristics. The discrete lag damper modal forcing at r_2 is obtained from

$$MF_{LD_i} = -F_D\sin\alpha_D v_i - F_D\cos\alpha_D l_2 v'_{2_i} \quad \text{for the } i^{th} \text{ mode} \qquad (3.41)$$

The discrete lag damper moment at position r is determined from

$$M_r = \begin{cases} 0 \\ -F_D[l_2\cos\alpha_D+(r_2-r)\sin\alpha_D] \\ -F_D[l_2\cos\alpha_D+(r_2-r)\sin\alpha_D]+F_D[l_1\cos\alpha_D+(r_1-r)\sin\alpha_D] \end{cases} \text{ if } \begin{cases} r_2 < r \\ r_1 < r \le r_2 \\ r \le r_1 \end{cases} \qquad (3.42)$$

3.2.12 Modelling of Structural Damping

Energy is dissipated in all dynamical system through internal friction or hysteresis of elastic material, so some form of structural damping representation is required. However, a mathematical description of structural damping that is both general and accurate does not yet exist. Through experimental studies, structural damping has been found to be both small and a function of a wide range of parameters.

By far the most practical approach for modelling structural damping has been to represent it either by a form of equivalent viscous damping or by a complex form of stiffness. In the latter form, the imaginary part of the stiffness is proportional to the energy dissipative structural damping. However the general observation is that the energy loss per cycle of oscillation is relatively invariant with respect to frequency, but the complex stiffness form pre-supposes that the motion of the structure is that of sustained simple harmonic motion. It is for this reason that we choose the equivalent viscous damping model as structural damping. The damping in each of the modes is proportional to the magnitude of the displacement and in-phase with the velocity. The modal response equation thus appears in the form;

$$\ddot{q}_i + 2\nu_i\lambda_i\dot{q}_i + \lambda_i^2 q_i = f_i$$

where ν_i is the equivalent viscous damping in %critical, which can be obtained using various experimental means.

3.2.13 Axial Mode Representation

In the derivation of the modal Lagrangian equation, the axial motion is included as an independent degree of freedom. However, unlike the blade lag and flap bending deformations, further consideration on the axial deformation is required.

Within the frequency range of interest, up to 12R (1R≡once per rev.), it is unlikely that a pure axial mode frequency is encompassed, which occurs typically at a frequency in excess of 30R. Thus the axial motion is not modelled and subsequently, the Coriolis term such as $2m\Omega\dot{u}$ cannot be represented.

It is shown in *Appendix* C that in order to include the effect of axial motion, it must be expressed as a fore-shortening term. This is done by considering the radial shear (V_x) expression and the u′ eliminant is defined, to $O(\varepsilon^3)$ accuracy, as

$$u' = \frac{V_x}{EA} + vV_p'' + wW_p'' - \frac{1}{2}(v'^2+w'^2) - k_A^2\vartheta'\phi'$$
$$+ [v'' + \phi(w'' + W_p'')]\ (e_{A2}\cos\vartheta - e_{A1}\sin\vartheta)$$
$$+ [w'' - \phi(v'' + V_p'')]\ (e_{A2}\sin\vartheta + e_{A1}\cos\vartheta) + O(\varepsilon^4) \qquad (3.43)$$

where $e_{A1}=\frac{\int\int E\xi d\eta d\xi}{\int\int E d\eta d\xi}$; $e_{A2}=\frac{\int\int E\eta d\eta d\xi}{\int\int E d\eta d\xi}$ are the flatwise and edgewise offsets of the tension centre from the elastic axis and $k_A^2=\frac{\int\int E(\eta^2+\xi^2)d\eta d\xi}{\int\int E d\eta d\xi}$ is the square of the radius of gyration about the tension axis. This is then substituted in the modal Lagrangian equation whereby the axial freedom is effectively eliminated and replaced by fore-shortening terms.

3.2.14 Elimination of Shear Flexibility

In the above derivation, the shear flexibility is retained such that a compatibility check with the CRFD can be made. As discussed in *Section* 3.2.5 in order that the analysis can be reduced to a manageable size, we assume that there is no distinction of the bending angles and slopes *ie.* $\zeta=v', \beta=w', ...etc$ in the Lagrangian equation. The reduction by eliminating shear flexibility is purely a numerical process and the equivalence between the dynamic and response systems, once demonstrated, remains valid.

3.2.15 Summary

In this section, the basic formulation of the modal Lagrangian equation for the coupled rotor-fuselage system has been presented. The Lagrangian equation, which is fully coupled, is valid for a rotor blade using real modes as state vectors. Only the kinematic effects of elastic hub motion and rigid aircraft motion are considered. Tedious algebra has been avoided as far as possible to provide clarity.

3.3 Modelling of Dynamics

3.3.1 Introduction

An essential ingredient in the modal analysis is a set of suitably defined modal vectors (state variables). The modes used can be, by definition, any admissible functions which approximate the natural modes and satisfy the boundary conditions of the dynamic system concerned. A finite sequence of these functions is then used in connection with the Galerkin or Rayleigh-Ritz method for the determination of the system characteristics, as illustrated by Bramwell [3.9]. The approach is referred to as the method of assumed modes.

For practical rotor applications, a set of hub-fixed structurally and inertially coupled rotating blade modes is usually used in rotor load prediction programs such as R150 [3.10] at WHL. These mode types, being more representative than those of admissible functions on the blade dynamics, allow more insight to be gained. However, because of the hub-fixed nature, these modes cannot represent the dynamic interactions between the rotor and the fuselage.

This can be illustrated qualitatively by considering a blade in the rotor when being forced by some unsteady loads. The unsteady loads will result in dynamic response of the blade which may be described by the natural modes of that blade. However, the response is dependent on the loads forcing the other blades in the rotor since the hub is free to move at the rotor centre-line. These hub translations and rotations are dependent on the dynamic characteristics of the fuselage and transmission system to which the rotor is attached. Indeed, each different combination of translational and rotational freedoms would, in general, yield a different blade response.

In order to model the dynamic interactions of the coupled rotor-fuselage system correctly, a complementary study was conducted by Juggins [3.1]. A number of methods were examined but were discarded as not being able to represent the dynamics of the coupled system correctly. For example, these methods included the classical impedance matching using free-free blade modes and hub-fixed modes superimposed on rigid body hub motion. The main conclusion drawn from this extensive study is that the dynamics of the coupled rotor-fuselage

system can only be correctly modelled using complex rotor modes. The dynamic coupling is achieved by transforming the blade motion to the fixed frame where hub motions are imposed. The hub motions represent the fuselage response and can be described by a set of free-free fuselage modes, which can be obtained analytically or experimentally.

The use of complex rotor modes will inevitably increase computational effort. However, not only does it enable coupling between the rotor and fuselage to be modelled, it also allows linear Coriolis and lag damper effects to be included in the modes calculation. Both effects cannot be modelled when real modes, *eg.* WHL's blade modes analysis program: J134 [3.11], are used but are treated as forcing functions in the response analysis [3.12]. Because the rotor modes are complex, special attention is needed to use these modes correctly. It is essential to understand how they are obtained and what implications they may have on the response analysis. The concept of complex rotor modes, not given before, and their solution are the subjects of the next few sections.

3.3.2 Description of Rotor Coordinates and Rotor Modes

The possible combinations of blade patterns within a rotor are infinite. However, it is possible to define a finite set of independent (orthogonal) rotor patterns, known as the rotor coordinates, from which any combination of blade motions may be described. This is analogous to the Fourier Transform method of re-constructing a time history from a set of orthogonal sine and cosine waveforms.

Rotor coordinates were first introduced by Coleman and Feingold [3.13] in their study of helicopter ground resonance (Coleman instability) based on a rigid rotor/fuselage system. However, the application of rotor modes is not widespread and is normally confined to stability calculation. For example, Done [3.14] demonstrated that the helicopter ground resonance problem could be reduced to a two degree of freedom model and was sufficient to provide an understanding of the physical mechanism.

The rotor coordinates are obtained from the blade coordinates via a fixed frame or multi-blade coordinate transformation. If x_k denotes a displacement, such as flap or lag deflection, on the k^{th} blade of an N-bladed rotor, then the corresponding rotor coordinates are defined as

$$x_0 = \frac{1}{N}\sum_{k=1}^{N} x_k \; ; \qquad x_C = \frac{2}{N}\sum_{k=1}^{N} x_k \cos\psi_k \; ; \qquad x_S = \frac{2}{N}\sum_{k=1}^{N} x_k \sin\psi_k \; ;$$

$$x_{nc} = \frac{2}{N}\sum_{k=1}^{N} x_k \cos n\psi_k \; ; \quad x_{ns} = \frac{2}{N}\sum_{k=1}^{N} x_k \sin n\psi_k \qquad n=2,... \qquad (3.44)$$

where x_0, x_C, x_S are known as the collective, cyclic cosine (longitudinal) and cyclic sine (lateral) coordinates and x_{nc}, x_{ns} are known as the n^{th} reactionless cosine and sine coordinates. ψ_k is the azimuth position occupied by the k^{th} blade, where $\psi_k = \psi_1 + \frac{2\pi(k-1)}{N}$ and ψ_1 is the arbitrary reference position of the first blade.

Diagrammatical representations of example lead-lag rotor coordinates, normalised by the blade tip deflection, for the 4 and 5-bladed rotor with $\psi_1 = 0^\circ$, are shown in *Figure* 3.9 below,

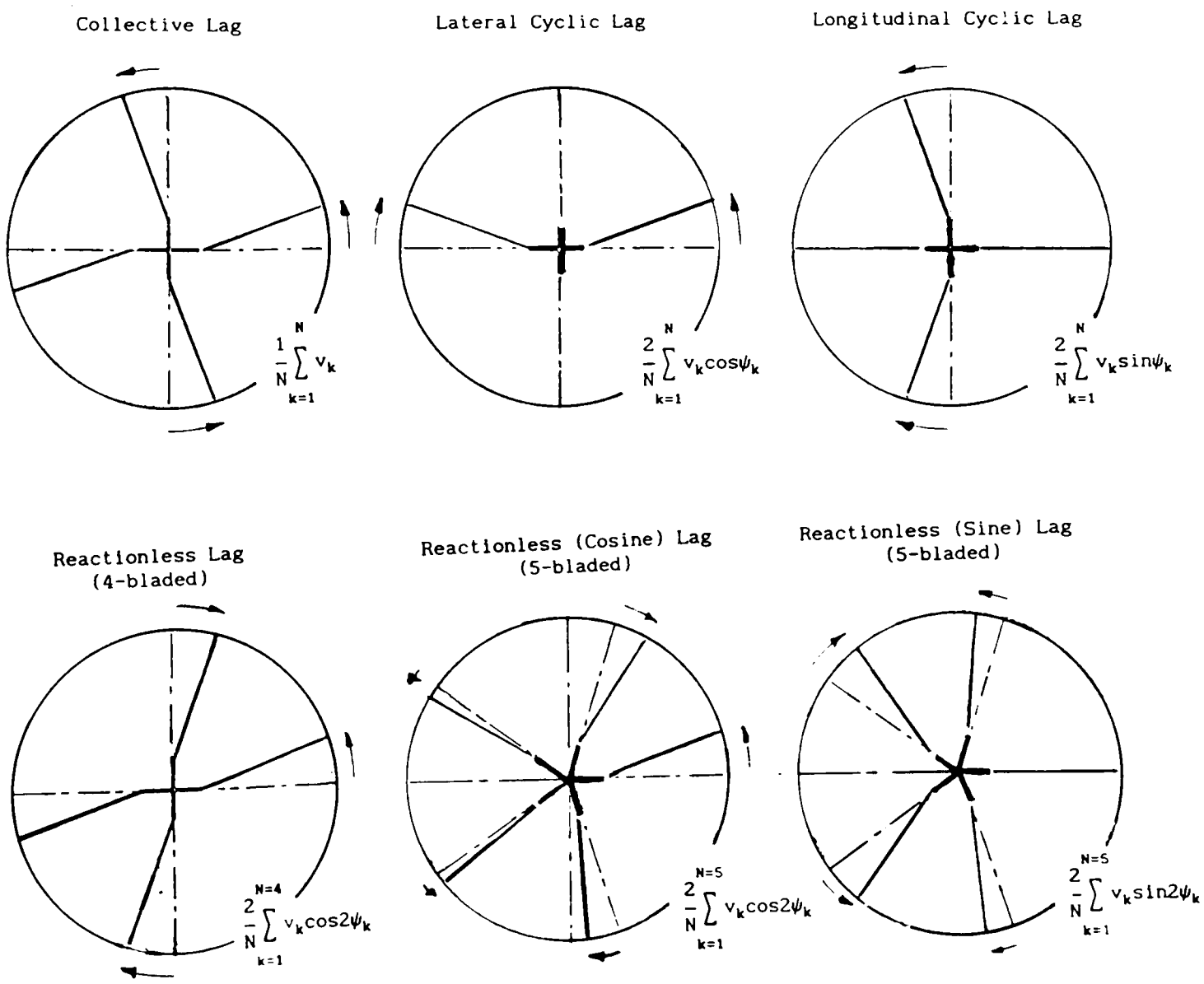

Figure 3.9: Example Lead-Lag Rotor Pattern with $\psi_1 = 0^\circ$

The corresponding inverse transformation from the fixed frame to the rotating blade coordinate system is

$$x_k = x_0 + x_c\cos\psi_k + x_s\sin\psi_k + \sum_{n=2}\left\{ x_{nc}\cos n\psi_k + x_{ns}\sin n\psi_k \right\} \qquad (3.45)$$

Two important features of this transformation must be noted. It is orthogonal and is independent of time for an odd-number (≥5) bladed rotor, but becomes time dependent for an even-number (≥4) bladed rotor. This is because for an odd-number bladed rotor, the number of reactionless patterns is always even and occur as independent pairs. It is possible to transform the pair into the fixed frame as higher harmonic component pairs *eg.* $\cos 2\Omega t, \sin 2\Omega t, \cos 3\Omega t, \sin 3\Omega t \ldots$ *etc.* For an even-number bladed rotor, the number of reactionless patterns is always odd, there will always be a rotor pattern which cannot be transformed into a pair of independent higher harmonic components. As a result, different solution methods can emerge depending on the number of blades in the rotor, as described by Holton [3.15].

To avoid this, Johnson [3.16] introduces the reactionless term as $x_R = \sum(-1)^k x_k$ in the transformation for an even-number bladed rotor and modifies the harmonic summation index n to range from 1 to $\mathrm{Int}(\frac{N-2}{2})$. However, this still leaves the frequency defined in the rotating frame and the transformation cannot be used for the response solution since the phasing of the forcing relative to the blade cannot be prescribed.

The number of independent rotor coordinates necessary to describe the possible rotor motion is clearly dictated by the number of blades in the rotor. However, not all of them will give rise to net motion at the hub. The collective motion x_0 is independent of azimuth position with each blade moving identically and resulting in net motion along or about the axis of rotation, *eg.* hub vertical and yaw motion. The cyclic motions x_c, x_s are dependent on the azimuth position, where the motion on each blade repeats itself once every rotor revolution resulting in net motion along and about axes in the plane of rotation, *eg.* hub inplane or disc tilt motion. Thus these coordinates: x_0, x_c and x_s, couple with the fixed frame motion and are therefore referred to as *coupled coordinates*.

The remaining coordinates: $x_{2c}, x_{2s}, \ldots, x_{nc}, x_{ns}$, necessary to complete the description of the rotor motion, do not couple with the hub motion.

The motion of each blade repeats twice or more in each rotor revolution resulting in no net motion at the hub. They are referred to as *reactionless coordinates* and can be treated in the same way as the rotating blade coordinates in a hub-fixed condition, *ie.* in the rotating frame, except that they include Coriolis effect.

The rotor modes, which describe the time independent natural motion of a complete rotor, are therefore made up of these 3 primary components; collective, cyclic and reactionless. Hence, only two mode types: the *coupled* modes (containing both collective and cyclic motions) defined in the fixed frame and the *reactionless* modes defined in the rotating frame, need to be considered. Once they are determined, the total response of a given blade can then be obtained by transforming the coupled motion from the fixed frame into the rotating frame and superimposing the reactionless motion for that blade.

The transformation (*Eqn.*3.45) merely introduces a convenient set of coordinates to enable coupling between the rotor and the fuselage to be carried out, the physics of the problem remains unchanged. Since x_k is a function of both time (t) and space (r), so must the rotor coordinates; $x_0, x_C, x_S, \ldots, x_{nc}$ and x_{ns}. Because of the nature of coupling, it is only necessary to consider the transformation up to and including the cyclic components, thus *Eqn.*3.45 reduces to

$$x_k(r,t) = x_0(r,t) + x_C(r,t)\cos\psi_k + x_S(r,t)\sin\psi_k \qquad (3.46)$$

It is important to note that by differentiating x_k with respect to time, gyroscopic and centrifugal terms are introduced,

$$\dot{x}_k = \dot{x}_0 + (\dot{x}_C + \Omega x_S)\cos\psi_k + (\dot{x}_S - \Omega x_C)\sin\psi_k \qquad (3.47a)$$

$$\ddot{x}_k = \ddot{x}_0 + (\ddot{x}_C + 2\Omega\dot{x}_S - \Omega^2 x_C)\cos\psi_k + (\ddot{x}_S - 2\Omega\dot{x}_C - \Omega^2 x_S)\sin\psi_k \qquad (3.47b)$$

where the notations of r,t dependencies are omitted from *Eqns.*3.47.

3.3.3 Modelling of Blade Dynamics

The determination of the dynamic characteristics: frequencies and mode shapes, for the coupled rotor-fuselage system is defined within the framework of CRFD. The full description of the solution process can be found in a number of reports by Juggins *eg.* [3.1,3.17A,3.17B]. A summary is provided here.

The intention of CRFD modelling is to provide a variety of mode types, ranging from undamped (real) blade modes to damped (complex) coupled modes, to be used for rotor response analysis. This enables the rotor modelling complexity to vary dependent upon the application. However the formulation is common to all mode types and is based on a single blade. The system equations differ only in the terms being retained, and subsequently, the dynamic characteristics vary.

In CRFD, the rotor blade is modelled by a continuous beam made up of a series of straight segments defining the locus of shear centres. Large pre-cone and pre-sweep angles are accommodated through numerical blade segment resolution. The blade is of a Timoshenko type beam with shear deformation included. Warping restraint is also included by modifying the torsional stiffness distribution.

The blade and hub are allowed to undergo elastic deformations similar to aeroelastic formulation. It is known that the blade steady state is influenced by many parameters, the most notable being the rotor thrust. A representative collective pitch ϑ_m is applied to achieve the required thrust calculated using quasi-steady or perturbatory aerodynamics.

The derivation of the equations of motion, defined at a point on the blade elastic axis, proceeds by the application of Hamilton's Principle using an ordering scheme. Once derived for a single blade, the equations are then transformed into the fixed frame to describe the motion of a blade point in a rotor made up of a number (>2) of identical blades. For a 2-bladed rotor, the collective can be described but there are two cyclic freedoms which have a time dependency between them and has not been dealt with.

The ordering assumption is similar to that adopted in the aeroelastic analysis, with the following exceptions;

(i) The precone, presweep and anhedral angles are not small;

(ii) The radial deflection (u) is assumed to be $O=O(\varepsilon)$ to accommodate the axial resolution through the blade kinks, because no small angle assumption is made to the pre-deformed angles;

(iii) Shear deformations are retained *ie.* blade section rotations (β,ζ) and bending slopes (w',v') are distinct; and

(iv) Both blade torsion inertias mk_{yy}^2 and mk_{zz}^2 are assumed to be $O(\varepsilon)$

instead of $O(\varepsilon^2)$. This is strictly incorrect but it allows the third order inertia terms to be retained in the torsion equation.

The equations of motion for a rotating (k^{th}) blade, including the hub motion, are written in terms of the coefficient matrices of which $A_0, A_1, A_2, B_0, B_1, B_2, B_3, B_4$ are constant for the blade variables and $B_5(t), B_6(t)$ are time dependent for the hub variables as shown,

$$A_0\underline{U}_k' + A_1\underline{U}_k + A_2\underline{F}_k + \underline{SA} = \underline{0}$$
$$B_0\underline{F}_k' + B_1\underline{U}_k' + B_2\underline{U}_k + B_3\dot{\underline{U}}_k + B_4\ddot{\underline{U}}_k + B_5(t)\dot{\underline{H}} + B_6(t)\ddot{\underline{H}} + \underline{SB} = \underline{0} \qquad (3.48)$$

where $\underline{U}_k=\{u,v,w,R_x,R_y,R_z\}^T$ is the vector of blade deformation variables;

$\underline{F}_k=\{V_x,V_y,V_z,M_x,M_y,M_z\}^T$ is the vector of blade forces and moments;

$\underline{H}=\{x_H,y_H,z_H,\phi_H,\vartheta_H,\psi_H\}^T$ is the vector of hub motions;

$\underline{SA}$ = vector of constants containing non-linear strain terms;

$\underline{SB}$ = vector of constants containing gravitational force and steady aerodynamic terms; and

$$()' = \frac{\partial()}{\partial r}; \quad \dot{()} = \frac{\partial()}{\partial t}.$$

The coefficient matrices (all real 6x6) possess the following properties;

$A_0^T = A_0$; $B_0 = I$; $B_3^T = -B_3$;

A_1 is general; B_1 is general; $B_4^T = B_4$;

$A_2 = -I$; $B_2^T = B_2$; B_5's and B_6's are general

and they satisfy the following important relationships;

(1) $A_1 = -B_1^T$; and

(2) $B_1A_0^{-1}A_1-B_2$ is symmetrical.

The system equation of this particular form is configured for the use of the transfer matrix solution method. It is however to be pointed that the form and the properties of coefficient matrices of the original CRFD system equations are *not* as shown in *Eqn.*3.48. As a result of proving the orthogonality relationship (*Section* 3.5.2) carried out within this study, the form of system equations was re-visited by Juggins [3.34], where inconsistencies were found and corrected with the revised form being shown above. Despite such changes, the solution procedure remains unaltered.

3.3.4 The Steady State and Modal Equations

The solution proceeds by defining the blade variables as the sum of the steady state and perturbatory components in both $\underline{U}_k$ and $\underline{F}_k$, and

perturbatory only in $\underline{H}$. The equations of motion are then linearised about the steady state. Upon separation, non-linear steady state and linearised modal equations are obtained.

The steady state solution is governed by the equations

$$A_0\underline{U}'_{ST} + A_1\underline{U}_{ST} + A_2\underline{F}_{ST} + \underline{SA} = \underline{0}$$
$$B_0\underline{F}'_{ST} + B_1\underline{U}'_{ST} + B_2\underline{U}_{ST} + \underline{SB} = \underline{0} \qquad (3.49)$$

where suffix ST refers to the blade steady state and is valid for all mode types.

The linearised modal equations in the single (k^{th}) blade form, are described by;

$$A_0\underline{U}'_k + A_1\underline{U}_k + A_2\underline{F}_k = \underline{0}$$
$$B_0\underline{F}'_k + B_1\underline{U}'_k + B_2\underline{U}_k + B_3\dot{\underline{U}}_k + B_4\ddot{\underline{U}}_k + (B_{50} + B_{5C}\cos\psi_k + B_{5S}\sin\psi_k)\dot{\underline{H}} + (B_{60} + B_{6C}\cos\psi_k + B_{6S}\sin\psi_k)\ddot{\underline{H}} = \underline{0} \qquad (3.50)$$

where the periodicity of matrices $B_5(t)$ and $B_6(t)$ is stated explicitly with $B_{50}, B_{5C}, B_{5S}, B_{60}, B_{6C}, B_{6S}$ being constant. *Eqns.* 3.50 provide the basic form of equation from which the system equations for various mode types are obtained.

3.3.5 Linearised Modal Equations

a. Real Blade Modes

By far, the simplest form of the system equations defined by CRFD is that for the undamped blade modes, where neither damping, hub motion nor Coriolis term is present. The system equations are obtained directly by eliminating these terms from *Eqns.* 3.50,

$$A_0\underline{U}'_k + A_1\underline{U}_k + A_2\underline{F}_k = \underline{0}$$
$$B_0\underline{F}'_k + B_1\underline{U}'_k + B_2\underline{U}_k + B_4\ddot{\underline{U}}_k = \underline{0} \qquad (3.51)$$

The solution is obtained in the rotating frame, with the assumption that the motions of all the blades are identical. Because there is no velocity term, the modes are real.

b. Undamped Complex Reactionless Modes

Since the reactionless modes involve no motion of the hub, they can be treated in the rotating frame. The system equations differ from those

for the real blade mode type in that they include the Coriolis terms, *ie.* $B_3\dot{\underline{U}}$,

$$\begin{aligned} &A_0\underline{U}'_k + A_1\underline{U}_k + A_2\underline{F}_k = \underline{0} \\ &B_0\underline{F}'_k + B_1\underline{U}'_k + B_2\underline{U}_k + B_3\dot{\underline{U}}_k + B_4\ddot{\underline{U}}_k = \underline{0} \end{aligned} \qquad (3.52)$$

This system resembles that of a gyroscopic system, and the dynamic characteristics are complex as shown by Lancaster [3.18].

c. Undamped Complex Coupled Modes via The Fixed Frame Transformation

For the coupled modes without damping, both Coriolis and hub motion terms are present, the system equations for these mode types in the rotating frame are those given by *Eqns.*3.50. They contain azimuthally dependent terms, which are removed by transforming the system equations into the fixed frame using *Eqn.*3.46. It is to be noted that the transformation is complete only by applying the following operators to the system equations,

$$\sum_{k=1}^{N} (..)\ 1\ ; \qquad \sum_{k=1}^{N} (..)\ \cos\psi_k\ ; \qquad \sum_{k=1}^{N} (..)\ \sin\psi_k\ .$$

By equating the coefficients of like terms, the following sets of coupled equations are obtained;

Collective Equations

$$\begin{aligned} &A_0\underline{U}'_0 + A_1\underline{U}_0 + A_2\underline{F}_0 = \underline{0} \\ &B_0\underline{F}'_0 + B_1\underline{U}'_0 + B_2\underline{U}_0 + B_3\dot{\underline{U}}_0 + B_4\ddot{\underline{U}}_0 + B_{50}\dot{\underline{H}} + B_{60}\ddot{\underline{H}} = \underline{0} \end{aligned}$$

Cyclic Cosine Equations

$$\begin{aligned} &A_0\underline{U}'_C + A_1\underline{U}_C + A_2\underline{F}_C = \underline{0} \\ &B_0\underline{F}'_C + B_1\underline{U}'_C + B_2\underline{U}_C + B_3(\dot{\underline{U}}_C+\Omega\underline{U}_S) + B_4(\ddot{\underline{U}}_C+2\Omega\dot{\underline{U}}_S-\Omega^2\underline{U}_C) + B_{5C}\dot{\underline{H}} + B_{6C}\ddot{\underline{H}} = \underline{0} \end{aligned}$$

Cyclic Sine Equations

$$\begin{aligned} &A_0\underline{U}'_S + A_1\underline{U}_S + A_2\underline{F}_S = \underline{0} \\ &B_0\underline{F}'_S + B_1\underline{U}'_S + B_2\underline{U}_S + B_3(\dot{\underline{U}}_S-\Omega\underline{U}_C) + B_4(\ddot{\underline{U}}_S-2\Omega\dot{\underline{U}}_C-\Omega^2\underline{U}_S) + B_{5S}\dot{\underline{H}} + B_{6S}\ddot{\underline{H}} = \underline{0} \end{aligned} \qquad (3.53)$$

where $\underline{U}_0, \underline{U}_C, \underline{U}_S$ are the collective, cyclic cosine and cyclic sine components of the coupled modes. These coupled sets of equations are far more complicated than those of reactionless modes. Apart from the hub terms, additional gyroscopic and centrifugal terms are also introduced as a result of the transformation. The system equations are

to be solved in the fixed frame. Despite such complexity, this system also resembles a gyroscopic system.

*Eqns.*3.53 describe only the blade-hub dynamics. The dynamics of the sub-system to which the rotor is attached, are included using an impedance representation. The frequency dependent impedance, Z, is obtained by considering a set of undamped normal modes defined in a free-free condition. The sub-system dynamic characteristics can be obtained either analytically *eg.* finite element method or experimentally. The hub compatibility equation, *ie.* the boundary condition, is derived from Hamilton's Principle by considering the variation of virtual work due to the hub motions, and equating the coefficients of individual variations to zero *ie.* $\frac{\delta W}{\delta h_i}\Big|_{r=0}=0$ where $h_i=x_H, y_H, z_H, \phi_H, \vartheta_H, \psi_H$. This is done by summing the shears and moments from all the blades, and by equating them to the hub values. The following matrix equation results

$$(\frac{1}{N}\,Z + S)\,\underline{H} = FC\cdot\underline{F}_C + FS\cdot\underline{F}_S + FO\cdot\underline{F}_O \qquad (3.54)$$

where N is the number of blades;

Z is the fuselage impedance matrix at the rotor hub (a function of coupled frequency);

S is a matrix containing linearised steady blade root forces;

$\underline{H}$ is the vector of hub motions (as before);

FC,FS,FO are the coefficient matrices of the blade root forces;

$\underline{F}_O, \underline{F}_C, \underline{F}_S$ are the root collective, cyclic cosine and sine forces.

*Eqn.*3.54 is then combined with those in *Eqns.*3.53 to obtain the solution for the coupled modes.

d. Reactionless and Coupled Modes with General (Real) Damping

The retention of velocity terms allows linear damping: structural, aerodynamic or viscous, to be included in the modes solution for both the reactionless and coupled modes. The system equations are those defined previously by *Eqns.*3.53 & 3.54 except $B_3^T \neq -B_3$ *ie.* the gyroscopic nature of the undamped system is destroyed. Indeed, the inclusion of damping effect is responsible for the vastly increased complexity during the analytical development of this study. Further discussion on this topic will be given in *Section* 3.5.2e.

3.3.6 Method of Modal Solution

The solution procedures for the steady state and the various mode types are based on the multi-blade transfer matrix approach.

Steady State Solution

The steady state solution proceeds as a single blade hub-fixed condition, by re-expressing the governing equations (*Eqn.*3.49) as

$$\underline{U}'_{ST} = -A_0^{-1}A_1\underline{U}_{ST} - A_0^{-1}A_2\underline{F}_{ST} - A_0^{-1}\underline{SA}$$
$$\underline{F}'_{ST} = -B_0^{-1}B_1\underline{U}'_{ST} - B_0^{-1}B_2\underline{U}_{ST} - B_0^{-1}\underline{SB}$$

or

$$\begin{bmatrix} I & 0 \\ B_0^{-1}B_1 & I \end{bmatrix}\begin{Bmatrix} \underline{U}' \\ \underline{F}' \end{Bmatrix}_{ST} = \begin{bmatrix} -A_0^{-1}A_1 & -A_0^{-1}A_2 \\ -B_0^{-1}B_2 & 0 \end{bmatrix}\begin{Bmatrix} \underline{U} \\ \underline{F} \end{Bmatrix}_{ST} + \begin{Bmatrix} -A_0^{-1}\underline{SA} \\ -B_0^{-1}\underline{SB} \end{Bmatrix}$$

$$\begin{Bmatrix} \underline{U}' \\ \underline{F}' \end{Bmatrix}_{ST} = \begin{bmatrix} I & 0 \\ -B_0^{-1}B_1 & I \end{bmatrix}\left\{ \begin{bmatrix} -A_0^{-1}A_1 & -A_0^{-1}A_2 \\ -B_0^{-1}B_2 & 0 \end{bmatrix}\begin{Bmatrix} \underline{U} \\ \underline{F} \end{Bmatrix}_{ST} + \begin{Bmatrix} -A_0^{-1}\underline{SA} \\ -B_0^{-1}\underline{SB} \end{Bmatrix} \right\}$$

$$= \begin{bmatrix} -A_0^{-1}A_1 & -A_0^{-1}A_2 \\ B_0^{-1}B_1A_0^{-1}A_1 - B_0^{-1}B_2 & B_0^{-1}B_1A_0^{-1}A_2 \end{bmatrix}\begin{Bmatrix} \underline{U} \\ \underline{F} \end{Bmatrix}_{ST} + \begin{Bmatrix} -A_0^{-1}\underline{SA} \\ B_0^{-1}B_1A_0^{-1}\underline{SA} - B_0^{-1}\underline{SB} \end{Bmatrix}$$

Using the known properties, A_2=-I, B_0=I (*Eqn.*3.48), it reduces to

$$\begin{Bmatrix} \underline{U}' \\ \underline{F}' \end{Bmatrix}_{ST} = \begin{bmatrix} -A_0^{-1}A_1 & A_0^{-1} \\ B_1A_0^{-1}A_1 - B_2 & -B_1A_0^{-1} \end{bmatrix}\begin{Bmatrix} \underline{U} \\ \underline{F} \end{Bmatrix}_{ST} + \begin{Bmatrix} -A_0^{-1}\underline{SA} \\ B_1A_0^{-1}\underline{SA} - \underline{SB} \end{Bmatrix} \qquad (3.55)$$

The solution can be obtained by integrating *Eqn.*3.55 along the blade using the known boundary condition at the tip (natural) *ie.* $\underline{F}_{TIP}=\underline{0}$ as the starting point and also the condition at the root (geometric) *ie.* $\underline{U}_{ROOT}$. The blade root forces and displacements can be written in transfer matrix form as

$$\begin{Bmatrix} \underline{U} \\ \underline{F} \end{Bmatrix}_{ROOT} = \begin{bmatrix} T_{11} & - \\ T_{21} & - \end{bmatrix} \cdot \begin{Bmatrix} \underline{U} \\ \underline{0} \end{Bmatrix}_{TIP} + \begin{Bmatrix} \underline{CD} \\ \underline{CS} \end{Bmatrix} \qquad (3.56)$$

where T_{11}, T_{21} are the transfer matrices and $\underline{CD}, \underline{CS}$ are the steady load vectors. The steady state solution in terms of the vectors $\underline{U}_{ST}$ and $\underline{F}_{ST}$ can then be evaluated iteratively.

Solution for The Blade and Reactionless Modes

The modal solutions for both the blade modes and the complex reactionless modes proceed in the same manner as in the steady state solution, except that the transfer matrix will be frequency dependent.

Solution for The Coupled Modes

In transfer matrix form, the blade root forces and displacements for the coupled modes can also be written as a set of coupled equations,

Collective

$$\begin{Bmatrix} \underline{U}_0 \\ \underline{F}_0 \end{Bmatrix}_{ROOT} = \begin{bmatrix} T_{11_0} & - \\ T_{21_0} & - \end{bmatrix} \cdot \begin{Bmatrix} \underline{U}_0 \\ \underline{0} \end{Bmatrix}_{TIP} + \begin{bmatrix} TH_{11} \\ TH_{21} \end{bmatrix} \cdot \{\underline{H}\}$$

Cyclic (cos)

$$\begin{Bmatrix} \underline{U}_C \\ \underline{F}_C \end{Bmatrix}_{ROOT} = \begin{bmatrix} T_{11_{CC}} & - \\ T_{21_{CC}} & - \end{bmatrix} \cdot \begin{Bmatrix} \underline{U}_C \\ \underline{0} \end{Bmatrix}_{TIP} + \begin{bmatrix} T_{11_{CS}} & - \\ T_{21_{CS}} & - \end{bmatrix} \cdot \begin{Bmatrix} \underline{U}_S \\ \underline{0} \end{Bmatrix}_{TIP} + \begin{bmatrix} TH_{11_C} \\ TH_{21_C} \end{bmatrix} \cdot \{\underline{H}\}$$

Cyclic (sin)

$$\begin{Bmatrix} \underline{U}_S \\ \underline{F}_S \end{Bmatrix}_{ROOT} = \begin{bmatrix} T_{11_{SC}} & - \\ T_{21_{SC}} & - \end{bmatrix} \cdot \begin{Bmatrix} \underline{U}_C \\ \underline{0} \end{Bmatrix}_{TIP} + \begin{bmatrix} T_{11_{SS}} & - \\ T_{21_{SS}} & - \end{bmatrix} \cdot \begin{Bmatrix} \underline{U}_S \\ \underline{0} \end{Bmatrix}_{TIP} + \begin{bmatrix} TH_{11_S} \\ TH_{21_S} \end{bmatrix} \cdot \{\underline{H}\}$$

(3.57)

where $T_{11_0}, T_{21_0} \ldots, TH_{21_S}$ are coefficient matrices which are functions of the complex natural frequencies. Substituting *Eqns.*3.57 into the hub compatibility equation (*Eqn.*3.54) leads to the matrix equation,

$$\begin{bmatrix} TH_{11_0} & T_{11_0} & 0 & 0 \\ TH_{11_C} & 0 & T_{11_{CC}} & T_{11_{CS}} \\ TH_{11_S} & 0 & T_{11_{SC}} & T_{11_{SS}} \\ FC \cdot TH_{21_C} + FS \cdot TH_{21_S} + FO \cdot TH_{21_0} - (\frac{1}{N}Z+S) & FO \cdot T_{21_0} & FC \cdot T_{21_{CC}} + FS \cdot T_{21_{SC}} & FC \cdot T_{21_{CC}} + FS \cdot T_{21_{SC}} \end{bmatrix} \cdot \begin{Bmatrix} \underline{H} \\ \underline{U}_0 \\ \underline{U}_C \\ \underline{U}_S \end{Bmatrix} = \begin{Bmatrix} \underline{0} \\ \underline{0} \\ \underline{0} \\ \underline{0} \end{Bmatrix}$$

or

$$D\ \underline{V} = \underline{0} \qquad (3.58)$$

The determinant of the coefficient matrix D, which is a function of the blade properties and the complex frequency, is evaluated successively for a given search frequency. The mode frequencies and shapes are then determined by finding the zero determinants of matrix D and the corresponding complex eigenvector $\underline{V}$, which contains the values of the coupled coordinates in the fixed frame. The complex modal vector $\underline{V}$ is normalised to unity and zero phase by the largest component in $\underline{V}$. The modal solution is thus complete.

3.4 Modelling of Aerodynamics

3.4.1 Introduction

The determination of blade aerodynamic loads is an integral part of a rotor aeroelastic analysis. For this purpose, it is essential to know the local components of airflow at any station along the blade and this, in turn, requires a knowledge of the air velocity, induced by the lift of the blades.

The flowfield through the rotor is extremely complex and the oscillatory pitching motion of the blade has a significant effect on the aerofoil section characteristics. The correct modelling of aerofoil behaviour undergoing these rapid changes in incidence around the azimuth is important to ensure the aerodynamic loadings are determined accurately.

When the rotor blades are treated as slender beams, the modelling of blade aerodynamics essentially reduces to one of finding the spanwise distribution of normal force, chordwise force and pitching moment coefficients *ie.* the lifting line theory. Even with such a simplification, the task is still a difficult one.

Development of aerodynamic models is not part of this study but description of models adopted is provided here for completeness. The aerodynamic models adopted, cumulating many years of development at both WHL and DRA (Farnborough), represent the state-of-the-art modelling of wake geometry and unsteady aerodynamics. No attempt is made here to discuss in detail all the theories upon which the aerodynamic model is based.

For many years, there have been doubts on the true definition of the angle of attack expression used for aerodynamic calculation. A rigorous approach is provided here to clarify such an issue.

3.4.2 Wake Induced Velocity and Fuselage Upwash Models

The determination of induced velocity distribution involves the modelling of the wake geometry shed from the rotor. Once the distribution of these vortex lines trailing from the rotor is

determined, the induced velocity at a given point of the flow can be calculated by applying the Biot-Savart law. Wake models of varying complexity are included as options in this analysis.

The simplest wake model included is due to Glauert [3.19], where the induced velocity increases linearly from the front to the rear of the disc and is constant across any lateral cross-section. A more representative wake model is the vortex ring model developed by Cook [3.20]. It consists of half vortex rings originating at the tip and root cut-out of the reference blade, with complete vortex rings being displaced down-stream. The family of vortex rings are assumed to be equally spaced in both the vertical and horizontal planes. The root and tip vortices are opposite but equal in strength such that circulation is constant along the blade. Both the Glauert and vortex ring wake models provide an overall representation of induced velocity for the rotor.

In a more detailed modelling of rotor induced velocity, it is common to model the wake geometry using both a near wake and a far wake. The near wake defines the interaction of the trailed vortices immediately behind the blade, and the far wake defines the significant part of the mean inflow levels and the blade vortex interactions (BVI's).

The interactive near wake model incorporated in this analysis is based on that developed by Young [3.21]. It is an extension to Cook's vortex ring model by replacing the half rings, at the tip and the root originating from the reference blade, with a series of half rings across the span. This allows a spanwise variation of circulation. The trailing wake *ie.* the system of complete rings, remains unchanged but both wake contraction and non-uniform vertical displacements of the vortex rings are incorporated. It is however assumed that at any given azimuth angle, the circulation does not vary along the half ring. Since the loading history is neglected, excessive computational effort is avoided. However, the error is small, as the velocity induced at the calculation points is dominated by the part of the ring closest to the blade, the effects from the rest of the rings are small. This model provides a reasonably accurate definition of the overall inflow model and the blade vortex interactions. It is computationally efficient and has been shown to improve the vibratory loads prediction in cases away from the retreating blade stall envelope [3.21].

In general, the far wake model is assumed to comprise the cycloidal path of the point on the blade from where the fully contracted tip vortex originates. The downwash at any point on the blade is calculated by summing the effects of a series of small straight line segments following the cycloidal path. This is computationally expensive. To avoid complexity, Beddoes' far wake model [3.22] is adopted in this analysis.

Beddoes' model replaces each spiral turn of the wake by only 2 straight line vortex elements, both having length equal to the contracted wake diameter and positioned tangentially to the cycloidal path and centrally on points, known as the critical points. They are defined as the only points where the normal to the cycloidal path passes through the control point on the blade, at which the induced velocity is evaluated. From the definition of the spiral path there are only two critical points ensuring one of which will always be closest on the spiral to the control points, hence the approximation of the spiral by 2 straight line elements. The induced velocity on the blade is calculated by applying the Biot-Savart law to the spiral.

This model has been well-validated in level flight. To include application to manoeuvring flight, it has been extended by Harrison [3.23] to include the effects on the wake distortion due to the 3-dimensional aircraft motion. This avoids the need to use a free wake model for which computation is intensive, although the incorporation of 3D aircraft motion is relatively easy.

The discussion has so far concentrated on the rotor induced flow field. Wilby *et al* [3.24] has shown that the flow about the helicopter fuselage has a major effect on the rotor behaviour and is recognised as an important source of oscillatory loading on a rotor. The fuselage produces an upwash over the inboard part of the blade at the front of the disc. This increases the blade incidence and can lead to premature blade stall. The upwash also keeps the tip vortex from the preceding blade closer to the plane of the disc thereby increasing the loading outboard of the crossing point. The effect of these additional loadings is to increase the forcings of certain modes, with frequencies in the vicinity of (N±1)R and hence the loads transmitted to the fuselage.

In this analysis, two fuselage upwash models are included. Young's model [3.25] is based on a panel-source method, developed originally for fixed-wing aircraft. The method had been modified to give velocity components in the rotor disc at any specified radial and azimuth position. A simple interpolative procedure is then used to determine the upwash distribution. The other upwash model, due to Hawkings [3.26], is based on a slender body theory using potential flow. The fuselage upwash distribution is interpolated from tabulated data.

3.4.3 Modelling of Unsteady Aerodynamics

The flow over the rotor blade is a complicated phenomenon with the aerofoil oscillating over a range of angles of attack and this affects the blade loading. The principal features of this mechanism, known as dynamic stall, are described by the flow separation, formation of the leading edge vortices and passage of these vortices. The timewise variation of the angle of attack along the blade determines the torsional damping when the flow is attached, and the high control load generated when the blade undergoes dynamic stall limits the flight envelope of the aircraft. The rapid increase in pitch link loads, *eg.* due to retreating blade stall, cannot be estimated accurately unless the dynamic stall process is modelled correctly. The modelling of unsteady aerodynamics is principally to simulate the dynamic stall mechanism.

The simplest unsteady aerodynamics model used for rotorcraft aeroelastic analysis is Theodorsen's theory. It is however well-known that the theory is not directly applicable for rotary-wing aircraft because the unsteady wake beneath a rotor is quite different from the wake postulated. Nevertheless, various quasi-steady and unsteady models for determining aerodynamic loads based on this theory have been developed for rotorcraft stability analysis *eg.* Friedmann's dynamic inflow model [3.27]. The dynamic inflow, defined as a combination of steady and perturbation inflows, captures the low frequency aerodynamic effects associated with the wake.

The two unsteady aerodynamic models adopted for this analysis are based on a semi-empirical approach and both are well-validated against wind tunnel test data. The first model is the original dynamic stall model,

developed by Beddoes [3.28] which is based on an indicial approach. It consists of distinct attached and separated flow regimes which simulates the physics of the separation process. The model of the dynamic stall process assumes that there are two distinct time delays, one due to the lift and the other due to the pitching moment coefficient. This determines the lift and moment break points when the angle of attack for static stall is exceeded. The method is robust and generally produces acceptable predictions for aerofoil sections that exhibit leading-edge stall. The second model, by Leishman & Beddoes [3.29], is an extension to [3.28] by including a trailing edge separation to account for the vortex shedding during dynamic stall. Both of these unsteady aerodynamics models are provided as a table of data for a range of Mach numbers from which the aerofoil section coefficients can be synthesised.

3.4.4 Angle of Attack for Aerodynamic Calculation

In *Section* 3.2.4, an integral term ϑ_b was derived. This second order change in pitch angle is induced by pure lag and flap bending whilst the torsion angle remains zero. A rigorous approach is given here to determine its significance on the definition of angle of attack used in the calculation of aerodynamics. Consider the following diagram;

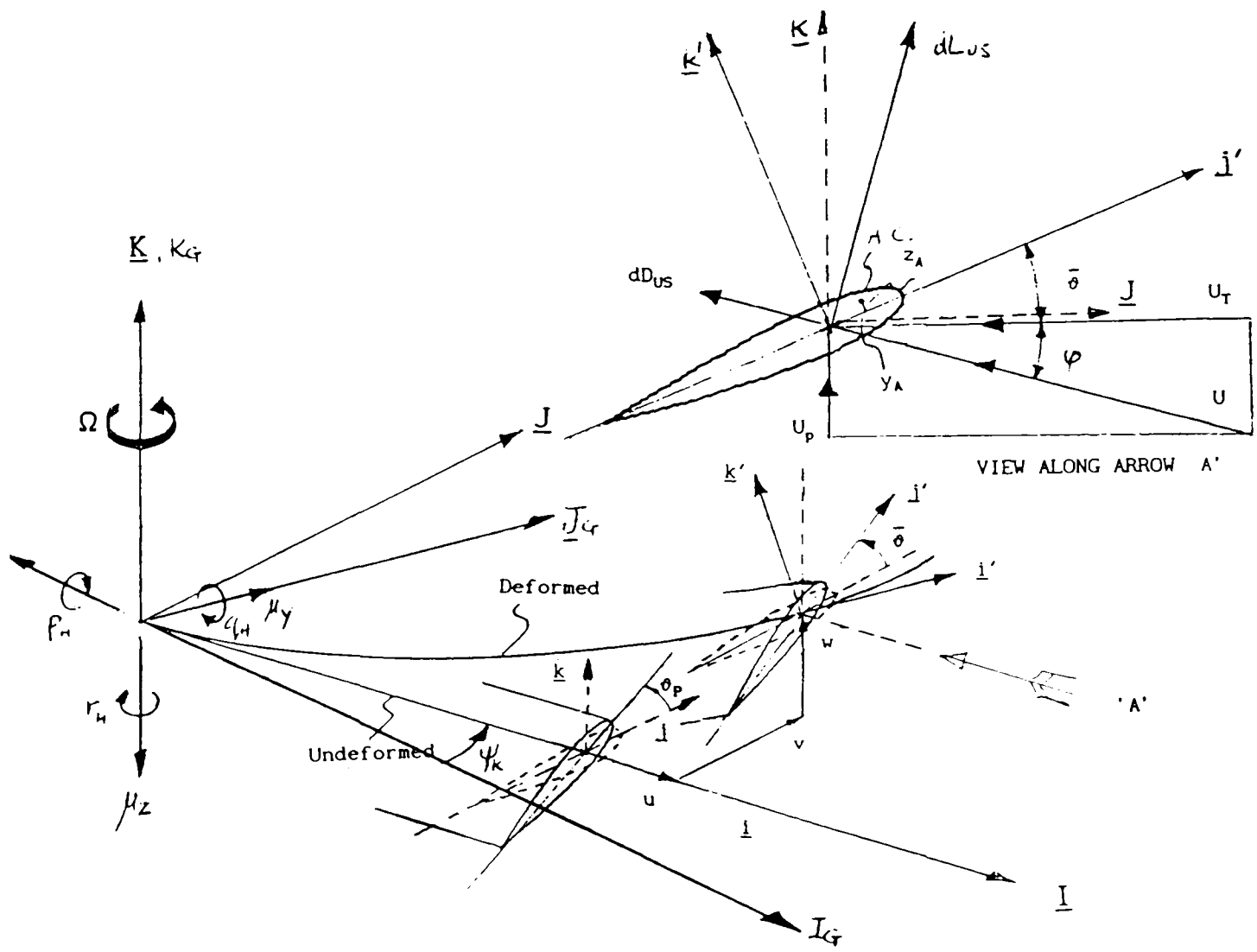

Figure 3.10: Angle of Attack on An Aerofoil Section

The angle of attack (α) for aerodynamic calculation is expressed as

$$\alpha = \bar{\vartheta} + \varphi \qquad (3.59)$$

$$= \bar{\vartheta} + \tan^{-1}\left(\frac{U_P}{U_T}\right)$$

where $\bar{\vartheta}$ ($=\hat{\vartheta}-\int\bar{v}''\bar{w}'dr$) is the pitch angle defined in *Eqn.*3.12 and φ is the inflow angle, U_p and U_T are the velocity components of air perpendicular and tangential to the blade in the undeformed blade axis ($\underline{i},\underline{j},\underline{k}$) coordinate system. These velocity components are related via the transformation matrix $\hat{T}$, as follows;

$$\begin{Bmatrix} U_R \\ -U_T \\ U_P \end{Bmatrix} = \hat{T}\cdot\begin{Bmatrix} U_i \\ U_j \\ U_k \end{Bmatrix}$$

$$= \begin{bmatrix} 1-\frac{(\bar{v}'^2+\bar{w}'^2)}{2} & \bar{v}' & \bar{w}' \\ -\bar{v}' & (1-\frac{\bar{v}'^2}{2}) & 0 \\ -\bar{w}' & -\bar{v}'\bar{w}' & (1-\frac{\bar{w}'^2}{2}) \end{bmatrix}\cdot\begin{Bmatrix} U_i \\ U_j \\ U_k \end{Bmatrix} + O(\varepsilon^3) \qquad (3.60)$$

where $\hat{T}$ is equivalent to T^T in *Eqn.*3.11 but the following are noted;

(1) $\hat{T}$ is devoid of the $\bar{\vartheta}$ component since U_R,U_T,U_P are the components of air velocity relative to the unpitched blade; and

(2) $\bar{v},\bar{w}$ contain both built-in (pre-deformed) and elastic deformations such that $\bar{v}=V_p+v,\bar{w}=W_p+w$, *etc.*

The velocity components U_i,U_j,U_k of the blade are defined as follows. Let the position vector of the aerodynamic centre $\underline{r}_A=\{0,y_A,z_A\}^T$ in the blade axis system, after deformation, be given by

$$\underline{r}_A = R(x+u)\underline{i} + R(\bar{v}+y_A)\underline{j} + R(\bar{w}+z_A)\underline{k} \qquad (3.61)$$

If $\underline{U}$ denotes the total velocity of the blade section relative to the air in the undeformed ($\underline{i},\underline{j},\underline{k}$) system, then

$$\underline{U} = \begin{Bmatrix} U_i \\ U_j \\ U_k \end{Bmatrix} = \underline{V} + \underline{\lambda} + \frac{\partial \underline{r}_A}{\partial t} + \underline{\Omega} \wedge \underline{r}_A \qquad (3.62)$$

where $\underline{V}$ is the hub velocity vector, $\underline{\lambda}$ is the induced velocity vector (+ve with axis) and $\underline{\Omega}$ is the rotation velocity vector, defined as

$$\underline{V}=\Omega R\begin{Bmatrix} -(\mu_x\cos\psi - \mu_y\sin\psi) \\ \mu_x\sin\psi + \mu_y\cos\psi \\ -\mu_z \end{Bmatrix};\ \underline{\lambda}=\Omega R\begin{Bmatrix}\lambda_i\\ \lambda_j\\ \lambda_k\end{Bmatrix};\ \underline{\Omega}=\Omega\begin{Bmatrix} -(p_H\cos\psi - q_H\sin\psi - \dot{\phi}) \\ p_H\sin\psi + q_H\cos\psi) \\ 1 - r_H \end{Bmatrix}$$

where all the quantities are normalised in accordance with *Table* 3.1. λ's, $y_A, z_A, \mu_y, \mu_z, u, \bar{v}, \bar{w}, \phi, p_H, q_H, r_H$ are at least $O(\varepsilon)$ quantities and μ_x, x are $O(1)$. It is to be noted that u is set to $O(\varepsilon)$ here in order that a check with other analyses can be made. Therefore,

$$\frac{\partial \underline{r}_A}{\partial t} + \underline{\Omega}\wedge\underline{r}_A = \Omega R\begin{Bmatrix} \dot{u} - (\bar{v}+y_A) + O(\varepsilon^2) \\ \dot{\bar{v}} + x + u - r_H x + O(\varepsilon^2) \\ \dot{\bar{w}} - (p_H\cos\psi - q_H\sin\psi - \dot{\phi})(\bar{v}+y_A) - (p_H\sin\psi + q_H\cos\psi)(x+u) + O(\varepsilon^3) \end{Bmatrix};$$

and

$$\therefore \underline{U} = \Omega R\begin{Bmatrix} -(\mu_x\cos\psi - \mu_y\sin\psi) + \lambda_i + \dot{u} - (\bar{v}+y_A) + O(\varepsilon^2) \\ x + \mu_x\sin\psi + \mu_y\cos\psi + \lambda_j + \dot{\bar{v}} + u - r_H x + O(\varepsilon^2) \\ -(\mu_z - \lambda_k - \dot{\bar{w}}) - (p_H\cos\psi - q_H\sin\psi - \dot{\phi})(\bar{v}+y_A) - (p_H\sin\psi + q_H\cos\psi)(x+u) + O(\varepsilon^3) \end{Bmatrix} \tag{3.63}$$

It is noted that the U_k component is expressed to an order higher than U_i, U_j such that they can be used to determine the inflow angle to $O(\varepsilon^2)$ accuracy. Hence from *Eqns.* 3.60 & 3.63,

$$\begin{Bmatrix} U_R \\ -U_T \\ U_P \end{Bmatrix} = \begin{bmatrix} 1-\frac{(\bar{v}'^2+\bar{w}'^2)}{2} & \bar{v}' & \bar{w}' \\ -\bar{v}' & (1-\frac{\bar{v}'^2}{2}) & 0 \\ -\bar{w}' & -\bar{v}'\bar{w}' & (1-\frac{\bar{w}'^2}{2}) \end{bmatrix} \cdot \Omega R\begin{Bmatrix} -(\mu_x\cos\psi - \mu_y\sin\psi) + \lambda_i + \dot{u} - (\bar{v}+y_A) + O(\varepsilon^2) \\ x + \mu_x\sin\psi + \mu_y\cos\psi + \lambda_j + \dot{\bar{v}} + u - r_H x + O(\varepsilon^2) \\ -(\mu_z - \lambda_k - \dot{\bar{w}}) - (p_H\cos\psi - q_H\sin\psi - \dot{\phi})(\bar{v}+y_A) - (p_H\sin\psi + q_H\cos\psi)(x+u) + O(\varepsilon^3) \end{Bmatrix} \tag{3.64}$$

which after some re-arranging,

$$\begin{aligned} U_R &= \Omega R[-(\mu_x\cos\psi - \mu_y\sin\psi) + \lambda_i + \dot{u} - (\bar{v}+y_A) + \bar{v}'(x+\mu_x\sin\psi)] + O(\varepsilon^2) \\ U_T &= -\Omega R[(x+\mu_x\sin\psi) + (\mu_y - \bar{v}'\mu_x)\cos\psi + \lambda_j + \dot{\bar{v}} + u - r_H x] + O(\varepsilon^2) \\ U_P &= \Omega R[-(\mu_z - \lambda_k - \dot{\bar{w}}) - (p_H\cos\psi - q_H\sin\psi - \dot{\phi})(\bar{v}+y_A) - (p_H\sin\psi + q_H\cos\psi)(x+u) \\ &\quad + \bar{w}'\{\mu_x\cos\psi - \mu_y\sin\psi - \lambda_i - \dot{u} + (\bar{v}+y_A)\} - \bar{v}'\bar{w}'(x+\mu_x\sin\psi)] + O(\varepsilon^3) \end{aligned} \tag{3.65}$$

from which the inflow angle φ is defined and the angle of attack α then takes the form,

$$
\begin{aligned}
\alpha &= \bar{\vartheta} + \varphi \\
&= \bar{\vartheta} + \tan^{-1}\left(\frac{U_P}{U_T}\right) \\
&\simeq \vartheta_p + \vartheta(\psi) + \phi - \int \bar{v}''\bar{w}'\,dr + \frac{U_P}{U_T} \\
&= \vartheta_p + \vartheta(\psi) + \phi - \int \bar{v}''\bar{w}'\,dr + \bar{v}'\bar{w}' + \\
&\quad \Big\{ -(\mu_z - \lambda_k - \dot{\bar{w}}) - (p_H\cos\psi - q_H\sin\psi - \dot{\phi})(\bar{v}+y_A) - (p_H\sin\psi + q_H\cos\psi)(x+u) \\
&\qquad + \bar{w}'\{\mu_x\cos\psi - \mu_y\sin\psi - \lambda_i - \dot{u} + (\bar{v}+y_A)\} \Big\} \\
&\quad \frac{}{\Big\{ -[(x+\mu_x\sin\psi) + (\mu_y - \bar{v}'\mu_x)\cos\psi + \lambda_j + \dot{\bar{v}} + u - r_H x] \Big\} + O(\varepsilon^3)}
\end{aligned}
\tag{3.66}
$$

This expression can be checked by letting $p_H=q_H=r_H=\mu_y=\lambda_i=\lambda_j=0$ and $\lambda_k=\nu, \vartheta(\psi)=0$ and α becomes

$$
\alpha = \underline{\vartheta_0} + \underline{\phi} - \underline{\int \bar{v}''\bar{w}'\,dr} + \underline{\bar{v}'\bar{w}'} + \frac{\mu_z \; \underline{-\nu} \; \underline{-\dot{\bar{w}}} \; \underline{-y_A\dot{\phi}} \; -\bar{w}'(\mu_x\cos\psi \; \underline{-\dot{u}} \; \underline{+\bar{v}})}{(x + \mu_x\sin\psi) + \mu_x\bar{v}'\cos\psi + \dot{\bar{v}} + u} + O(\varepsilon^3)
\tag{3.67}
$$

which is the same as that obtained by Walker [3.6] but without aircraft rate terms. The underlined terms are those derived by Peters [3.3] for the hover condition.

*Eqn.*3.66 is accurate to $O(\varepsilon^2)$ and is indeed complicated. In practice, the velocity components U_T, U_p are evaluated numerically from which the inflow angle φ is determined. The derivation here is rigorous and clarifies the effect of the second order pseudo torsion term due to pure bending in the α expression (*Eqn.*3.67). It should also be regarded as a definitive treatment of the blade pre-deformations, such as geometric anhedral and sweep, in the calculation of aerodynamic loads. If these pre-deformations are defined in the blade segment geometry for the modes calculation, then they are automatically included in the steady state twist and their effect must be removed from α, otherwise spurious torsion will be introduced. It is worth noting that for an accurate determination of aerodynamic loads, the blade section coefficients should also be evaluated to a comparable accuracy. The latter is however often carried out in a semi-empirical approach.

3.5 Method of Solution for The Rotor Response

The modal Lagrangian equation derived in *Section* 3.2 is valid for a rotor system modelled with real blade modes. Having introduced the concept of complex rotor modes, we examine their application in the rotor response calculation. The analytical concept that follows is entirely new.

3.5.1 Modal Representation of Rotor Coordinates

The response of the rotor is described by the time history of all the blades around the azimuth. On the basis that the rotor behaviour can be completely described by the responses of both coupled and reactionless modes, the motion of the individual k^{th} blades ($\underline{x}_k$) in the rotor can be uniquely determined from the following representation;

$$\begin{aligned}\underline{x}_k(r,\psi) &= \underline{x}_{ST}(r) + \sum_{i=1}^{N_c} \eta_{c_i}(\psi)\underline{x}_{\mathbb{C}_i}(r,\psi_k) + \sum_{i=1}^{N_r} \eta_{r_i}(\psi)\underline{x}_{r_i}(r) \\ &= \underline{x}_{ST}(r) + \sum_{i=1}^{N_c} \eta_{c_i}(\psi)[\underline{x}_0(r) + \underline{x}_C(r)\cos\psi_k + \underline{x}_S(r)\sin\psi_k] \\ &\quad + \sum_{i=1}^{N_r} \eta_{r_i}(\psi)\underline{x}_{r_i}(r) \qquad (3.68)\end{aligned}$$

where suffices $\mathbb{C}$(or c),r refer to the coupled and reactionless modes respectively. η_{c_i}, η_{r_i} are the generalised coordinates (modal responses) for the i^{th} mode and N_c, N_r are the numbers of respective mode types used in the response analysis. It is noted that the azimuthal dependence of the i^{th} coupled mode shape, $\underline{x}_{\mathbb{C}_i}(r,\psi_k)$, arises from the cyclic motion and that the k^{th} blade occupies the position of ψ_k at time t.

It has been noted in *Section* 3.2 that when hub motions are included in the modes, they are also expressible in terms of the generalised coordinates as follows;

$$\underline{H}(\psi) = \sum_{i=1}^{N_c} \eta_{c_i}(\psi)\underline{h}_i \qquad (3.69)$$

where $\underline{h}_i$ is the vector of hub motions in the i^{th} coupled mode and *Eqns.*3.20 & 3.21 must be extended as follows;

$$\frac{\partial}{\partial \dot{\eta}_{c_i}} = \sum \frac{\partial}{\partial \dot{x}} \frac{\partial \dot{x}}{\partial \dot{\eta}_{c_i}} + \frac{\partial}{\partial \dot{H}} \frac{\partial \dot{H}}{\partial \dot{\eta}_{c_i}} \qquad (3.20a)$$

$$\frac{\partial}{\partial \eta_{c_i}} = \sum \frac{\partial}{\partial x} \frac{\partial x}{\partial \eta_{c_i}} + \frac{\partial}{\partial H} \frac{\partial H}{\partial \eta_{c_i}} \qquad (3.20b)$$

Substituting these expressions into the Lagrangian equation will yield two sets of response equations,

$$\frac{d}{dt}\left(\frac{\partial K}{\partial \dot{\eta}_{c_i}}\right) - \frac{\partial K}{\partial \eta_{c_i}} + \frac{\partial U}{\partial \eta_{c_i}} = \frac{\delta W}{\delta \eta_{c_i}} = Q_{c_i} \qquad i=1,2,\ldots,N_c \qquad (3.70a)$$

$$\frac{d}{dt}\left(\frac{\partial K}{\partial \dot{\eta}_{r_i}}\right) - \frac{\partial K}{\partial \eta_{r_i}} + \frac{\partial U}{\partial \eta_{r_i}} = \frac{\delta W}{\delta \eta_{r_i}} = Q_{r_i} \qquad i=1,2,\ldots,N_r \qquad (3.70b)$$

The response equations described by *Eqns.*3.70 are fully coupled. By applying the modes orthogonality relationship, they can be reduced to a set of (N_c) uncoupled modal response equations representing the coupled modes system and (NxN_r) uncoupled equations representing the reactionless system for an N-bladed rotor *ie.* N_r number for each blade. The structures of the response equations are similar but the forcing functions differ. The forcing functions clearly depend on the features modelled in the system modes, any features, not modelled, will subsequently result as RHS forcings. Since the single blade response equation is derived (*Section* 3.2) in such a way that all possible forcings present in the rotor system can be identified, there is no need to invoke the Lagrangian equation twice using *Eqns.*3.70.

For the coupled rotor-fuselage system, we only need to identify the forcing functions which are appropriate for the system modes concerned. Because the reactionless system is hub-fixed, the forcings which are confined to fixed frame *ie.* hub and rate terms will be absent and can be obtained from the single blade equation by removing these terms from the RHS forcings to give Q_{r_i} in *Eqn.*3.70b. Furthermore, the linearised Coriolis terms, if included in the modes, must be removed. Similarly, the response equations for the coupled system modes can be obtained but this time, the linearised hub motion terms are removed from the RHS forcings as they are already included in the modes to give Q_{c_i} in *Eqn.*3.70a. A more detailed treatment will be provided in *Section* 3.5.3.

Before we proceed to obtain these equations, we first need to prove the orthogonality relationship of the complex rotor modes. This is followed by the examination of the effect of this relationship on the solution method. A full report on the orthogonality proof is provided by the author [3.30], only a summary is given here.

3.5.2 Proof of Orthogonality Relationship for The System Modes Defined by CRFD

The orthogonality relationship of the mode shapes is a powerful feature in that it allows a reduced number of these modal vectors to be used in the response analysis. The task of providing a mathematical proof of the orthogonality relationship for the complex rotor modes, configured in a form suitable for the transfer matrix solution method, has proved to be one of the most formidable tasks undertaken within this study. Significant efforts and numerous attempts throughout much of the study were made but a rigorous proof was elusive for some time.

Essentially, the CRFD system equations define the loads equilibrium of the blade in a linearised fashion (*Section* 3.3). It takes the form of a set of first order spatial differential equations in displacements and rotations as well as internal forces and moments at a point along the blade. As noted previously, the CRFD system equations (*Eqns.*3.48) include additional terms *eg.* Coriolis, hub motions or damping terms together with the gyroscopic and centrifugal terms introduced from the multi-blade coordinate transformation. It provides flexibility for varying the modelling complexity for the rotor dynamic system, in which case the forms of system equations would differ. In the absence of damping, the system resembles a gyroscopic system for which an orthogonality relationship exists for the system modes as shown by Meirovitch [3.31]. The viability of this technique depends on the system equation being described by a set of second order differential equations in terms of displacements only with explicit mass, damping and stiffness matrices. It is herein referred to as the *classical form ie.* $m\ddot{x} + c\dot{x} + kx = 0$.

The existing CRFD system equations do not automatically yield the required form. Subsequent discussions and communications with academics [3.32,3.33] revealed that concerted effort would be needed to examine the matrix structure of the system equations. It is only then possible to decide whether any viable proof exists for such a complex system.

A further literature survey has also revealed three important facts:-

(1) All linear dynamical system equations must be reducible to the classical form;

(2) The form of modal orthogonality relationship for the various dynamical systems depends on the type of damping represented; and
(3) A generalised relationship of modal orthogonality must be reducible to all simpler systems.

The proof of a generalised modal orthogonality relationship, known as bi-orthogonality, employing both the left-hand (LH) and the right-hand (RH)-eigenvectors, is first established and is given in *Appendix* D. The CRFD system equations, especially in the presence of hub motions, are not readily reducible to the classical form. The prime effort must be that of converting the system equations into the classical form.

A viable approach to re-configure the CRFD system equations is to use a dynamic stiffness matrix formulation, as suggested by Simpson [3.32]. Essentially, the approach is to establish the elemental stiffness matrix, as well as the inertia (and damping, if any) matrix, between the neighbouring nodes of a continuous system. Thence by assembling these elements, a global system equation in the required classical form can be constructed and the orthogonality proof follows.

a. Structure of The CRFD System Equations

The rotor blade is essentially a continuous system in which the CRFD system equations derived originally are of the form,

$$\left\{\begin{matrix}\underline{U}' \\ \underline{F}'\end{matrix}\right\}_i = \begin{bmatrix} T_{11} & T_{12} \\ T_{21} & T_{22}\end{bmatrix}_i \cdot \left\{\begin{matrix}\underline{U} \\ \underline{F}\end{matrix}\right\}_i$$

ie. the spatial derivative of displacement and forces (state variables) are related to the local variables via the transfer matrix. The constituent matrices $T_{11}, T_{12}, \ldots$ are functions of the structural and inertia properties of the blade system. For system equations of this form, Walker [3.34] has by inspection laid down a sufficient, but not necessary, condition upon which the orthogonality relationship is assured. The proof is furnished by converting the system equations from the form suitable for the transfer matrix solution method to the classical form. The condition is conveniently described by a single matrix equation,

$$\left\{\begin{matrix}\underline{U}' \\ \underline{F}'\end{matrix}\right\}_i = \begin{bmatrix} B & A \\ C & -B^T\end{bmatrix}_i \cdot \left\{\begin{matrix}\underline{U} \\ \underline{F}\end{matrix}\right\}_i \qquad (3.71)$$

where matrices A,B & C (all real) describe the beam properties of which A and C are self-adjoint, $()' = \frac{\partial()}{\partial x}$ and suffix i refers to the i^{th} element. *Eqn.* 3.71 relates the blade displacements and their derivatives and is reversible. This condition implies that all of the sub-sets of CRFD can be converted into the classical form with the nature of the LH-eigenvectors shown in *Table* 3.3 below;

Case	System Description (CRFD System Equivalent)	Frame of Reference	Form of CRFD System Eqn. (Homogeneous)	Nature of eigen-sol'n eigenvalue (λ) eigenvector ($\underline{\phi}$ or $\underline{\Phi}$)	Order of System	Solution
1	Undamped System a) Single Blade (No Coriolis)	Rotating	$m\ddot{\underline{x}} + k\underline{x} = \underline{0}$; c=0	Imaginary Real ($\lambda=-i\omega$ where ω is real)	n 2nd order	$\underline{x} = \underline{\phi}e^{\lambda t}$ $[\gamma]\equiv[\phi]$
2	Symmetrically Damped System b) (a) + Symmetric Damping	Rotating	$m\ddot{\underline{x}} + c\dot{\underline{x}} + k\underline{x} = \underline{0}$; $c^T=c$ $I\dot{\underline{z}} - S\underline{z} = 0$; *ie.* $\begin{bmatrix} I & 0 \\ 0 & I \end{bmatrix}\begin{Bmatrix} \ddot{\underline{x}} \\ \dot{\underline{x}} \end{Bmatrix} - \begin{bmatrix} m^{-1}c & m^{-1}k \\ I & 0 \end{bmatrix}\begin{Bmatrix} \dot{\underline{x}} \\ \underline{x} \end{Bmatrix} = \begin{Bmatrix} \underline{0} \\ \underline{0} \end{Bmatrix}$	Complex Complex	2n 1st order	$\underline{z} = \underline{\Phi}e^{\lambda t}$ $[\Gamma]\equiv[\Phi]$
3	Undamped Gyroscopic System c) Reactionless Modes (Single Blade with Coriolis) ——— or c) Blade ± Coriolis d) Coupled Modes ± Coriolis (Gyroscopic with Hub motion ± Coriolis)	Rotating ——— Fixed Fixed	$m\ddot{\underline{x}} + g\dot{\underline{x}} + k\underline{x} = \underline{0}$; $g^T=-g$ $I\dot{\underline{z}} - S\underline{z} = 0$; *ie.* $\begin{bmatrix} I & 0 \\ 0 & I \end{bmatrix}\begin{Bmatrix} \ddot{\underline{x}} \\ \dot{\underline{x}} \end{Bmatrix} - \begin{bmatrix} -m^{-1}g & -m^{-1}k \\ I & 0 \end{bmatrix}\begin{Bmatrix} \dot{\underline{x}} \\ \underline{x} \end{Bmatrix} = \begin{Bmatrix} \underline{0} \\ \underline{0} \end{Bmatrix}$ or in a special form $B\dot{\underline{z}} - A\underline{z} = \underline{0}$ $\begin{bmatrix} m & 0 \\ 0 & k \end{bmatrix}\begin{Bmatrix} \ddot{\underline{x}} \\ \dot{\underline{x}} \end{Bmatrix} - \begin{bmatrix} -g & -k \\ k & 0 \end{bmatrix}\begin{Bmatrix} \dot{\underline{x}} \\ \underline{x} \end{Bmatrix} = \begin{Bmatrix} \underline{0} \\ \underline{0} \end{Bmatrix}$ *NB*: k must be +ve definite.	Imaginary Complex ——— Imaginary Complex	2n 1st order	$\underline{z} = \underline{\Phi}e^{\lambda t}$ $[\Gamma]\equiv[\Phi]^*$
4	Linearly Damped Gyroscopic System e) Reactionless Modes ——— f) Coupled Modes	Rotating ——— Fixed	$m\ddot{\underline{x}} + b\dot{\underline{x}} + k\underline{x} = \underline{0}$; b general $I\dot{\underline{z}} - S\underline{z} = 0$; *ie.* $\begin{bmatrix} I & 0 \\ 0 & I \end{bmatrix}\begin{Bmatrix} \ddot{\underline{x}} \\ \dot{\underline{x}} \end{Bmatrix} - \begin{bmatrix} -m^{-1}b & -m^{-1}k \\ I & 0 \end{bmatrix}\begin{Bmatrix} \dot{\underline{x}} \\ \underline{x} \end{Bmatrix} = \begin{Bmatrix} \underline{0} \\ \underline{0} \end{Bmatrix}$	Complex Complex	2n 1st order	$\underline{z} = \underline{\Phi}e^{\lambda t}$ $[\Gamma]$=general

Table 3.3: Summary of CRFD System Characteristics

It was noted in *Section* 3.3.3 that the original CRFD system equations DID NOT, in fact, meet Walker's condition and this proved to be the major obstacle in all the previous attempts at establishing the modes orthogonality. The requirement for the system equations to meet Walker's condition prompted an investigation by Juggins [3.35] into the basis of the original formulation. During that process, a number of inconsistencies were identified and corrected in order to meet Walker's condition. The main findings are that the coefficient matrix B_1 is now associated with $\underline{U}'$ (instead of $\underline{F}$) and also that the sequential blade moments (a non-orthogonal set) are now used instead of the original instantaneous set.

In the absence of damping, the revised CRFD system equations in the single (k^{th}) blade form are repeated below;-

$$A_0\underline{U}'_k + A_1\underline{U}_k + A_2\underline{F}_k = \underline{0}$$
$$B_0\underline{F}'_k + B_1\underline{U}'_k + B_2\underline{U}_k + B_3\dot{\underline{U}}_k + B_4\ddot{\underline{U}}_k + (B_{50}+B_{5C}\cos\psi_k+B_{5S}\sin\psi_k)\dot{\underline{H}}$$
$$+ (B_{60}+B_{6C}\cos\psi_k+B_{6S}\sin\psi_k)\ddot{\underline{H}} = \underline{0} \qquad (3.48)$$

where the coefficients matrices (all real 6x 6) possess the following properties;

$A_0^T = A_0$;	$B_0 = I$;	$B_3^T = -B_3$;
A_1 is general;	B_1 is general;	$B_4^T = B_4$;
$A_2 = -I$;	$B_2^T = B_2$;	B_5's and B_6's are general

with $A_1=-B_1^T$. It can be easily demonstrated that *Eqns.*3.48 conforms to *Eqn.*3.71 by considering the equivalent *quasi-steady* form *ie.*

$$A_0\underline{U}' + A_1\underline{U} + A_2\underline{F} = \underline{0}$$
$$B_0\underline{F}' + B_1\underline{U}' + B_2\underline{U} = \underline{0}$$

where the suffix k is dropped for clarity. After re-arranging and substituting $A_2=-I$ and $B_0=I$, we get

$$\begin{Bmatrix}\underline{U}'\\ \underline{F}'\end{Bmatrix} = \begin{bmatrix} -A_0^{-1}A_1 & A_0^{-1} \\ B_1A_0^{-1}A_1-B_2 & -B_1A_0^{-1}\end{bmatrix}\begin{Bmatrix}\underline{U}\\ \underline{F}\end{Bmatrix} = \begin{bmatrix} B & A \\ C & -B^T\end{bmatrix}\begin{Bmatrix}\underline{U}\\ \underline{F}\end{Bmatrix} \qquad (3.72)$$

using the matrix properties,

$$A = A_0^{-1}$$
$$B = -A_0^{-1}A_1 \quad [ie.\ -B^T=(A_0^{-1}A_1)^T=A_1^T(A_0^{-1})^T=A_1^T(A_0^T)^{-1}=A_1^TA_0^{-1}=-B_1A_0^{-1}]$$
$$C = B_1A_0^{-1}A_1-B_2 = C^T \qquad (3.73)$$

Thus Walker's condition is met.

b. Conversion of CRFD System Equations into The Classical Form using The Dynamic Stiffness Matrix Formulation

In order to perform the conversion of the system equations into the classical form, it is necessary to invoke an integration scheme. It is concluded in [3.35] that the only requirement is that the integration scheme is reversible in order to ensure the solution is independent of the direction in which it is progressed. A slope averaging integration scheme is adopted, but it should not be regarded as the only one possible.

Define the slope average integration scheme (from tip to root) between two neighbouring nodes, Stations i and i+1, as

$$\underline{U}_{i+1} = \underline{U}_i + \frac{\delta x}{2}(\underline{U}'_{i+1} + \underline{U}'_i)$$

$$\underline{F}_{i+1} = \underline{F}_i + \frac{\delta x}{2}(\underline{F}'_{i+1} + \underline{F}'_i) \qquad (3.74)$$

Substituting *Eqn.*3.71 into *Eqns.*3.74 yields

$$\underline{U}_{i+1} = \underline{U}_i + \frac{\delta x}{2}(B\underline{U}_{i+1} + A\underline{F}_{i+1} + B\underline{U}_i + A\underline{F}_i)$$

$$\underline{F}_{i+1} = \underline{F}_i + \frac{\delta x}{2}(C\underline{U}_{i+1} - B^T\underline{F}_{i+1} + C\underline{U}_i - B^T\underline{F}_i)$$

Re-arranging,

$$[I - \frac{\delta x}{2}B\ ]\underline{U}_{i+1} = [I + \frac{\delta x}{2}B\ ]\underline{U}_i + \frac{\delta x}{2}A\underline{F}_{i+1} + \frac{\delta x}{2}A\underline{F}_i$$

$$[I + \frac{\delta x}{2}B^T]\underline{F}_{i+1} = [I - \frac{\delta x}{2}B^T]\underline{F}_i + \frac{\delta x}{2}C\underline{U}_{i+1} + \frac{\delta x}{2}C\underline{U}_i$$

Expressing this in a conventional finite element formulation *ie.* introducing $-\underline{F}_i$ as a state vector, results in

$$\begin{bmatrix} \frac{\delta x}{2}A & -\frac{\delta x}{2}A \\ I-\frac{\delta x}{2}B^T & I+\frac{\delta x}{2}B^T \end{bmatrix} \begin{Bmatrix} -\underline{F}_i \\ \underline{F}_{i+1} \end{Bmatrix} = \begin{bmatrix} I+\frac{\delta x}{2}B & -(I-\frac{\delta x}{2}B) \\ \frac{\delta x}{2}C & \frac{\delta x}{2}C \end{bmatrix} \begin{Bmatrix} \underline{U}_i \\ \underline{U}_{i+1} \end{Bmatrix} \qquad (3.75)$$

For illustrative purpose, one can choose δx such that $\frac{\delta x}{2}$ =1, then

$$\begin{bmatrix} A & -A \\ I-B^T & I+B^T \end{bmatrix} \begin{Bmatrix} -\underline{F}_i \\ \underline{F}_{i+1} \end{Bmatrix} = \begin{bmatrix} I+B & B-I \\ C & C \end{bmatrix} \begin{Bmatrix} \underline{U}_i \\ \underline{U}_{i+1} \end{Bmatrix}$$

$$\begin{Bmatrix} -\underline{F}_i \\ \underline{F}_{i+1} \end{Bmatrix} = \begin{bmatrix} A & -A \\ I-B^T & I+B^T \end{bmatrix}^{-1} \begin{bmatrix} I+B & B-I \\ C & C \end{bmatrix} \begin{Bmatrix} \underline{U}_i \\ \underline{U}_{i+1} \end{Bmatrix}$$

The inversion can be carried out using the method of sub-matrices *eg.* Collar & Simpson [3.36]

$$\begin{Bmatrix} -\underline{F}_i \\ \underline{F}_{i+1} \end{Bmatrix} = \frac{1}{2} \begin{bmatrix} (I+B^T)A^{-1} & I \\ (B^T-I)A^{-1} & I \end{bmatrix} \begin{bmatrix} I+B & B-I \\ C & C \end{bmatrix} \begin{Bmatrix} \underline{U}_i \\ \underline{U}_{i+1} \end{Bmatrix}$$

$$= [K_e] \begin{Bmatrix} \underline{U}_i \\ \underline{U}_{i+1} \end{Bmatrix} \qquad (3.76)$$

On expanding $[K_e]$,

$$[K_e] = \frac{1}{2}\begin{bmatrix} (I+B^T)A^{-1} & I \\ (B^T-I)A^{-1} & I \end{bmatrix} \begin{bmatrix} I+B & B-I \\ C & C \end{bmatrix} = \begin{bmatrix} (I+B^T)A^{-1}(I+B)+C & (I+B^T)A^{-1}(B-I)+C \\ (B^T-I)A^{-1}(I+B)+C & (B^T-I)A^{-1}(B-I)+C \end{bmatrix}$$

and its transpose,

$$[K_e]^T = \frac{1}{2}\begin{bmatrix} I+B^T & C \\ B^T-I & C \end{bmatrix} \begin{bmatrix} A^{-1}(I+B) & A^{-1}(B-I) \\ I & I \end{bmatrix} = \begin{bmatrix} (I+B^T)A^{-1}(I+B)+C & (I+B^T)A^{-1}(B-I)+C \\ (B^T-I)A^{-1}(I+B)+C & (B^T-I)A^{-1}(B-I)+C \end{bmatrix}$$

$$= [K_e]$$

where $C^T=C$ and $(A^{-1})^T=(A^T)^{-1}= A^{-1}$ are used. Using *Eqns.*3.72, $[K_e]$ can be expressed in terms of the CRFD coefficient matrices as

$$\left[K_e\right] = \begin{bmatrix} (A_0-B_2)-(A_1-A_1^T) & -(A_0+B_2)+(A_1^T-A_1) \\ -(A_0+B_2)+(A_1-A_1^T) & (A_0-B_2)+(A_1-A_1^T) \end{bmatrix} = \begin{bmatrix} \alpha & \beta \\ \beta^T & \gamma \end{bmatrix} \qquad (3.77)$$

It is apparent that the 12x12 elemental stiffness matrix $[K_e]$ is symmetric. Past experiences indicate that it is useful to know the algebraic form of $[K_e]$ in terms of the blade properties as this can often provide physical insight. However, an attempt to evaluate $[K_e]$ algebraically using the known coefficient matrices has proved to be extremely cumbersome. Even for a straight blade without any section centre offsets, $[K_e]$ is fully populated with lengthy expressions of structural and inertia properties. One must therefore revert to numerical evaluation. This implies that any orthogonality relationship subsequently identified cannot be easily expressed algebraically without extensive manipulation. However, the fact that conversion of the system equations is possible enables one to proceed.

c. System Equations for The Undamped Reactionless Modes

The above conversion process can be easily extended for the undamped reactionless mode system equations, where $\underline{H}=\underline{0}$. *Eqns.*3.52 are repeated below,

$$\begin{aligned} &A_0\underline{U}_k' + A_1\underline{U}_k + A_2\underline{F}_k = \underline{0} \\ &B_0\underline{F}_k' + B_1\underline{U}_k' + B_2\underline{U}_k + B_3\dot{\underline{U}}_k + B_4\ddot{\underline{U}}_k = \underline{0} \end{aligned} \qquad (3.52)$$

Using the above procedure, one obtains

$$\begin{aligned} \begin{Bmatrix} \underline{U}' \\ \underline{F}' \end{Bmatrix} &= \begin{bmatrix} -A_0^{-1}A_1 & A_0^{-1} \\ B_1A_0^{-1}A_1-B_2 & -B_1A_0^{-1} \end{bmatrix} \begin{Bmatrix} \underline{U} \\ \underline{F} \end{Bmatrix} + \begin{bmatrix} 0 \\ -B_3 \end{bmatrix} \begin{Bmatrix} \dot{\underline{U}} \end{Bmatrix} + \begin{bmatrix} 0 \\ -B_4 \end{bmatrix} \begin{Bmatrix} \ddot{\underline{U}} \end{Bmatrix} \\ &= \begin{bmatrix} B & A \\ C & -B^T \end{bmatrix} \begin{Bmatrix} \underline{U} \\ \underline{F} \end{Bmatrix} + \begin{bmatrix} 0 \\ -B_3 \end{bmatrix} \begin{Bmatrix} \dot{\underline{U}} \end{Bmatrix} + \begin{bmatrix} 0 \\ -B_4 \end{bmatrix} \begin{Bmatrix} \ddot{\underline{U}} \end{Bmatrix} \end{aligned} \qquad (3.78)$$

By inspection, *Eqn.*3.78 also conforms to Walker's condition (*Eqn.*3.71), with C being modified to be $\hat{C} = C-\lambda B_3-\lambda^2 B_4$ and λ is complex, *ie.* $\hat{C}$ is Hermitian: $X=Y+iZ$ with and $Y^T=Y, Z^T=-Z$ and is self-adjoint. Applying the reversible integration scheme as before, one obtains,

$$[I - \frac{\delta x}{2}B\ ]\underline{U}_{i+1} = [I + \frac{\delta x}{2}B\ ]\underline{U}_i + \frac{\delta x}{2}A\underline{F}_{i+1} + \frac{\delta x}{2}A\underline{F}_i$$

$$[I + \frac{\delta x}{2}B^T]\underline{F}_{i+1} = [I - \frac{\delta x}{2}B^T]\underline{F}_i + \frac{\delta x}{2}C(\underline{U}_{i+1}+\underline{U}_i) - \frac{\delta x}{2}B_3(\dot{\underline{U}}_{i+1} + \dot{\underline{U}}_i)$$

$$- \frac{\delta x}{2}B_4(\ddot{\underline{U}}_{i+1} + \ddot{\underline{U}}_i)$$

or when $\frac{\delta x}{2}$ =1,

$$\begin{bmatrix} A & -A \\ I-B^T & I+B^T \end{bmatrix}\begin{Bmatrix} -\underline{F}_i \\ \underline{F}_{i+1} \end{Bmatrix} = \begin{bmatrix} I+B & B-I \\ C & C \end{bmatrix}\begin{Bmatrix} \underline{U}_i \\ \underline{U}_{i+1} \end{Bmatrix} + \begin{bmatrix} 0 & 0 \\ -B_3 & -B_3 \end{bmatrix}\begin{Bmatrix} \dot{\underline{U}}_i \\ \dot{\underline{U}}_{i+1} \end{Bmatrix} \begin{bmatrix} 0 & 0 \\ -B_4 & -B_4 \end{bmatrix}\begin{Bmatrix} \ddot{\underline{U}}_i \\ \ddot{\underline{U}}_{i+1} \end{Bmatrix}$$

$$[L]\begin{Bmatrix} -\underline{F}_i \\ \underline{F}_{i+1} \end{Bmatrix} = [P]\begin{Bmatrix} \underline{U}_i \\ \underline{U}_{i+1} \end{Bmatrix} + [Q]\begin{Bmatrix} \dot{\underline{U}}_i \\ \dot{\underline{U}}_{i+1} \end{Bmatrix} + [R]\begin{Bmatrix} \ddot{\underline{U}}_i \\ \ddot{\underline{U}}_{i+1} \end{Bmatrix}$$

$$\begin{Bmatrix} -\underline{F}_i \\ \underline{F}_{i+1} \end{Bmatrix} = [L]^{-1}[P]\begin{Bmatrix} \underline{U}_i \\ \underline{U}_{i+1} \end{Bmatrix} + [L]^{-1}[Q]\begin{Bmatrix} \dot{\underline{U}}_i \\ \dot{\underline{U}}_{i+1} \end{Bmatrix} + [L]^{-1}[R]\begin{Bmatrix} \ddot{\underline{U}}_i \\ \ddot{\underline{U}}_{i+1} \end{Bmatrix}$$

$$= [K_e]\begin{Bmatrix} \underline{U}_i \\ \underline{U}_{i+1} \end{Bmatrix} + [C_e]\begin{Bmatrix} \dot{\underline{U}}_i \\ \dot{\underline{U}}_{i+1} \end{Bmatrix} + [M_e]\begin{Bmatrix} \ddot{\underline{U}}_i \\ \ddot{\underline{U}}_{i+1} \end{Bmatrix} \qquad (3.79)$$

where from *Eqn.*3.76, $[L]^{-1}=\frac{1}{2}\begin{bmatrix} (I+B^T)A^{-1} & I \\ (B^T-I)A^{-1} & I \end{bmatrix}$ and $[K_e]$ is the elemental symmetric stiffness matrix given by *Eqn.*3.77 and the corresponding damping and inertia matrices are

$$[C_e] = [L]^{-1}[Q] = \frac{1}{2}\begin{bmatrix} -B_3 & -B_3 \\ -B_3 & -B_3 \end{bmatrix} = -[C_e]^T$$

$$[M_e] = [L]^{-1}[R] = \frac{1}{2}\begin{bmatrix} -B_4 & -B_4 \\ -B_4 & -B_4 \end{bmatrix} = [M_e]^T$$

Noting that $B_3=-B_3^T$ and $B_4=B_4^T$, it is apparent that $[C_e]$ and $[M_e]$ are skew-symmetric and symmetric respectively. It is interesting to point out here that both $[C_e]$ and $[M_e]$ are 6-fold degenerate (rank=6) but this is of no particular concern. It is merely the result of the deployment of a reversible integration scheme where the mass is concentrated at the mid-point of each element and zero at each end. Other reversible schemes can of course be employed instead.

On assembling, the global system equation becomes;

$$\begin{Bmatrix} \underline{F}_{tip}=\underline{0} \\ \vdots \\ \underline{0} \\ \underline{0} \\ \vdots \\ \underline{F}_0 \end{Bmatrix} = \begin{bmatrix} & \begin{bmatrix} \begin{bmatrix} \end{bmatrix} \end{bmatrix} & \\ & & \end{bmatrix} \begin{Bmatrix} \underline{U}_{tip} \\ \vdots \\ \underline{U}_i \\ \underline{U}_{i+1} \\ \vdots \\ \underline{U}_0 \end{Bmatrix} + \begin{bmatrix} & \begin{bmatrix} \begin{bmatrix} \end{bmatrix} \end{bmatrix} & \\ & & \end{bmatrix} \begin{Bmatrix} \dot{\underline{U}}_{tip} \\ \vdots \\ \dot{\underline{U}}_i \\ \dot{\underline{U}}_{i+1} \\ \vdots \\ \dot{\underline{U}}_0 \end{Bmatrix}$$

$$+ \begin{bmatrix} & \begin{bmatrix} \begin{bmatrix} \end{bmatrix} \end{bmatrix} & \\ & & \end{bmatrix} \begin{Bmatrix} \ddot{\underline{U}}_{tip} \\ \vdots \\ \ddot{\underline{U}}_i \\ \ddot{\underline{U}}_{i+1} \\ \vdots \\ \ddot{\underline{U}}_0 \end{Bmatrix}$$

or

$$M\,\ddot{\underline{U}}_B + C\,\dot{\underline{U}}_B + K\,\underline{U}_B = \underline{F} \tag{3.80}$$

where $\underline{U}_B$ is the 6nx1 global state vector for the blade and each [ ] is a square matrix of order 12. Suffices tip,0 refer to the tip and root values respectively. It is noted that the force vector $\underline{F}$ is everywhere zero (including the tip) except at the root $\underline{F}_0 \neq \underline{0}$ where the geometric boundary condition is applied. Thus, the required classical form is obtained and the orthogonality relationship follows immediately.

d. System Equations for The Undamped Coupled Modes

It has been shown that the system equations for the undamped blade and reactionless modes, both defined in the rotating frame, can be converted to the classical form and that the LH-eigenvectors are known in relation to the RH-eigenvectors (*Table* 3.1). However, for the coupled modes system with hub motions included, the dynamic characteristics are to be solved in the fixed frame, further consideration is required.

Eqns.3.53 can be re-expressed as 3 sets of coupled matrix equations,

$$\begin{Bmatrix} \underline{U}_0' \\ \underline{F}_0' \end{Bmatrix} = \begin{bmatrix} B & A \\ C & -B^T \end{bmatrix} \begin{Bmatrix} \underline{U}_0 \\ \underline{F}_0 \end{Bmatrix} + \begin{bmatrix} 0 \\ -B_3 \end{bmatrix} \{\dot{\underline{U}}_0\} + \begin{bmatrix} 0 \\ -B_4 \end{bmatrix} \{\ddot{\underline{U}}_0\} + \begin{bmatrix} 0 \\ -B_{50} \end{bmatrix} \{\dot{\underline{H}}\} + \begin{bmatrix} 0 \\ -B_{60} \end{bmatrix} \{\ddot{\underline{H}}\}$$

$$\begin{Bmatrix} \underline{U}_C' \\ \underline{F}_C' \end{Bmatrix} = \begin{bmatrix} B & A \\ C & -B^T \end{bmatrix} \begin{Bmatrix} \underline{U}_C \\ \underline{F}_C \end{Bmatrix} + \begin{bmatrix} 0 \\ -B_3 \end{bmatrix} \{\dot{\underline{U}}_C + \Omega \underline{U}_S\} + \begin{bmatrix} 0 \\ -B_4 \end{bmatrix} \{\ddot{\underline{U}}_C + 2\Omega \dot{\underline{U}}_S - \Omega^2 \underline{U}_C\} + \begin{bmatrix} 0 \\ -B_{5C} \end{bmatrix} \{\dot{\underline{H}}\} + \begin{bmatrix} 0 \\ -B_{6C} \end{bmatrix} \{\ddot{\underline{H}}\}$$

$$\begin{Bmatrix}\underline{U}_S'\\ \underline{F}_S'\end{Bmatrix}=\begin{bmatrix}B & A\\ C & -B^T\end{bmatrix}\begin{Bmatrix}\underline{U}_C\\ \underline{F}_C\end{Bmatrix}+\begin{bmatrix}0\\ -B_3\end{bmatrix}\left\{\dot{\underline{U}}_S-\Omega\underline{U}_C\right\}+\begin{bmatrix}0\\ -B_4\end{bmatrix}\left\{\ddot{\underline{U}}_S-2\Omega\dot{\underline{U}}_C-\Omega^2\underline{U}_S\right\}+\begin{bmatrix}0\\ -B_{5S}\end{bmatrix}\left\{\dot{\underline{H}}\right\}+\begin{bmatrix}0\\ -B_{6S}\end{bmatrix}\left\{\ddot{\underline{H}}\right\} \tag{3.81}$$

where matrices A,B,C are those defined in *Eqn.*3.73. When assembled in sub-global matrix form, the following equations are obtained,

$$\begin{Bmatrix}\underline{U}_0'\\ \underline{U}_C'\\ \underline{U}_S'\\ \underline{F}_0'\\ \underline{F}_C'\\ \underline{F}_S'\end{Bmatrix}=\begin{bmatrix}B & & & A & & \\ & B & & & A & \\ & & B & & & A\\ C & & & -B^T & & \\ & C+\Omega^2B_4 & -\Omega B_3 & & -B^T & \\ & \Omega B_3 & C+\Omega^2B_4 & & & -B^T\end{bmatrix}\begin{Bmatrix}\underline{U}_0\\ \underline{U}_C\\ \underline{U}_S\\ \underline{F}_0\\ \underline{F}_C\\ \underline{F}_S\end{Bmatrix}+\begin{bmatrix}-B_3 & & \\ & -B_3 & -2\Omega B_4\\ & 2\Omega B_4 & -B_3\end{bmatrix}\begin{Bmatrix}\dot{\underline{U}}_0\\ \dot{\underline{U}}_C\\ \dot{\underline{U}}_S\end{Bmatrix}$$
$$+\begin{bmatrix}-B_4 & & \\ & -B_4 & \\ & & -B_4\end{bmatrix}\begin{Bmatrix}\ddot{\underline{U}}_0\\ \ddot{\underline{U}}_C\\ \ddot{\underline{U}}_S\end{Bmatrix}+\begin{bmatrix}0\\ 0\\ 0\\ -B_{50}\\ -B_{5C}\\ -B_{5S}\end{bmatrix}\dot{\underline{H}}+\begin{bmatrix}0\\ 0\\ 0\\ -B_{60}\\ -B_{6C}\\ -B_{6S}\end{bmatrix}\ddot{\underline{H}} \tag{3.82}$$

where each of the elements is a square matrix of order 6 and the blank elements are null matrices. Re-expressing this in the form of *Eqn.*3.80 yields,

$$\begin{Bmatrix}\underline{U}_{\mathbb{C}}'\\ \underline{F}_{\mathbb{C}}'\end{Bmatrix}=\begin{bmatrix}\mathbb{B} & \mathbb{A}\\ \mathbb{C} & -\mathbb{B}^T\end{bmatrix}\begin{Bmatrix}\underline{U}_{\mathbb{C}}\\ \underline{F}_{\mathbb{C}}\end{Bmatrix}+\begin{bmatrix}0\\ -\mathbb{B}_3\end{bmatrix}\left\{\dot{\underline{U}}_{\mathbb{C}}\right\}+\begin{bmatrix}0\\ -\mathbb{B}_4\end{bmatrix}\left\{\ddot{\underline{U}}_{\mathbb{C}}\right\}+\begin{bmatrix}0\\ -\mathbb{B}_5\end{bmatrix}\left\{\dot{\underline{H}}\right\}+\begin{bmatrix}0\\ -\mathbb{B}_6\end{bmatrix}\left\{\ddot{\underline{H}}\right\} \tag{3.83}$$

where $\underline{U}_{\mathbb{C}}=\begin{Bmatrix}\underline{U}_0\\ \underline{U}_C\\ \underline{U}_S\end{Bmatrix}$, $\underline{F}_{\mathbb{C}}=\begin{Bmatrix}\underline{F}_0\\ \underline{F}_C\\ \underline{F}_S\end{Bmatrix}$ and the matrices $\mathbb{A}=\begin{bmatrix}A & 0 & 0\\ 0 & A & 0\\ 0 & 0 & A\end{bmatrix}$, $\mathbb{C}=\begin{bmatrix}C & 0 & 0\\ 0 & C+\Omega^2B_4 & -\Omega B_3\\ 0 & -\Omega B_3 & C+\Omega^2B_4\end{bmatrix}$

which are still self-adjoint. Thus Walker's condition is maintained in the (18x18) matrices $\mathbb{A},\mathbb{B},\mathbb{C}$'s. When $\underline{H}=\underline{0}$, *Eqn.*3.83 is directly analogous to *Eqn.*3.78 and must therefore represent the system equations for the reactionless modes, being transformed into the fixed frame. As the reactionless modes possess the orthogonality relationship in the rotating frame, this must also be true when the system equations are transformed into the fixed frame since the multi-blade coordinate transformation (*Eqn.*3.45) is itself orthogonal.

However, in the presence of hub motion, it is not obvious that *Eqn.*3.82 is readily expressible in the classical form. It is recalled that the blade motion defined by CRFD is relative to the moving hub. It is shown in *Appendix* E that the following relationship between the relative and total (absolute) blade displacement holds;

$$\begin{Bmatrix} \underline{U}_O \\ \underline{U}_C \\ \underline{U}_S \end{Bmatrix}_T = \begin{Bmatrix} \underline{U}_O \\ \underline{U}_C \\ \underline{U}_S \end{Bmatrix}_R + \begin{bmatrix} [HO] \\ [HC] \\ [HS] \end{bmatrix} \underline{H}$$

or

$$\underline{U}_{C_T} = \underline{U}_{C_R} + [HM]\ \underline{H} \tag{3.84}$$

where the suffices T,R refer to the total and relative quantities. The matrix [HM] and its constituents are defined in *Appendix* E for a straight blade with coincidental blade centres. To ensure the orthogonality relationship holds for the coupled mode system, the system equations (*Eqn.*3.82) must also be reducible to a form similar to *Eqn.*3.80. Now express *Eqn.*3.82 in terms of the absolute blade displacement, and in so doing, the hub motion terms will be implicit in the total displacement vector and the displacement at the centre line will, in effect, be the hub displacements.

$$\begin{Bmatrix} \underline{U}'_{O_R}+[HO]'\underline{H} \\ \underline{U}'_{C_R}+[HC]'\underline{H} \\ \underline{U}'_{S_R}+[HS]'\underline{H} \\ \underline{F}'_O \\ \underline{F}'_C \\ \underline{F}'_S \end{Bmatrix} = \begin{bmatrix} B & & & A & & \\ & B & & & A & \\ & & B & & & A \\ C & & & -B^T & & \\ & C+\Omega^2B_4 & -\Omega B_3 & & -B^T & \\ & \Omega B_3 & C+\Omega^2B_4 & & & -B^T \end{bmatrix} \begin{Bmatrix} \underline{U}_{O_R}+[HO]\underline{H} \\ \underline{U}_{C_R}+[HC]\underline{H} \\ \underline{U}_{S_R}+[HS]\underline{H} \\ \underline{F}_O \\ \underline{F}_C \\ \underline{F}_S \end{Bmatrix}$$

$$+ \begin{bmatrix} -B_3 & & \\ & -B_3 & -2\Omega B_4 \\ & 2\Omega B_4 & -B_3 \end{bmatrix} \begin{Bmatrix} \dot{\underline{U}}_{O_R}+[HO]\dot{\underline{H}} \\ \dot{\underline{U}}_{C_R}+[HC]\dot{\underline{H}} \\ \dot{\underline{U}}_{S_R}+[HS]\dot{\underline{H}} \end{Bmatrix} + \begin{bmatrix} -B_4 & & \\ & -B_4 & \\ & & -B_4 \end{bmatrix} \begin{Bmatrix} \ddot{\underline{U}}_{O_R}+[HO]\ddot{\underline{H}} \\ \ddot{\underline{U}}_{C_R}+[HC]\ddot{\underline{H}} \\ \ddot{\underline{U}}_{S_R}+[HS]\ddot{\underline{H}} \end{Bmatrix} \tag{3.85}$$

*Eqn.*3.85 must be interchangeable with that of *Eqn.*3.83 and matrices B_5's and B_6's are related to the matrices B_3, B_4 when appropriate ordering is imposed (*Appendix* E).

$$\begin{aligned} -B_3[HO] &= -B_{50} \\ -B_3[HC] - 2\Omega B_4[HS] &= -B_{5C} \\ -B_3[HS] + 2\Omega B_4[HC] &= -B_{5S} \\ -B_4[HO] &= -B_{60} \\ -B_4[HC] &= -B_{6C} \\ -B_4[HS] &= -B_{6S} \end{aligned} \tag{3.86}$$

Even when this substitution is applied, there are residual $\underline{H}$ terms in *Eqn.*3.85. Since the hub terms are perturbatory in the CRFD system *ie.* only $\dot{\underline{H}}, \ddot{\underline{H}}$ terms exist, there will be no steady state $\underline{H}$ terms. Bearing

this in mind, the original equation *Eqn.*3.83 is recovered. This is not at all surprising as the physics of dynamic system cannot be altered, the system equations are only described by a different set of coordinates. Clearly the above relationship can be easily generalised to a blade with pre-deformations and section centre offsets.

Thus *Eqn.*3.85 can be re-expressed in terms of the total displacement vector (*ie.* $\underline{H}$ is implicit in $\underline{U}$) as

$$\begin{Bmatrix} \underline{U}_0' \\ \underline{U}_C' \\ \underline{U}_S' \\ \underline{F}_0' \\ \underline{F}_C' \\ \underline{F}_S' \end{Bmatrix}_T = \begin{bmatrix} B & & & & A & & \\ & B & & & & A & \\ & & B & & & & A \\ C & & & & -B^T & & \\ & C+\Omega^2 B_4 & -\Omega B_3 & & & -B^T & \\ & \Omega B_3 & C+\Omega^2 B_4 & & & & -B^T \end{bmatrix} \begin{Bmatrix} \underline{U}_0 \\ \underline{U}_C \\ \underline{U}_S \\ \underline{F}_0 \\ \underline{F}_C \\ \underline{F}_S \end{Bmatrix}_T + \begin{bmatrix} -B_3 & & \\ & -B_3 & -2\Omega B_4 \\ & 2\Omega B_4 & -B_3 \end{bmatrix} \begin{Bmatrix} \dot{\underline{U}}_0 \\ \dot{\underline{U}}_C \\ \dot{\underline{U}}_S \end{Bmatrix}_T$$

$$+ \begin{bmatrix} -B_4 & & \\ & -B_4 & \\ & & -B_4 \end{bmatrix} \begin{Bmatrix} \ddot{\underline{U}}_0 \\ \ddot{\underline{U}}_C \\ \ddot{\underline{U}}_S \end{Bmatrix}_T$$

or

$$\begin{Bmatrix} \underline{U}_{\mathbb{C}}' \\ \underline{F}_{\mathbb{C}}' \end{Bmatrix}_T = \begin{bmatrix} \mathbb{B} & \mathbb{A} \\ \mathbb{C} & -\mathbb{B}^T \end{bmatrix} \begin{Bmatrix} \underline{U}_{\mathbb{C}} \\ \underline{F}_{\mathbb{C}} \end{Bmatrix}_T + \begin{bmatrix} 0 \\ -\mathbb{B}_3 \end{bmatrix} \{ \dot{\underline{U}}_{\mathbb{C}} \}_T + \begin{bmatrix} 0 \\ -\mathbb{B}_4 \end{bmatrix} \{ \ddot{\underline{U}}_{\mathbb{C}} \}_T \qquad (3.87)$$

which is of the identical form as *Eqn.*3.78. By applying the same technique shown in *Section* 3.5.2c, the classical form is obtained,

$$\begin{Bmatrix} \underline{F}_{\mathbb{C}tip}=\underline{0} \\ \vdots \\ \underline{0} \\ \underline{0} \\ \vdots \\ \underline{F}_{\mathbb{C}o} \end{Bmatrix} = \begin{bmatrix} & & \\ & \left[\begin{bmatrix} & \\ & \end{bmatrix} \right] & \\ & & \end{bmatrix} \begin{Bmatrix} \underline{U}_{\mathbb{C}tip} \\ \vdots \\ \underline{U}_{\mathbb{C}i} \\ \underline{U}_{\mathbb{C}i+1} \\ \vdots \\ \underline{U}_{\mathbb{C}o} \end{Bmatrix} + \begin{bmatrix} & & \\ & \left[\begin{bmatrix} & \\ & \end{bmatrix} \right] & \\ & & \end{bmatrix} \begin{Bmatrix} \dot{\underline{U}}_{\mathbb{C}tip} \\ \vdots \\ \dot{\underline{U}}_{\mathbb{C}i} \\ \dot{\underline{U}}_{\mathbb{C}i+1} \\ \vdots \\ \dot{\underline{U}}_{\mathbb{C}o} \end{Bmatrix}$$

$$+ \begin{bmatrix} & & \\ & \left[\begin{bmatrix} & \\ & \end{bmatrix} \right] & \\ & & \end{bmatrix} \begin{Bmatrix} \ddot{\underline{U}}_{\mathbb{C}tip} \\ \vdots \\ \ddot{\underline{U}}_{\mathbb{C}i} \\ \ddot{\underline{U}}_{\mathbb{C}i+1} \\ \vdots \\ \ddot{\underline{U}}_{\mathbb{C}o} \end{Bmatrix}$$

or

$$\mathbb{M}\ddot{\underline{U}}_{\mathbb{C}_T} + \mathbb{C}\dot{\underline{U}}_{\mathbb{C}_T} + \mathbb{K}\underline{U}_{\mathbb{C}_T} = \underline{F}_{\mathbb{C}} \qquad (3.88)$$

where $\mathbb{M},\mathbb{K}$ are the global (banded diagonal) symmetric mass, stiffness matrices and $\mathbb{C}$ is the skew-symmetric velocity matrix *ie.* the coupled modes system without damping also resembles the gyroscopic system. The exercise here has provided two important conclusions:-

(1) It has been proved possible to convert the system equations into the classical form and the required LH-eigenvectors can be deduced from the conventional system characteristics; and

(2) The orthogonality relationship of the coupled modes is thus assured even if the modes are still obtained using the transfer matrix solution method.

Thus prior to the use of damped modes, which is not anticipated for some time, the modes obtained using the existing transfer matrix solution method remain valid.

However, it must be stressed here that the need to use absolute coordinates is primarily to ensure that the conversion is feasible. This is not a necessary condition for the orthogonality proof, should the system equation be derived as an eigenvalue problem using relative blade and hub displacement.

e. System Equations for The Blade, Coupled and Reactionless Modes with General Damping

The conversion of the system equation in transfer matrix form into the classical form has been demonstrated for the systems of blade, reactionless and coupled modes without damping. These systems considered belong to the specific types in which the required LH-eigenvectors can be identified without actually being evaluated. Thus the transfer matrix solution method, currently adopted for the CRFD analysis, can be retained. However, this will no longer be the case for any of the systems when general damping is present *ie.* the velocity matrix $[B_3]$ does not have any special properties. Although the above technique of conversion can be employed, the LH-eigenvectors must be determined by other means. Two further important conclusions can be drawn from this observation;

Either

(1) All the RH-eigenvectors must be determined in order that the similarity transformation (*Appendix* D) can be used to uncouple the forced response equation;

or

(2) One must formulate the system equations for these cases with general damping as an eigenvalue problem at the outset.

Neither method seems particularly favourable at this stage as the first is not computationally feasible and the second requires a fundamental change of solution method for the CRFD system equation. However, in the long term, the eigenvalue problem formulation approach would be a far better choice. Not only will it assure the orthogonality relationship, but it will also allow the use of standard algorithms, which are readily available, in solving the system dynamic characteristics. It is strongly recommended that the approach using eigen-formulation should be adopted in CRFD[1].

3.5.3 Complex Mode Response Equation in Modal Form - An Orthogonalisation Process

Having established that the various system modes defined by CRFD do possess the required orthogonality relationship, we proceed to examine its application in the forced response equation. Let us first recall a number of key issues:

(1) The Lagrangian equation derived in *Section* 3.2 is valid for a single blade on the basis that the blade motions are modally represented using a set of real blade modes (*Eqn.*3.1);

(2) The complete blade motion can be described in terms of both coupled and reactionless mode responses (*Eqns.*3.68 & 3.69); and

(3) The orthogonality relationship for the complex modes is available only in numerical form. Although a mathematical derivation of the mode orthogonality relationship for the real blade modes system is furnished in *Appendix* F, the algebraic evaluation process is still far from straightforward.

---

1 As a result, the CRFD system has been re-formulated as an eigenvalue problem by Holton [3.37]. However, it is currently limited to only a small number of spanwise stations for the blade properties definition because of computer storage problem. Refinements are still required before it is fully operational.

To derive the system response equations modelled with complex rotor modes, one can proceed in the same manner as CRFD. This can be achieved by transforming the blade coordinates into the rotor coordinates and then applying the Lagrangian equation in terms of complex rotor modes as in *Eqns.*3.70. However the algebraic process will be extremely laborious and instead, we employ a process termed as orthogonalisation.

The CRFD system solves the free response of the coupled rotor-fuselage system about a steady state, and provides a set of modes (state vectors) to be used in CRFA. CRFA identifies *all* the possible forcings, including those not modelled by CRFD. By subtracting the steady state and linear terms from the forcings derived for CRFA, the additional forcings present in the response equations can be defined. These additional forcings are essentially the non-linear, perturbatory aerodynamic, time varying and rigid body motion terms. Although the two system equations are derived independently using different assumptions, they are the same systems. Based upon the same assumptions, the two systems must be identical.

Hence the process of deriving the modal response equations for the various mode types reduces to one of identifying the RHS forcing terms in the exact manner. This process is best described as a reversed Hamiltonian Principle by which the modal Lagrangian equation can be constructed, if necessary. This avoids the need to derive different system response equations for each mode type considered. And by applying the mode orthogonality, the system response equation can be further reduced to the uncoupled modal form, suitable for a solution. Although for the case of complex modes, one needs to reduce the system response equation to the first order form, this is only a numerical process by which the modal response solution can be obtained.

This orthogonalisation process has a number of advantages;

(1) It simplifies the algebraic derivation process;

(2) It correctly identifies the RHS forcings for the forced response equations for all mode types used; and

(3) It provides an option to include certain forcing terms for parametric study without introducing complexity to the dynamic modelling *eg.* to include measured hub motions as forcing functions for the real mode system.

The determination of the RHS forcings is accomplished by first deriving the structural loads for the CRFA system (*Appendix* G), where a more detailed description will be given in *Section* 3.6.3. The analytical expressions for the CRFD system equations and the CRFA structural loads are summarised in *Appendix* H1.

Because some of the modelling and basic assumptions between CRFD and CRFA are different (*Section* 3.3.3), in order to ensure that compatible forcing terms can be identified, certain algebraic processes are still needed. The following approach is adopted;

(1) The structural loads for the CRFA system are derived using the same ordering scheme as CRFD initially *ie.* $u,\dot{u},\ddot{u}=O(\varepsilon)$ (*NB.* $u'=O(\varepsilon^2)$ in both analyses) and $mk\bar{m}=O(\varepsilon)$ - this ensures the energy functions for both systems are accurate to the same order before any algebraic process is applied;

(2) The blade shear flexibility in CRFD is removed by imposing $R_z=v'+O(\varepsilon^4), R_y=-w'+O(\varepsilon^4)$ after the equations are obtained;

(3) The axial degree of freedom is retained in the CRFA structural load equations to provide clarity; and finally,

(4) The CRFD equations are expressed using the same notation as those used in CRFA.

Principally, this can be achieved and has been successfully applied to the kinetic energy function. However the different blade models assumed in the two systems lead to some algebraic inconsistency, leaving a number of residual terms in the structural stiffness expression. We need to examine the conditions for which both systems are compatible.

The system equations for CRFD are derived for a blade model made up of a number of straight segments which are connected at 'kinks'. This allows large blade pre-deformed angles to be modelled. The resolution of loads and displacements from one segment to another is accomplished by a numerical transformation at each of these kinks. In CRFA, the equations are derived for a generally curved blade model where pre-deformed curvature terms (V_p'',W_p'') exist. In addition, the blade pre-deformed slopes (V_p',W_p'), and likewise the curvatures, are assumed to be $O(\varepsilon)$ in order to reduce the problem to a manageable size (*Section* 3.2.5). In essence, the CRFD system equations do not contain any pre-deformed curvature terms and this can be readily seen by examining the strain tensor components for both CRFD and CRFA (*Appendix* H2).

However, if it is assumed that the curved blade is made up of a large but finite number of straight segments and that the small pre-deformed angle assumption is imposed, a direct equivalence between the variables defined for the straight and curved segments can be established (*Appendix* H3). By using this variable transformation, it is possible to reduce the CRFA load equations to those of CRFD. The only residual terms are those not accounted for in CRFD. However, algebraic inconsistency arises, leaving a number of residual pre-deformed curvature terms in the CRFA expressions. This inconsistency is solely induced by the ordering analysis and the simplification carried out by REDUCE. The transformation would require the strain energy for CRFA to be raised to an order higher such that terms can be appropriately grouped for simplification. If the above transformation is applied rigorously, all these pre-deformed curvature terms will vanish and the CRFA load equations reduce to those of CRFD. Unless the same assumption is made in both systems, this problem is always present.

To reduce algebraic complication in ensuring system equivalence, the following restriction is imposed. The blade models used in both analyses are made up of straight segments with small pre-deformed angles imposed. This is justified in practice. For example, the large tip sweep and anhedral for the EH101 main rotor blade are not modelled as kinked segments but as c.g. offsets to avoid problem with undesired geometric coupling [3.38]. The precone angle for the Lynx CMRB blade is 3° so that the assumption of small pre-deformed angles is satisfied. However this restriction must be accompanied by the numerical transformation of the loads and displacements between the segments as is done in CRFD.

Based on this restriction, the CRFD system equations, after being re-expressed in the CRFA notation, are given in *Appendix* H4. They are directly compatible with the structural loads of CRFA, given in *Appendix* H5. The additional terms appearing in the CRFA equations are, as expected, those associated with the time varying (*eg.* $\dot{\vartheta}, \dot{W}_p$ *etc.*) and aircraft rate (*eg.* p_H, q_H *etc.*) terms. There are also the non-linear terms since CRFD equations are linearised. They are not obvious since CRFD exhibits non-linearity which are subsequently linearised. These terms, together with those explicit ones, will result on the RHS as forcing functions. When multiplied by the appropriate modal vectors, they become the modal forcing for the system mode concerned.

Having identified the forcing functions, we proceed to describe the process by which the Lagrangian equation can be constructed using effectively a reversed Hamiltonian Principle. The process is described in *Appendix* H6 where the coefficients associated with each of the virtual displacements (*Eqn.*G14) are treated to provide the coefficient in terms of each q_i's. In order to provide insight, the indirect terms are re-expressed. This allows the non-linear and pitch perturbation terms to be identified analytically since the modes are linearised and calculated at a constant pitch angle ϑ_m. In addition, by combining the technique described in *Appendix* H6 with the expressions given by *Appendix* H5, the analytical expressions of modal inertia and stiffness for the single blade system can be constructed. If $(C)_A$ and $(C)_D$ are the total coefficient with each of the generalised coordinates for the CRFA and CRFD systems respectively, then by invoking orthogonality,

$$(C)_A = 0 = (C)_D + f_i; \quad (C)_D = -I_{ij}\ddot{q}_j - S_{ij}q_j \text{ where } I_{ij}=0 \text{ ; } S_{ij}=0 \quad \text{if } i\neq j$$
$$=I_i \quad =\lambda_i^2 I_i \quad \text{if } i=j$$

For the real blade modes system, the system response (Lagrangian) equation, without structural damping, can thus be written in the form of a set of second order differential equations as,

$$\ddot{q}_i + \lambda_i^2 q_i = \frac{\int_R f_i dr}{\Omega^2 R I_i} = \frac{\int_R \underline{\phi}_i^T \underline{f} dr}{\Omega^2 R I_i} \qquad i = 1,2, \ldots\ldots,N \qquad (3.89a)$$

where $\lambda_i, I_i, f_i, \underline{\phi}_i$ are the i^{th} mode frequency, inertia, generalised force and modal vector, N is the number of modes considered. The forcing vector $\underline{f}$ for a single (k^{th}) blade, occupying the azimuth position ψ_k, is defined in *Appendix* I. $\underline{f}$ is defined such that

1) The hub inertia terms are present as external forcings;
2) The ordering is consistent with the CRFA assumption;
3) The axial freedom (u) has been eliminated; and
4) The non-linear stiffness and pitch perturbation (evaluated $[\ ]_{\vartheta_m}^{\vartheta}$) forcing terms are separately identified.

For systems using complex modes as state vectors, the dynamic models differ only in the form of the velocity matrix and damping modelled. The system response equation can be uncoupled using the bi-orthogonality relationship (*Appendix* D). This enables the response equation for the system concerned: coupled or reactionless, damped or undamped, to be expressed in the form of a set of first order differential equations as,

$$\dot{\eta}_i - \lambda_i \eta_i = \frac{\int_0^R g_i dr}{C_i} = \frac{\int_0^R \underline{\Gamma}_i^T \begin{Bmatrix} m^{-1}\underline{f} \\ \underline{0} \end{Bmatrix} dr}{C_i} \qquad i = 1,2, \ldots\ldots,2N \qquad (3.89b)$$

with the various modal parameters summarised conveniently in *Table* 3.4 below;

Case	System Mode Description	Frame of Reference	Form of System Response Eqn.	Definition of Normalising Factor	Definition of Generalised Force	Order of System
1	Undamped Blade Modes	Rotating	$\ddot{q}_i + \lambda_i^2 q_i = \frac{f_i}{C_i}$	$C_i = \underline{\phi}_i^T m \underline{\phi}_i$	$f_i = \underline{\phi}_i^T \underline{f}$	Second
2	Blade Modes with Symmetrical Damping	Rotating	$\dot{\eta}_i - \lambda_i \eta_i = \frac{g_i}{C_i}$	$C_i = \underline{\Phi}_i^T \underline{\Phi}_i$	$g_i = \underline{\Phi}_i^T \begin{Bmatrix} m^{-1}\underline{f} \\ \underline{0} \end{Bmatrix}$ where $\underline{\Gamma}_i = \underline{\Phi}_i$	First
3	Undamped Gyroscopic System c) Reactionless Modes d) Coupled Modes	 Rotating Fixed	$\dot{\eta}_i - \lambda_i \eta_i = \frac{g_i}{C_i}$	$C_i = \underline{\Phi}_i^H \underline{\Phi}_i$	$g_i = \underline{\Phi}_i^H \begin{Bmatrix} m^{-1}\underline{f} \\ \underline{0} \end{Bmatrix}$ where $\underline{\Gamma}_i = \underline{\Phi}_i^*$	First
4	Linearly Damped Gyroscopic System e) Reactionless Modes with Damping f) Coupled Modes with Damping	 Rotating Fixed	$\dot{\eta}_i - \lambda_i \eta_i = \frac{g_i}{C_i}$	$C_i = \underline{\Gamma}_i^H \underline{\Phi}_i$	$g_i = \underline{\Gamma}_i^H \begin{Bmatrix} m^{-1}\underline{f} \\ \underline{0} \end{Bmatrix}$ where $\underline{\Gamma}_i$=general	First

Table 3.4: Forms Of System Response Equation

The modal parameters: normalising factor C_i, mode frequency (eigenvalue) λ_i and mode shapes (eigenvectors) $\underline{\Phi}_i, \underline{\Gamma}_i$, are obtained directly from CRFD and are complex quantities. The terminology of normalising factor is used here rather than modal mass since the latter is normally associated with real modes. When complex modes are used, C_i is not only associated with the inertia of the system but also with the complex frequency.

Depending on the system modes used *ie.* coupled or reactionless, the modal parameters will be defined in different reference frames. This is immaterial as the coupled mode shapes can be re-constructed in the rotating frame. Thus the RHS forcings for all mode types can be conveniently represented by a single expression $\underline{f}$ already given in *Appendix* I. The function $\underline{f}$ defines all the possible forcings for the single blade system, where the following must be noted, before it is used to construct the modal forcing.

In the case of reactionless modes, being hub-fixed, the hub and rate terms are to be removed from $\underline{f}$. In addition, the linearised Coriolis forces must also be subtracted. Similarly for the coupled modes, the linearised hub terms need to be removed from $\underline{f}$ since they are already included in the modes. Finally, for modes including a linear lag damper, the linear damper loads must also be removed.

This orthogonalisation process correctly identifies all the forcing functions for any mode type used without reverting to laborious algebra. Should it become necessary to express the modal response equations for all mode types in full, they would only differ in two aspects: the number of RHS forcing terms being retained, and the definition of modal forcing *ie.* the mode shape function to which the applied force is multiplied. This process is a systematic way of identifying the forcing vector even when complex modes are used, and is made easier when the eigenvalue formulation is adopted in CRFD.

In the next section, the technique of filtering the forcings appropriate to the coupled and reactionless modes is introduced.

3.5.4 Method of Solution for The Modal Response Equation

The method of solution for the rotor response is to determine the time history of both the coupled and reactionless mode responses, *ie.* $\eta_{c_i}(\psi), \eta_{r_{i_k}}(\psi)$, for all the blades within a rotor. The need to treat both mode types simultaneously when they are defined in different frames of reference requires special attention to the solution method and a novel numerical technique is introduced by the author [3.39]. A summary is given here.

In the presence of the hub motion, the response on a blade will become dependent on the loads forcing the other blades in the rotor. One cannot solve the response on an isolated blade without first determining the loads on the other blades. The generalised forces on the coupled modes are obtained by summing the load components from each of the blades. For the blade motions, independent of the hub, the reactionless mode response can be determined separately in the rotating frame, hub-fixed condition. The total response of a single blade at position ψ_k would then be the sum of the responses of the coupled and of the reactionless modes.

The loads on a blade at any azimuth ψ_k, can be determined fully from aerodynamic and dynamic considerations. Part of these loads would force the coupled modes and the residual loads would only force the reactionless modes. The blade loads, such as aerodynamic lift, are known in the rotating frame, and the load components that force the coupled modes must first be transformed into the fixed frame. The residual loads remain in the rotating frame.

There are two ways of determining the blade total response. The first approach is to transform algebraically the single blade response equation into the fixed frame and then determine the response in the fixed frame using the coupled mode shapes directly. The residual loads on each of the blades are then used to determine the reactionless mode response. The total blade response can be obtained by first resolving the coupled mode responses back to the rotating frame and added to the reactionless mode responses. The second approach, which is much simpler, performs this transformation numerically using only the single blade equation defined at the ψ_k position.

This numerical method, which is applicable to a rotor with a number of blades greater than 2, eliminates the need to express the modal response equations for different numbers of blades. In fact, the method is also applicable to a 2-bladed rotor, but in this case, there is a time dependency between the two cyclic freedoms about the fore/aft and lateral axes. Certain modifications are required to adopt this solution method to a 2-bladed rotor. As the application of CRFD to the 2-bladed rotor is not planned for some time, the modifications required are not dealt with here.

It is to be noted that all the RHS forcing terms in $\underline{f}$ (*Appendix* I) are either azimuthally or time dependent. The most obvious azimuthally dependent terms are those associated with the hub motion and aircraft rates. The implicit time dependence is in the aerodynamic loadings, the control pitch variation and the pre-deformed coordinates, which in turn are functions of the pitch variations. Since the reactionless modes are independent of the hub, the fixed frame forcings *ie.* hub and rate terms need not be evaluated. Otherwise, it is generally not possible to isolate analytically the time dependent forces on the blade for the coupled or reactionless modes.

The generalised forces can be conveniently described in the form of a product of an applied force $F_k(r)=F(r,\psi_k)$ with a modal quantity $x_{i_k}(r)=x_i(r,\psi_k)$ on the k^{th} blade. The applied forces, either linear or non-linear, can be determined on all the blades. The coupled mode applied forces can be obtained by filtering the blade forces using the fixed frame transformation. The generalised forces acting on each of the blades, are obtained by multiplying these applied forces with the coupled mode shapes, being transformed into the rotating frame. The generalised force for the coupled mode on the blade is re-constituted by summing the contributions over all the blades, hence the coupled mode responses.

The residual applied force on each of the blades is determined by subtracting the load component, already used for the coupled mode response, from the total blade force. Similarly the generalised force for the reactionless modes is obtained by multiplying the residual applied force with the reactionless mode shape. This is then used to determine the responses on each blade.

The above procedure can be more easily understood using simple mathematics, by defining the coupled mode modal forcings as

$$MF_{\mathbb{C}}(\psi) = \sum_{k=1}^{N} \int_{0}^{R} F_{\mathbb{C}}(r,\psi_k)\cdot x_{\mathbb{C}_i}(r,\psi_k)\, dr \qquad (3.90)$$

where $x_{\mathbb{C}_i}$ and $F_{\mathbb{C}_i}$ are the i^{th} coupled mode shape and applied forces on the k^{th} blade and defined as

$$x_{\mathbb{C}_i}(r,\psi_k) = x_{0_i}(r) + x_{c_i}(r)\cos\psi_k + x_{s_i}(r)\sin\psi_k; \qquad (3.91a)$$

$$F_{\mathbb{C}}(r,\psi_k) = F_0(r) + F_c(r)\cos\psi_k + F_s(r)\sin\psi_k; \qquad (3.91b)$$

with F_0,F_C and F_S are the collective, cyclic cosine and cyclic sine components of forcings, defined as;

$$F_0(r) = \frac{1}{N}\sum_{k=1}^{N} F(r,\psi_k)$$

$$F_c(r) = \frac{2}{N}\sum_{k=1}^{N} F(r,\psi_k)\cos\psi_k$$

$$F_s(r) = \frac{2}{N}\sum_{k=1}^{N} F(r,\psi_k)\sin\psi_k \qquad (3.92)$$

and the reactionless mode modal forcing,

$$MF_{\mathbb{R}}(\psi_k) = \int_0^R F_{\mathbb{R}}(r,\psi_k)\cdot x_{\mathbb{R}_i}(r)\,dr \tag{3.93}$$

where $x_{\mathbb{R}_i}(r)$ is the reactionless mode shape and the residual blade force on the k^{th} blade is determined from

$$F_{\mathbb{R}}(r,\psi_k) = F(r,\psi_k) - F_{\mathbb{C}}(r,\psi_k) \tag{3.94}$$

The above procedure, which can be performed numerically, acts as a filtering process such that the coupled and reactionless mode modal forcings are separated. This will ensure that the modes are correctly excited and minimise any numerical errors.

The procedure can be easily programmed and is best described in the form of a flowchart, illustrated using the lift modal forcing $\int(\frac{dL}{dr})(r,\psi_k)w_{k_i}dr$. The technique is applicable to *all* the RHS forcing terms of the response equation, but is clearly not needed on the fixed frame forcings since they are only present in the coupled mode system, *ie.* the residual loads from these terms for the reactionless modes are identically zero.

For the non-linear forcings, *eg.* the Coriolis ($\int 2m\Omega v_i \int \dot{v}' v' dr dr$) or bending-torsion coupling terms, the difference hinges only on the calculation of the applied force. That is the total function values *eg.* v' and $\dot{v}'$, are first determined from

$$\begin{aligned}
v'(r,\psi_k) &= \sum_{i=1}^{N_c} \eta_{c_i}(\psi_{k-1})[v'_{0_i}+v'_{C_i}\cos\psi_k+v'_{S_i}\sin\psi_k] + \sum_{i=1}^{N_r} \eta_{r_i}(\psi_{k-1})v'_{r_i}(r) \\
\dot{v}'(r,\psi_k) &= \sum_{i=1}^{N_c} \dot{\eta}_{c_i}(\psi_{k-1})[v'_{0_i}+v'_{C_i}\cos\psi_k+v'_{S_i}\sin\psi_k] \\
&\quad + \sum_{i=1}^{N_c} \eta_{c_i}(\psi_{k-1})[-v'_{C_i}\sin\psi_k+v'_{S_i}\cos\psi_k] + \sum_{i=1}^{N_r} \dot{\eta}_{r_i}(\psi_{k-1})v'_{r_i}(r)
\end{aligned} \tag{3.95}$$

where $\eta_i(\psi_{k-1})$ is the response from the previous time step and the process is performed as a timewise solution.

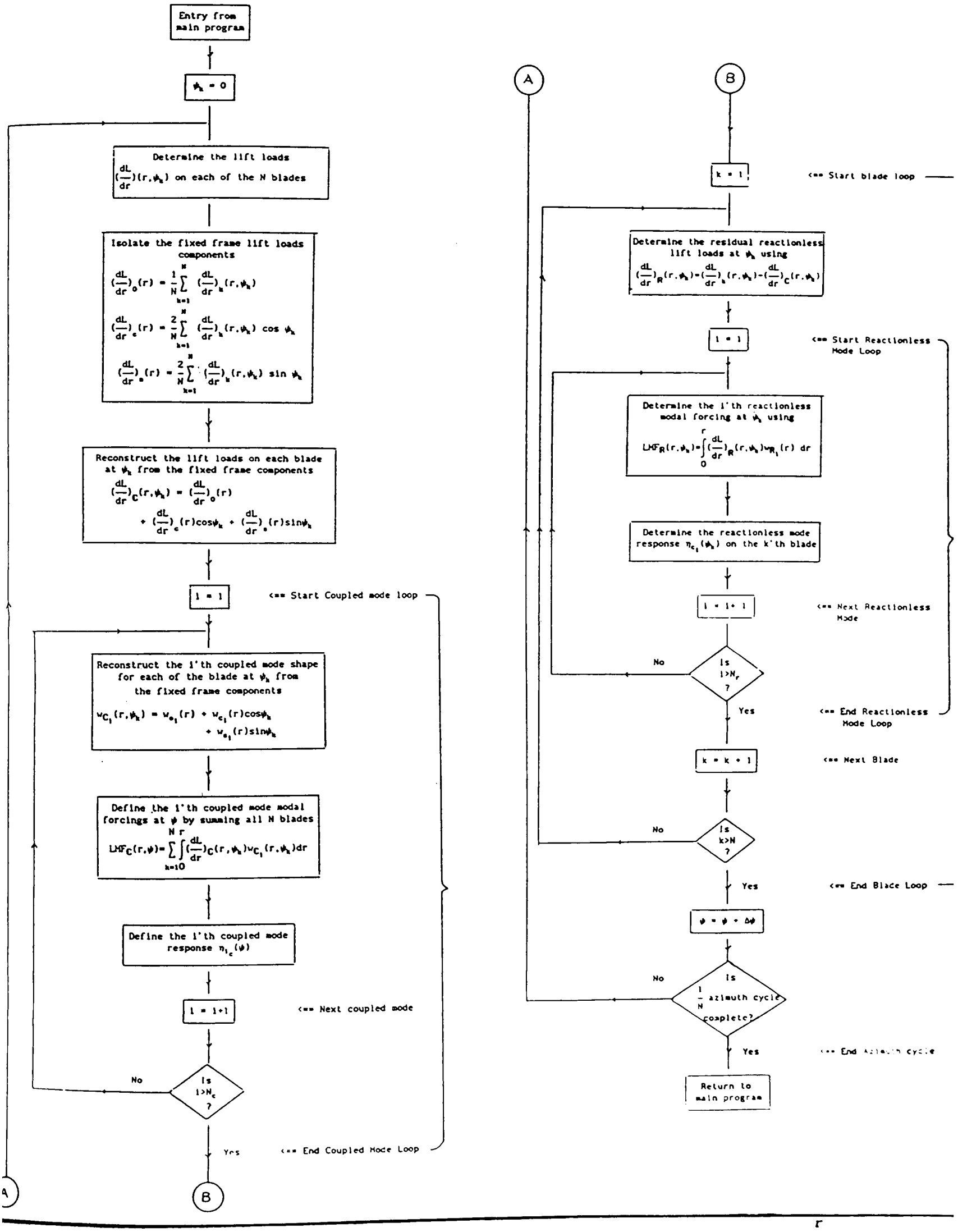

Rotor Mode Solution Method in CRFA - Illustrated using Aerodynamic Lift Modal Forcings $\int_0^r (\frac{dL}{dr})(r,\psi_k)w_i dr$

3.5.5 Timewise Solution

The filtering process described previously separates the forcings for the coupled and reactionless modes at each time step. An azimuthal integration scheme is then employed to determine the response history. In view of the extensive computation needed, a separate investigation to identify suitable solution algorithm(s) was conducted by Hawkings [3.40] under the CRFM development.

In Hawking's study, a series of tests were carried out on a selection of algorithms and their performance was compared based on a number of criteria - accuracy, stability and efficiency. The findings concluded that the NAG FORTRAN routine (D02CBF) is the most efficient algorithm and should be incorporated into the response analysis. However the structure of implementation is significantly different from the other algorithms, which are also recommended. The NAG routine is based on a predictor-corrector method and for improved efficiency, it has a built-in varying steplength mechanism. The other algorithms are either explicit or predictor-corrector types but they are all based on a fixed stepsize.

A separate study undertaken by the author [3.41] has demonstrated that the NAG routine, due to its variable stepsize feature, misses important discrete forcings arising from blade vortex interactions unless a very fine tolerance is imposed. Further evaluations by the author [3.42] also revealed that other algorithms, except the 4^{th} order Runge-Kutta method, failed to model the highly non-linear lag damper behaviour accurately and they were eliminated. Although the Z-transform method was not recommended from [3.40], its robustness and effectiveness in dealing with non-linear forcings as shown in [3.10] warrants its re-instatement. It has shown comparable accuracy with the 4^{th} order Runge-Kutta method but is more computationally efficient for application for real modes. The only deficiency would be its application to the response equation in the first order form, for which the formulation is not readily available. For the above reasons, the chosen algorithm is the 4^{th} order Runge-Kutta method.

The solution algorithm for the Runge-Kutta method is defined as follow. The response equation is conveniently described by a set of differential equations in the form,

$$y'' + 2\zeta\omega y' + \omega^2 y = F(x,y,y')$$

or

$$y'' = G(x,y,y') = F - 2\zeta\omega y' - \omega^2 y \tag{3.96}$$

where y = the modal response ($=\eta_i$; i=1,2,...,N), x = the azimuth angle ($=\psi$), ζ,ω are the normalised structural damping and modal frequency.

In the first order form,

$$\underline{Y}' = H(x,\underline{Y}) \quad \text{or} \quad \begin{Bmatrix} y \\ z \end{Bmatrix}' = \begin{Bmatrix} z \\ f-2\zeta\omega y-\omega^2 y \end{Bmatrix} \tag{3.97}$$

For many modes, there is a family of the above equations, one for each mode. In the formulation below, h($=\Delta\psi$) denotes the integration time interval, the solution at time t_{n+1} is given by

$$\left.\begin{aligned} y_{n+1} &= y_n + h\left\{y'_n + \frac{1}{6}(k_1+k_2+k_3)\right\} \\ y'_{n+1} &= y'_n + \frac{1}{6}\left\{k_1 + 2k_2 + 2k_3 + k_4\right\} \end{aligned}\right\} \tag{3.98}$$

where $k_1 = h\ G(x_n,\ y_n,\ y'_n)$

$$k_2 = h\ G\left(x_n+\frac{h}{2},\ y_n+\frac{hy'_n}{2}+\frac{hk_1}{8},\ y'_n+\frac{k_1}{2}\right)$$

$$k_3 = h\ G\left(x_n+\frac{h}{2},\ y_n+\frac{hy'_n}{2}+\frac{hk_1}{8},\ y'_n+\frac{k_2}{2}\right)$$

$$k_4 = h\ G\left(x_n+h,\ y_n+hy'_n+\frac{hk_3}{2},\ y'_n+k_3\right)$$

3.6 Formulation of Blade Structural Loads

3.6.1 Introduction

The determination of the responses for the CRFD modes constitutes only part of the complete aeroelastic solution for this analysis. Once the modal responses, and hence deflections, are known, the next task is to determine the blade structural loads.

The structural loads are the resultant forces and moments experienced by the blade and hub due to all external and internal loadings. The blade loads are used to determine the stresses, hence the fatigue life and static strength of various components in the rotor system. The hub loads are required to determine the mean and vibratory loads at the blade passing frequency to assess the vibration level in the airframe.

Traditionally, two different techniques have been employed to determine the blade structural loads. The most widely used is the Modal Summation method, which expresses blade loads as the sum, over the modes considered, of the product of modal responses with modal load distributions. The latter are obtained directly from the modal solution in the form of modal bending moments and shears *ie.* the eigenvectors. The other technique, which is still favoured, is the Force Integration method. This involves the direct integration of all loading actions on the blade, both aerodynamic and dynamic.

There are relative advantages and disadvantages with both methods. Modal Summation is easy to implement and is computationally efficient. It is particularly favoured for the physical insight it provides in identifying the sources of oscillatory loads. Ormiston [3.43] described a notable exercise comparing the results of different rotor load methods for a hypothetical rotor. One of his observations was the degree of variation of predicted bending moment at the hinge position. The Modal Summation method, due to the nature of the modal solution, inherently produces a zero hinge moment for an articulated rotor while the Force Integration method does not necessarily satisfy this boundary condition.

Both techniques were evaluated by Bielawa [3.44] with the conclusion that Modal Summation is inadequate in its modelling of discontinuous

applied loads when using only a limited number of modes. The two methods were again compared by Walker [3.45], the results however were not totally conclusive since Force Integration showed relatively inferior flatwise moment predictions in the root region, yet chordwise moments were better predicted in the presence of lag damper loads.

The concern over the accuracy of Modal Summation is not restricted to lag damper load modelling. It is associated with the general inability to model discrete or loading distributions due to higher order mode shapes because of the mode truncation inherent in this method. Indeed, variable spanwise pitching moments cannot be properly represented by the inclusion of a single torsion mode. Also, the discrete nature of impulsive loadings due to blade vortex interactions may also require higher order modal modelling.

The method has however performed satisfactorily in the past, since it offers better insight into the physical source of structural loads and such higher modal forcings are generally not very significant. This is of course, not true when a lag damper is present in the rotor system. The presence of a lag damper induces discrete loads, and the vortex interaction at low speeds could induce higher modal forcings which cannot be adequately represented using Modal Summation alone. There is another potential difficulty which is associated with the elimination of the axial degree of freedom. The axial motion is expressed in terms of flap and lag freedoms. As a result, Modal Summation mis-represents the radial loads as flap and lag shear components. These loads should strictly be re-aligned after the summation process. For the above reasons, Force Integration would appear to offer greater potential accuracy by the direct integration of applied loadings.

Force Integration has however, a reputed history of numerical problems as it involves the process of finding small differences between large load fields. It is obviously more computationally intensive due to the repeated spanwise integrations required at each azimuth position. The airloads are integrated in the exact form rather than by an equivalent modal representation. Hence, the modal contribution to the structural loads are not immediately available, as they are in Modal Summation. However, by appropriate post-processing of applied loads determined using the Force Integration method, the structural loads can be analysed in terms of their modal components to provide the necessary

insight. It is therefore decided to implement Force Integration as an option in this analysis in addition to the Modal Summation option.

A hybrid technique known as the Unified Formulation method was introduced by Hansford [3.46]. It combines the potential accuracy of Force Integration with the simplicity of Modal Summation by introducing a correction term due to higher mode forcing. Thus the advantages of both computational speed and insight can be retained. The fundamental principle for Unified Formulation is however dependent upon the knowledge of the orthogonality condition for the modes. Although the orthogonality relationship has been established for the complex rotor modes, it only exists in numerical form. Further work is still required to use such a relationship for Unified Formulation. Consequently, it cannot yet be incorporated as an option for structural load calculation. One reason why it might still be valuable would be if the computation of Force Integration becomes too excessive.

The determination of structural loads based on Modal Summation and Force Integration is described in the next 2 sections. This is followed by the description of a novel analytical integration technique, developed to alleviate the inherent numerical problem with Force Integration.

3.6.2 Modal Summation Method

Once the response solutions *ie.* generalised coordinates of both the coupled and reactionless modes are determined using the method described in *Section* 3.5.4, the structural loads can be obtained directly if Modal Summation is used. The total structural loads, as a radial and azimuthal distribution, are the sum of contributions from both mode types as,

$$\underline{F}(r,\psi_k) = \sum_{i=1}^{N_c} \eta_{c_i}(\psi_k)[\underline{F}_{O_i}(r) + \underline{F}_{C_i}(r)\cos\psi_k + \underline{F}_{S_i}(r)\sin\psi_k] + \sum_{i=1}^{N_r} \eta_{r_i}(\psi_k)\,\underline{F}_{r_i}(r) \qquad (3.99)$$

where $\underline{F}_{O_i}, \underline{F}_{C_i}, \underline{F}_{S_i}$ are the collective, cyclic (cosine) and cyclic (sine) components of the modal load-vector (radial distribution) of the i^{th} coupled mode and $\underline{F}_{r_i}$ is the modal load-vector of the i^{th} reactionless mode.

3.6.3 Force Integration Method

The structural load expressions are derived by the application of Hamilton's principle, similar to those of CRFD. The main differences are that the effects due to aircraft motion, non-linear, pitch perturbation terms,..*etc.* are also included.

Hamilton's Principle states

$$\int_{t_1}^{t_2} \left[\delta(K-U) + \delta W\right] dt = 0$$

or in terms of the energy functions f,g,

$$\int_{t_1}^{t_2} \left[\int_{0}^{r} \delta(g-f)\, dr + \delta W \right] dt = 0 \qquad (3.100)$$

By considering the variations of f,g with respect to each of the blade freedoms (u,v,w,ϕ,β,ζ) and the virtual work, the structural load expressions can be derived. Details of the derivation are given in *Appendix* G. The analytical expressions for the structural loads are defined as

$$\left.\begin{aligned}
V'_x &= \frac{d}{dt}\left(\frac{\partial g}{\partial \dot{u}}\right) - \frac{\partial g}{\partial u} + \frac{\partial (f+U_s)}{\partial u} - \frac{dA}{dr} \\
V'_y &= \frac{d}{dt}\left(\frac{\partial g}{\partial \dot{v}}\right) - \frac{\partial g}{\partial v} + \frac{\partial (f+U_s)}{\partial v} + \frac{dD}{dr} \\
V'_z &= \frac{d}{dt}\left(\frac{\partial g}{\partial \dot{w}}\right) - \frac{\partial g}{\partial w} + \frac{\partial (f+U_s)}{\partial w} - \frac{dL}{dr} \\
\underbrace{M'_x + (\zeta M_y)' + (\beta M_z)'}_{M'_{x_{def}}} &= \frac{d}{dt}\left(\frac{\partial g}{\partial \dot{\phi}}\right) - \frac{\partial g}{\partial \phi} + \frac{\partial (f+U_s)}{\partial \phi} - \frac{dM}{dr} + O(\varepsilon^3) \\
\underbrace{-(M_y)' + (\zeta M_x)'}_{-M'_{y_{def}}} &= \frac{d}{dt}\left(\frac{\partial g}{\partial \dot{\beta}}\right) - \frac{\partial g}{\partial \beta} + \frac{\partial (f+U_s)}{\partial \beta} + O(\varepsilon^3) \\
M'_{z_{def}} &= \frac{d}{dt}\left(\frac{\partial g}{\partial \dot{\zeta}}\right) - \frac{\partial g}{\partial \zeta} + \frac{\partial (f+U_s)}{\partial \zeta}
\end{aligned}\right\} \qquad (3.101)$$

where the suffix (def) denotes the loads are in the blade deformed $Or\eta\xi$-axis system. The boundary conditions, obtained as a by-product of applying Hamilton's Principle, are

$$
\left.
\begin{aligned}
V_x &= \frac{\partial f}{\partial u'} \\
V_y &= \frac{\partial f}{\partial v'} \\
V_z &= \frac{\partial f}{\partial w'} \\
\underbrace{M_x + \zeta M_y + \beta M_z}_{M_{x_{def}}} &= \frac{\partial f}{\partial \phi'} + O(\varepsilon^3) \\
\underbrace{-M_y + \zeta M_x}_{-M_{y_{def}}} &= \frac{\partial f}{\partial \beta'} + O(\varepsilon^3) \\
M_{z_{def}} &= \frac{\partial f}{\partial \zeta'}
\end{aligned}
\right\} \qquad (3.102)
$$

The structural load expressions, derived using REDUCE, are given in *Appendix* J1, where the axial freedom is retained and in *Appendix* J2, where it has been re-expressed as fore-shortening terms.

3.6.4 Chebyshev Polynomial Integration Technique

Because of the need to find small differences between large load fields, potential numerical error is always present in Force Integration. This numerical deficiency is compounded by the fact that only a limited number of stations are generally available for spanwise integration. The inaccuracy is reflected in the erroneous boundary condition, characterised by the non-vanishing hinge bending moment for an articulated blade, and can lead to significant error in load prediction. In order to apply Force Integration successfully, it is essential to ensure that these errors are reduced to a minimum.

A detailed study leading up to the development of an analytical integration technique was conducted by the author [3.47]. The theory and conclusions are summarised here. The approach took a number of steps. First, it proved that this numerical ill-conditioning is always present unless all the radial integrations are carried out over the same (R_M) stations at which the dynamic characteristics are calculated. However, because of the varying properties of the rotor blade, the number of stations is necessarily large, in excess of 500, and this is clearly not computationally feasible at every azimuth position. Thus it is necessary to establish an accurate integration scheme using only a limited number of radial stations. The technique was initially

demonstrated using an analytical example and then applied to a simplified, but real, blade problem.

a. Description of Problem

Consider a simplified form of the blade response equation,

$$\ddot{q}_i + 2\nu_i\lambda_i\dot{q}_i + \lambda_i^2 q_i = \frac{1}{\Omega^2 I_i}\int_e^R \frac{dL}{dr} w_i \, dr \qquad \text{for } i= 1,2,..,N \qquad (3.103)$$

where only the lift modal forcing is shown and the usual meanings apply to the various parameters. The lift modal forcing is defined as the product of the aerodynamic lift $\frac{dL}{dr}$ and the flap mode shape w_i. The lift is normally defined over the aerodynamic (R_G) stations, typically 25 points spanning from the root cut-out to the tip with the assumption that inboard of the root cut-out, the aerodynamic loadings are uniformly zero. The flap mode shape is described by a distribution over the dynamic output (R_F) stations, typically 25 points spanning from the blade root to the tip. Unless these R_F stations are carefully chosen, accurate details of the mode shapes and properties cannot be guaranteed. The normal procedure is to integrate radially the product of $\frac{dL}{dr}$ with the flap shape interpolated at the R_G stations.

It is shown in *Appendix* K1 that the expressions for the flap hinge bending moment for both Modal Summation and Force Integration, due to pure flapping motion, are given respectively by;

$$M_{MS}(e) = \sum_{i=1}^{N} q_i M_i(e) = \sum_{i=1}^{N} q_i \int_e^{R_M} m\Omega^2\left[\lambda_i^2(r-e) - r\right]w_i \, dr \qquad (3.104)$$

$$M_{FI}(e) = \int_e^{R_F}\left\{ \left(\frac{\partial L}{\partial r} - m\Omega^2 \frac{\sum_{i=1}^{N} w_i \int_e^{R_G} \frac{\partial L}{\partial r} w_i dr}{\Omega^2 I_i} \right)(r-e) - m\Omega^2 r \sum_{i=1}^{N} q_i\left[\lambda_i^2(r-e)-r\right]w_i \right\} dr \qquad (3.105)$$

such that

$$M_{FI}(e) = M_{MS}(e) + \left(\int_o^{R_F} - \int_0^{R_G} \right) m\Omega^2 r \sum_{i=1}^{N} q_i\left[\lambda_i^2(r-e)-r\right]w_i \, dr \qquad (3.106)$$

It should be noted that even though the calculation of response coefficient q_i may be in error, the correct boundary condition is

always assured for Modal Summation. For Force Integration, unless all the integrations are carried out using the most populated array, namely the dynamic integrated (R_M) stations, erroneous boundary conditions will result. This incompatibility of using integration stations other than R_M will always be present. In addition, unless the true features of the blade properties, which are often largely varying and discontinuous, are captured, errors induced from radial integration will be significant. An example mass distribution is given in *Figure* 3.11 below.

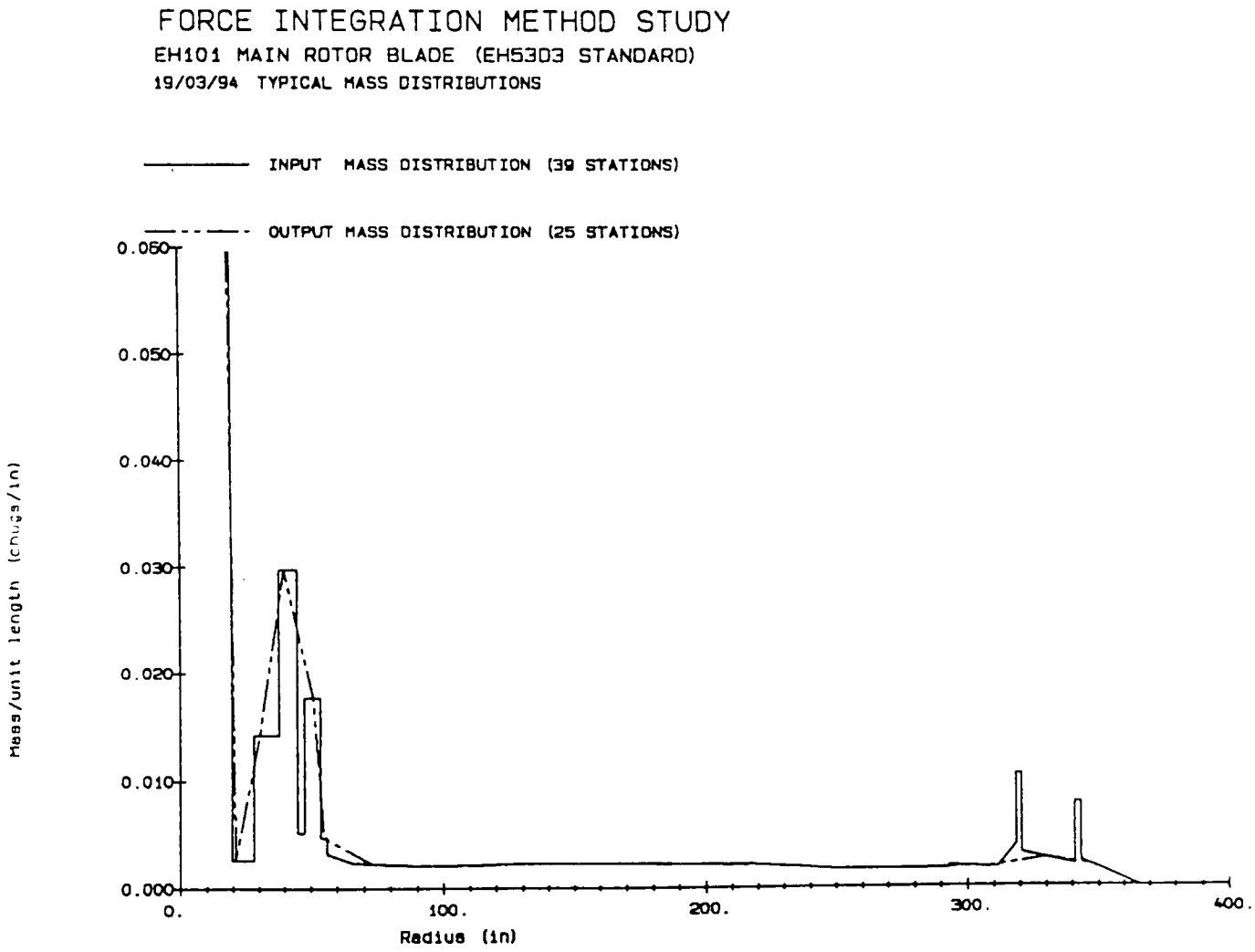

Figure 3.11: Example Mass Distribution of Rotor Blade (EH101)

In order to implement Force Integration successfully, numerical errors from these origins must be minimised.

b. The Theory

The shortcoming of defining mode shapes at limited R_F stations can be overcome by fitting a polynomial through these stations. For this, the Chebyshev polynomials are chosen because of the accuracy they provide and computational routines for fitting and integration are readily available *eg.* the NAG FORTRAN library.

The Chebyshev polynomial approximates a set of data points by an analytical function, p(x), using a least square method;

$$p(x) = \frac{1}{2}a_0T_0(x) + a_1T_1(x) + a_2T_2(x) + \cdots\cdots + a_nT_n(x) \qquad (3.107)$$

where $T_0(x) = 1$

$T_1(x) = x$

$T_2(x) = 2x^2 - 1$

:

etc..

:

$T_{n+1}(x) = 2xT_n(x) - T_{n-1}(x)$ for $n \geq 1$

are simple analytical and orthogonal functions. The fitting process involves the determination of the coefficients $a_0, a_1, a_2, \ldots . a_n$ defined in p(x) [3.48]. Providing a high enough order of polynomial is taken, the fitting process will always produce the most accurate curve fit of maximum order R_F-1 to the mode shape. Products of mode shapes, where required, can be found by multiplying the fitted polynomials and the mode slopes by analytical differentiation. The problem of dealing with integrands of mode shape weighted with a discontinuous function *eg.* mass, can be accommodated by treating the distribution as a piecewise analytical linear function, f(x).

The principle of the Chebyshev Polynomial Integration technique, thence named as CPI, involves the piecewise analytical integration of a product of discontinuous f(x) and continuous functions p(x) as shown schematically in *Figure* 3.12 below;

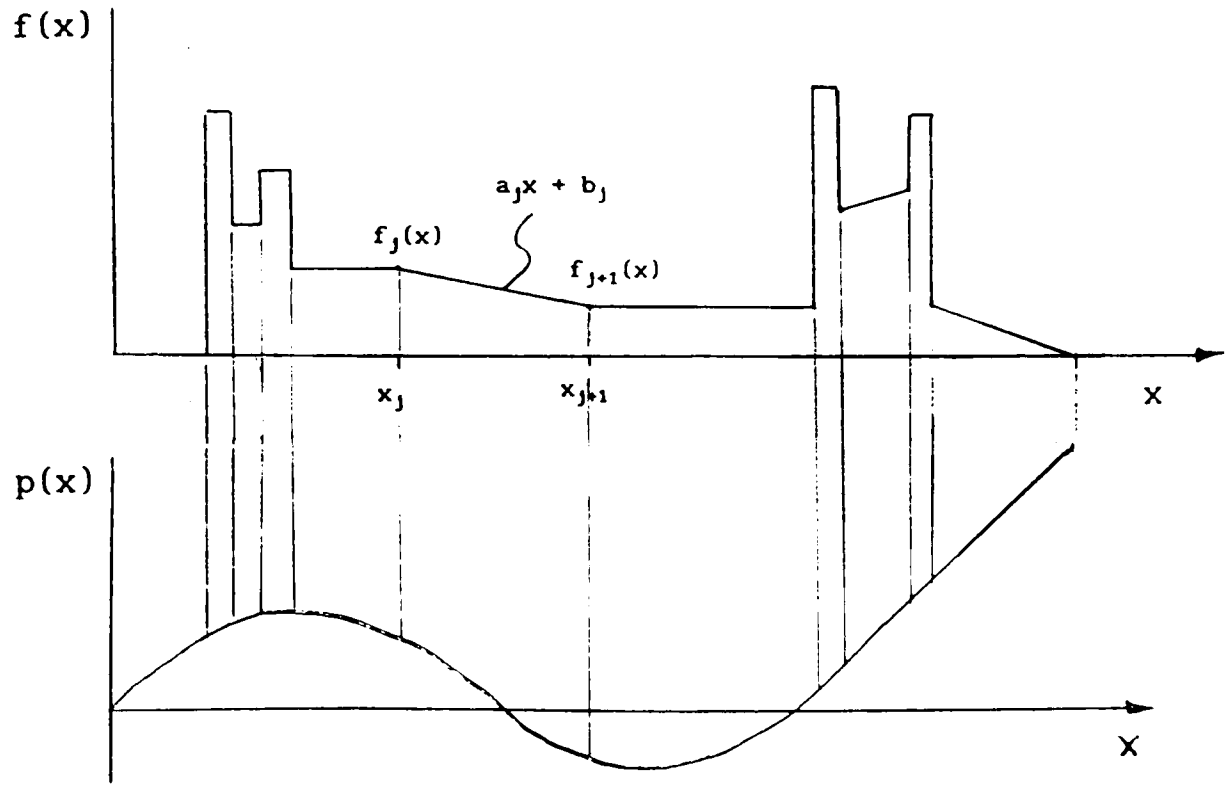

Figure 3.12: Treatment of Continuous and Discontinuous Functions

Consider f(x) being defined over the range of (x_0,x_1), each of the bays defining f(x) over (x_j,x_{j+1}) can be conveniently written as

$$f_j(x) = a_j x + b_j \qquad \text{where } x_j \le x \le x_{j+1} \tag{3.108}$$

where the segment coefficients a_j,b_j are defined as

$$a_j = \frac{f_{j+1} - f_j}{x_{j+1} - x_j}$$

$$b_j = \frac{(f_{j+1} + f_j) - a_j(x_{j+1} + x_j)}{2}$$

Consider the fitted polynomial p(x) which is defined over the range $(\bar{x}_0,\bar{x}_1)$. Noting that (x_0,x_1), $(\bar{x}_0,\bar{x}_1)$ are not necessarily the same, however, (x_0,x_1) must lie within $(\bar{x}_0,\bar{x}_1)$. The bay integral for the product of $f_j(x)$ and p(x) is then given by

$$I_j = \int_{x_j}^{x_{j+1}} f_j(x)\, p(x)\, dx$$

$$= \int_{x_j}^{x_{j+1}} \left(a_j x + b_j\right) p(x)\, dx$$

$$= a_j \int_{x_j}^{x_{j+1}} xp(x)\, dx + b_j \int_{x_j}^{x_{j+1}} p(x)\, dx$$

Integrating the first term by parts leads to,

$$I_j = \left(a_j x + b_j\right) \int_{x_j}^{x_{j+1}} p(x)\, dx - a_j \int_{x_j}^{x_{j+1}} \int_{x_j}^{x_{j+1}} p(x)\, dx\, dx \tag{3.109}$$

This analytical technique is exact and can easily be adopted for other applications involving integration of similar products.

c. An Application

Validation of the technique in application to a rotor blade based on a set of uncoupled single blade modes; 4 flap, 3 lag and 1 torsion, can be found in [3.47]. Being uncoupled, the forcings associated with flap, lag and torsion are conveniently separated.

The mode response coefficients are first determined from the following simplified form of the response equation,

$$\ddot{q}_i + 2\nu_i\omega_i\dot{q}_i + \omega_i^2 q_i = \frac{1}{\Omega^2 R I_i}\int_e^R \Bigg\{ \underbrace{\frac{dL}{dr}w_i - \frac{dD}{dr}v_i + \frac{dM}{dr}t_i}_{\text{Aerodynamic}} + \underbrace{m\Omega^2\left(-2v_i\int_0^r (v'\dot{v}'+w'\dot{w}')\,dr - 2\dot{v}\int_0^r (v'v_i'+w_i'w_i')\,dr\right)}_{\text{Coriolis}} \Bigg\} dr - \underbrace{F_D l_D v_{2_i}'}_{\text{Damper}}$$

(3.110)

where ν_i is the structural damping for the i^{th} mode. The corresponding hinge bending moment expressions are defined as:

$$-M_{y_{def}}(e) = \underbrace{\iint_{er}^{RR} \frac{dL}{dr}\,drdr}_{\text{Applied}} - \underbrace{\iint_{er}^{RR} m\Omega^2\ddot{w}\,drdr}_{\text{Inertia}} - \underbrace{\int_e^R w'\int_r^R m\Omega^2 r\,drdr}_{\text{CF}} - \underbrace{\int_e^R w'\int_r^R 2m\Omega^2\dot{v}\,drdr}_{\text{Coriolis}}$$

$$M_{z_{def}}(e) = \underbrace{-\iint_{er}^{RR}\frac{dD}{dr}drdr}_{\text{Applied}} - \underbrace{\iint_{er}^{RR} m\Omega^2\ddot{v}\,drdr}_{\text{Inertia}} + \underbrace{\iint_{er}^{RR} m\Omega^2 v\,drdr}_{\text{CF}} + \underbrace{\iint_{er}^{RR}\int_0^r 2m\Omega(v'\dot{v}'+w'\dot{w}')drdrdr}_{\text{Coriolis}}$$

$$\underbrace{-\int_e^R v'\int_r^R m\Omega^2 r\,drdr}_{\text{CF}} - \underbrace{\int_e^R v'\int_r^R 2m\Omega^2\dot{v}\,drdr}_{\text{Coriolis}} - \underbrace{F_D l_D}_{\text{Lag damper}} \qquad (3.111)$$

By inspection, all the integrands, except the Coriolis terms, are defined as products of discontinuous and fitted functions for which the CPI technique can be applied. Further consideration to the treatment of Coriolis and non-linear torsion-flap-lag forcings is given below.

d. Treatment of Coriolis and Non-linear Forcings

Coriolis Forcing

The non-linear Coriolis modal forcing is given by

$$CMF = \frac{1}{\Omega^2 R I_i}\int_e^R -m\Omega^2\left(-2v_i\int_0^r (v'\dot{v}'+w'\dot{w}')\,dr - 2\dot{v}\int_0^r (v'v_i'+w'w_i')\,dr\right) dr \qquad (3.112)$$

and it involves double integrations with the inner integrals defining the fore-shortenings as,

$$\int_0^r v'\dot{v}'+w'\dot{w}'\,dr = \int_0^r \left(\sum_{i=1}^N q_i v_i' \sum_{j=1}^N \dot{q}_j v_j' + \sum_{i=1}^N q_i v_i' \sum_{j=1}^N \dot{q}_j w_j'\right) dr$$

$$\int_0^r v' v_i' + w' w_i' \, dr = \int_0^r \left(v_i' \sum_{j=1}^{N} q_j v_j' + w_i' \sum_{j=1}^{N} q_j w_j' \right) dr \qquad (3.113)$$

which must first be evaluated from root to tip. It is possible to follow a similar process by fitting polynomials to individual mode shapes and differentiating to give the mode slopes. However, this proves to be cumbersome and non-beneficial due to the presence of a large number of non-linear terms. It can be more effectively dealt with by fitting a polynomial to the non-linear integrand as a global function defined at R_F stations and performing analytical integration from root to tip. The outer integrals are treated similarly by first defining $v_i \int (v'\dot{v}' + w'\dot{w}')dr$ *etc* as a product of two fitted polynomials and then integrating with the mass function.

To ensure compatibility, a similar technique must also be applied to the Coriolis component in the lag bending moment expression, which involves triple integrals,

$$M_{z_{cor}}(r) = \int_{er}^{RR} \int_0^r 2m\Omega \, (v'\dot{v}' + w'\dot{w}') \, drdrdr \qquad (3.114)$$

The predictions of vibratory flatwise and edgewise bending moment, including the lag damper loads, using both Force Integration and Modal Summation (with and without the Unified Formulation treatment of the damper load) are shown in *Figure* 3.13 below, extracted from [3.47];

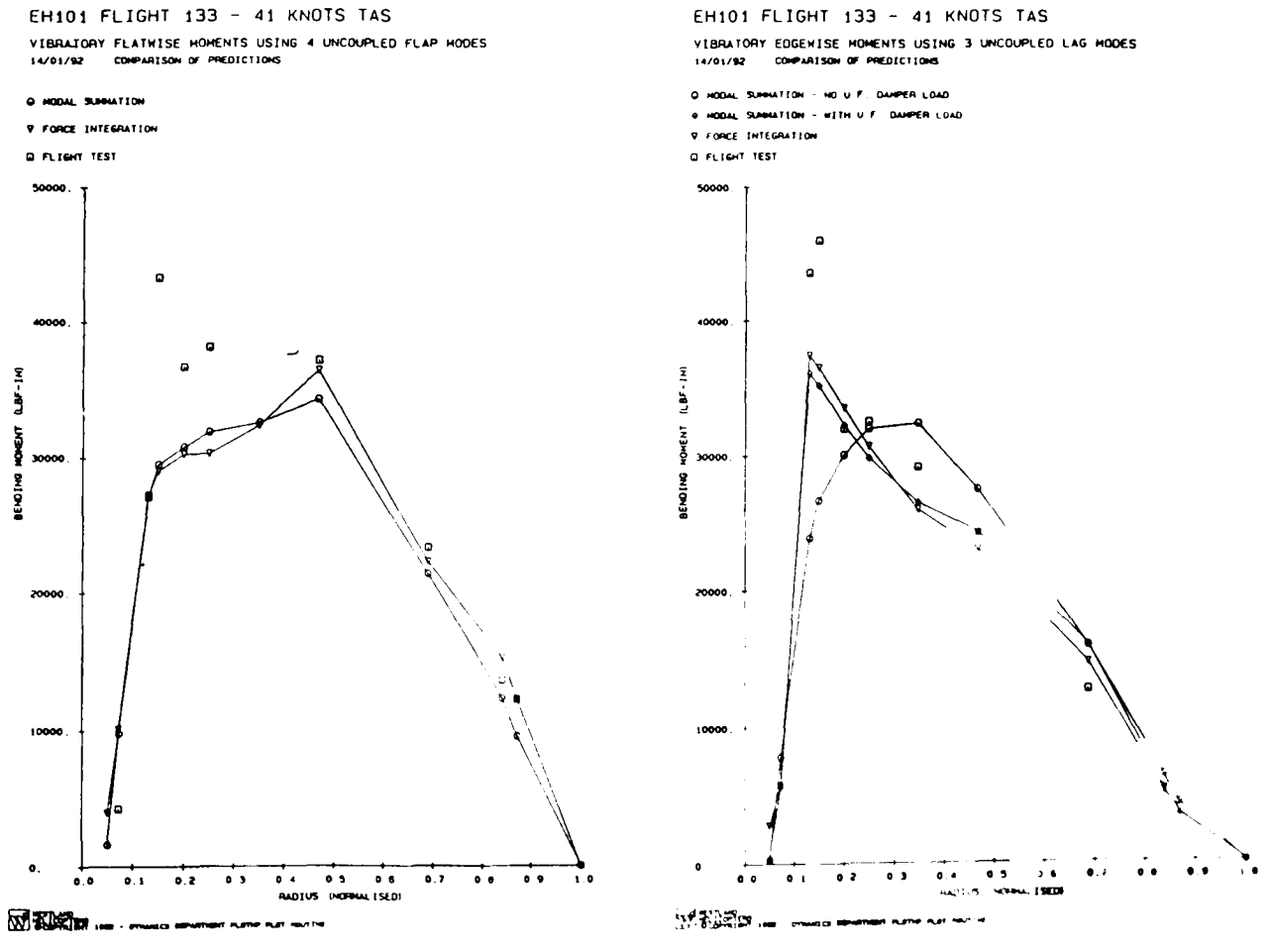

Figure 3.13 - Application of CPI Method in Vibratory Moment Calculation

It can be seen clearly that Force Integration shows comparable accuracy with Modal Summation in flatwise moment prediction. In edgewise moment prediction, Force Integration shows considerable improvement over Modal Summation and compares well with Modal Summation when Unified Formulation treatment of the lag damper load is included. The results confirm that Force Integration is a preferred method in the structural load calculation, since the Unified Formulation method is currently limited in its application to lag damper and aerodynamic pitching moment forcings only.

Torsion-Flap-Lag Forcing

An extension to apply the CPI technique to deal with non-linear torsion-flap-lag forcing terms was carried out by Griffiths [3.49]. These terms involve the product of modal curvature and stiffness functions, which are both discontinuous. The approach is to re-express these terms as a product of the inverse of stiffness and bending moment, where the latter can be fitted with polynomials. The formulation can be found in *Appendix* K2.

3.7 Summary of Analytical Model

In this chapter, the development of the analytical rotor response model has been described in detail. The model is valid for the coupled rotor-fuselage system modelled using either real blade modes or complex rotor modes as state vectors. Owing to algebraic complexity, tedious algebra has been avoided as far as possible in order to provide clarity and insight.

CHAPTER 4 - CORRELATIONS AND DISCUSSION OF RESULTS

4.1 Introduction

The concept and application of complex rotor modes for the rotor response analysis were described in Chapter 3. A FORTRAN program, the Coupled Rotor-Fuselage Aeroelastics (CRFA), is being jointly developed by WHL and DRA (Farnborough)[2]. The program is based on the foregoing theory and is used to calculate the rotor loads in flight. To provide an understanding of the algorithm, its main features are described in this chapter.

Owing to unforeseen delays in the software development, not all the analytical features described in Chapter 3 have been incorporated in CRFA to-date. CRFA currently solves the in-flight forced response for an isolated rotor using either blade modes or real rotor modes as state vectors. The software implementation of the complex rotor modes solution [4.1] has been started but is not anticipated to be completed for some time. Thus the application of complex rotor modes in rotor response analysis cannot yet be evaluated. However a correlation exercise using CRFA is undertaken and the results obtained in a variety of applications are discussed and compared with flight test data. Wherever appropriate, results from Program R150 [4.2] will be presented so that a direct comparison of the analytical capability can be made.

While CRFA is continuously being developed, a parallel activity to extend the single rotor trim capability to the complete rotorcraft trim (multiple rotors), is being undertaken by Young [4.3]. The requirement is needed to define a trim state to be used as an initial condition for a manoeuvre simulation. The ability to simulate manoeuvre constitutes the third and final phase of the Coupled Rotor-Fuselage Model (CRFM) development. The completion of software development is not expected, realistically, for at least a few more years.

4.2 Description of The Computer Software - Program CRFA

Program CRFA is the main rotor load module among a suite of programs. The integration of these programs is described in *Figure* 4.1 below;

---

2 The author would especially like to thank Mr C Young of DRA for furnishing most of the software.

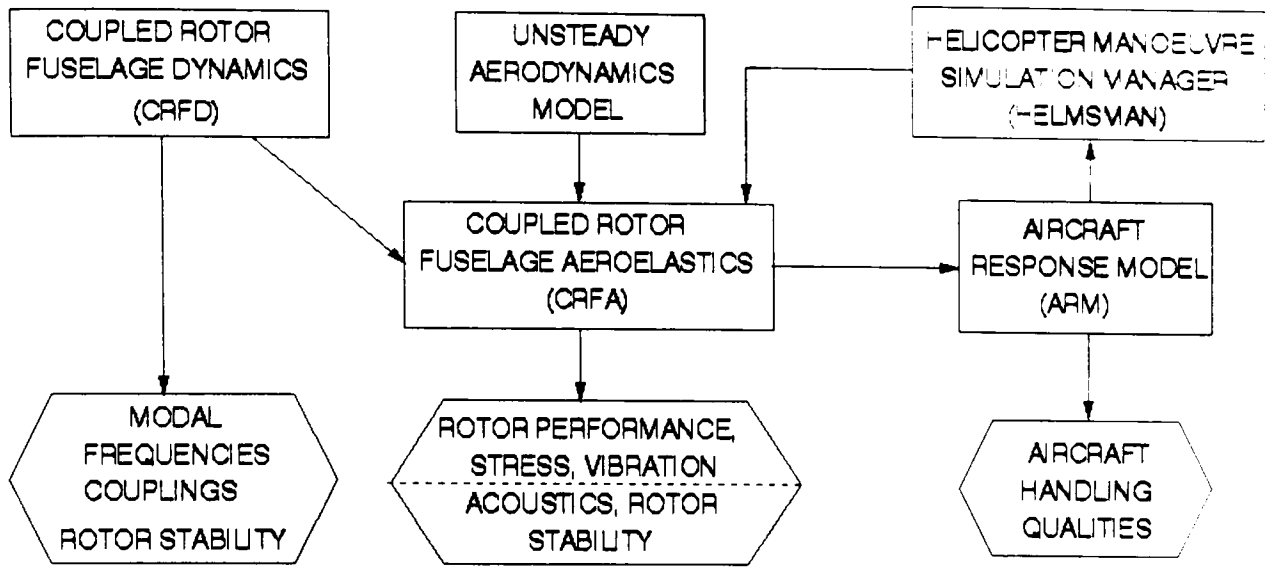

Figure 4.1: Primary Structure of The Coupled Rotor-Fuselage Model

Briefly, CRFA reads the dynamic characteristics of the rotor, *ie.* mode frequencies and shapes, from Program CRFD [4.4] and performs the forced response analysis. The main processing algorithm and the convergence logic used in CRFA, not furnished before, are provided in the flow-charts (*Figures* 4.2 and 4.3). The rotor response calculation is similar to all dynamic models defined in CRFD. The main difference lies only in the definition of forcing functions and the treatment of the solution method for the mode types used, as described in *Sections* 3.5.3 and 3.5.4.

The loadings on all the blades, both aerodynamic and dynamic (including the non-linear and the time varying terms,..,*etc*) are calculated and used as forcing functions for the rotor response evaluation. The blade loads can then be determined and used to assess the blade stresses and airframe vibration. Even for an isolated rotor in flight, the task is still a demanding one.

The other modules, the Aircraft Response Model (ARM) [4.3] solves the aircraft response through a manoeuvre and the HELicopter Manoeuvre Simulation MANager (HELMSMAN) [4.5] determines the pilot input required to maintain the flight path. The pilot inputs so determined are then fed back into the loads module (CRFA) to solve the forced response of the rotor during manoeuvre. Both modules are continuously being developed and are outside the scope of this study. Together they form the complete CRFM.

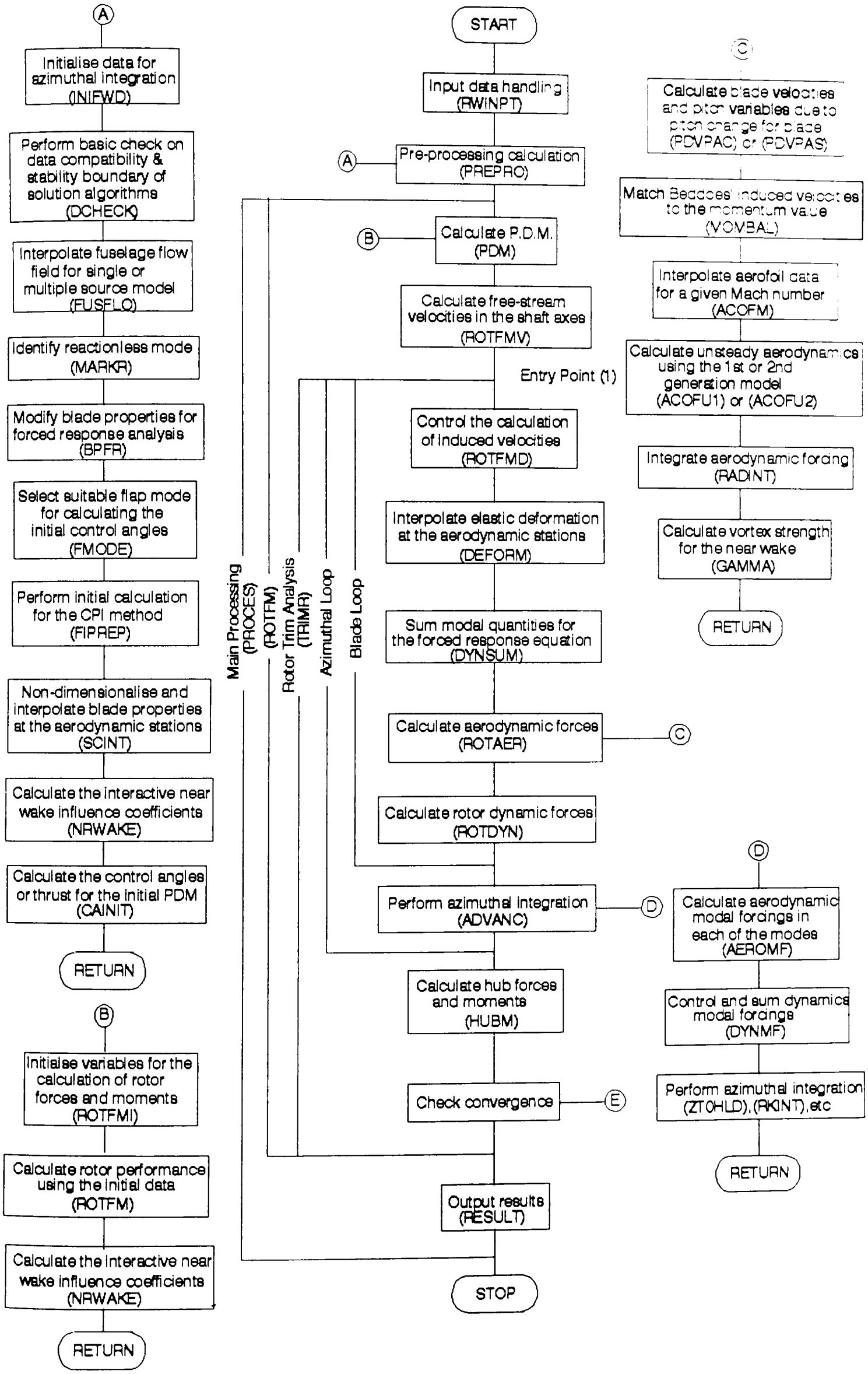

Figure 4.2 - Main Processing of Program CRFA

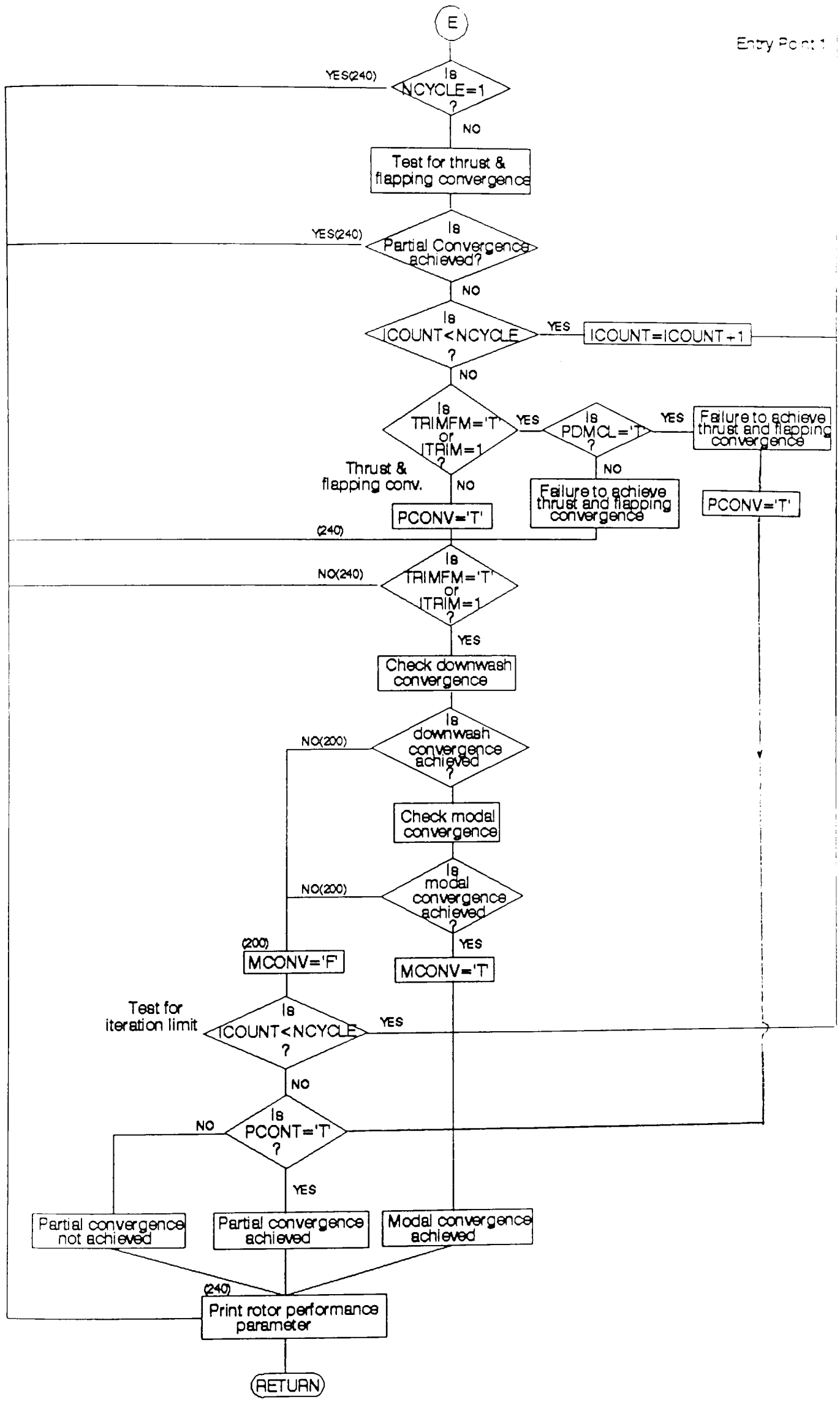

Figure 4.3 - Convergence Logic used in Program CRFA (Subroutine ROTFM)

4.3 Correlation using Program CRFA

4.3.1 The Approach

The approach on correlation using CRFA is carried out in stages. Initially, a set of datum cases using hub-fixed blade modes for a range of rotor and flight conditions are performed. The results are compared with those obtained from Program R150 and flight test data.

Program R150 is chosen as the benchmark mainly because many of its features are similar to CRFA and they adopt similar aerodynamic models. Furthermore, it is a proven model, culminating many years of development at WHL, and has been validated against numerous flight test conditions. The correlation with flight test data between both R150 and CAMRAD/JA can be found in the WHL/NASA collaborative report [4.6]. The simulated conditions cover a wide-range of thrust and speed combinations for a Lynx aircraft fitted with metal blades. The correlation shown represents the general level of prediction capability in the rotorcraft industry. By comparing the results with those obtained from R150, this will ensure that CRFA can be operated in the current level of capability, which will still be extensively used in the foreseeable future.

Based on a single blade model, the effects of hub motion on rotor loads are examined by introducing measured hub motions as external (fixed frame) forcings on the EH101 aircraft. Then the application of CRFA on rotor load calculation on a simulated Lynx loop exit manoeuvre is demonstrated. Finally, the rotor mode concept is demonstrated by applying CRFA to a Lynx case with the transmission system flexibility included. Appropriate explanations on the modelling philosophy will be given.

4.3.2 Datum Correlations

The purpose of performing the datum correlation is not to show advancement in the theory. It aims to provide an opportunity to put together a working model and to address discrepancies, if any, seen between analytical results.

The cases studied include 2 WHL aircraft: Lynx fitted with both metal and BERP blades and EH101 fitted with early development blades. The flight conditions for these cases are at nominal disc loading and over a range of speed. In addition, cases of BERP Lynx in high disc loading are also examined. The latter cases reveal the program characteristics in handling conditions close to the edge of the flight envelope - an area which is generally difficult to simulate.

The process taken is described as follows. Initially, the blade dynamics for the various rotor models are obtained using CRFD. The steady state, based on a hover model [4.7], is first calculated. The hover model calculates the aerodynamic loads for a rotor in hover or axial flight by setting up a wake model consisting of both a near wake sheet and a far wake (a system of tip and root vortex rings). The loads are iterated to the required thrust and pitch angle.

After the steady state, the modes are calculated by searching the eigenvalues of the system. Without damping, the real blade mode shapes (eigenvectors) are defined as radial distributions of deflections and rotations, as well as shears and moments, and are normalised by the largest tip deflection, either in flap, lag or torsional sense. They are referred to as the fundamental, second, third,.. flap, lag or torsion modes. The first 8 modes, comprising 4 flap, 3 lag and 1 torsion modes for each blade, are used for the datum correlation. The modal frequencies and tip couplings for the 4 different blade models at the required thrust are summarised in *Table* 4.1.

The main rotor assembly, blade planform geometry and a schematic diagram of the blade and control system for the metal-bladed Lynx (4-bladed semi-rigid rotor) and the EH101 (5-bladed articulated rotor) are shown in *Figures* 4.4 & 4.5 respectively. Both blades are modelled by a straight segment rotating at a constant angular velocity Ω. The control system stiffness is modelled as a secondary load path to earth attached to the blade. The inertia and structural properties *ie.* mass, flatwise, edgewise and torsional stiffnesses, c.g., centroidal offsets and radii of gyration, defined as radial distributions, for the two blade models are shown in *Figures* 4.6. Imperial units are used throughout.

TITLE: LYNX MAIN ROTOR METAL BLADE AT 9500 LB THRUST - SINGLE BLADE COUPLED MODES
NEWMETAL: CRFA/R150 CORRELATION - MODAL DATA AT Ω= 34.167 R/S

MODE NUMBER	S.S.	1	2	3	4	5	6	7	8
MODAL FREQUENCY (Ω)	-	.64695	1.10952	2.69264	4.32476	4.85113	5.90906	7.95160	9.90764
MODAL DISPLACEMENT-FLAP	2.99806	-.01051	1.00000	1.00000	.07269	1.00000	-.81438	1.00000	.34345
LAG	-.90615	1.00000	.00354	-.12327	1.00000	.00480	.32138	-.24802	1.00000
TORSION	-.01918	-.00002	.00101	-.00190	-.00311	.03071	1.00000	-.03058	-.00915
MODAL INERTIA(CHUGS-IN**2)	-	.07183	.07518	.07597	.08663	.11600	1.85588	.13715	.18856

TITLE: LYNX MAIN ROTOR MONOBLOC HUB BERP BLADE AT 9540 LB. THRUST
LXBERPLO: CRFA/R150 CORRELATION - MODAL DATA AT Ω= 34.167 R/S

MODE NUMBER	S.S.	1	2	3	4	5	6	7	8
MODAL FREQUENCY (Ω)	-	.66542	1.11382	2.63607	4.51109	5.01813	5.35253	8.23150	10.43734
MODAL DISPLACEMENT-FLAP	3.78136	-.01236	1.00000	1.00000	.14281	1.00000	1.00000	1.00000	.32731
LAG	.14149	1.00000	.00338	-.11306	1.00000	-.11965	.52746	-.15345	1.00000
TORSION	-.00578	-.00017	.00100	-.00348	-.02126	-.04838	.59548	.01323	-.00048
MODAL INERTIA(CHUGS-IN**2)	-	.07067	.07385	.06525	.07663	.07526	.77841	.06273	.12972

TITLE: EH101 MRB 15JAN92 EH53 FLAT TIPPED STD. DEV. BLADE + ADD. ALTIP
EH53D3NEW: CRFA/R150 CORRELATION - MODAL DATA AT Ω= 21.967 R/S

MODE NUMBER	S.S.	1	2	3	4	5	6	7	8
MODAL FREQUENCY (Ω)	-	.28254	1.03368	2.88118	4.91954	5.88786	6.58553	10.99203	12.87110
MODAL DISPLACEMENT-FLAP	13.7273	-.00538	1.00000	1.00000	.34732	1.00000	1.00000	1.00000	.10099
LAG	-21.4222	1.00000	.00622	-.19472	1.00000	-.22666	-.18302	-.14083	1.00000
TORSION	-.00684	-.00041	-.00073	.00157	-.00402	-.04676	.12504	.00624	.00736
MODAL INERTIA(CHUGS-IN**2)	-	.24810	.24533	.14871	.22534	.17011	.49815	.09163	.23098

TITLE: LYNX MAIN ROTOR MONOBLOC HUB BERP BLADE AT 11905 LB. THRUST (CRFD)
LXBERPHI: CRFA/R150 CORRELATION - MODAL DATA AT Ω= 32.801 R/S

MODE NUMBER	S.S.	1	2	3	4	5	6	7	8
MODAL FREQUENCY (Ω)	-	.67343	1.11356	2.65679	4.54521	5.10296	5.54942	8.37279	10.39574
MODAL DISPLACEMENT-FLAP	9.3120	-.02331	1.00000	1.00000	.09763	1.00000	1.00000	1.00000	.59258
LAG	-4.1697	1.00000	.00682	-.19215	1.00000	-.09098	.53511	-.32921	1.00000
TORSION	0.04792	-.00035	.00102	-.00281	-.02763	-.04695	.49881	.01126	-.00090
MODAL INERTIA(CHUGS-IN**2)	-	.07055	.07388	.06692	.07987	.07266	.55919	.06530	.15056

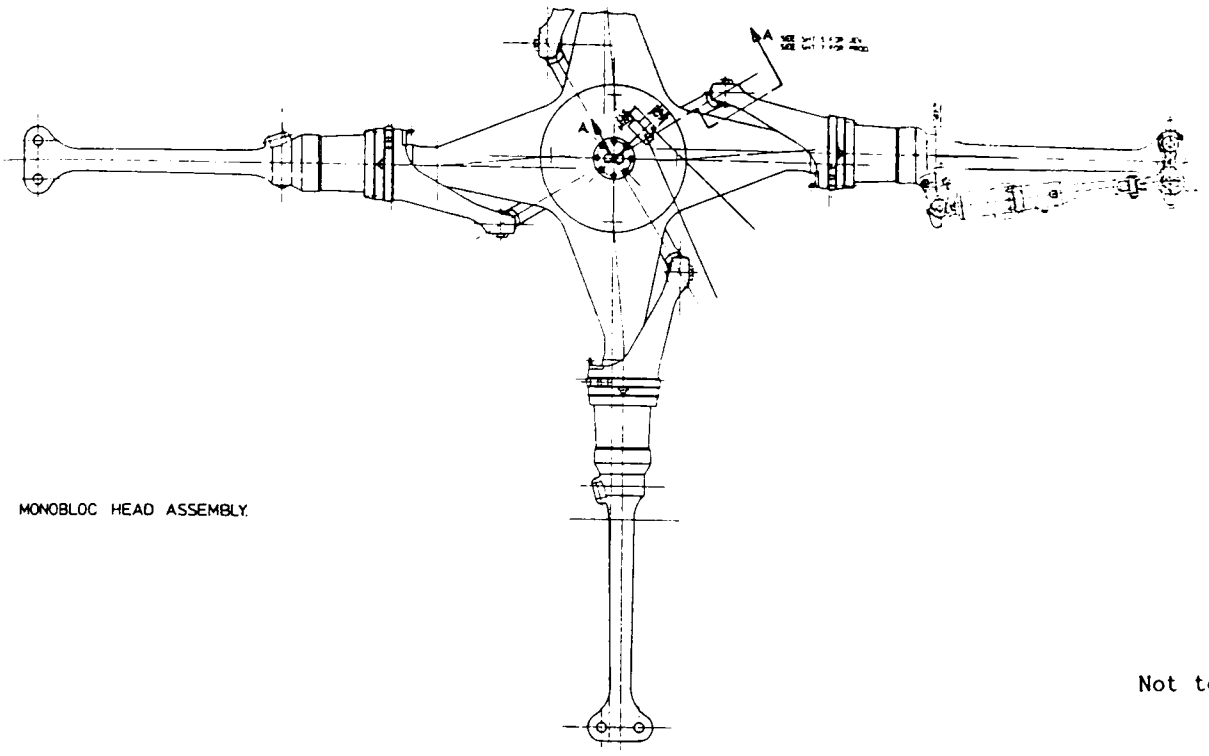

MONOBLOC HEAD ASSEMBLY.

Not to Scale

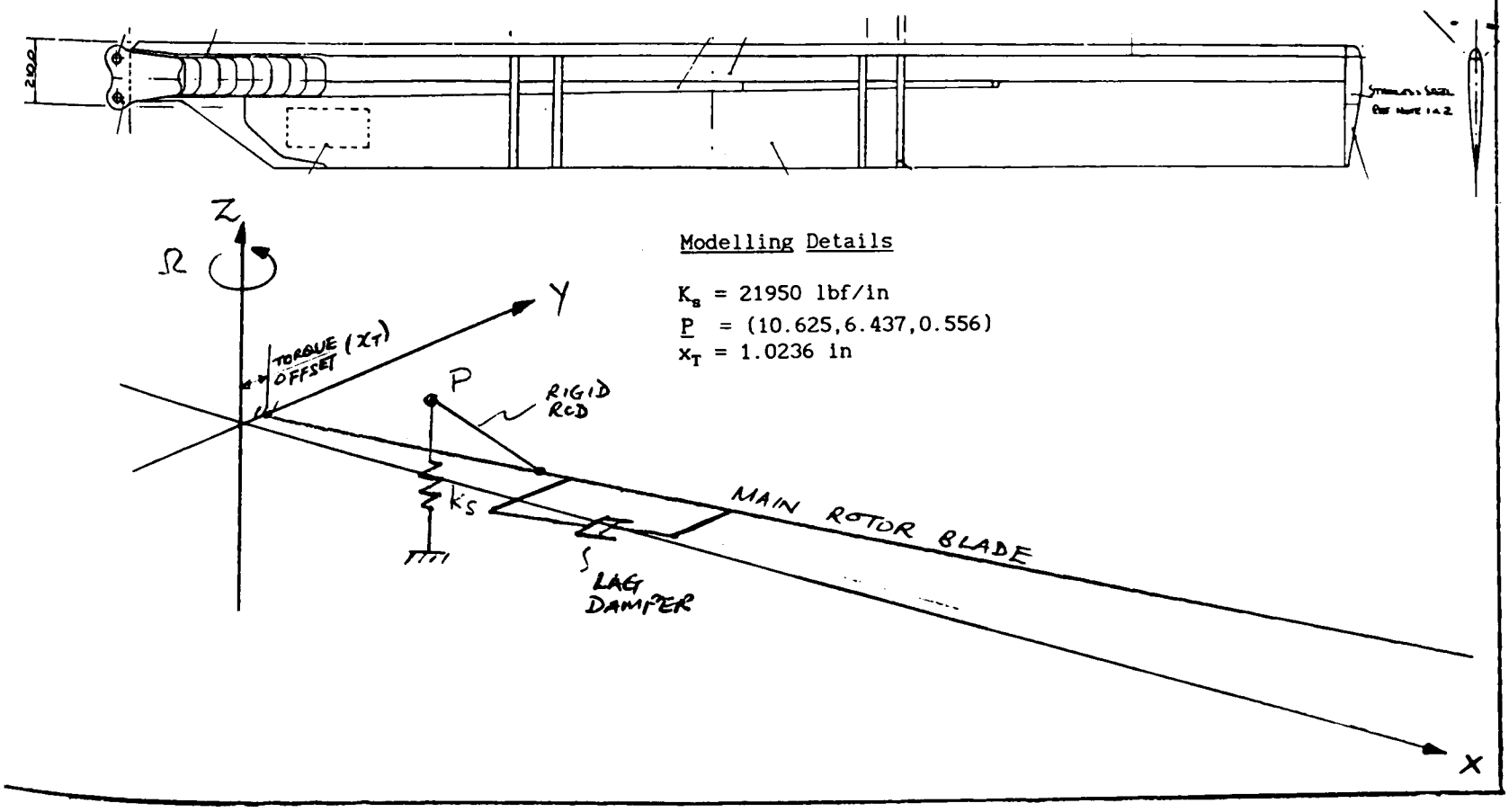

Modelling Details

K_s = 21950 lbf/in

P = (10.625, 6.437, 0.556)

x_T = 1.0236 in

Figure 4.4 - Lynx Main Rotor Assembly and Model Schematic Diagram

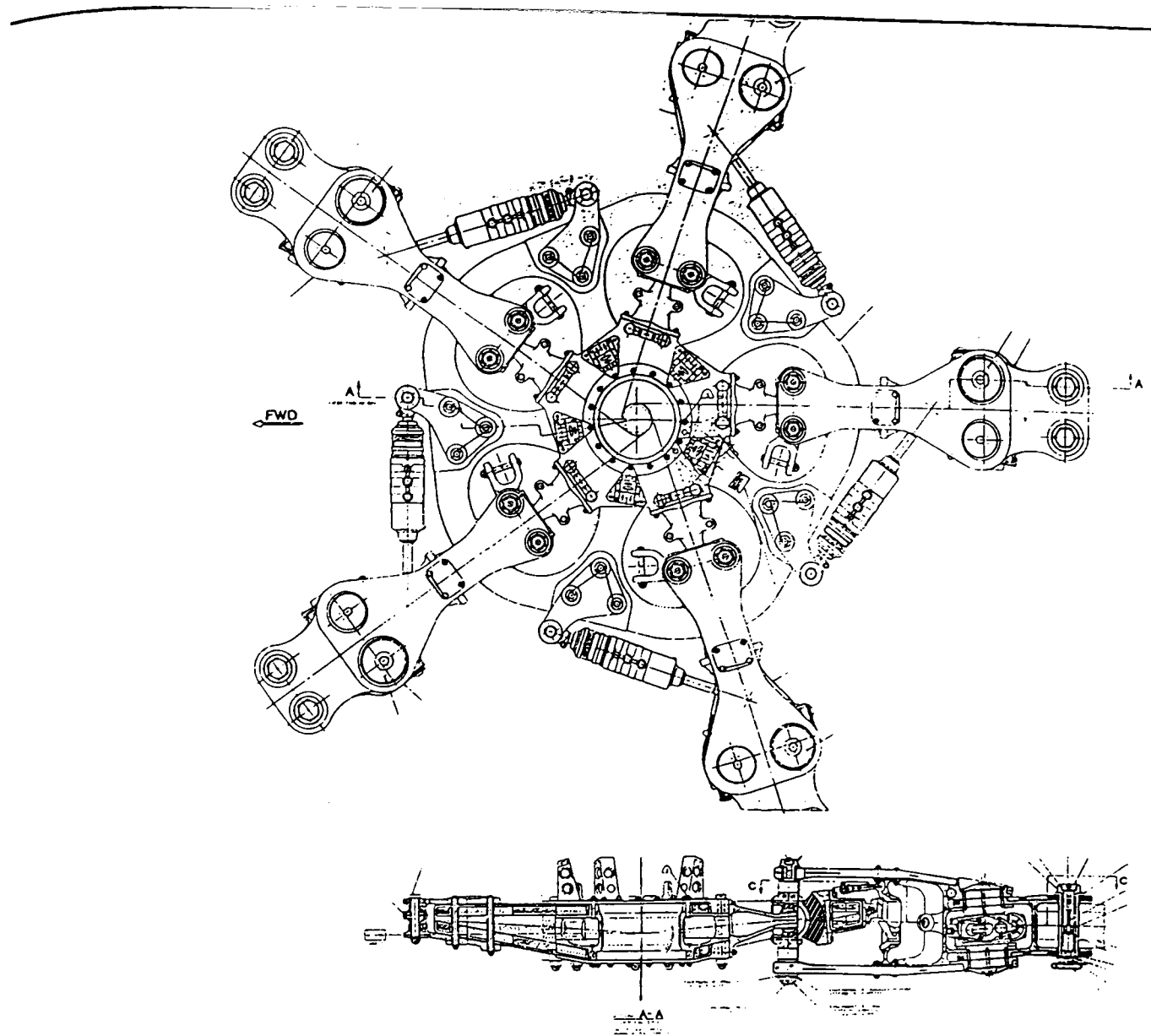

Modelling Details

K_s = 56000 lbf/in

$\underline{P}$ = (16.507, -4.807, 1.162)

x_T = 1.89 in

Hinge Stiffness

K_x = 9454 lbf-in/rad

K_y =25439 lbf-in/rad

K_z =25439 lbf-in/rad

Figure 4.5 - EH101 Main Rotor Assembly and Model Schematic Diagram

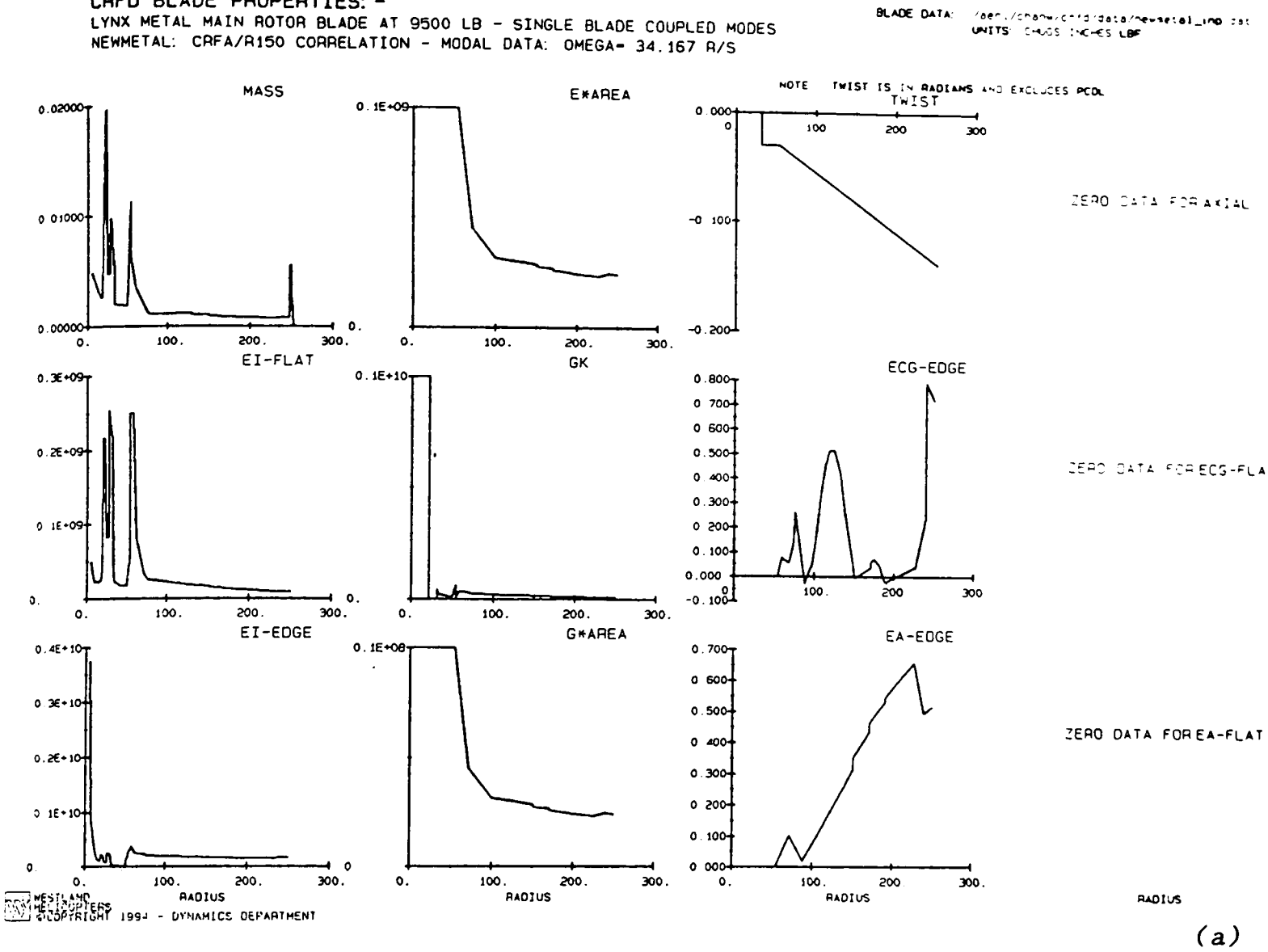

Figure 4.6 - Blade Structural Properties (a) Lynx (Metal) (b) EH101 (Dev.Std.)

Now for the forced response calculation. For all the datum cases, the rotor is trimmed to the required thrust and head moments by adjusting the collective and cyclic pitch angles. The thrust and head moment values are derived from flight test data using the Strain Modal Synthesis (SMS) method [4.8]. SMS is a technique by which a best fit, using the same blade mode set, is made to the harmonic components of the measured bending moment. The solution of the modal quantities from the best fit is then used to construct other loads, particularly hub loads, and deflections that are not measured.

The blade geometry *ie.* chord, sweep angle, aerodynamic centre offset, aerofoil section, *etc* are input as radial distributions. The section coefficients (C_L, C_D & C_M) are determined using Beddoes' indicial aerodynamic model [4.9]. Both the fuselage upwash model based on the slender body theory [4.10] and the non-linear lag damper model are included.

Using the procedure briefly described above, the results for all the datum correlation cases were obtained and reported in detail [4.11]. The results for all the metal and BERP Lynx cases at nominal disc loadings compared extremely well between the two programs and favourably with flight test data. The results on the two speeds each for the EH101 and the high disc loading Lynx cases are presented here. The rotor performance parameters are tabulated in *Table* 4.2 alongside the R150 results. The corresponding structural loads, calculated using Modal Summation with unified formulation of lag damper loads, are presented as waveform plots in *Figures* 4.7 and compare well with only detailed differences.

For the EH101 rotor, the prediction for both flatwise and edgewise loads are similar in both programs (*Figures* 4.7(a) and 4.7(b)) It is evident that both programs under-predict the 3R flatwise loads at the two speeds but for reasons which are still unclear. The inability to predict the 3R load at low speed is initially thought to be attributed to the induced velocity modelling around the azimuth. However the NASA/WHL collaborative study [4.6] has revealed that there was no particular benefit when the free wake model was introduced. The slight improvement in the control load prediction using CRFA on the advancing side and in the mid-span torque for the high speed case, was attributed to an error found in R150.

For the BERP Lynx cases, a deficiency with the trim process using the partial derivative matrix (PDM) method in CRFA has been highlighted. The problem is due to the numerical sensitivity in this highly non-linear region of the lift-incidence curve. *Figure* 4.7(c) shows the typical variations of rotor parameters during the trimming process for both the low and high disc loading conditions. The PDM method calculates the changes of rotor parameters by perturbing each of the rotor controls in turn. It assumes the variation is linear over the range of perturbation and is used to relate the out of trim conditions. The use of PDM, a process which is mathematically simple, does not always guarantee that the required trim can be achieved in this region since the linear assumption is no longer valid. Although a trim in this regime was achieved using CRFA, earlier results showed large discrepancies in the rotor power between CRFA and R150. These discrepancies were attributed to the different amount of stall penetration characterised by the two programs. This was eventually overcome by ensuring that both rotor models generate the same H-force, a measure of stall penetration, using an iterative trim process.

Using the revised trim in both programs, the comparison of rotor performance is shown in *Table* 4.2 and is considered reasonably good in such a flight regime. When correlating the loads prediction with flight test data, shown in *Figures* 4.7(d) & (e), CRFA has shown improvement in the peak-to-peak flatwise loads prediction as the over-predictions of the 5R content exhibited by R150 no longer exist. However, the control load comparisons indicate that there is a slight degradation on the advancing side at the low speed.

The conclusions from this datum correlation are that the agreement in the rotor performance and structural loads on a range of rotor and flight conditions is very good. The main difficulty lies with the trim calculation for the high disc loading cases using the PDM method in Program CRFA. However, directly comparable results between the two programs can be obtained provided that care is taken to ensure similar amount of stall penetration are experienced by both rotor models. This is, in fact, more representative than trimming the rotor in isolation. Nevertheless, refinement of the PDM method is needed in order that it can deal with various flight regimes. Once this is carried out, it is possible to turn CRFA into an operational tool with at least the same level of capability as R150.

le 4.2 - Datum Correlation: Comparison of Rotor Performance Parameters for EH101 & BERP Lynx

Aircraft	EH101 (DEV.STD.)		EH101 (DEV.STD.)		LYNX (BERP)		LYNX (BERP)	
TAS (kts)	40.0		150.0		66.0		102.0	
Date Run	12/05/94	11/05/94	12/05/94	11/05/94	14/12/93	04/01/94	18/01/94	04/01/94
Version	R150SS	CRFA	R150SS	CRFA	R150SW3	CRFA	R150SW3	CRFA
Control Angles (deg)	(-ve Fourier Series)							
Collective, A0	15.527	15.881	17.522	18.421	15.547	14.719	16.687	14.593
Lateral, A1	-6.044	-6.044	-2.254	-2.940	-4.809	-4.805	-3.831	-4.839
Longitudinal, B1	6.238	6.238	10.585	11.422	6.478	6.577	8.622	9.282
Tip Flapping (deg)	(-ve Fourier Series)							
Coning, a0	5.24	5.532	4.65	4.996	4.74	5.195	4.58	5.076
Longitudinal, a1	-2.84	-2.701	-1.26	-1.222	-0.221	-0.217	-0.476	-0.107
Lateral, b1	0.718	0.709	1.51	1.519	0.088	0.031	0.040	0.057
Tip Mean Lag (deg)	-0.074	-0.491	-1.20	-1.729	0.106	-0.009	0.370	0.189
Tip Torsion (deg)	(-ve Fourier Series)							
Mean	-0.350	-0.358	-0.192	-0.165	0.198	0.419	-0.050	0.005
A1	0.488	0.478	-1.24	-1.276	-0.952	-0.967	-1.47	-1.221
B1	-0.425	-0.375	-0.441	-0.441	-0.507	-0.453	-0.831	-0.976
Rotor Forces (lbf)								
Thrust	26931.4	26874.4	26213.3	26308.8	11754.9	11766.8	11612.7	11634.9
X-Force	1514.0	1464.2	784.7	723.9	209.6	166.1	381.1	261.0
Y-Force	-1144.7	-1092.5	-603.5	-550.8	-541.4	-561.6	-546.1	-562.0
Rotor Moments(lbf-in)								
MX	5809	6846	13078	16216	-9070	-7638	-11301	-9639
MY	-176740	-180397	-80155	-80417	-6814	-9784	12403	9746
Power (hp)								
Induced Power	1867.9	1945.3	2181.2	2237.0	638.7	654.6	187.2	177.0
Profile Power	466.5	497.1	608.1	673.4	306.0	262.5	550.2	587.0
Total Power	2334.4	2442.4	2789.3	2910.3	944.7	917.1	737.4	764.0
Convergence Level	Thrust & Moment Trim only	Modal	Thrust & Moment Trim only	Partial	Thrust & moment trim only	Partial	Thrust & Moment Trim only	Partial
Modes	J134	J134	J134	J134	CRFD	CRFD	CRFD	CRFD

FLATWISE BENDING MOMENT ~ AZIMUTH
X = 0.470

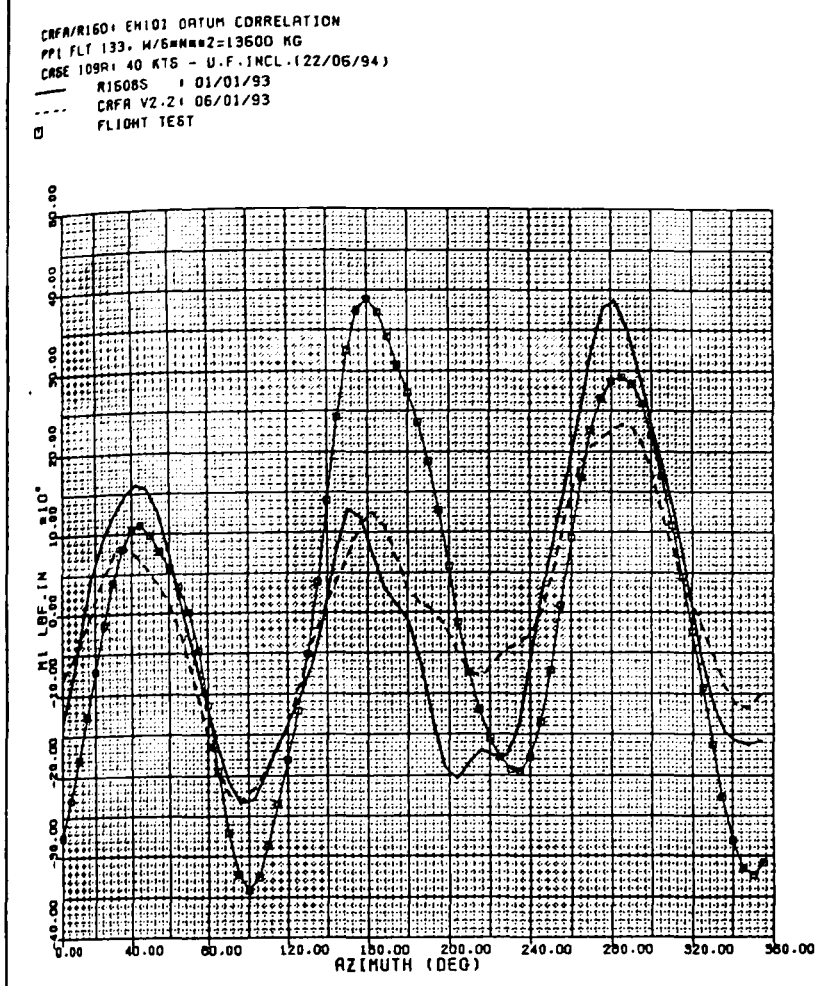

EDGEWISE BENDING MOMENT ~ AZIMUTH
X = 0.470

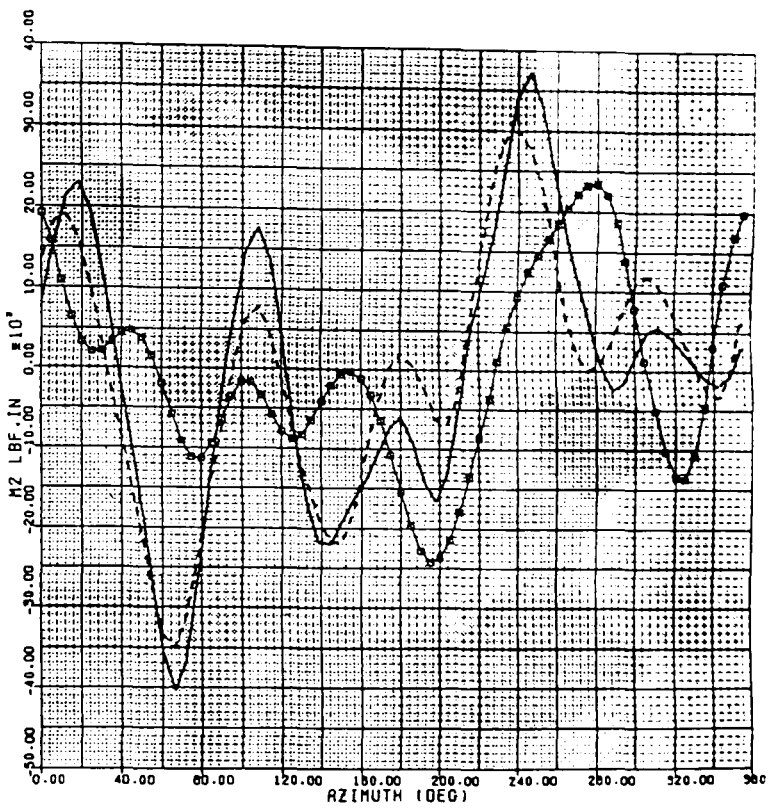

CONTROL LOAD ~ AZIMUTH

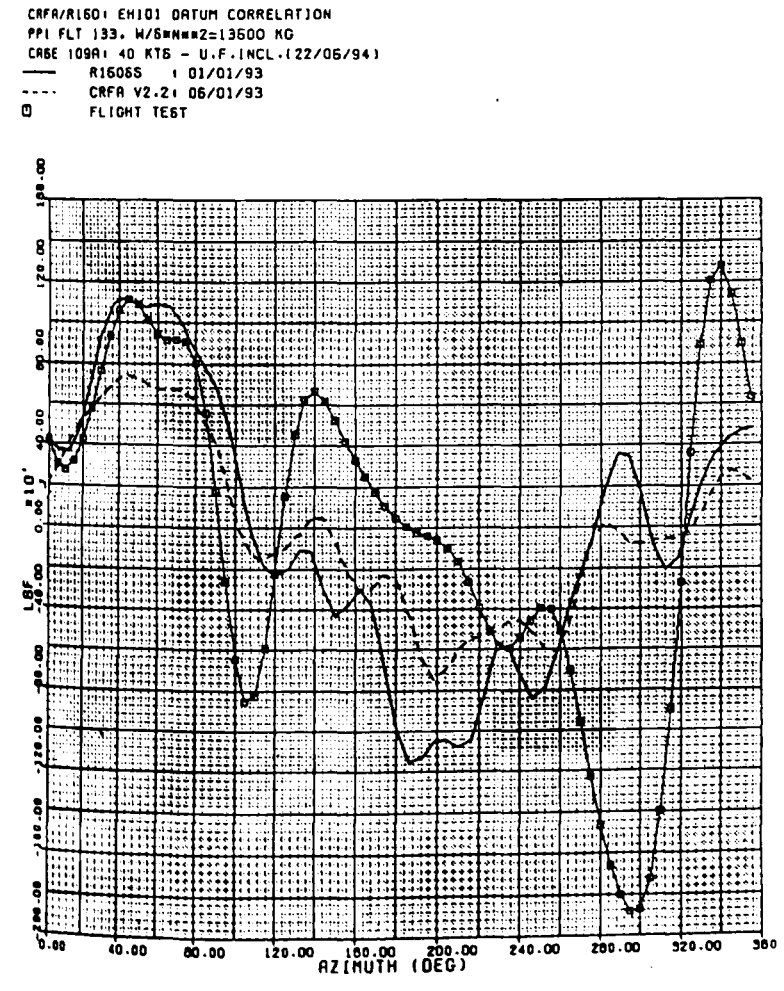

TORQUE ~ AZIMUTH (DEFORMED AXES)
X = 0.470

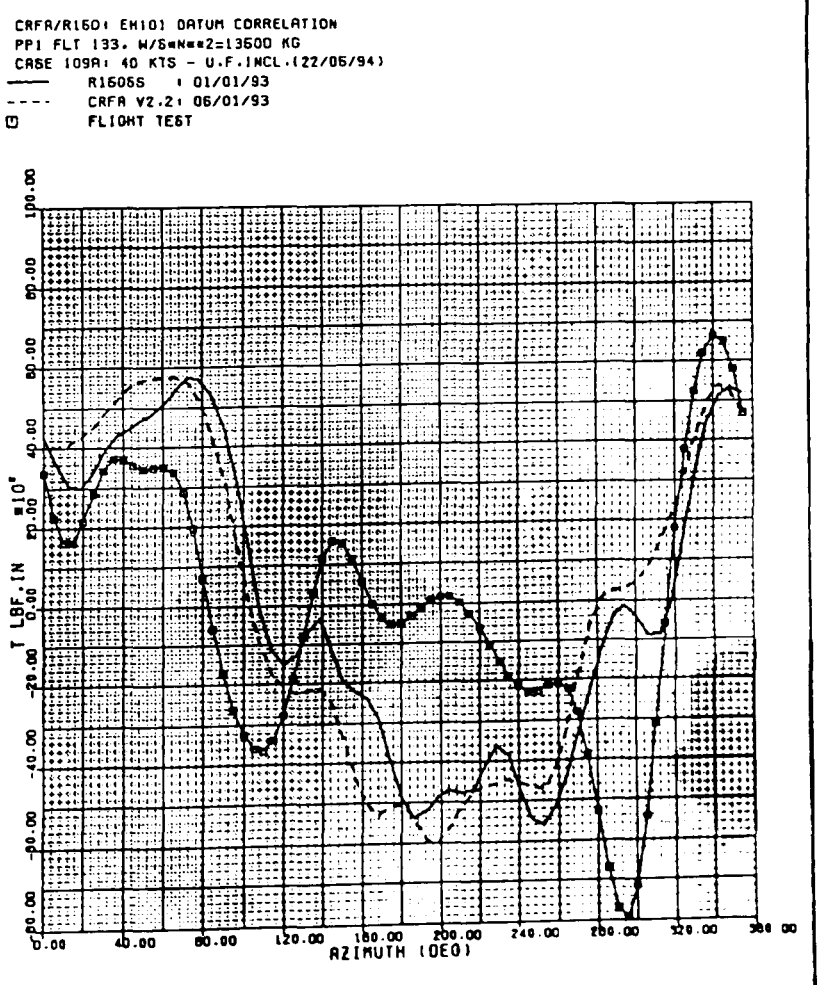

Figure 4.7(a) - Structural Loads Comparison for EH101 (40 ktas)

FLATWISE BENDING MOMENT ~ AZIMUTH
X = 0.470

CRFA/R160: EH101 DATUM CORRELATION
PP1 FLT 133. W/S=N=*2=13600 KG
CASE 109C:160 KTS - U.F.INCL.(22/06/94)
—— R1606S : 01/01/93
---- CRFA V2.2: 06/01/93
□ FLIGHT TEST

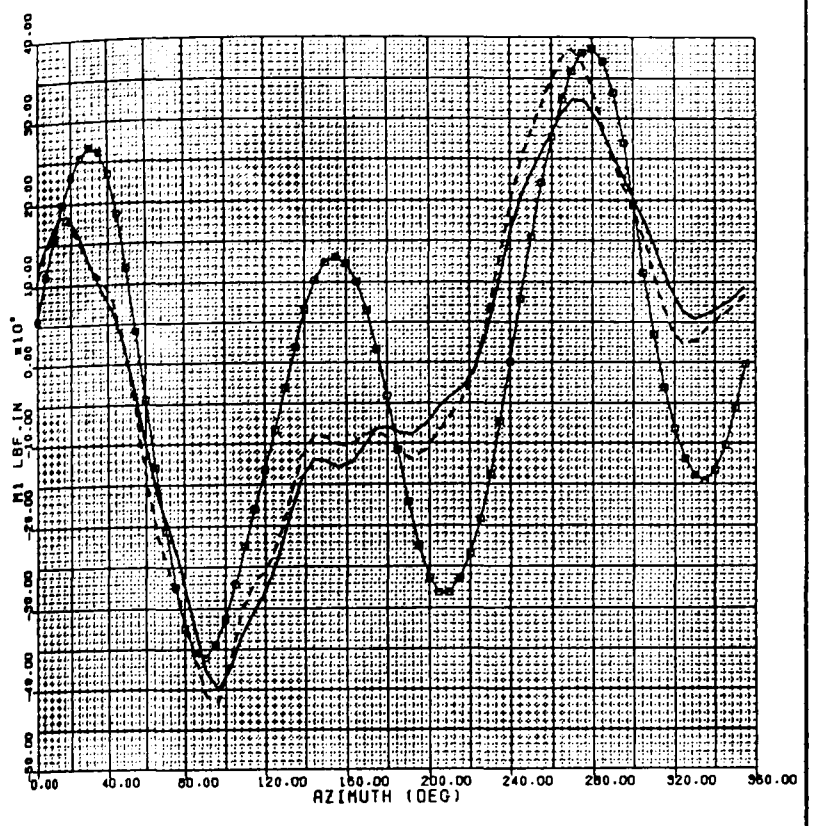

EDGEWISE BENDING MOMENT ~ AZIMUTH
X = 0.470

CRFA/R160: EH101 DATUM CORRELATION
PP1 FLT 133. W/S=N=*2=13600 KG
CASE 109C:160 KTS - U.F.INCL.(22/06/94)
—— R1606S : 01/01/93
---- CRFA V2.2: 06/01/93
□ FLIGHT TEST

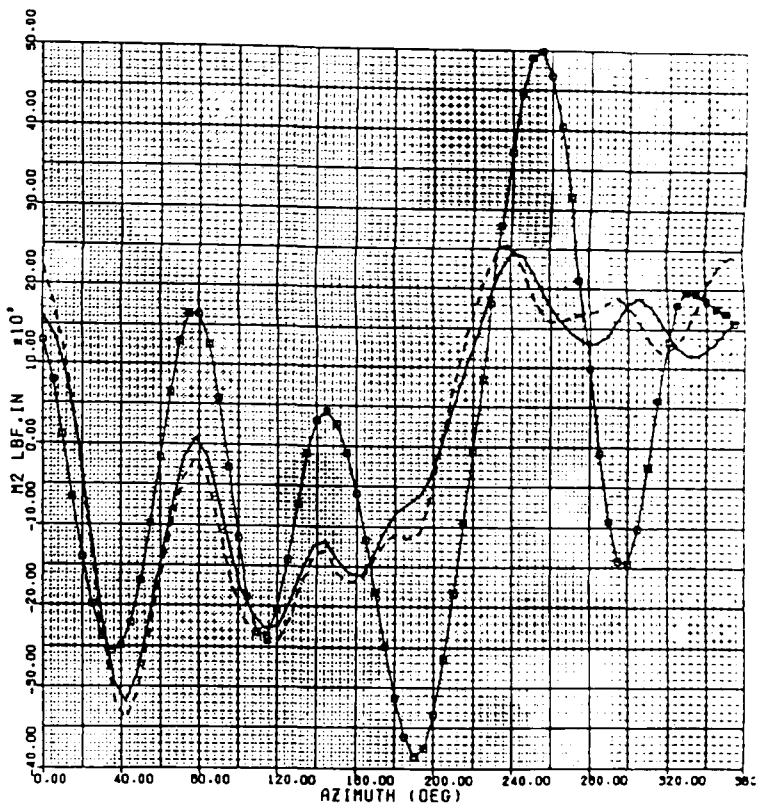

CONTROL LOAD ~ AZIMUTH

CRFA/R160: EH101 DATUM CORRELATION
PP1 FLT 133. W/S=N=*2=13600 KG
CASE 109C:160 KTS - U.F.INCL.(22/06/94)
—— R1606S : 01/01/93
---- CRFA V2.2: 06/01/93
□ FLIGHT TEST

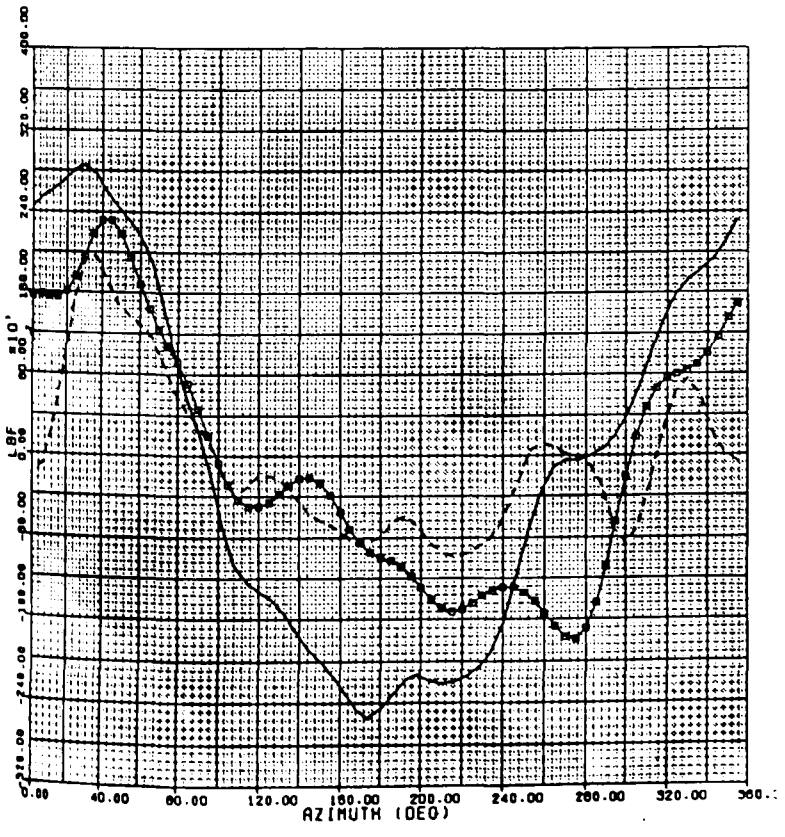

TORQUE ~ AZIMUTH (DEFORMED AXES)
X = 0.470

CRFA/R160: EH101 DATUM CORRELATION
PP1 FLT 133. W/S=N=*2=13600 KG
CASE 109C:160 KTS - U.F.INCL.(22/06/94)
—— R1606S : 01/01/93
---- CRFA V2.2: 06/01/93
□ FLIGHT TEST

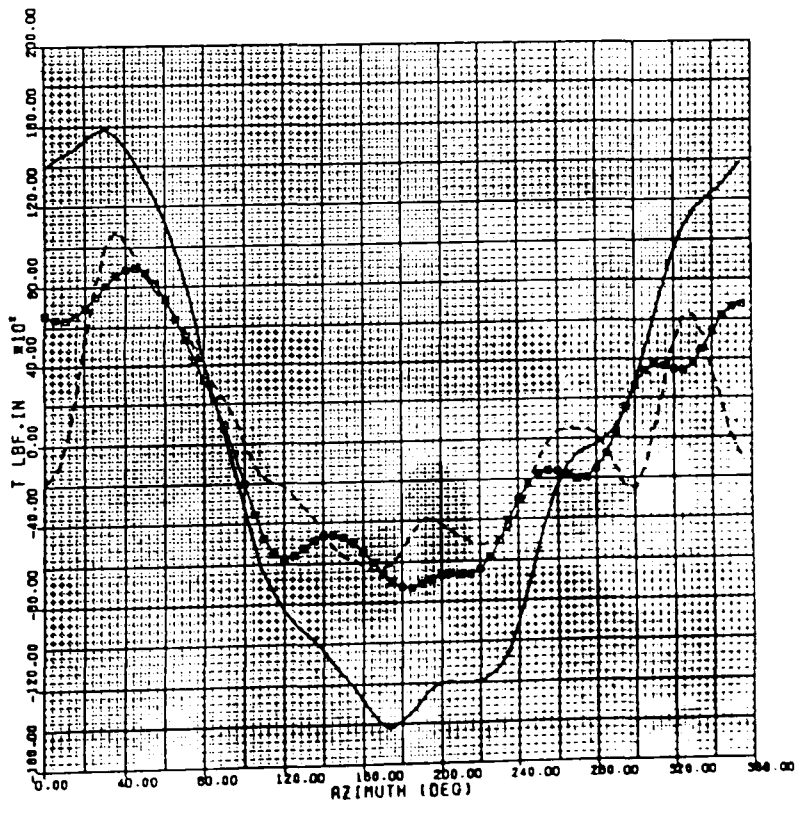

Figure 4.7(b) - Structural Loads Comparison for EH101 (150 ktas)

COUPLED ROTOR FUSELAGE ANALYSIS
TRACES OF TRIM PARAMETERS

21.12.94

CRFA/R150 BERP3 LYNX DATUM CORRELATION - SINGLE BLADE MODES
NEW 107C: V3.0 BM CASE 2: COLL. PRESET 16.5 (21/12/94)

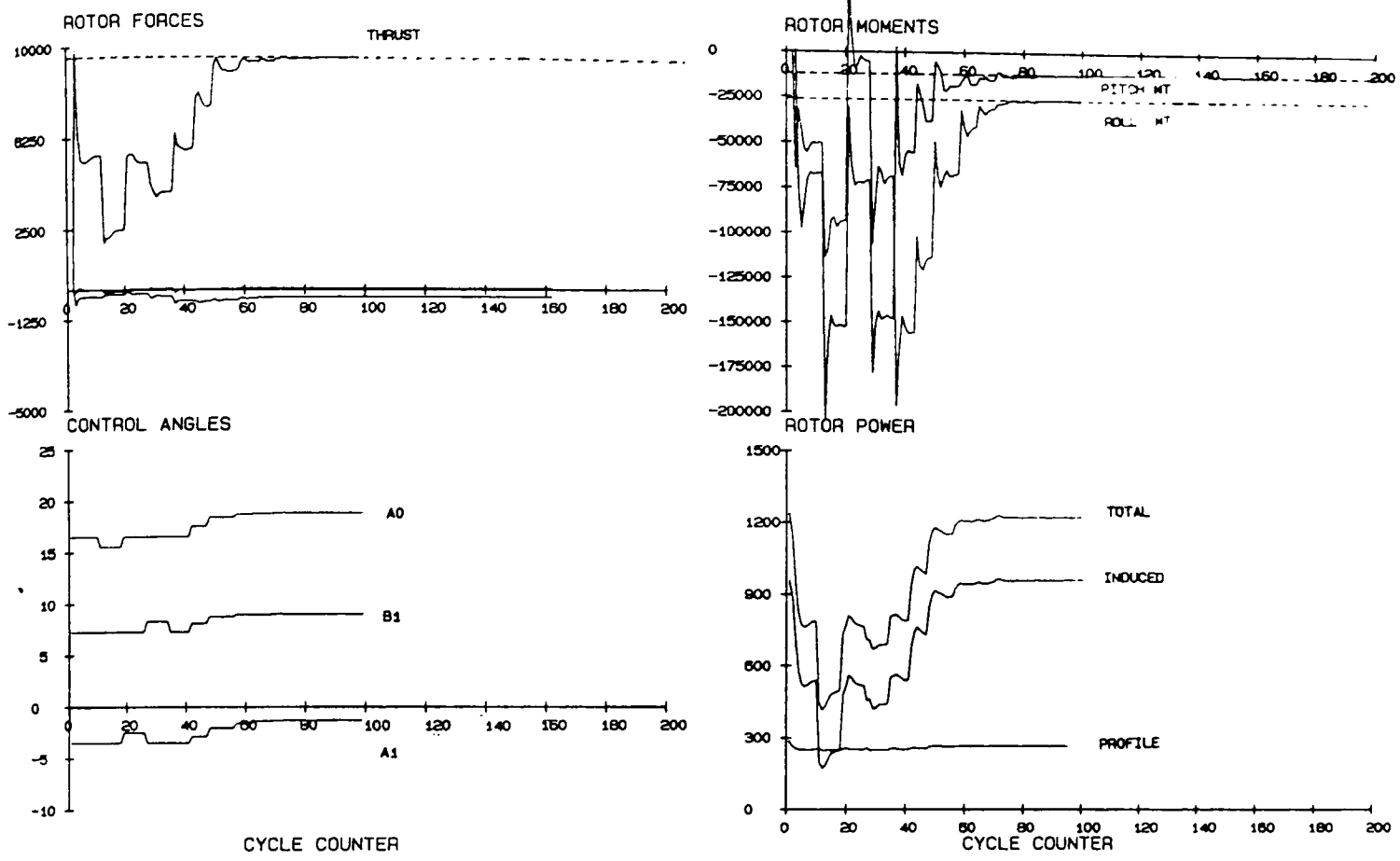

COUPLED ROTOR FUSELAGE ANALYSIS
TRACES OF TRIM PARAMETERS

7.2.95

CRFA/R150 BERP LYNX DATUM CORRELATION - CRFD MODES - NO P-G CORR
TEMP108A: V3.0 BENCHMARK CASE 4A: HD LOADING, NO A1MOD (07/02/95)

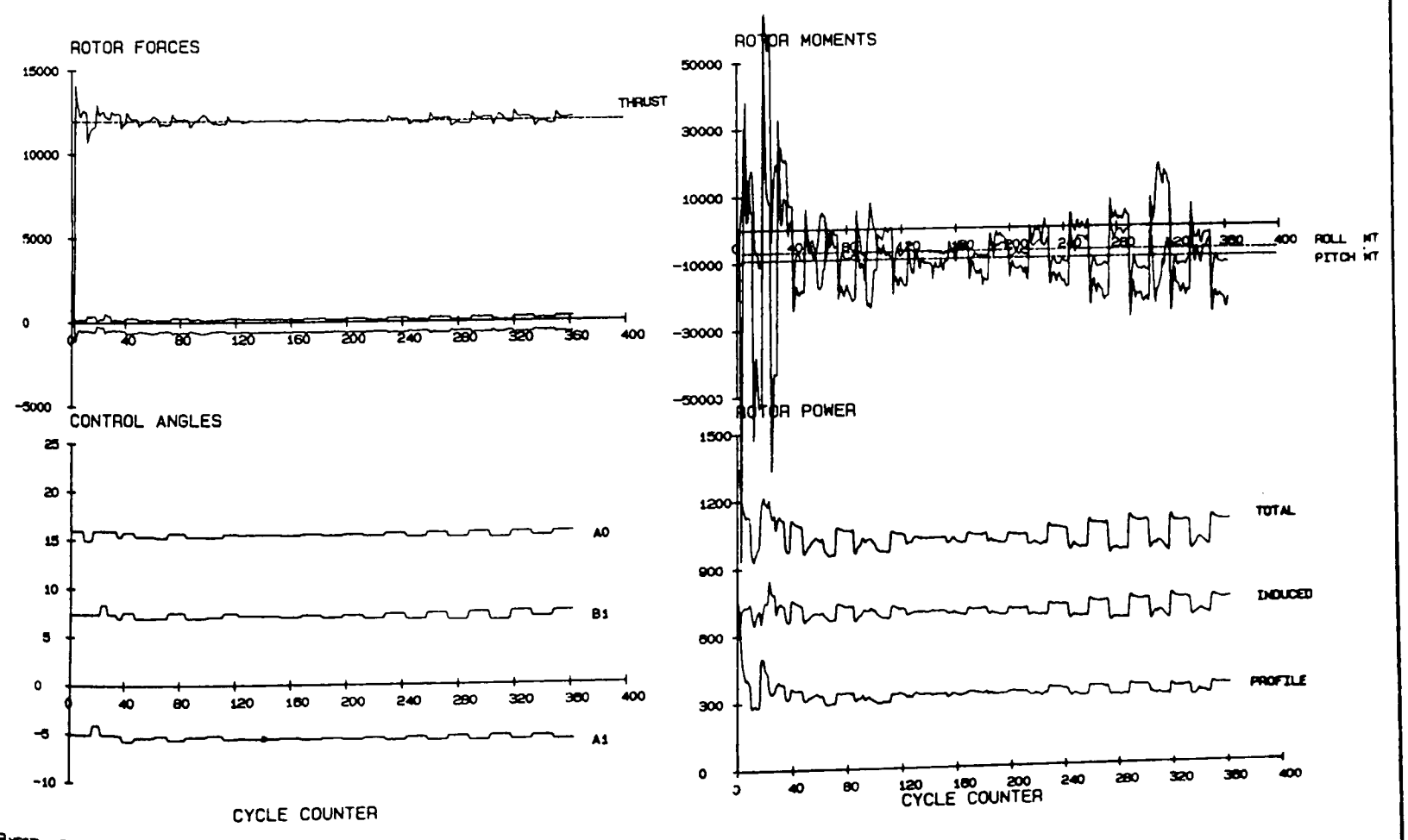

Figure 4.7(c) - Example of Trim Parameter Traces using The PDM method (BERP Lynx)

FLATWISE BENDING MOMENT ~ AZIMUTH
X = 0.640

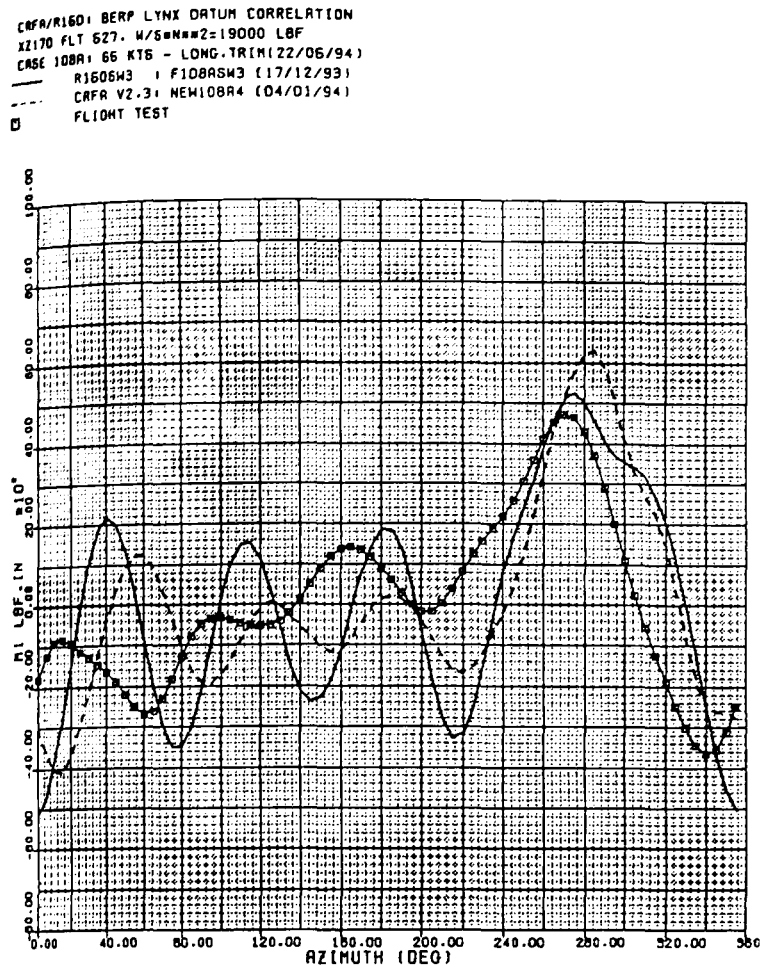

EDGEWISE BENDING MOMENT ~ AZIMUTH
X = 0.311

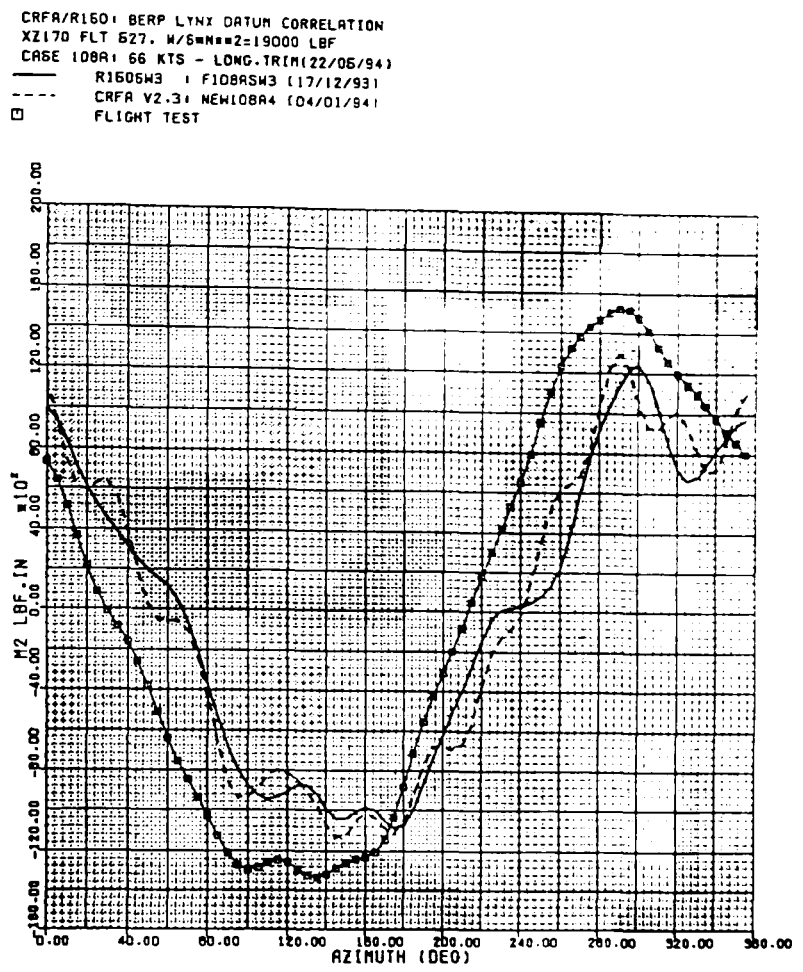

CONTROL LOAD ~ AZIMUTH

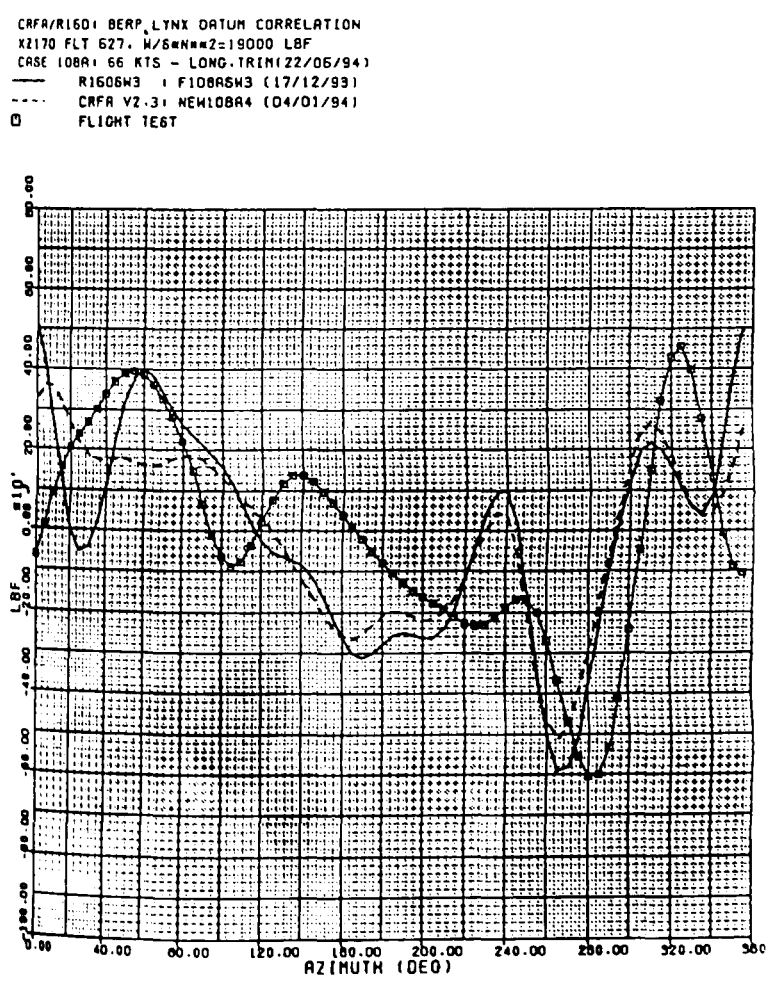

FLATWISE BENDING MOMENT ~ AZIMUTH
X = 0.311

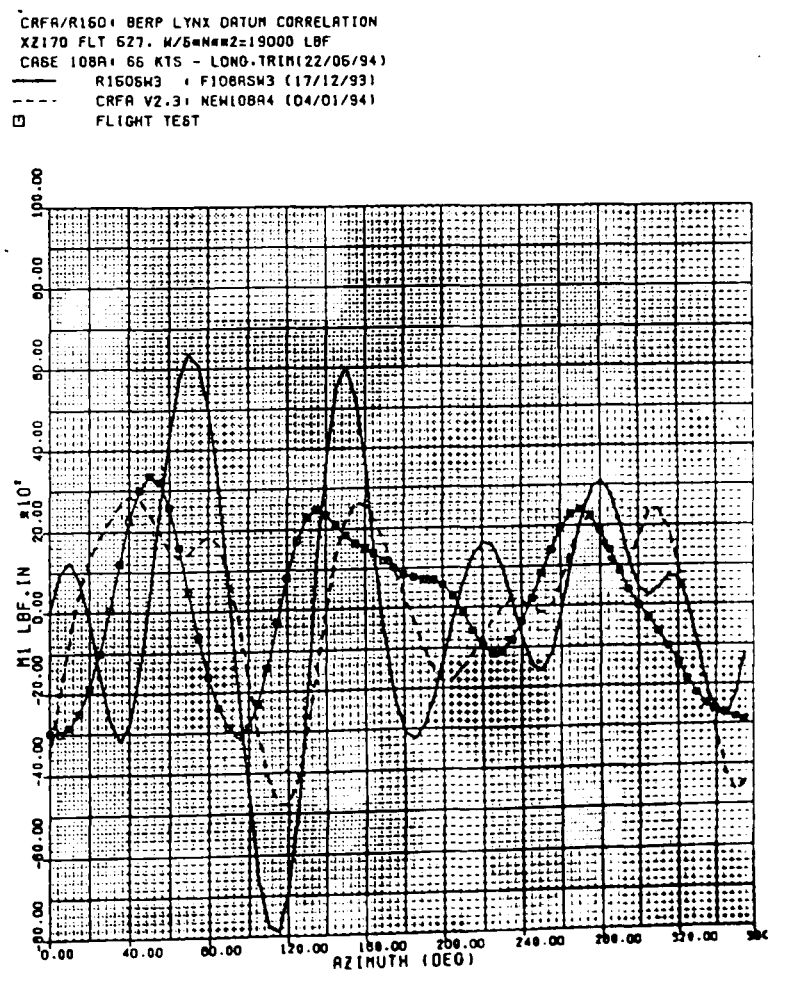

Figure 4.7(d) - Structural Loads Comparison for BERP Lynx (66 ktas)

FLATWISE BENDING MOMENT ~ AZIMUTH
X = 0.640

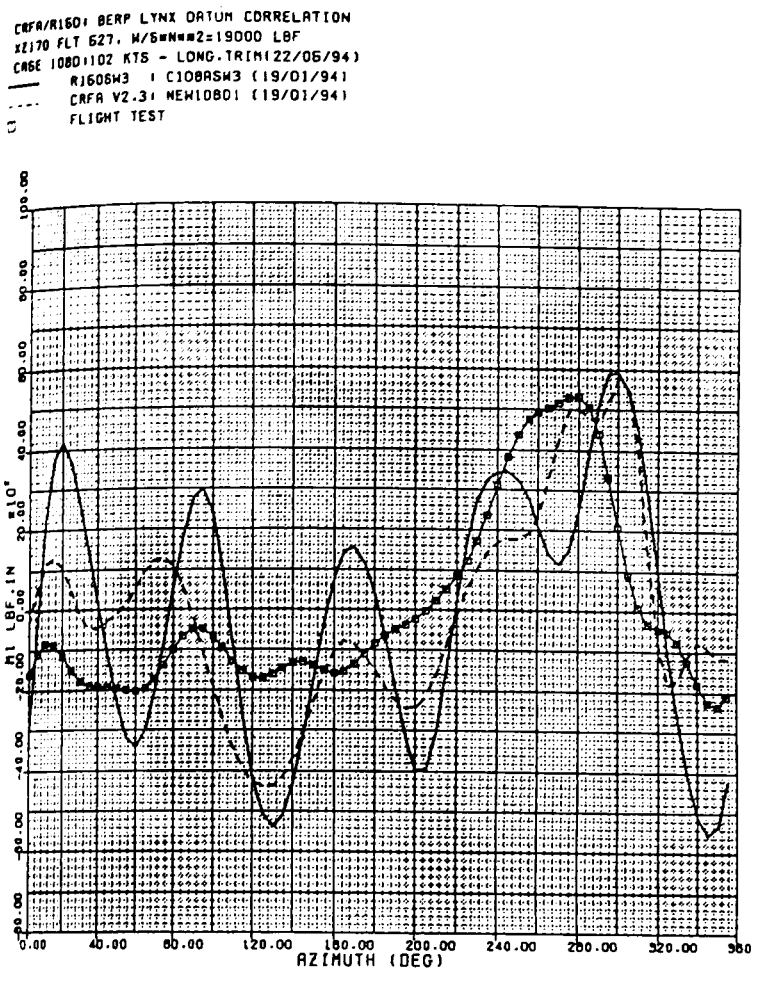

EDGEWISE BENDING MOMENT ~ AZIMUTH
X = 0.311

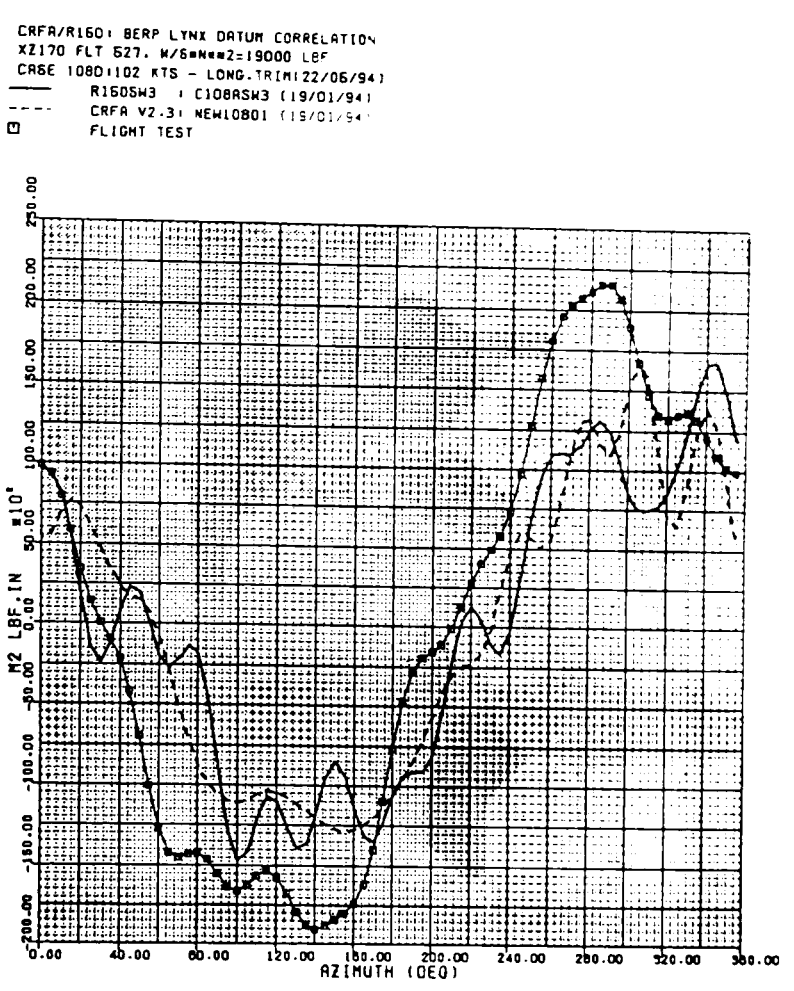

CONTROL LOAD ~ AZIMUTH

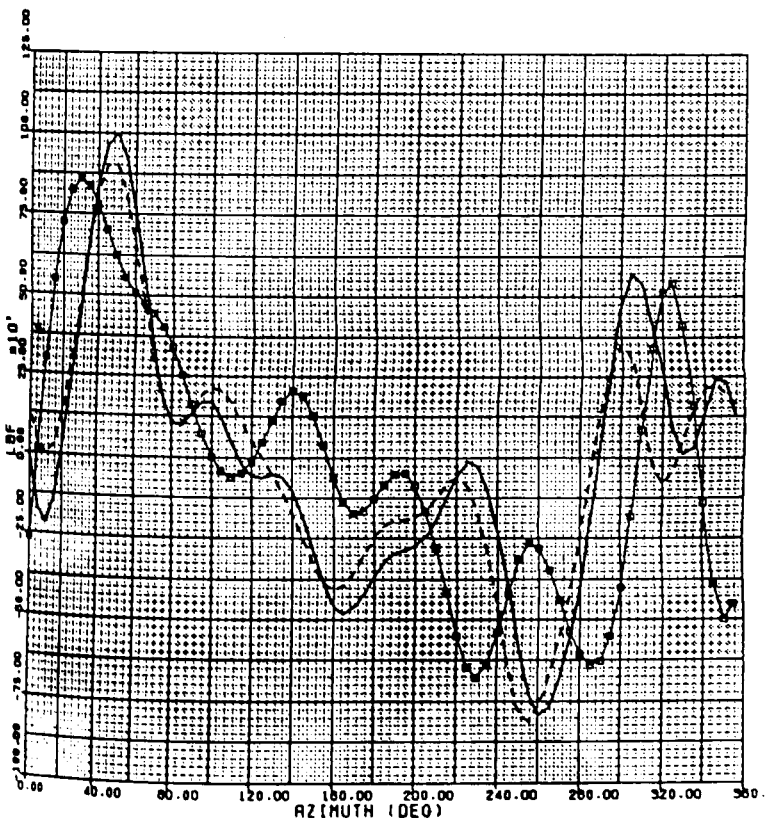

FLATWISE BENDING MOMENT ~ AZIMUTH
X = 0.311

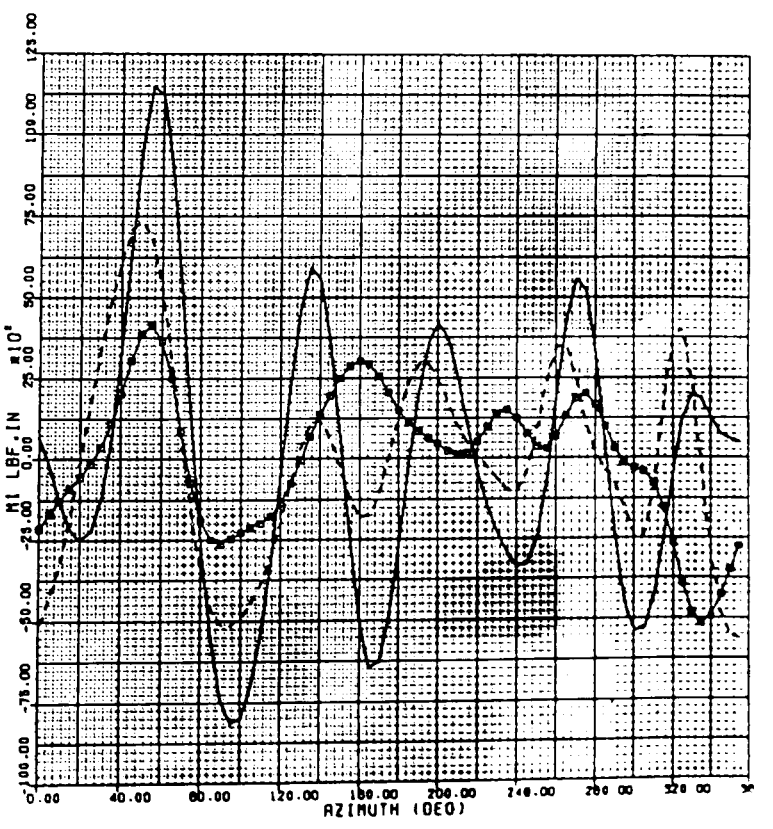

Figure 4.7(e) - Structural Loads Comparison for BERP Lynx (102 ktas)

4.3.3 Effects of Hub Motions on Rotor Vibratory Loads

One of the two main objectives of this study is to include the effects of hub motion on rotor loads and hence, airframe vibration. The effects of hub motion can be introduced using complex rotor modes as state vectors in the forced response analysis. Alternatively, they can be introduced as external forcings on a single blade modelled with real modes. Since the software development for incorporating the complex rotor modes solution is currently being carried out, it is decided to adopt the latter approach. Program CRFA is modified to incorporate hub motions as external NR (N/rev) fixed frame forcings, N being the number of blades. The hub motion modal forcing, for the i^{th} blade mode, is defined by the following terms (extracted from *Appendix* I),

$$HMF_i = -\frac{1}{\Omega^2 R I_i}\int_0^R \Big\{ m\{v_i[r\ddot{\psi}_H - \ddot{x}_H\sin\psi_k + \ddot{y}_H\cos\psi_k] + w_i[\ddot{z}_H - r(\ddot{\vartheta}_H\cos\psi_k - \ddot{\phi}_H\sin\psi_k)]\} + 2m\Omega r w_i(\dot{\vartheta}_H\sin\psi_k - \dot{\phi}_H\cos\psi_k)\Big\}\, dr + O(\varepsilon^3)$$

Based on modal summation, these additional forcings will result in different blade inertia responses from the case when the hub is assumed fixed. Providing a sufficient number of modes are used, the N/R effects due to hub motion, in both flap and lag senses, will be properly accounted for. Since no axial mode is included in the forced response analysis, correction to the radial shear is needed. The radial shear, calculated by the modal summation method (Vx_M), must be modified by an additional term due to hub motion (Vx_H),

$$ie.\quad Vx = Vx_M + Vx_H \qquad \text{where}\quad Vx_H = \int_r^R [2m\Omega r\dot{\psi}_H - m(\ddot{x}_H\cos\psi_k + \ddot{y}_H\sin\psi_k)]\, dr$$

$$Vx_M = \int_r^R m\Omega^2 r\, dr$$

It is noted here that Vx_M normally include the $2m\Omega\dot{v}$ term but to assess the effect due to hub motion, this terms is purposely excluded.

Flight test data reveals that the EH101 aircraft exhibits some hub motions in flight and is therefore chosen for this study. The elastic hub motions are introduced as 5R hub velocity components in terms of both magnitude and phase, in all six directions. They are determined by performing spectral analysis on vibrations (g) measured on the gearbox at 3 (tri-axial) locations: two on the engine drive-shafts and

one on top of the gearbox. The interconnecting structure between the gearbox and the rotor head is assumed rigid. A least-squares fit is then applied to the 5R contents of the measured data to obtain the hub motions [4.12]. Two speeds (44 and 167 ktas) are selected and the corresponding flight test data are analysed using SMS. The derived 5R hub motions are given in the table below, where the phase angles are relative to ψ=0°;

	$\dot{x}_H$	$\dot{y}_H$	$\dot{z}_H$	$\dot{\phi}_H$	$\dot{\vartheta}_H$	$\dot{\psi}_H$
44 KTAS						
Magnitude (in/sec)	1.38	2.59	1.92	0.0375	0.0173	0.0366
Phase (deg)	305	-48	239	148	-52	300
167 KTAS						
Magnitude (in/sec)	3.90	4.11	1.33	0.0483	0.0829	0.0832
Phase (deg)	26	-18	220	138	-328	8

To understand the effects of hub motion on rotor vibratory loads, we consider the following. The main rotor vibratory loads transmitting to the airframe, are the NR fixed frame head loads. They are, in turn, obtained from summing the loads of (N-1)R,NR,(N+1)R harmonics in the rotating frame at the hub. In lag and flap senses, the blade inertia effects cancel with the applied hub motion in the fundamental modes. Thus the hub motion effects on the other hub load components: vertical shear, pitch and roll moments are small. They predominantly affect the inplane (longitudinal and lateral) shears due primarily to the radial load in the rotating frame. Since there is no axial mode used in the analysis, the hub motion effects result in a direct change in the radial shear, primarily be the (N-1)R and (N+1)R in the rotating frame. To account for the effects of hub motion on these rotating harmonics, the inertia loads due to hub motion in the fixed frame are first transformed into the rotating frame and then added to the radial shear.

Figures 4.8(a) & (b) show the effects of hub motions on all the fixed frame (5R) hub load components for the two speeds examined. The components corresponding to (x) are for the datum case without hub motion, (Δ) for the case with hub motion and (□) for the test data. The loads are plotted in an Argand diagram form where the Fourier coefficients of cos5ψ and sin5ψ, *ie.* A5 and B5 components, are plotted on the x-y axes. In this manner, both the magnitude and phase correlation with flight test data can be assessed.

It is evident from *Figures* 4.8 that for the low speed case, both the magnitude and phasing of the 5R lateral shears (F_y) are much improved. Although the magnitude of the 5R longitudinal shear (F_x) is still under-predicted, the phasing is improved. For the high speed where the biggest effect is, both inplane shear components are much better predicted. The effects of hub motion on other components are small, as expected. A more qualitative assessment on the effect of hub motions can be made by comparing the ratios of the root mean square of the inplane shears $S=\sqrt{(F_x^2+F_y^2)}$ for the 2 cases with flight data, which are;

ktas	$\frac{S_{Datum}}{S_{SMS}}$	$\frac{S_{Hub}}{S_{SMS}}$
44	0.2607	0.8472
167	0.2024	0.7599

It is clear that the ratios have increased by more than 3 folds when hub motion is included.

The conclusions drawn from this exercise is that the inclusion of hub motions have shown significant improvement on the hub vibratory load calculations and must be included in order to provide a better estimate of airframe vibration. The observation is in line with expectation and confirmed by the vastly improved correlation. This represents a significant milestone in the ability to include hub motion effects on vibratory load calculation.

However, it should be pointed out in order to substantiate the effects of hub motion on vibratory loads, an accurate knowledge of measured hub motions and fixed axis loads is needed. This depends on many factors, which include the fitting process used to infer the hub motion data and the assumption of a rigid interconnecting structure used in the spectral analysis. Both must be sufficiently sound to ensure the correct phasing of the inferred hub motions is defined. Also when inferring flight load data in SMS, care must also be taken to ensure the true rotor dynamics are modelled.

A more qualitative study would be to use complex rotor modes in both the forced response analysis and SMS. However, even if this approach is taken, the calculated loads will still depend on factors such as the accuracy of the fuselage modes used and the hub impedance calculation.

PROGRAM CRFA V3.0 - HUB MOTION EFFECTS

EH101 FLT 514 TAS= 44.0 KTAS - PREDICTION vs TEST DATA (SMS)

COMPARISON OF 5R FIXED FRAME LOADS

5/08/96

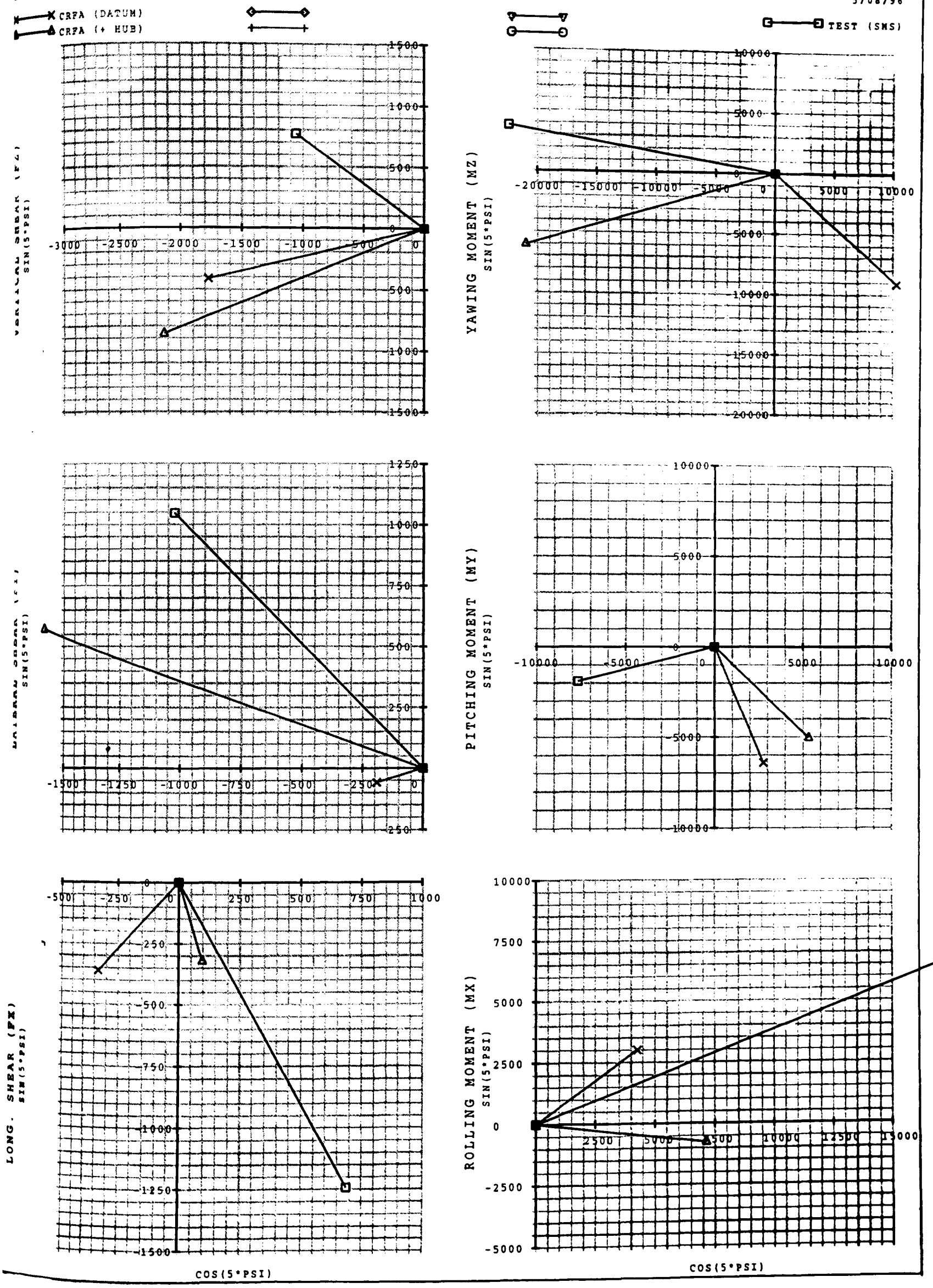

Figure 4.8(a) - Hub Motion Effects: EH101 5R Fixed Frame Loads (44 ktas)

PROGRAM CRFA V3.0 - HUB MOTION EFFECTS

EH101 FLT 514 TAS=167.0 KTAS - PREDICTION vs TEST DATA (SMS)

COMPARISON OF 5R FIXED FRAME LOADS

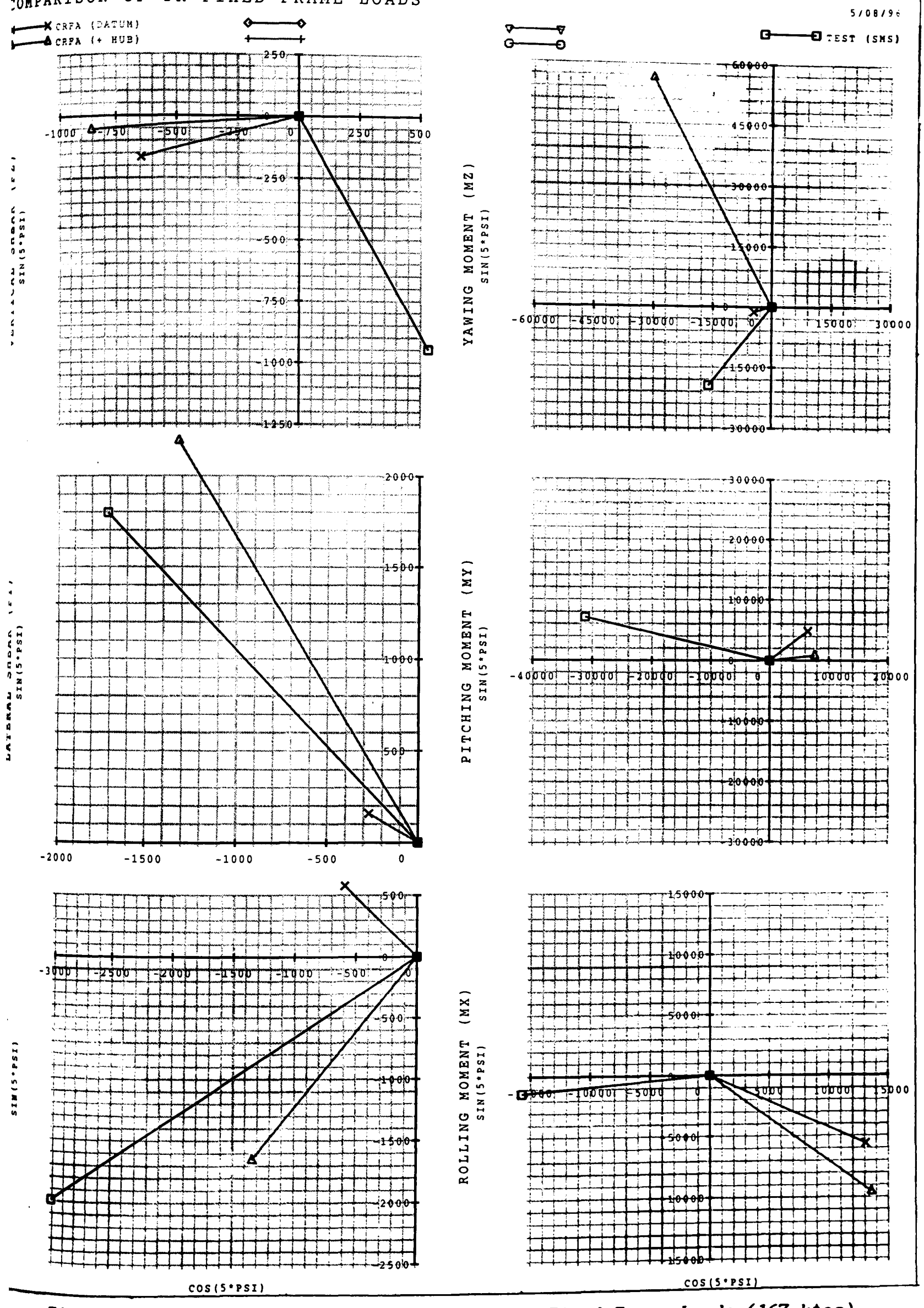

Figure 4.8(b) - Hub Motion Effects: EH101 5R Fixed Frame Loads (167 ktas)

4.3.4 Rotor Loads Evaluation for a Manoeuvre

The second objective of this study is to develop a method capable of predicting rotor loads during manoeuvre flight. In an ideal manoeuvre simulation, the aim is to model the rotorcraft behaviour over time as if there were a pilot in the loop. This leads to a set of pilot controls and aircraft states which are then fed back into CRFA from which the loads are determined. The rotor loads so determined are then used to define the fuselage motion during the manoeuvre. The process is repeated at each time step throughout the manoeuvre.

For non-steady flight, a multi-bladed rotor model should be used as each blade would behave differently. Since the software for the rotor mode solution is not yet available in CRFA, we proceed in the same manner as the hub motion study *ie.* use the single blade rotor model.

A comprehensive manoeuvre flight trial on the Lynx aircraft, fitted with both metal and BERP blades, was carried out in 1990. The exercise was carried out primarily to establish both the behaviour and the absolute level of performance of the BERP rotor in manoeuvring flight and was reported by Phipps [4.13]. The manoeuvre of a loop with high "g" load factor on exit was chosen to demonstrate the application of this model in calculating rotor loads in manoeuvres.

The time history traces of C_T/s v μ and some selected parameters for this transient condition are shown in *Figure* 4.9(a). The loop manoeuvre was performed by pitching the aircraft and increasing the pitch rate over the top of the loop and on exit, the aircraft load factor reached 3.3g. At such a high $C_T/s(\cong 0.4)$, the aircraft experienced deep stall.

In steady flight conditions, the rotor is normally operating in a non-stalled condition and the aircraft trim state is well-defined. For manoeuvre simulation of this kind, we adopt the following approach. We define a snap-shot trim state by selecting a time slice of the event and assume the condition is quasi-steady on a chosen cycle. The flight condition data: true airspeed, descent rate, fuselage attitude, aircraft pitch and roll rates, are obtained from the measured data. The thrust can then be estimated using an iterative aircraft trim analysis and the head moment inferred from gauge data.

The theoretical model cannot be expected to simulate the manoeuvre exactly by matching all the aircraft state parameters simultaneously. It is therefore decided that one of the constraints - shaft incidence, is allowed to be varied in order to obtain a power match since the power available from the engines is a real physical constraint. This method of trimming is chosen because the primary influence on the blade loads will be the level of stall penetration which can be controlled by matching the power. Hence the blade load characteristics are more likely to be modelled correctly. The following trim condition is defined for this loop exit manoeuvre;

Flight Data	Loop Exit
True air speed (ktas)	143.490
Fuselage attitude (deg)	36.580
Roll rate (deg/s)	0.0
Pitch rate (deg/s)	30.789
Rotor speed (%NR)	107.5
Thrust (lbf)	22200
Roll moment (lbf-in)	33290
Pitch moment (lbf-in)	56090
Rotor power, P_R (hp)	640
σ	0.9189
C_T/s (-)	0.4055
μ (-)	0.3236

This manoeuvre simulation is proceeded by first generating a set of blade modes using CRFD. This time, the steady state is obtained by trimming the rotor to the required thrust to ensure that the modes are still small perturbations. The process used in CRFA to trim the rotor to the required thrust/head moment and matching the rotor power simultaneously has, as expected, proved to be not straightforward.

Initially, the simulation was performed using zero pitch rate *ie.* using the level of capability available in R150. This has been unsuccessful in acquiring the trim condition with the highest achievable thrust being some 2000 lbf short of that required. When the pitch rate was included, the required thrust was achievable. This result has substantiated the existence of the physical phenomenon known as pitch rate alleviation [4.14]. Positive pitch rate developed during the manoeuvre resulted in a favourable gyroscopic moment acting on the rotor. This gyroscopic moment provided a starboard down flapping moment *ie.* positive flapping on the retreating side. In order to generate the same longitudinal flapping motion required for trim, the aerodynamic moment on the retreating side was reduced. This was achieved by a decrease in blade incidence which relieved the stall and it was this mechanism which enabled the trim to be achieved.

Although a trim was achieved, the deficiency associated with the PDM trim method to handle such a highly non-linear flight regime was once again highlighted (*Fig.*4.9b). Because of the numerical sensitivity and non-linearity in this regime, even a numerical difference of 0.05° in the shaft incidence could switch the rotor condition from a moderately stalled to a stalled one. Clearly in reality, this would not occur. After a number of attempts, a thrust/moment trim was eventually achieved but the predicted power was some 800hp lower than that required. Because of the approximations inherent in this simulation, it was felt that further improvement could not be guaranteed by refining the trim process, therefore the acquired trim was accepted.

Examination of the control load waveform (*Fig.*4.9b) reveals that apart from the phase shift on the 1R and some missing higher harmonics on the advancing side, the correlation is good when considering the extreme aerodynamic environment encountered and the approximations of the manoeuvre by a quasi-steady rotor state used.

Figures 4.9(c) also show the flatwise and edgewise moments at the root and mid-span positions. It is evident that the correlation of the peak-to-peak flatwise loads and the general shape of the waveforms is very good. Although at the mid-span, there is an over-prediction of the peak value at ψ=40°, the overall magnitude is much less than the inboard value and so represents only a relatively small error. For the edgewise moments, the 1R loads at the inboard region are slightly under-predicted but the mid-span correlation is truly excellent.

The main conclusion drawn from this exercise is that the inclusion of the pitch rate in the analytical model has correctly alleviated the retreating blade stall. This has allowed the simulation to be performed even in such a high C_T/s ($\cong$0.4) manoeuvre, which would otherwise not be possible. This value represents a physical limit at which most existing rotors can operate and it forms the basis for limit loads correlation for the EH101 certification [4.15]. Thus it is important to be able to predict the loads at such an extreme condition. The ability of this model to simulate severe manoeuvres with the level of correlation similar to the level flight represents an important achievement. When the HELMSMAN and ARM modules, together with the rotor modes solution, are incorporated, the full potential of CRFA in manoeuvres can be explored.

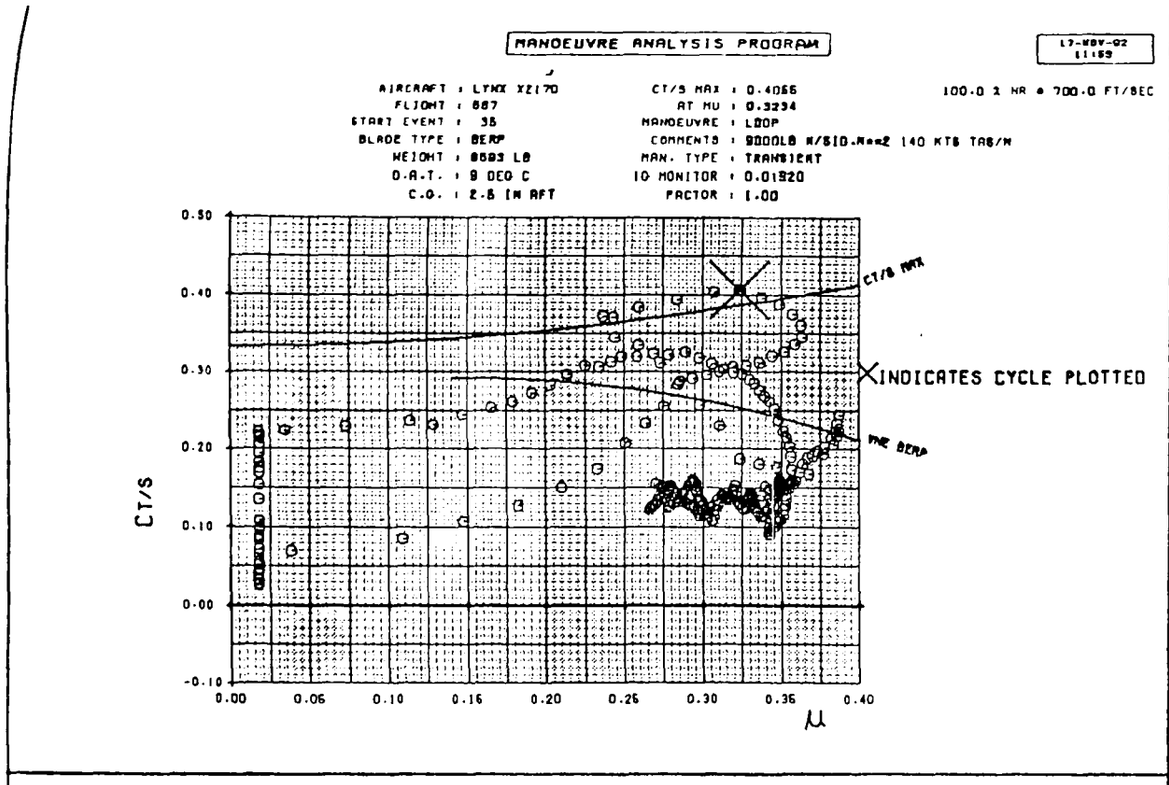

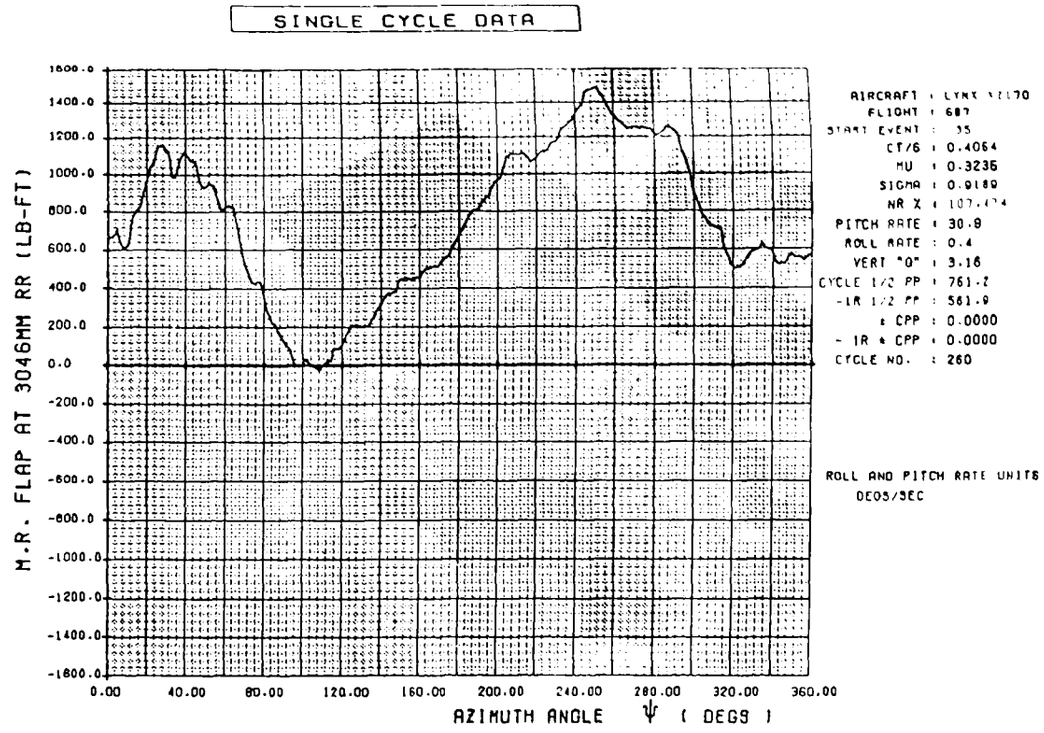

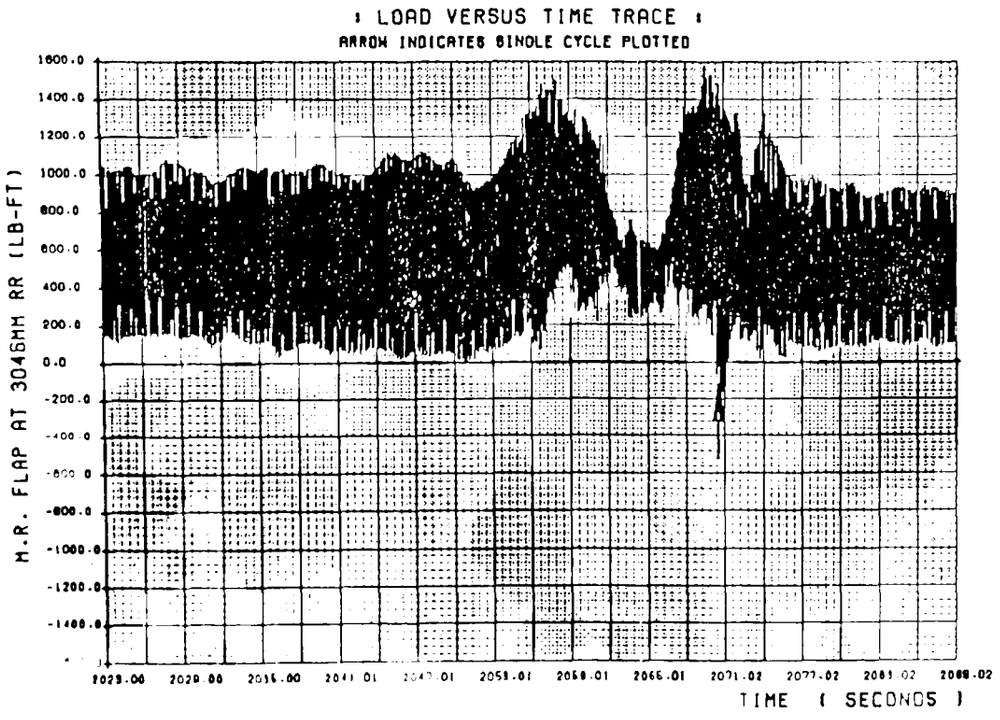

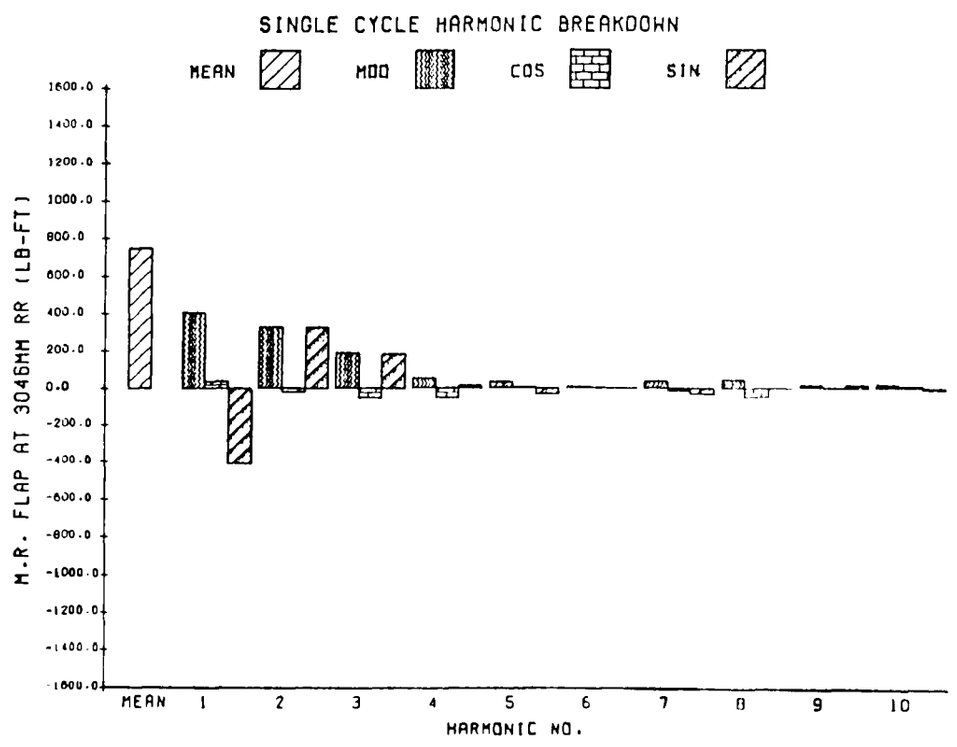

Figure 4.9(a) - Lynx 3.3g Loop Exit: Flight Test Time History Trace

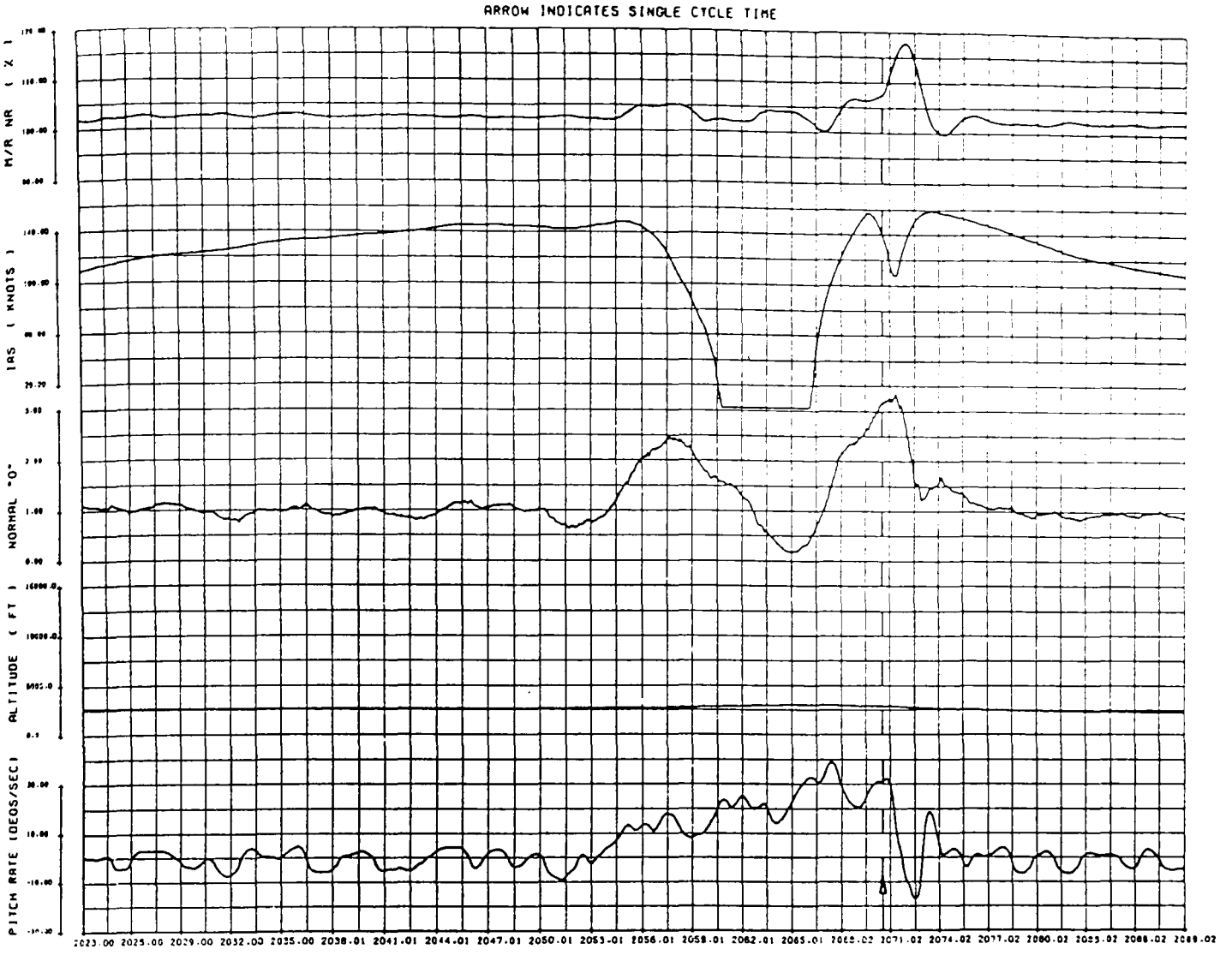

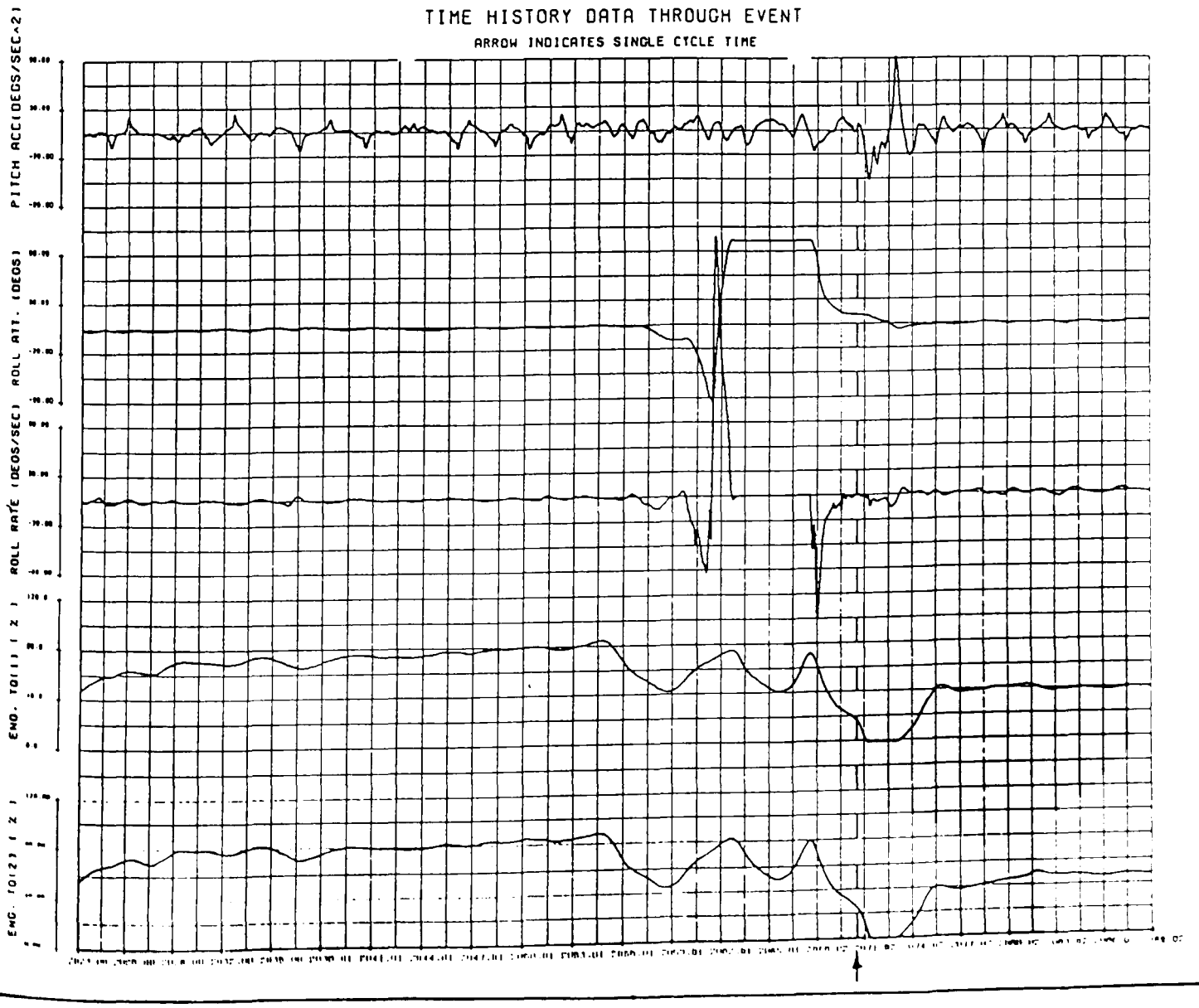

Figure 4.9(a) - Lynx 3.3g Loop Exit: Flight Test Time History Trace (Cont'd)

COUPLED ROTOR FUSELAGE ANALYSIS
TRACES OF TRIM PARAMETERS

7.3.95

CRFA (V3.0): LYNX 3G LOOP EXIT 2 MODES TRIM : 50 47 49 TH+100
LYNXLOOP4: 105%NR 160 KTAS, 33.50 12.01, -3.00, 6.00 (07/03/95)

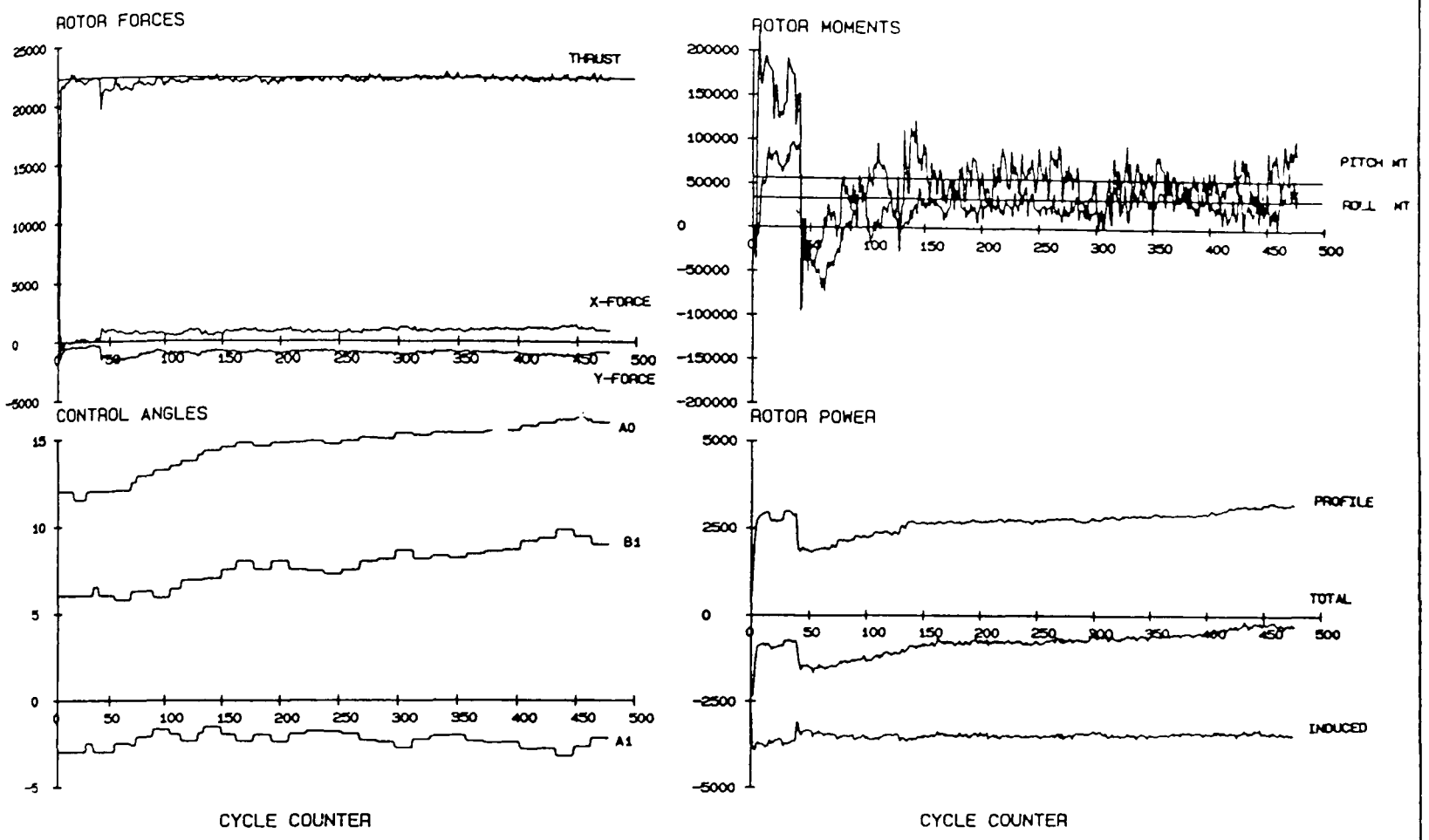

PROGRAM CRFA V3.0 - MANOEUVRING CORRELATION USING BERP LYNX
FLIGHT 687-EV.35 3.3G LOOP EXIT AT 140 KTAS - LIMIT LOAD STUDY
8/03/95 AZIMUTHAL VARIATION OF CONTROL LOAD (ZERO MEAN)

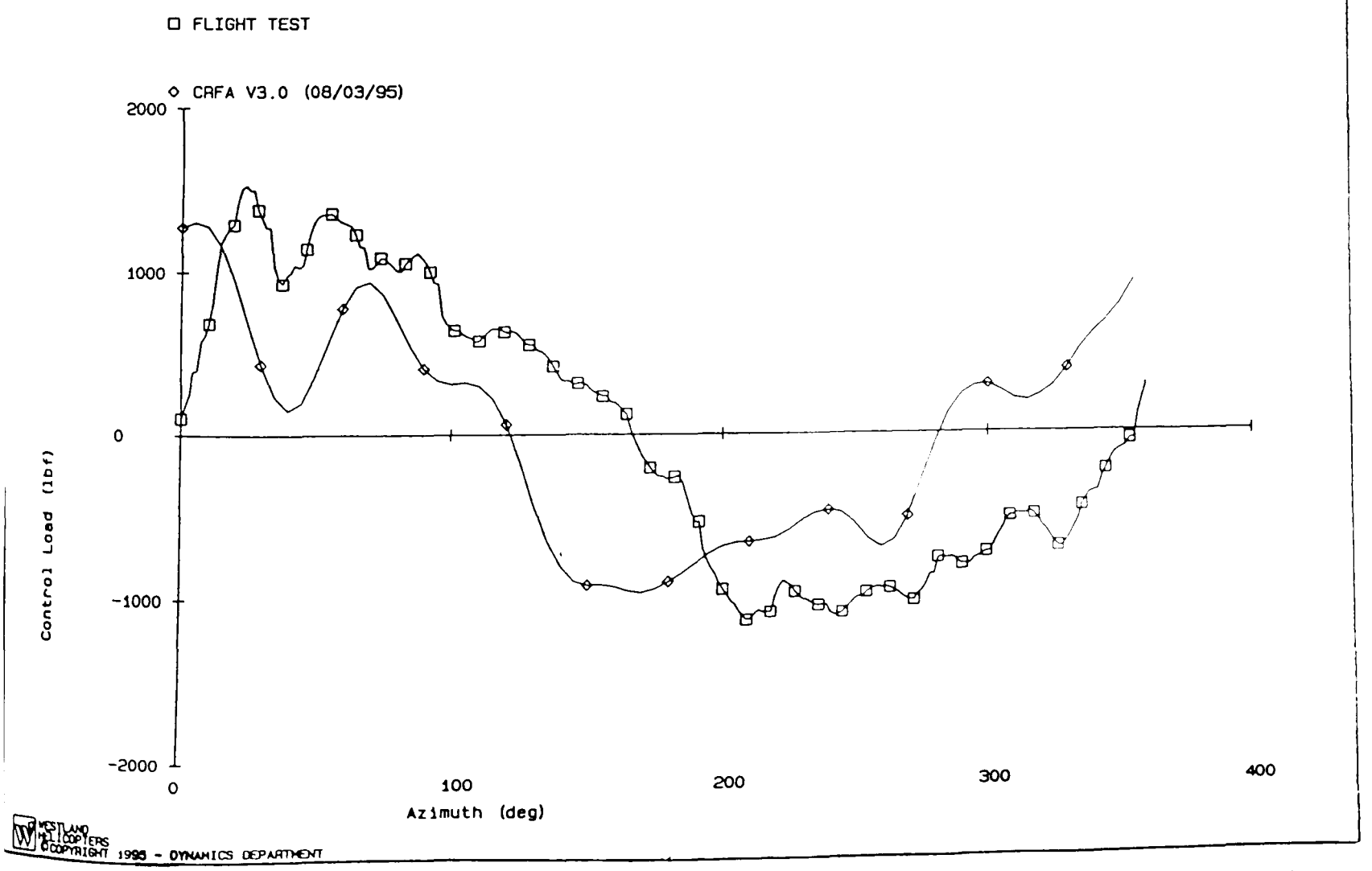

Figure 4.9(b) - Lynx 3.3g Loop Exit: Trim Parameter Traces & Control Load Waveform

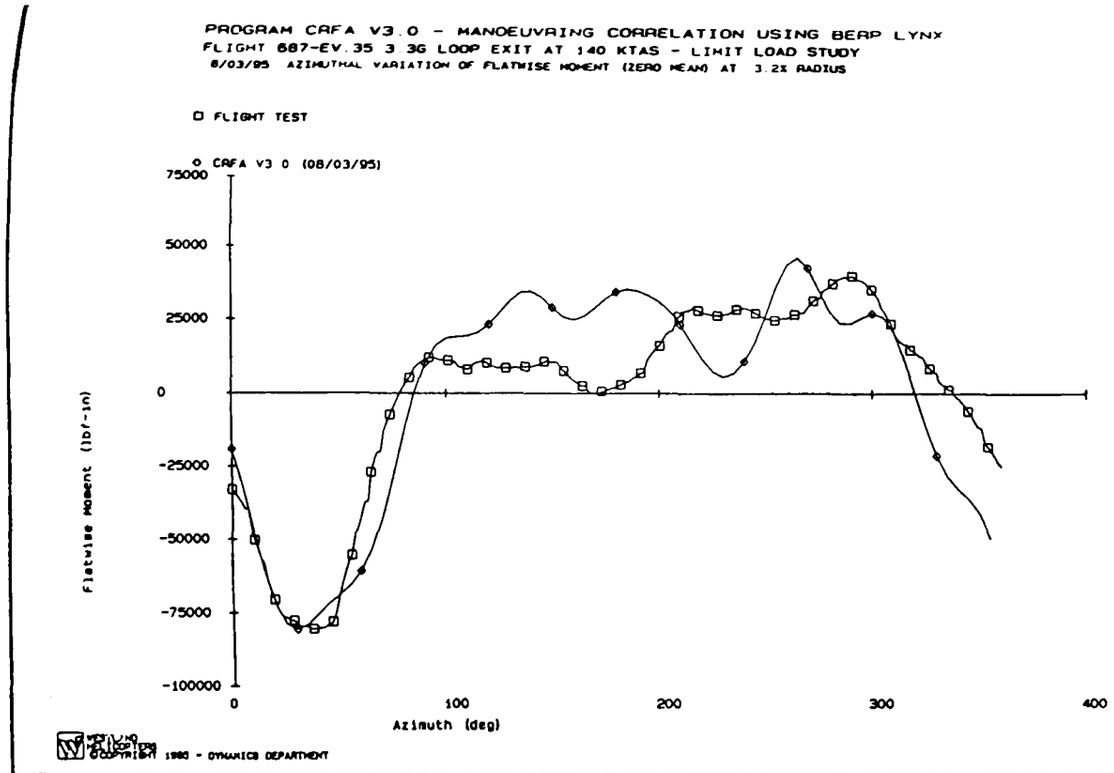

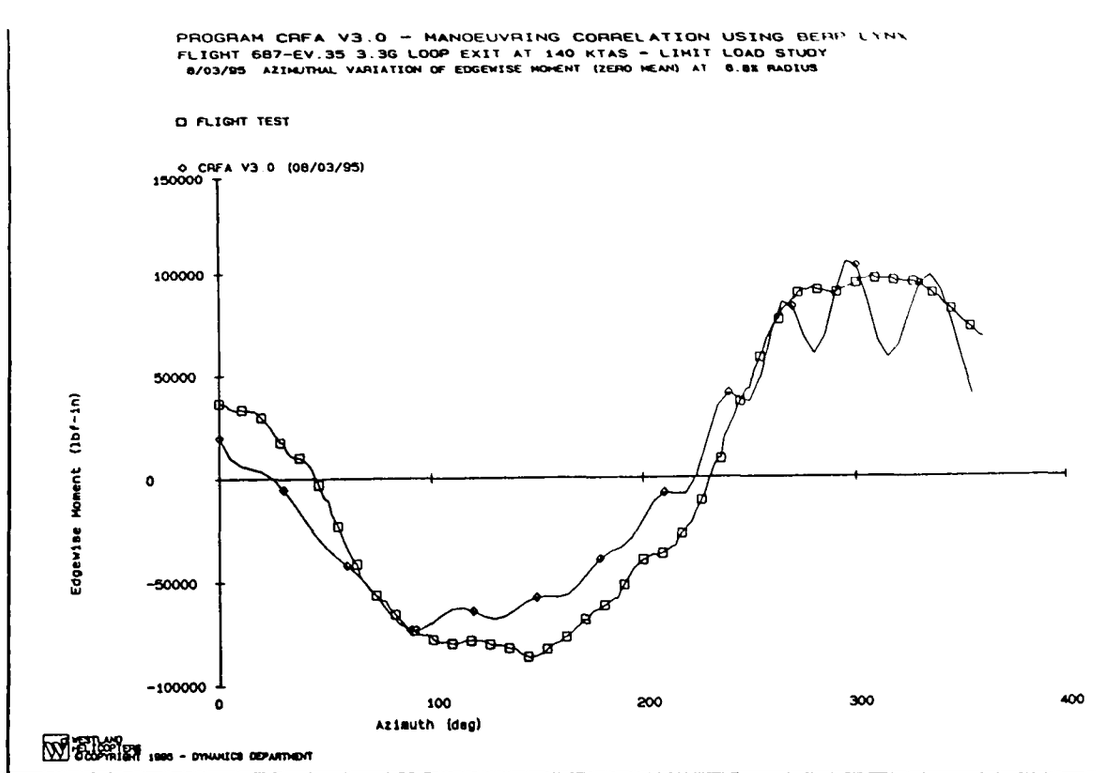

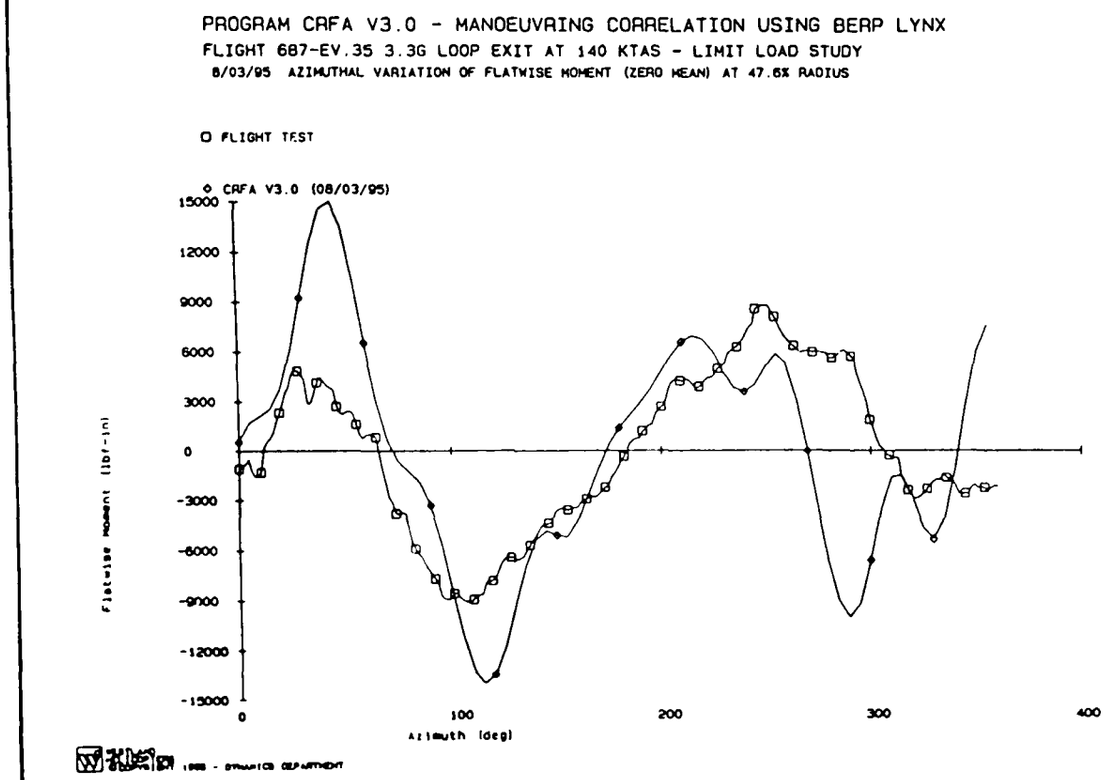

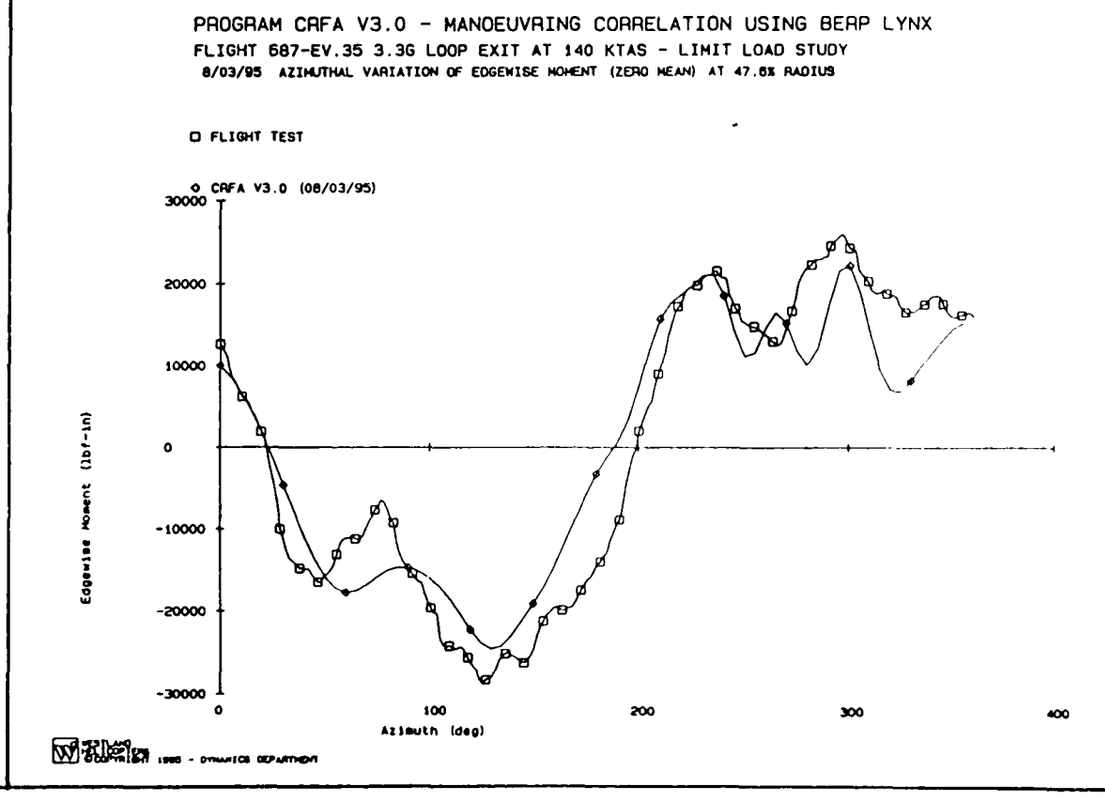

Figure 4.9(c) - Lynx 3.3g Loop Exit: Comparison of Structural Loads with Flight Test

4.3.5 Application of Rotor Modes
- Effect of Including Transmission System Dynamics

This analytical model adopts a new dynamic modelling strategy based on the concept of rotor modes. Before the full (complex) rotor mode solution is used, it is necessary to gain some insight into its application. This will provide a sound basis for applying this technique to the more comprehensive dynamic modelling.

Rotor modes are normally complex. However, by examining the rotor system, it is not difficult to see that certain types of rotor/sub-system coupling involve only collective motions of all the blades, with each blade moving identically. This results in net motion along or about the axis of rotation *eg.* hub vertical and yaw motion. Thus, these systems can be modelled using only the collective and reactionless modes and are conveniently separated from the cyclic modes. In the absence of damping, aerodynamic or Coriolis coupling, the collective mode eigenvectors are real and can be expressed in either the rotating or non-rotating frames. The reactionless modes, which involve no motion of the hub and with all motion being confined to the rotor, are also real and are expressed in the rotating frame. Hence, under the preceding conditions the rotor modes, which can be treated as wholly real, are the reactionless and the collective modes, both expressed in the rotating frame. This forms the basis of the intermediate, as opposed to the full, rotor mode solution as introduced by Holton [4.16] and has been programmed in CRFA.

The test case for the rotor mode concept is to include transmission flexibility for the Lynx rotor system. *Figure* 4.10(a) shows the Lynx transmission system gear diagram and the dynamics torsion model. Two sets of (real) modes; the reactionless (*ie* single blade) and collective modes (calculated with 10 transmission system modes) are set up using CRFD and the modal properties are given in *Table* 4.3. The three lag mode shapes and modal bending moment distribution for the two sets of mode types are shown in *Figure* 4.10(b). The differences, primarily in the lead-lag dynamics, are attributed to the transmission flexibility being included and are shown in the table of frequencies below;

Mode	Reactionless (Ω)	Collective (Ω)
L1	0.66222	1.00876
L2	4.45706	3.40387
L3	10.12104	6.57788

The most significant change is in the second lag mode frequency, where it has moved from above 4R to below 4R. This will clearly affect the edgewise loads. The change in the fundamental lag frequency is attributed to the stiffening effect whereby the 2 isolated systems, free-free (transmission) and fixed-free (blade), are moving out-of-phase with each other. The blade is effectively shortened as a result of the shift of the node in the lag mode shape from the blade centre line to some 30%R (*Figure* 4.10(b)).

The biggest effect of including transmission flexibility is on the NR loads whilst the rotor trim parameters, mainly steady components, are unaffected by the changes in the lag modes. To ensure that the application of rotor modes is correct, the check is made on the modal responses. This is performed using the harmonic balance method *ie.* by re-constructing the harmonic contents of modal responses from the modal forcings. Consider

$$\ddot{q}_i + 2\nu_i\lambda_i\dot{q}_i + \lambda_i^2 q_i = f_i$$

where

$$q_{An} = \frac{f_{An} - \delta f_{Bn}}{(\lambda^2-n^2)I(1+\delta^2)} \; ; \quad q_{Bn} = \frac{f_{Bn} + \delta f_{An}}{(\lambda^2-n^2)I(1+\delta^2)} \quad \text{where } \delta = \frac{2\nu\lambda n}{(\lambda^2-n^2)}$$

where I,λ,ν are the modal inertia, frequency, damping and f,q are the modal forcing and response for the second lag mode and n=4 here. The suffices An,Bn refer to the Fourier coefficients of a positive Fourier series. The 4R modal responses are summarised below;

Case	L2 Modal Data		Modal Forcing	Response Calculated	H.Balance
Collective + Reactionless	λ= 3.40387	A4	-0.000028	0.000060	0.000057
	ν= 0.01	B4	0.000000	0.000009	-0.000004
	I= 0.11070				

The calculated modal responses compared well to those based on the harmonic balance method. Further scrutiny of the modal responses reveals that all collective modes respond only at 0R,4R,8R (for the 4-bladed Lynx rotor) as expected confirming the correct mode is responding at the correct harmonics. Likewise, the reactionless modes respond to all other forcing harmonics except, of course, the collective forcing harmonics.

Figures 4.10(c) show the edgewise moment waveforms for a number of radial stations and the overall changes are slight but, as previously noted, the biggest improvement would be on the fixed frame edgewise loads. The 4R edgewise moment at 31.1%R is shown in the Argand diagram *Figure* 4.10(d) below.

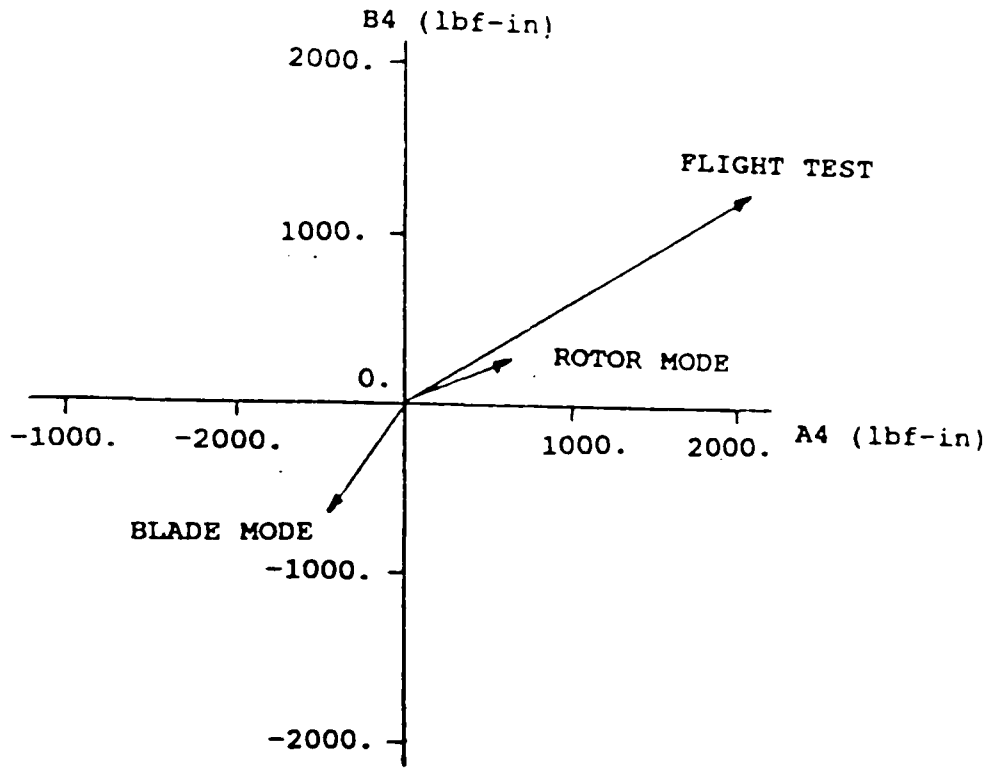

Figure 4.10(d) - Comparison of 4R Edgewise Moment at 31.1%R

It is clear that the use of rotor modes has improved the phasing correlation. The improvement is due primarily to the correct second lag mode frequency (below 4R) being used, thereby changing the phasing of 4R response. Although the amplitude has not been improved, the prediction is of the same order as the single blade case. A simple calculation reveals that in the proximity of 4R lag resonance, assuming 1% structural damping, an increase in lag mode frequency typically of 13% would be sufficient to quadruple the 4R edgewise moment. This reflects the fact that a relatively small frequency discrepancy near resonance, can lead to significant changes in the amplitude of structural loads at the near resonant frequency. This is especially important in a flyaway simulation where the rotor speed variation can sweep across the resonant frequency.

This exercise has provided the insight into the use of rotor modes in response analysis and the observations are in line with those seen in [4.17]. It provides the confidence and forms the basis of applying the full (complex) rotor modes in the forced response analysis in the future when the software becomes available.

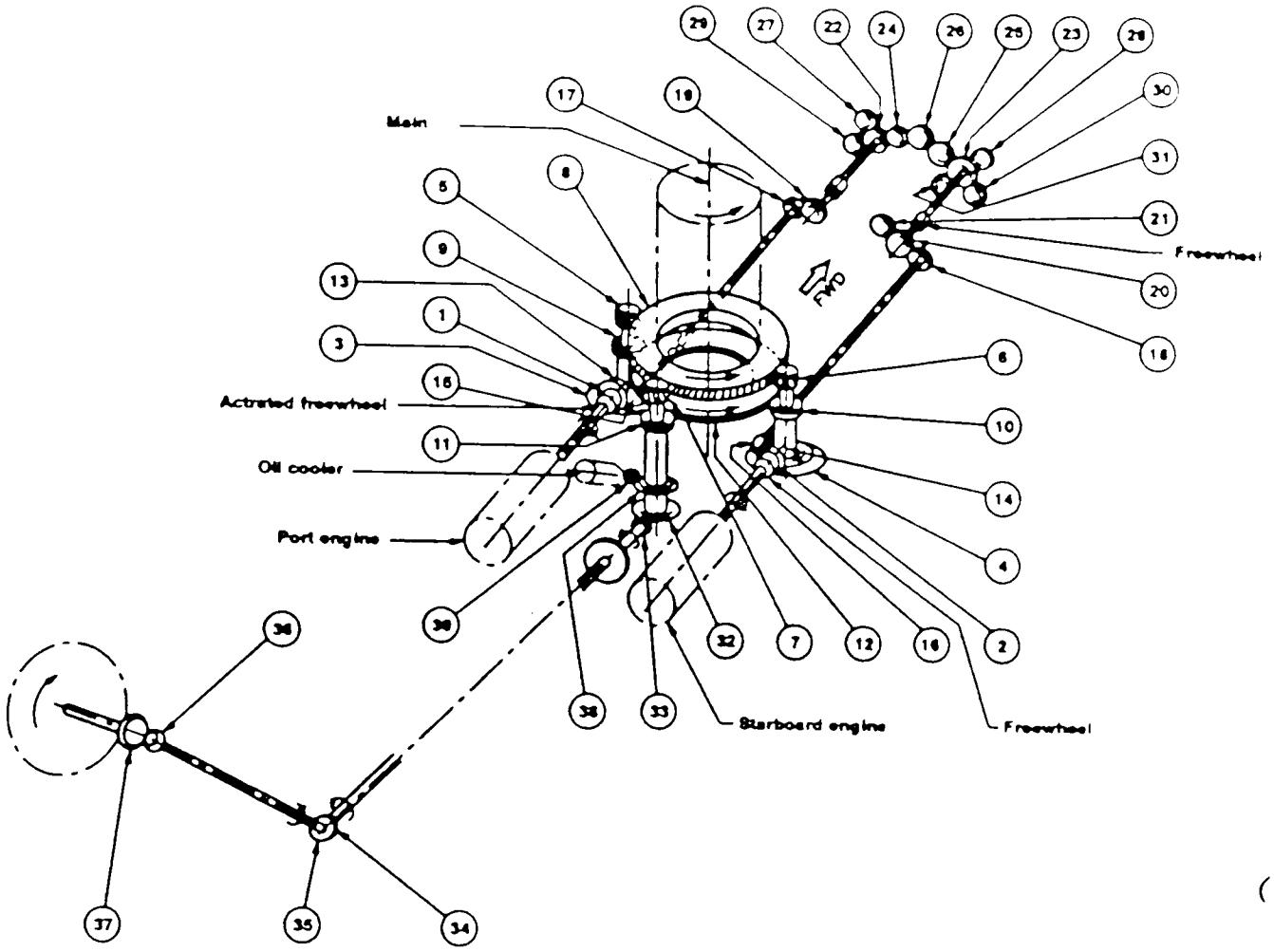

Figure 4.10(a) - Lynx Transmission System (3-Pinion Gear Box)
(a) Gear Diagram (b) Dynamics Torsion Model

Table 4.3 - Blade Modal Data for The Lynx with Transmission Flexibility

Reactionless Modal Data

Title: LYNX MAIN ROTOR BERP BLADE 9500 LB. THRUST - REACTIONLESS MODES
LXBERP_REAC: NO TRANSMISSION SYSTEM - Ω=34.167 R/S, Collective=14.5315 DEG

MODES NUMBER		S.S.	1	2	3	4	5	6	7	8
MODAL FREQUENCY (Ω)		-	.66222	1.11142	2.62495	4.45706	4.97108	5.31862	8.14309	10.12104
MODAL DISPLACEMENT-FLAP		3.37660	-.01165	1.00000	1.00000	.14147	1.00000	1.00000	1.00000	.29150
	LAG	0.21978	1.00000	.00301	-.11163	1.00000	-.11857	.35110	-.15259	1.00000
	TORSION	-0.00625	-.00017	.00096	-.00325	-.02042	-.05279	.48677	.01118	-.00007
MODAL INERTIA(CHUGS-IN**2)		-	.07085	.07415	.06518	.07665	.07542	.53482	.05891	.12594

Collective Modal Data

Title: LYNX MAIN ROTOR BERP BLADE 9500 LB. THRUST - COLLECTIVE MODES
LXBERP_COLL: 10 TRANSMISSION MODES - Ω=34.167 R/S, Collective=14.5315 DEG

MODES NUMBER		S.S.	1	2	3	4	5	6	7	8
MODAL FREQUENCY (Ω)		-	1.00876	1.11145	2.61850	3.40387	4.96901	5.30270	6.57788	8.15675
MODAL DISPLACEMENT-FLAP		3.37660	-.06900	1.00000	1.00000	.29045	1.00000	1.00000	.36623	1.00000
	LAG	0.21978	1.00000	.00859	-.15882	1.00000	-.18376	-.03212	1.00000	-.23256
	TORSION	-0.00625	-.00066	.00096	-.00304	-.00905	-.04936	.56389	.01421	.01112
MODAL INERTIA(CHUGS-IN**2)		-	.05902	.07417	.06636	.11070	.07649	.70419	.09044	.06137

Transmission System Modes used in the calculation of Collective Modes:

Mode	Frequency (R/S)	Modal Deflection at the hub (normalised to unit modal mass)
1	4.9464E-05	1.254E-02
2	46.310	4.759E-03
3	99.458	1.507E-04
4	237.89	5.290E-02
5	431.45	3.034E-02
6	738.71	1.096E-02
7	970.41	9.640E-04
8	1676.3	1.596E-04
9	1903.4	1.966E-05
10	2502.5	1.057E-02

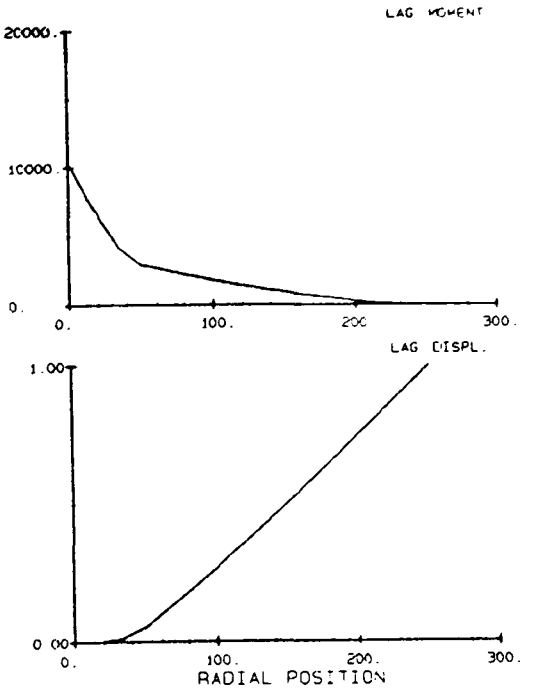

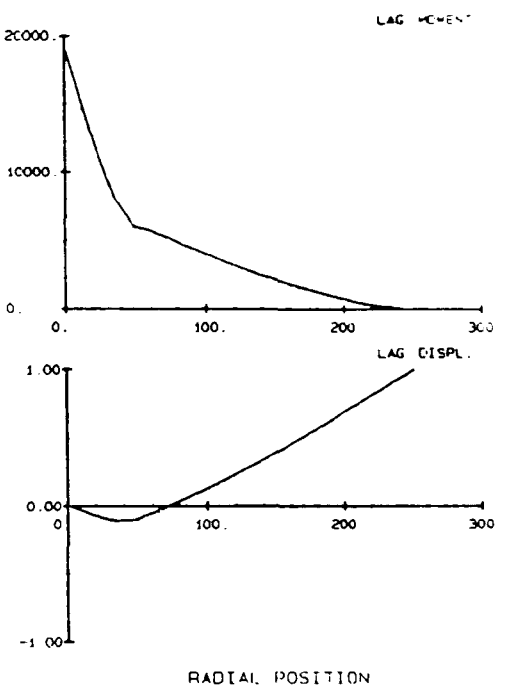

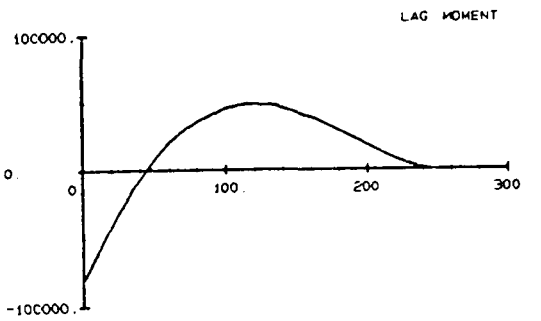

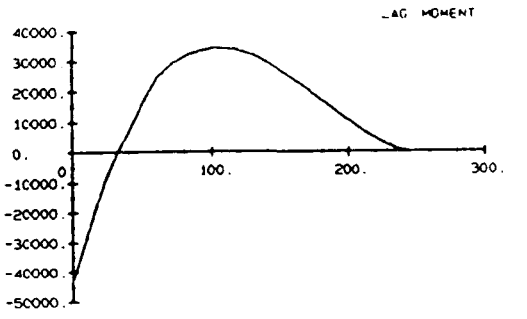

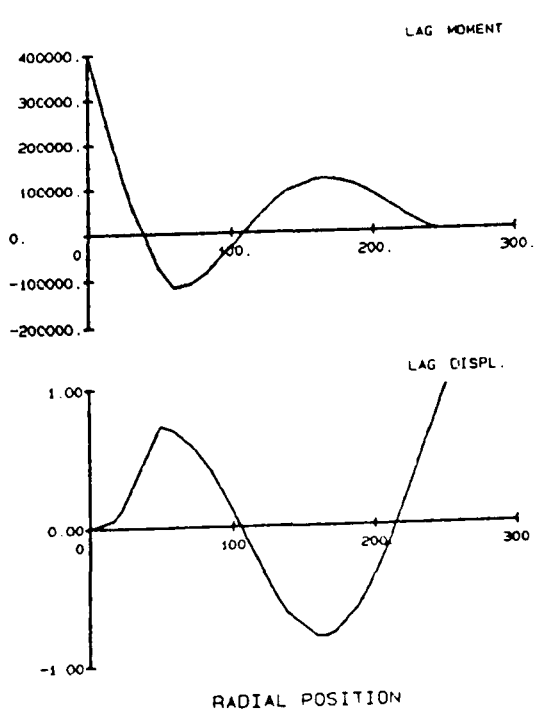

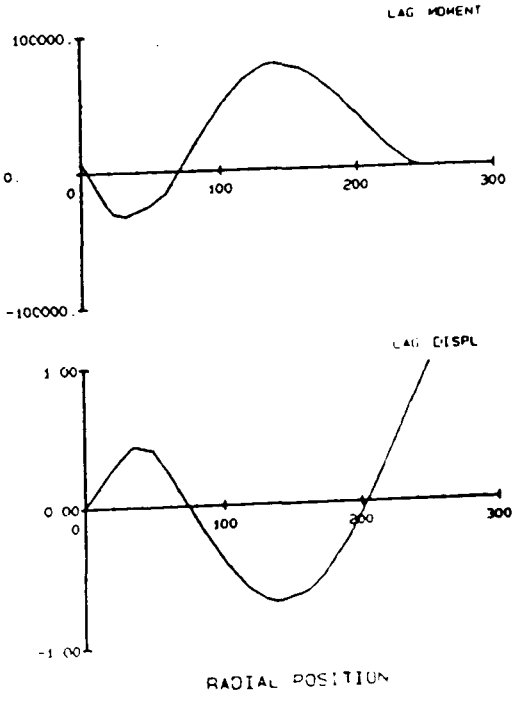

(a) Reactionless (Blade) *(b) Collective (Rotor)*

Figure 4.10(b) - Lynx Lag Mode Shapes and Modal Bending Moments (a) Reactionless (Blade) (b) Collective (Rotor)

EDGEWISE BENDING MOMENT ~ AZIMUTH
X = 0.640

PROGRAM CRFA V2.3 CONVERSION CHECK
XZ170 BERP3 BLADE AT W/S=N**2=9000 LBF TAS=160
INTERMEDIATE ROTOR MODE SOLUTION STUDY
—— CRFA V2.3: NEWBM6A: REACTIONLESS MODE (22/11/93)
---- CRFA V2.3: NEWBM6B: COLL + REAC MODE (12/01/94)
□ FLIGHT TEST

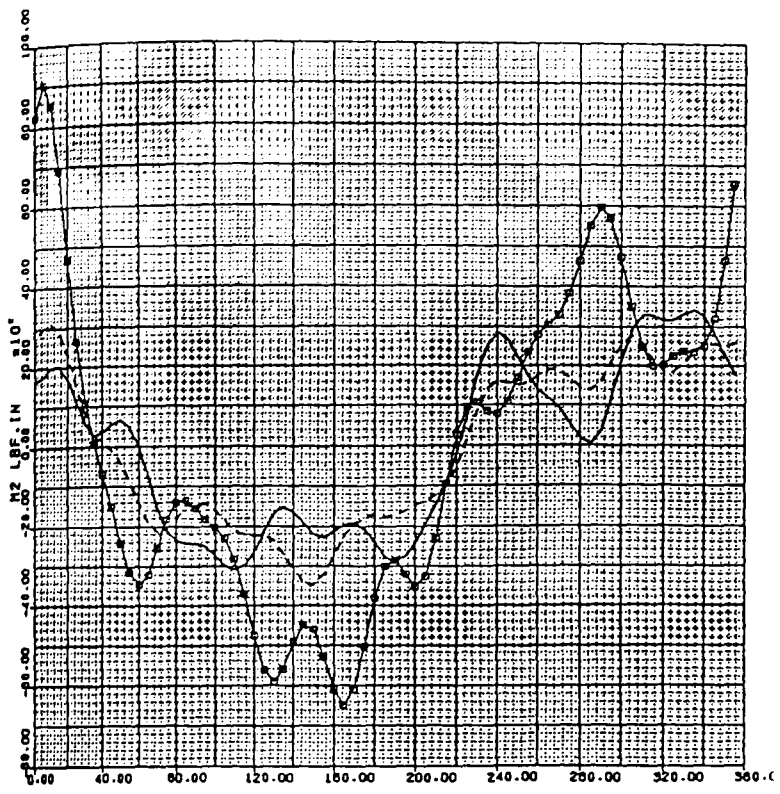

EDGEWISE BENDING MOMENT ~ AZIMUTH
X = 0.813

PROGRAM CRFA V2.3 CONVERSION CHECK
XZ170 BERP3 BLADE AT W/S=N**2=9000 LBF TAS=160
INTERMEDIATE ROTOR MODE SOLUTION STUDY
—— CRFA V2.3: NEWBM6A: REACTIONLESS MODE (22/11/93)
---- CRFA V2.3: NEWBM6B: COLL + REAC MODE (12/01/94)
□ FLIGHT TEST

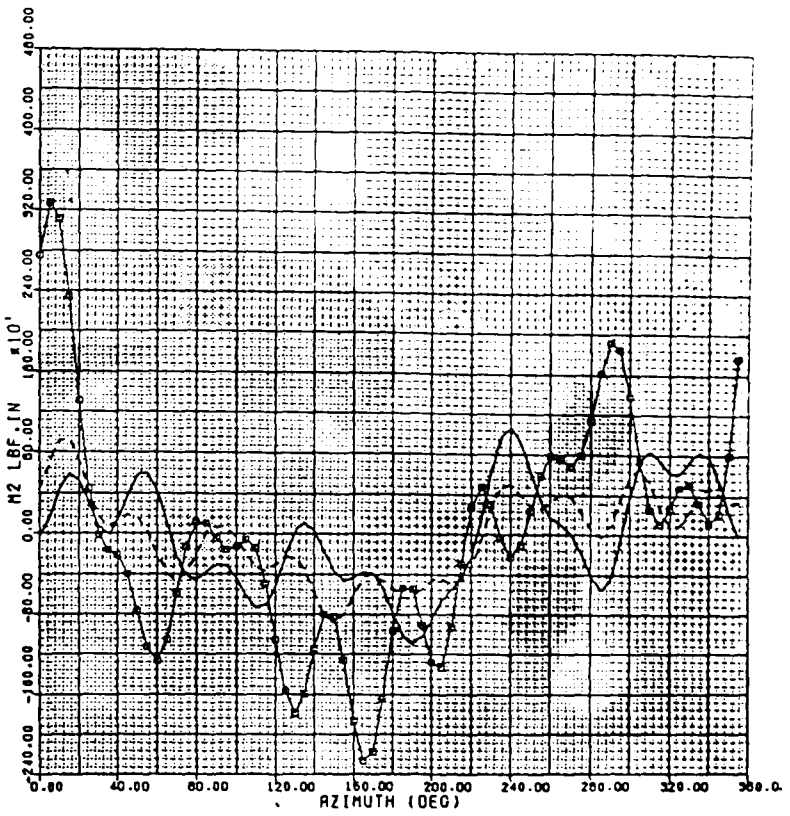

EDGEWISE BENDING MOMENT ~ AZIMUTH
X = 0.068

PROGRAM CRFA V2.3 CONVERSION CHECK
XZ170 BERP3 BLADE AT W/S=N**2=9000 LBF TAS=160
INTERMEDIATE ROTOR MODE SOLUTION STUDY
—— CRFA V2.3: NEWBM6A: REACTIONLESS MODE (22/11/93)
---- CRFA V2.3: NEWBM6B: COLL + REAC MODE (12/01/94)
□ FLIGHT TEST

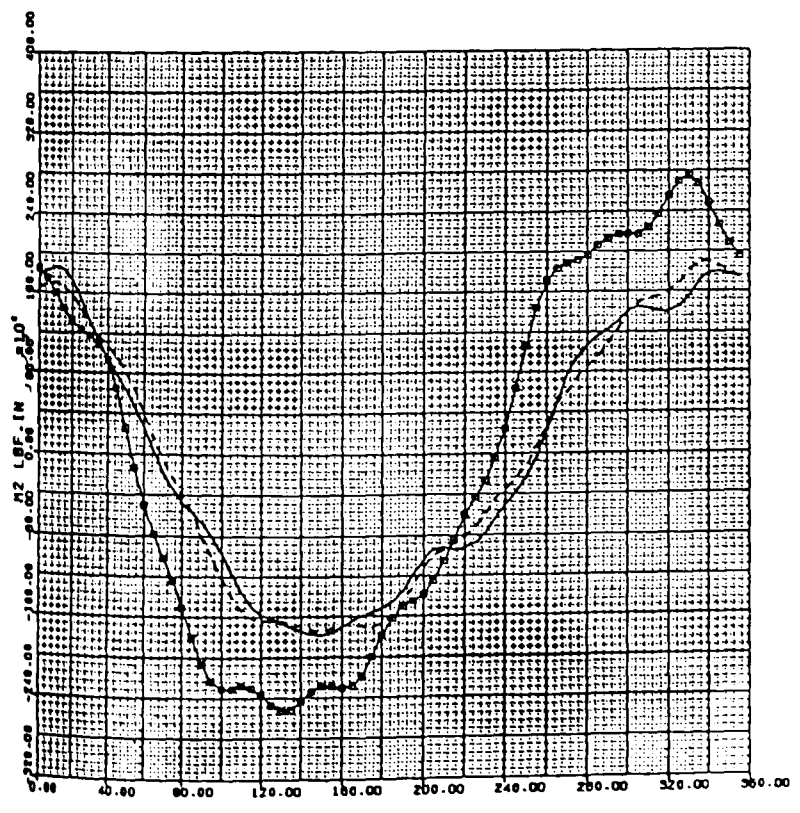

EDGEWISE BENDING MOMENT ~ AZIMUTH
X = 0.311

PROGRAM CRFA V2.3 CONVERSION CHECK
XZ170 BERP3 BLADE AT W/S=N**2=9000 LBF TAS=160
INTERMEDIATE ROTOR MODE SOLUTION STUDY
—— CRFA V2.3: NEWBM6A: REACTIONLESS MODE (22/11/93)
---- CRFA V2.3: NEWBM6B: COLL + REAC MODE (12/01/94)
□ FLIGHT TEST

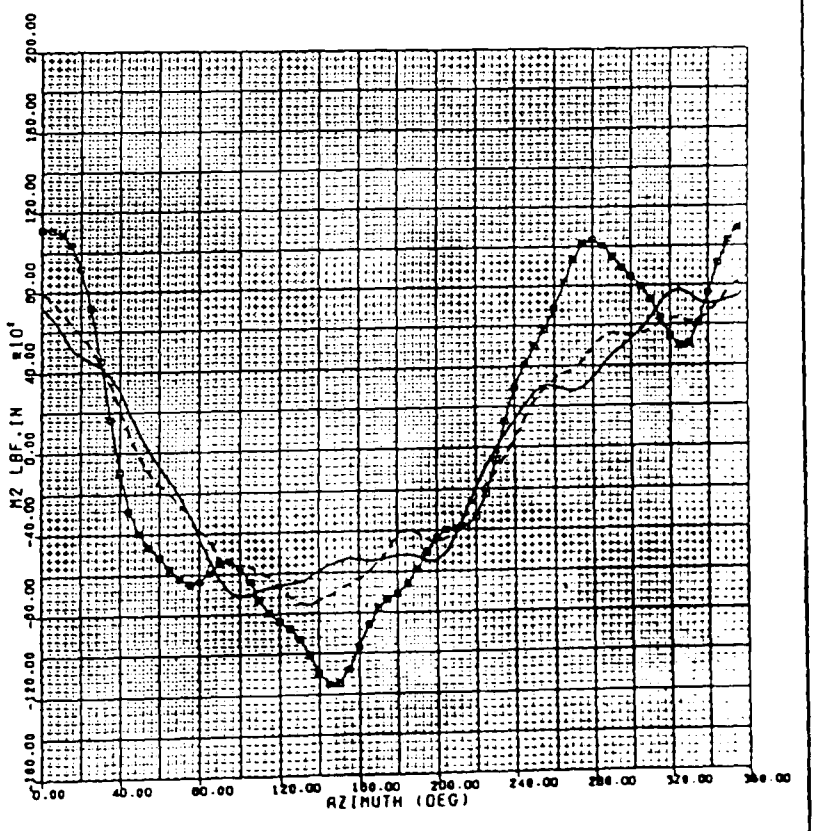

Figure 4.10(c) - Structural Loads Comparison for BERP Lynx (160 ktas) using Reactionless (Blade) and Collective (Rotor) Modes

CHAPTER 5 - CONCLUSIONS AND RECOMMENDATIONS

5.1 The Conclusions

A new modal method capable of analysing the rotorcraft aeroelastic response in both steady and manoeuvring flight has been developed. The two main objectives of the study: to include the effects of hub motion in the rotor loads calculation and to be able to analyse rotor loads during manoeuvring flight, have been achieved. The rigid aircraft motion is introduced in the analytical model as a set of aircraft velocities and rates. The effects of elastic hub motions on rotor loads are included (1) as external hub inertia forcings on a rotor modelled using real blade modes; and (2) as the main constituent of the rotor dynamic model by way of complex rotor modes.

The main conclusions drawn from this study are;

- In order to provide the thorough modelling and insight of the dynamic interactions between the rotor and the fuselage systems, complex rotor modes are needed. The use of complex modes as state variables in rotor response analysis is a concept which is both new and analytically demanding.

- The various rotor mode types differ in the type of damping and velocity terms modelled in the rotor dynamic system, but the solution treatments are significantly different. For the simplest rotor dynamic model without damping or gyroscopic coupling, *ie.* real rotating blade modes, the rotor response can be solved wholly in terms of real quantities. For the general rotor model using a complex modes representation, *ie.* coupled and reactionless modes with or without damping, the rotor response must be solved in the form of first order complex differential equations.

- The coupled and reactionless rotor modes are both needed to define the total response of the coupled rotor-fuselage system. The modes are necessarily expressed in different frames of reference: rotating (reactionless modes) and fixed (coupled modes). Care must be exercised to ensure that the forcings appropriate to each mode type are correctly identified. As a result, a numerical filtering process to isolate the forcing has been developed. This method, combined

with the use of complex rotor modes, can be easily adopted to solve the forced response of other dynamical systems consisting of both rotating and non-rotating components.

- The successful application of the modal method depends on the modes being orthogonal. This ensures that any subset of the modes forms an independent set and allows the use of a reduced number of degrees of freedom for the response analysis. The task of providing a text-book proof of the orthogonality relationship for the complex rotor modes, originally configured in the form suitable for the transfer matrix solution method, proved to be one of the most formidable tasks undertaken within this study. A generalised proof is furnished by way of the bi-orthogonality relationship employing both the left-hand and right-hand eigenvectors and has revolutionised the traditional approach in rotor dynamic analysis. Important conclusions drawn from this proof include;
  (1) A set of complex left-hand eigenvectors are required, together with the right-hand set, in order to reduce the system to a subset of modal response equations suitable for a solution; and
  (2) It is necessary for the modes analysis to be re-formulated as a classical eigenvalue problem replacing the transfer matrix solution procedure.

- In order to use the modes correctly, it is necessary to ensure that the dynamic and the aeroelastic systems are compatible - a process which requires significant algebraic manipulation of complicated expressions. The complexity of the reduction of the response equation to the uncoupled modal form has been minimised by employing an orthogonalisation process. The concept is simple and the process can be applied to all system modes for the coupled rotor-fuselage system with the added advantages;
  (1) It simplifies the algebraic derivation process and correctly identifies the RHS forcing terms for all the mode types used; and
  (2) It provides the option to include certain forcing terms for parametric study without adding complexity to the dynamic model.

- Because some of the modellings and basic assumptions used in the dynamic and aeroelastic analyses are different, to ensure compatibility it is necessary to restrict the blade model representation to straight segments with small pre-deformed angles.

This restriction is in line with practical modelling but requires future review when other applications are necessary.

- Much of the derivation of various algebraic expressions is performed using the symbolic algebraic package REDUCE. The deficiencies of REDUCE in dealing with expansion of linearised polynomials are highlighted. However it remains as an indispensable tool in the formulation and manipulation of lengthy equations.

- In the derivation of both the modal response equation and structural load expressions, the important non-linear terms were retained by employing an ordering scheme. The ordering scheme was based on both physical and practical reasonings.

- The fundamental issues regarding the true definition of aerodynamic incidence (α) expression is addressed. It is necessary to include the second order pseudo-torsion term in the α-expression. The derivation provided is rigorous and should be regarded as definitive when pre-deformation and aircraft rate terms are included in the response analysis. However, in order to use this definition effectively, it should also be complemented by an accurate determination of the aerodynamic loads.

- The numerical problem inherent with the Force Integration procedure used for structural loads calculation has been addressed. This is overcome by the deployment of a novel analytical integration procedure known as the Chebyshev Polynomial Integration (CPI) method. Application of the method in predicting vibratory edgewise moment has shown a definite improvement over Modal Summation and comparable accuracy to Modal Summation when Unified Formulation treatment to lag damper load is included. This novel method is numerically exact and can be easily adopted to other applications involving integration of similar product of discontinuous and continuous functions.

- Application of the analytical model to include the effects of elastic hub motion is demonstrated by introducing the latter as external inertia forcings in the loads calculation. This has improved the hub vibratory load calculations significantly, establishing an important milestone in the ability to provide a better estimate of airframe vibration. However, this approach depends on the integrity of the

process of inferring hub motion data from measured accelerations. This applies equally to the case when the complex rotor modes are used where the fuselage dynamics must also be accurately modelled in order to use this aeroelastic model successfully.

- Application of the model to manoeuvring flight has been successfully demonstrated on a loop exit manoeuvre by approximating it as a quasi-steady condition. The inclusion of pitch rate has correctly alleviated the retreating blade stall thus allowing simulation to be performed even in such a severe manoeuvre, which is otherwise not possible. The ability of this model to simulate such a severe manoeuvre with the level of correlation similar to the level flight represents an important achievement.

- The application of rotor modes in response analysis is demonstrated by including transmission flexibility in the rotor dynamic model. The improvement in the phasing calculation of the edgewise loads is due to the use of correct second lead-lag frequency. This exercise has provided the insight into the mechanism of the dynamic interactions between the rotor and the subsystem. It has also increased the confidence in the use of complex rotor modes.

5.2 Recommendations for Future Work

Having achieved the research objectives of this study, a number of key areas have been identified for future research topics. The immediate requirement is clearly to refine the PDM trim method and to complete the implementation of the rotor mode solution method in Program CRFA. These are essential in exploring the potential applications of this model to the complete helicopter.

Other tasks which could be undertaken as future works include;

. The integration of the HELMSMAN and ARM into this model to explore its application through a manoeuvre;
. The extension of this model to other rotorcraft configurations and other applications such as aeroelastic tailoring.

On completion of these tasks, the full potential of this model can be further explored and indeed be turned into an analytical tool with a wide range of applications.

REFERENCES

Chapter 1

1.1 Bramwell A R S
"Helicopter Dynamics"
Edward Arnold, 1976

1.2 Johnson W
"Helicopter Theory"
Princeton University Press, 1980

1.3 Loewy R G
"Review of Rotary-Wing V/STOL Dynamic and Aeroelastic Problems"
Journal of AHS, Vol.14, No.3, July 1969

1.4 Ormiston R A
"A Comparison of Several Methods for Predicting Loads on A Hypothetical Rotor"
AHS Publication SP-352, February 1974

1.5 Arcidiacono P J & Sopher R
"Review of Rotor Load Prediction Methods"
AGARD Conference Proceeding No.334, April 1982

1.6 Bousman W G & Mantay W R
"A Review of Research in Rotor Loads"
NASA/Army Rotorcraft Research Technology Conference, March 1987

1.7 Friedmann P P
"Recent Trends in Rotary-Wing Aeroelasticity"
VERTICA, Vol.11,No 1/2 *pp.*139-170, April 1987

1.8 Griffiths N
"Program R150 Working File"
WHL Aerodynamics Department Software Quality Document 1980-

1.9 Johnson W
"Recent Development in The Dynamics of Advanced Rotor Systems"
VERTICA, Vol.10, No.1 *pp.*73-150, 1986

1.10A Stephens W B, Rutkowsky M J & Ormiston R A (2GCHAS)
"Review of 2GCHAS Mathematical Model on Dynamics and Aerodynamics"
2nd Technical Workshop on Dynamics and Aeroelastic Stability Modelling of Rotorcraft Dynamics, November 1987

1.10B Ormiston R A, Ruzicka G C, Tan C M & Rutkowski M J (2GCHAS)
"First Level Release of 2GCHAS for Comprehensive Helicopter Analysis"
17th ERF Paper 91-09, September 1991

1.11A Johnson W (CAMRAD)
"Development of a Comprehensive Analysis for Rotorcraft
- Part 1: Rotor Model and Wake Analysis
- Part 2: Assessment of Aircraft Model, Solution Procedure & Applications
VERTICA, Vol.5, No.2 *pp.*99-129 & No.3 *pp.*185-216, 1981

1.11B Johnson W (CAMRAD/II)
"Technology Drivers in The Development of CAMRAD/II"
Paper Presented at The AHS Aeromechanics Specialists Conference, San Francisco, January 1994

1.12 Sopher R & Hallock D W (RDYNE)
"Development and Application of a Time History Analysis for Rotorcraft Dynamics based on a Component Approach"
Paper presented at The AHS 2nd Decennial Specialists Meeting on Rotorcraft Dynamics, November 1984

1.13 Hurty W C
"Dynamic Analysis of Structural System using Component Modes"
AIAA Journal Vol.3, No.4, April 1965

1.14 Strehlow H (MBB)
"An Advanced Rotorcraft Model using A Hybrid Multi-body Algorithm"
Paper presented at The 2nd Technical Workshop on Dynamics and Aeroelastic Stability Modelling of Rotorcraft Dynamics, Nov.1987

1.15 Hodges D H, Hopkins A S, Kunz D L & Hinnant H E (GRASP)
"Introduction to GRASP - General Rotorcraft Aeromechanical Stability Program - A Modern Approach to Rotorcraft Modelling"
Paper presented at The AHS 42nd Forum, June 1986

1.16 Friedmann P P & Straub F
"Application of The Finite Element Method to Rotary-Wing Aeroelasticity"
Journal of AHS, Vol.25, No.1, January 1980

1.17 Done G T S & Gibbons M P
"Automatic Generation of Helicopter Rotor Aeroelastic Equations"
Paper presented at The 8th ERF, September 1982

1.18 Hansford R E
"A Unified Formulation of Rotor Load Prediction Method"
Journal of AHS, Vol.31, No.2, April 1986

Chapter 2

2.1 Coleman R P & Feingold A M
"Theory of Self-Excited Mechanical Oscillations of Helicopter Rotors with Hinged Blades"
NACA Report 1351, 1958

2.2 Hohenemser K H & Yin S K
"Some Applications of The Method of Multi-blade Coordinates"
Journal of AHS, Vol.17, No.3, July 1972

2.3 Done D T S
"A Simplified Approach to Helicopter Ground Resonance"
Royal Aeronautical Society Aeronautical Quarterly, May 1974

2.4 Sopher R & Kottapalli S B R
"Correlation of Predicted Vibrations and Test Data for a Wind Tunnel Helicopter Model"
Paper presented at The 38th AHS Forum, Anaheim, USA, May 1982

2.5 Griffiths N
"Analysis of BERP Structural Loads and Vibration"

WHL Dynamics Department Report RP-739, July 1988

2.6 Vickers E G

A) "Lynx CMRB - Simulation of High Lag Loads during a Fly Away"
WHL Dynamics Department Note, DYN/92/28, May 1992

B) "Lynx Main Rotor Fly Away Loads - Metal *v* CMRB Blades"
WHL Dynamics Department Note, DYN/91/28, July 1991

2.7 Gabel R & Sankewitsch V

"Rotor-fuselage Coupling by Impedance"
Paper presented at The 42nd AHS Forum, June 1986

2.8 Rutkowski M J

"Assessment of Rotor-Fuselage Coupling on Vibration Prediction using a Simple Finite Element Method"
Journal of AHS, Vol.28, No.3, July 1983

2.9 Holton S A

"Investigation of The Stability of The Sea King Mk42B Tail Rotor"
WHL Dynamics Department Note, DYN/85/14, July 1985

2.10 King S P

"Lynx Main Rotor Lag Mode Frequencies"
WHL Dynamics Department Note, DYN/85/21, October 1985

2.11 Corrigan J J, Schillings J J & Yin S K (COPTER)

"Developments in Dynamics Methodology at Bell"
Paper Presented at The AHS 44th Annual Forum, June 1988

2.12 Shirk M H, Hertz T J & Weisshaar T A

"A Survey of Aeroelastic Tailoring: Theory, Practice, Promise"
AIAA Paper 84-0982, 1982

2.13 Hodges D H

"Review of Composite Rotor Blade Modelling"
AIAA Journal, Vol.28, No.3, *pp*.561-565, March 1990

2.14 Bauchau O A & Hong C H

"Non-linear Composite Beam Theory"
Journal of Applied Mechanics, Vol.110, *pp*.156-163, March 1988

2.15 Dowell E H & Hodges D H
"Non-linear Equations of Motion for The Elastic Bending and Torsion of Twisted Non-uniform Rotor Blades"
NASA Technical Note TN-7818, December 1974

2.16 Bauchau O A & Liu S P
"Finite Element Based Modal Analysis of Helicopter Rotor Blades"
VERTICA Vol.13, No.2, *pp.*197-206, 1989

2.17 Hodges D H
A) "Non-linear Beam Kinematics for Small Strain & Finite Rotations"
VERTICA Vol.11, No.3, *pp.*573-589, 1987
B) "A Mixed Variational Formulation based on Exact Intrinsic Equations for Dynamics of Moving Beams"
AHS Specialists' Meeting on Rotorcraft Dynamics, November 1989

2.18 Simpson A
"Derivation of Modal Lagrangian Equations for Motion for A Multi-Blade Flexible Rotor on A Flexible Shaft"
RAE Report 31, August 1988

2.19 REDUCE V3.2 - Users' Manual
Rand Cooperation, 1987

2.20 Garrad A D & Quarton
"Symbolic Computing as A Tool in Wind Turbine Dynamics"
Journal of Sound & Vibration, Vol.109, No.1, 1986

Chapter 3

3.1 Juggins P T W
"Development of an Analysis for The Coupled Rotor-Fuselage Dynamics"
WHL Dynamics Department Note DYN/88/27, August 1988

3.2 Hamm J C
"The Development of Helicopter Pilot Models to Control Engineering Simulations"

Presented at The RAeS/AHS Symposium Rotorcraft Simulations in London, 18-19 May 1994.

3.3 Peters D A & Ormiston R A
"The Effects of Second Order Blade Bending on The Angle of Attack of Hingeless Rotor Blade"
Journal of AHS, Vol.18, No.4, Technical Notes *pp.*45-48, 1972

3.4 Hodges D H, Ormiston R A & Peters D A
"On The Non-linear Deformation Geometry of Euler-Bernoulli Beams"
NASA Technical Report 80-A-1, TP-1566, 1980

3.5 Hodges D H & Dowell E H
"Non-linear Equations of Motion for The Elastic Bending and Torsion of Twisted Non-uniform Rotor Blades"
NASA Technical Notes, TN-7818, December 1974

3.6 Walker W R
"Equations of Motion for a Fibre Composite Helicopter Rotor Blade"
RAE Technical Report TR-88053, August 1988

3.7 Simpson A
"Derivation of Modal Lagrangian Equations for Motion for a Multi-Blade Flexible rotor on a Flexible Shaft"
RAE Report 31, August 1988

3.8 Goodbody A M
"Cartesian Tensors - With Application to Mechanics, Fluid Mechanics & Elasticity" - Chapter 7 *pp.*229 *et seq.*
Ellis Horwood Ltd, 1982

3.9 Bramwell A R S
"Helicopter Dynamics"
Edward Arnold, 1976

3.10 Griffiths N
"Program R150 Working File"
WHL Aerodynamics Department Software Documents, 1980-

3.11 King S P
"Blade Equation by Energy Method"
WHL Dynamics Department Report, GEN/DYN/209N, November 1978

3.12 Hansford R E
"Non-Linear Equations of Motion for Combined Flapwise, Lagwise and Torsional Deflections of A Twisted Bent Non-Uniform Rotor Blade"
WHL Dynamics Department (Unpublished) Report, 1980

3.13 Coleman R P & Feingold A M
"Theory of Self-Excited Mechanical Oscillations of Helicopter Rotors with Hinged Blades"
NACA Report 1351, 1958

3.14 Done G T S
"A Simplified Approach to Helicopter Ground Resonance"
RAeS Aeronautical Quarterly, May 1974

3.15 Holton S A
"A Note on The Implementation of Coupled Rotor-Fuselage Modes in Aeroelastic Analysis"
WHL Dynamics Department Note, DYN/91/20, July 1991

3.16 Johnson W
"Helicopter Theory" - Chapter 8, *pp.*334-377
Princeton University Press, 1980

3.17 Juggins P T W
A) "A Comprehensive Approach to Coupled Rotor-Fuselage Dynamics"
Paper presented at The 14th ERF, Milano, Italy, September 1988
B) "Application of The Westland CRFD Program to Total Helicopter Dynamics"
Paper presented at The AHS National Specialists Meeting on Rotorcraft Dynamics at Arlington, Texas, November 1989

3.18 Lancaster P
"Lambda Matrices and Vibrating Systems" - Chapter 7
Pergamon Press Inc, 1966

3.19 Glauert H
"A General Theory of The Autogyro"
Aeronautical Research Council, Research Memorandum 1111, 1926

3.20 Cook C V
"Induced Flow Through a Helicopter Rotor in Forward Flight"
WHL Research Paper 374, 1970

3.21 Young C Y
"Development of The Vortex Ring Wake Model and Its Influence on The Prediction of Rotor Loads"
AGARD Conference Proceeding No.334, Paper 11, May 1982

3.22 Beddoes T S
"A Wake Model for High Resolution Airloads"
Paper Presented at The US Army/AHS Conference on Rotorcraft Basic Research, North Carolina, USA, February 1985

3.23 Harrison R J
"A Manoeuvre Wake Model for The Coupled Rotor-Fuselage Model (Phase 2)"
WHL Research Paper 775, January 1991

3.24 Wilby P G, Young C and Grant J
"An Investigation of The Influence of Fuselage Flow Field on Rotor Loads and The Effects of Vehicle Configuration"
Paper presented at The 4th ERF, Stresa, Italy, September 1978

3.25 Young C Y
"A Method of Predicting The Loading on Helicopter Rotor Blade"
RAE Technical Report 82096, 1982

3.26 Hawkings D L
"Slender Body Theory for Helicopter Fuselages"
WHL Research Memorandum No.369, July 1976

3.27 Friedmann P P
"Arbitrary Motion Unsteady Aerodynamics and Its Application to Rotary-wing Aeroelasticity"
Proceedings 42nd Forum of AHS, Washington D.C. June 1986

3.28 Beddoes T S
"A Synthesis of Unsteady Aerodynamic Effects Including Stall Hysteresis"
Paper presented at The 1st ERF, Southampton, UK, September 1975

3.29 Leishman J G & Beddoes T S
"A Second Generation Model for Aerofoil Unsteady Aerodynamic Behaviour and Dynamic Stall"
WHL Research Paper No.704, 1986

3.30 Chan W Y F
"Proof of Modal Orthogonality for The CRFD System"
WHL Dynamics Department Report, DYN/93/06, May 1993

3.31 Meirovitch L
A) "A New Method of Solution of The Eigenvalue Problem for Gyroscopic Systems"
AIAA Journal, *pp.*1337-1342, October 1974
B) "A Modal Analysis for The Response of Linear Gyroscopic Systems"
Journal of Applied Mechanics, *pp.*446-450, June 1975

3.32 Simpson A
Private Correspondence
dated: 20/05/90; 31/05/90; 03/06/92; 05/06/92.

3.33 Noble B
Private Correspondence
dated: 27/12/89; 01/01/90; 20/01/90; 22/01/90;
28/01/90; 31/01/90; 13/02/90.

3.34 Walker W R
Private Correspondence dated 10/04/91.

3.35 Hansford R E, Juggins P T W, Chan W Y F, Hamm J C, Sotiriou C P, Harrison R J & Hawkings D
"Final Report on MOD Contract H22A/47 - The Coupled Rotor-Fuselage Model - Phase 2
WHL Research Paper RP-785, DYN/91/45, Vol.1, December 1991

3.36 Collar A R & Simpson A
"Matrices and Engineering Dynamics"
Ellis Horwood Ltd, 1987

3.37 Holton S A
"CRFD Stiffness Method Implementation to Enable The application of Rotor Mode Orthogonality Condition"
WHL Dynamics Department Research Paper 946,DYN/95/11, February'95

3.38 Auger C J
"BERP Tip Axis Modelling Investigation"
WHL Dynamics Department (Unpublished) Note, DYN/91/33

3.39 Chan W Y F
"Method of Solution for The Response Equation of a Rotor with Any Number of Blades Greater Than 2"
WHL Dynamics Department Report, DYN/91/38, December 1991

3.40 Hawkings D L
"Timewise Integration Techniques for Blade Modal Response - Final Study Report"
Westland Systems Assessment Limited, Report WSAR 760, May 1990

3.41 Chan W Y F
"Investigation- Applicability of NAG Routine D02CBF for The CRFM"
WHL Dynamics Department Report DYN/90/49, October 1990

3.42 Chan W Y F
"Progress Report on Program CRFA Correlation 5/5/93"
WHL Dynamics Department Note, DYN/93/76, May 1993

3.43 Ormiston R A
"Comparison of Several Methods for Predicting Loads on a Hypothetical Helicopter Rotor"
Presented at AHS/NASA Ames Specialist Meeting on Rotorcraft Dynamics, Moffett Field, California, February 1974

3.44 Bielawa R L
"Blade Stress Calculation - Mode Deflection *v* Force Integration"
AHS Symposium on Rotor Technology, August 1976

3.45 Walker W R
"A Comparison of Two Methods for Calculating Loads in Helicopter Rotor Blades"
RAE Technical Memorandum, Structures 975, June 1980

3.46 Hansford R E
"A Unified Formulation of Rotor Load Prediction Methods"
Journal of AHS, Vol.31, No.2, April 1986

3.47 Chan W Y F
"Investigation into The Practical Implementation of A Force Integration Method - An Option for Structural Load Formulation"
WHL Dynamics Department Note, DYN/91/27, December 1991

3.48 Press W H, Flannery R B, Teukolsky S A & Vetterling W T
"Numerical Recipes - The Art of Scientific Computing"
Cambridge University Press, 1989

3.49 Griffiths N
"The CPI Technique for Force Integration Applied to The Nonlinear Flap-Lag-Torsion Term"
WHL Dynamics Department Note, DYN/93/11, April 1993

Chapter 4

4.1 Chan W Y F
"Implementation of The Full (Complex) Rotor Modes Solution in Program CRFA for Both Level and Manoeuvring Flight"
WHL Research Proposal B3401, September 1994

4.2 Griffiths N
"Program R150 Working File"
WHL Dynamics Department Software Quality Document, 1980-

4.3 Young C
"Aircraft Response Model - General Rotorcraft Trim Analysis"
DRA Draft Document - 1992

4.4 Holton S A
"Software Description and User Manual for The Coupled Rotor-Fuselage Dynamics Program - CRFD Version 2.0 (J167B)"
WHL Dynamics Department Report, DYN/95/28, May 1995

4.5 Hamm J C
"The Development of helicopter Pilot Models to Control Engineering Simulations"
Paper Presented at The RAeS/AHS Symposium Rotorcraft Simulations in London, 18-19 May 1994.

4.6 Lau B.H, Louie A W, Sotiriou C P & Griffiths N
"Correlation of The Lynx XZ-170 Flight Test Results Up To and Beyond Stall Boundary"
Paper Presented at The AHS 49th Annual Forum at St.Louis USA, May 1993

4.7 Holton S A
"Implementation of a Hover Model in Program J134"
WHL Dynamics Department Software Quality Document, 1987 -

4.8 Holton S A
"Input Data Specification and Brief Description of Program J168 - Strain Modal Synthesis"
WHL Dynamics Department Note, DYN/91/36, September 1991

4.9 Beddoes T S
"A Synthesis of Unsteady Aerodynamic Effects including Stall Hysteresis"
Paper Presented at The 1st ERF, Southampton, UK, September 1975

4.10 Hawkings D L
"Slender Body Theory for Helicopter Fuselages"
WHL Research Memorandum No.369, July 1976

4.11 Chan W Y F & Griffiths N
A) "Datum Correlation of CRFA *vs* R150"
WHL Dynamics Department Note, DYN/93/02, January 1993
B) "Further Validation of CRFM (Single Blade Capability)"
WHL Dynamics Department Note, DYN/94/03, January 1994

4.12 Brooker S
"Software Application Manual for EH101 Rotor Head Absorber"
WHL Dynamics Department Note, DYN/89/33, September 1989

4.13 Phipps P D
"Manoeuvre Capability of BERP Blade"
WHL Aerodynamics Department Report RP 769, June 1990

4.14 Stepniewski W Z & Keys C N
"Rotary Wing Aerodynamics"
Dover Publications, Inc. 1984

4.15 Hansford R E, Puricelli G, Auger C J, Griffiths N, Chan W Y F, Vickers E G & Hamilton J R
"The Philosophy for The Definition of Conditions for The Loads Book for The EH101 Main Rotor" - Issue 1
WHL EH101 Document EC62L003J, July 1994

4.16 Holton S A
"An Intermediate Solution Method for The Coupled Rotor-Fuselage Analysis"
WHL Dynamics Department Note, DYN/93/10, January 1993

4.17 Griffiths N
"Analysis of BERP Structural Loads and Vibrations"
WHL Dynamics Department Report, RP-739, July 1988

A P P E N D I X

Appendix A: Derivation of The Eulerian Angle ϑ from Blade Deformation

Consider a small rotation $\underline{\omega}dr$ of the blade-fixed system as shown in *Figure* 1 which occurs as r goes through the increment dr.

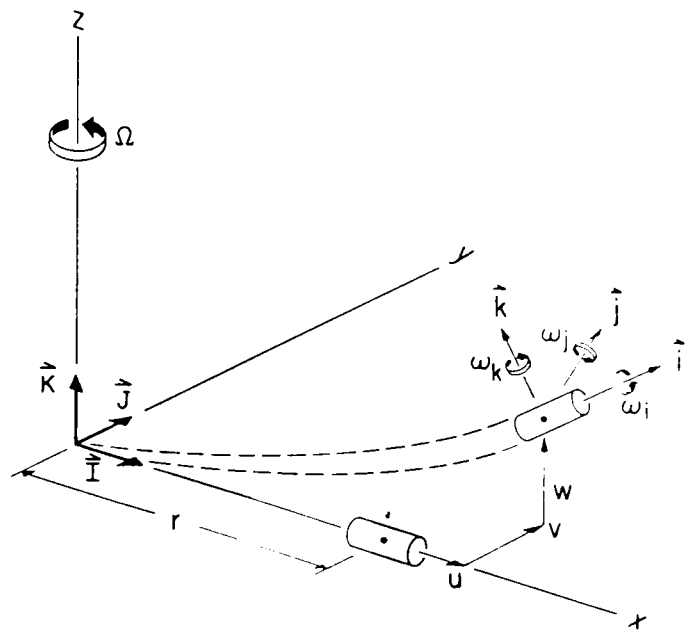

Figure 1. Blade coordinate systems.

To second order, there is no distinction between the distance along the deformed dr and the undeformed dx elastic axes, hence dr≅dx. The vector components of the rate of rotation $\underline{\omega}$ can be identified as the torsional rotation rate $\omega_i=\phi'$ and the bending curvatures ω_j and ω_k as shown. Consider the transformation from the undeformed $(\underline{i},\underline{j},\underline{k})$-system to the deformed $(\underline{i}',\underline{j}',\underline{k}')$-system (*Eqn.*3.8) in the order $\zeta,-\beta,\vartheta$ (*NB.* ϑ is devoid of the control pitch $\vartheta(\psi)$) such that

$$\begin{Bmatrix}\underline{i}\\ \underline{j}\\ \underline{k}\end{Bmatrix} = T \begin{Bmatrix}\underline{i}'\\ \underline{j}'\\ \underline{k}'\end{Bmatrix}$$

where $T=T_\zeta T_\beta T_\vartheta$; $T_\zeta = \begin{pmatrix} c\zeta & -s\zeta & 0\\ s\zeta & c\zeta & 0\\ 0 & 0 & 1\end{pmatrix}$; $T_\beta = \begin{pmatrix} c\beta & 0 & -s\beta\\ 0 & 1 & 0\\ s\beta & 0 & c\beta\end{pmatrix}$; $T_\vartheta = \begin{pmatrix} 1 & 0 & 0\\ 0 & c\vartheta & -s\vartheta\\ 0 & s\vartheta & c\vartheta\end{pmatrix}$ with the notations $c\vartheta=\cos\vartheta$, $s\vartheta=\sin\vartheta$, ... *etc.* used. Consider the orthonormality relation of T,

$$T^TT = I$$

Take the first variation,

$$\delta(T^TT) = \delta T^TT + T^T\delta T = 0; \quad \text{where } \delta(T^T) = (\delta T)^T \equiv (\delta T^T) \text{ is used.}$$

$$\Rightarrow \quad \delta T^TT = -T^T\delta T$$

Take the transpose of the left hand side,

$$\Rightarrow (\delta T^TT)^T = T^T\delta T$$

$$\therefore \delta T^TT = \begin{pmatrix} 0 & \omega_k & -\omega_j\\ -\omega_k & 0 & \omega_i\\ \omega_j & -\omega_i & 0\end{pmatrix}$$ is necessarily skew-symmetric and is expressed in terms of $\omega_i,\omega_j,\omega_k$, which are to be determined as follows.

First consider the transformation, $\tau = T_\zeta T_\beta$.

$$\begin{aligned}
\delta\rho &= \delta(\tau^T\tau) \\
&= \delta(T_\beta^T T_\zeta^T)\ T_\zeta T_\beta \\
&= (\delta T_\beta^T T_\zeta^T + T_\beta^T \delta T_\zeta^T)\ T_\zeta T_\beta \\
&= \delta T_\beta^T T_\beta + T_\beta^T \delta T_\zeta^T T_\zeta T_\beta
\end{aligned}$$

where

$$\delta T_\beta^T T_\beta = \delta\beta \begin{bmatrix} -s\beta & 0 & c\beta \\ 0 & 0 & 0 \\ -c\beta & 0 & -s\beta \end{bmatrix} \begin{bmatrix} c\beta & 0 & -s\beta \\ 0 & 1 & 0 \\ s\beta & 0 & c\beta \end{bmatrix} = \delta\beta \begin{bmatrix} 0 & 0 & 1 \\ 0 & 0 & 0 \\ -1 & 0 & 0 \end{bmatrix}$$

$$T_\beta^T \delta T_\zeta^T T_\zeta T_\beta = T_\beta^T\ \delta\zeta \begin{bmatrix} -s\zeta & c\zeta & 0 \\ -c\zeta & -s\zeta & 0 \\ 0 & 0 & 0 \end{bmatrix} \begin{bmatrix} c\zeta & -s\zeta & 0 \\ s\zeta & c\zeta & 0 \\ 0 & 0 & 1 \end{bmatrix} T_\beta$$

$$= \begin{bmatrix} c\beta & 0 & s\beta \\ 0 & 1 & 0 \\ -s\beta & 0 & c\beta \end{bmatrix}\ \delta\zeta \begin{bmatrix} 0 & 1 & 0 \\ -1 & 0 & 0 \\ 0 & 0 & 0 \end{bmatrix} \begin{bmatrix} c\beta & 0 & -s\beta \\ 0 & 1 & 0 \\ s\beta & 0 & c\beta \end{bmatrix}$$

$$= \begin{bmatrix} c\beta & 0 & s\beta \\ 0 & 1 & 0 \\ -s\beta & 0 & c\beta \end{bmatrix}\ \delta\zeta \begin{bmatrix} 0 & 1 & 0 \\ -c\beta & 0 & s\beta \\ 0 & 0 & 0 \end{bmatrix}$$

$$= \delta\zeta \begin{bmatrix} 0 & c\beta & 0 \\ -c\beta & 0 & s\beta \\ 0 & -s\beta & 0 \end{bmatrix}$$

$$\delta\rho \equiv \begin{bmatrix} 0 & \delta\rho_{n2} & -\delta\rho_{n1} \\ -\delta\rho_{n2} & 0 & \delta\rho_t \\ \delta\rho_{n1} & -\delta\rho_t & 0 \end{bmatrix} = \begin{bmatrix} 0 & \delta\zeta c\beta & \delta\beta \\ -\delta\zeta c\beta & 0 & \delta\zeta s\beta \\ -\delta\beta & -\delta\zeta s\beta & 0 \end{bmatrix}$$

where $\delta\rho_t, \delta\rho_{n1}, \delta\rho_{n2}$ are the rotations about the local t,n1,n2 directions respectively. In view of the *Figure* 2 below,

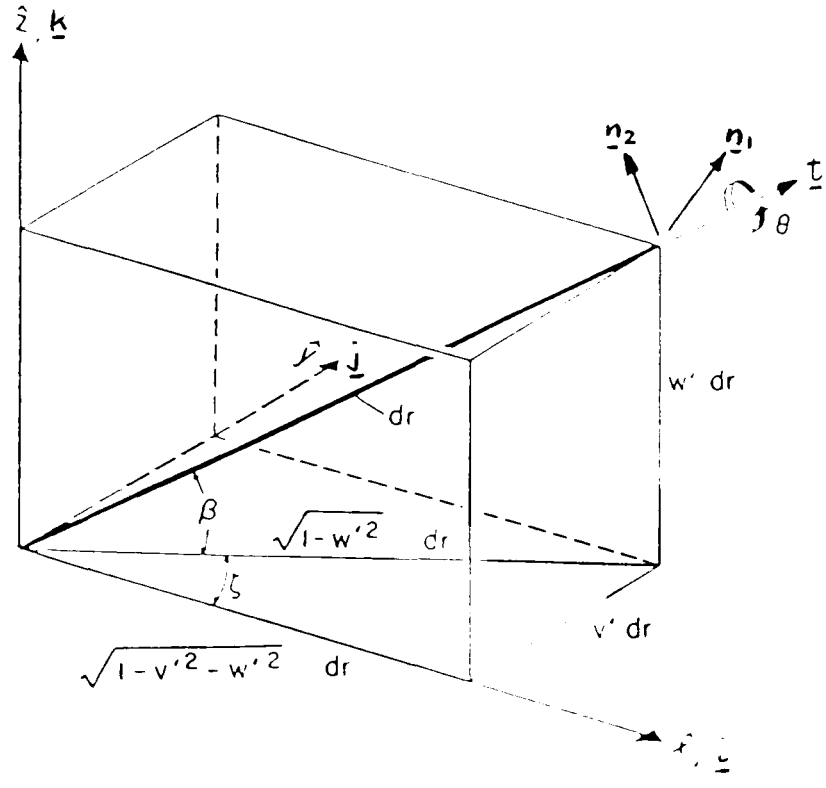

Figure 2. Euler angles.

the following *exact* relations can be established

$$\sin\beta = w',\ \cos\beta = \sqrt{1-w'^2};\ \sin\zeta = \frac{v'}{\sqrt{1-w'^2}};\ \cos\zeta = \frac{\sqrt{1-v'^2-w'^2}}{\sqrt{1-w'^2}}$$

where $()' \equiv \frac{\partial()}{\partial r}$, denotes the derivative with respect to the running length along the elastic axis, r. From which we deduce that

$$\delta\zeta = \frac{\delta v'}{\sqrt{1-v'^2-w'^2}} + \frac{v'w'\delta w}{\sqrt{1-v'^2-w'^2}(1-w'^2)}$$

and $\delta\beta = \frac{\delta w'}{\sqrt{1-w'^2}}$

$$\Longrightarrow \quad \delta\rho_t = \delta\zeta \sin\beta = \frac{w'\delta v'}{\sqrt{1-v'^2-w'^2}} + \frac{v'w'^2\delta w'}{\sqrt{1-v'^2-w'^2}(1-w'^2)}$$

$$\delta\rho_{n1} = -\delta\beta = \frac{-\delta w'}{\sqrt{1-w'^2}}$$

$$\delta\rho_{n2} = \delta\zeta \cos\beta = \frac{\delta v'\sqrt{1-w'^2}}{\sqrt{1-v'^2-w'^2}} + \frac{v'w'\delta w'}{\sqrt{1-v'^2-w'^2}\sqrt{1-w'^2}}$$

The variation $\delta\rho_t$, which is due to the resolution of bending slopes rather than elastic torsion (ϕ), is the quasi-torsion, ϑ_b where

$$\vartheta_b = \int_0^r \rho_t'\, dr = \int_0^r \left[\frac{w'v''}{\sqrt{1-v'^2-w'^2}} + \frac{v'w'^2w''}{\sqrt{1-v'^2-w'^2}(1-w'^2)} \right] dr$$

where $\delta \equiv ()'$ has been used. To determine the torsional rate ϑ' and the bending curvatures $\omega_i, \omega_j, \omega_k$, consider the variation of T in full,

$$\delta T^T T = \begin{pmatrix} 0 & \omega_k & -\omega_j \\ -\omega_k & 0 & \omega_i \\ \omega_j & -\omega_i & 0 \end{pmatrix} = \delta(T_\vartheta^T \rho^T)\rho T_\vartheta$$

$$= (\delta T_\vartheta^T \rho^T + T_\vartheta^T \delta\rho^T)\ \rho T_\vartheta$$

$$= \delta T_\vartheta^T T_\vartheta + T_\vartheta^T \delta\rho^T \rho T_\vartheta$$

Again,

$$\delta T_\vartheta^T T_\vartheta = \delta\vartheta \begin{pmatrix} 0 & 0 & 0 \\ 0 & -s\vartheta & c\vartheta \\ 0 & -c\vartheta & -s\vartheta \end{pmatrix} \begin{pmatrix} 1 & 0 & 0 \\ 0 & c\vartheta & -s\vartheta \\ 0 & s\vartheta & c\vartheta \end{pmatrix} = \delta\vartheta \begin{pmatrix} 0 & 0 & 0 \\ 0 & 0 & 1 \\ 0 & -1 & 0 \end{pmatrix}$$

$$T_\vartheta^T \delta\rho^T \rho T_\vartheta = \begin{pmatrix} 1 & 0 & 0 \\ 0 & c\vartheta & s\vartheta \\ 0 & -s\vartheta & c\vartheta \end{pmatrix} \begin{pmatrix} 0 & \delta\rho_{n2} & -\delta\rho_{n1} \\ -\delta\rho_{n2} & 0 & \delta\rho_t \\ \delta\rho_{n1} & -\delta\rho_t & 0 \end{pmatrix} \begin{pmatrix} 1 & 0 & 0 \\ 0 & c\vartheta & -s\vartheta \\ 0 & s\vartheta & c\vartheta \end{pmatrix}$$

$$\therefore\ \delta T^T T = \begin{pmatrix} 0 & \omega_k & -\omega_j \\ -\omega_k & 0 & \omega_i \\ \omega_j & -\omega_i & 0 \end{pmatrix} = \begin{pmatrix} 0 & \delta\rho_{n2}c\vartheta - \delta\rho_{n1}s\vartheta & -\delta\rho_{n2}s\vartheta - \delta\rho_{n1}c\vartheta \\ & 0 & \delta\rho_t + \delta\vartheta \\ \text{skew symm.} & & 0 \end{pmatrix}$$

where the virtual rotation vector $\delta\underline{\psi}$ is defined as

$$\delta\underline{\psi} = \delta\zeta\underline{k} + \delta\beta(\cos\zeta\underline{j} - \sin\zeta\underline{i}) + \delta\vartheta\underline{i}'$$
$$= \delta\psi_i\underline{i}' + \delta\psi_j\underline{j}' + \delta\psi_k\underline{k}'$$
$$\Rightarrow\ \delta\psi_i = \delta\vartheta + \delta\zeta\sin\beta$$
$$\delta\psi_j = -\delta\beta\cos\vartheta + \delta\zeta\cos\beta\sin\vartheta$$
$$\delta\psi_k = \delta\beta\sin\vartheta + \delta\zeta\cos\beta\cos\vartheta$$

On replacing the variation parameter, $\delta\equiv()'$, then

$$\omega_i = \rho_t' + \vartheta' = \vartheta_b' + \vartheta_p' + \phi' - \vartheta_b' = \vartheta_p' + \phi'$$

$$\Rightarrow\ \boxed{\vartheta' = \vartheta_p' + \phi' - \rho_t'}$$

which yields the *exact* expression for the third Eulerian angle, ϑ, as

$$\vartheta = \vartheta_p + \phi - \int_0^r \left[\frac{w'v''}{\sqrt{1-v'^2-w'^2}} + \frac{v'w'^2w''}{\sqrt{1-v'^2-w'^2}(1-w'^2)} \right] dr$$

The expressions for ω_j, ω_k are also given by

$$\omega_j = \delta\rho_{n2}\sin\vartheta + \delta\rho_{n1}\cos\vartheta$$
$$= \frac{\sin\vartheta(v'' - v''w'^2 + v'w'w'') - \cos\vartheta w''\sqrt{1-v'^2-w'^2}}{\sqrt{1-v'^2-w'^2}\sqrt{1-w'^2}}$$
$$\omega_k = \delta\rho_{n2}\cos\vartheta - \delta\rho_{n1}\sin\vartheta$$
$$= \frac{\cos\vartheta(v'' - v''w'^2 + v'w'w'') + \sin\vartheta w''\sqrt{1-v'^2-w'^2}}{\sqrt{1-v'^2-w'^2}\sqrt{1-w'^2}}$$

ie. $\omega_i, \omega_j, \omega_k$ are identical to those obtained in [3.5]. To $O(\varepsilon^2)$, they may be simplified to

$$\vartheta = \vartheta_p + \phi - \int_0^r w'v''dr + O(\varepsilon^3)$$

and

$$\omega_j = v''\sin(\vartheta_p + \phi) - w''\cos(\vartheta_p + \phi) + O(\varepsilon^3)$$
$$\omega_k = v''\cos(\vartheta_p + \phi) + w''\sin(\vartheta_p + \phi) + O(\varepsilon^3)$$

Appendix B - Modelling of Control Circuit System Stiffness

B.1 Control Circuit System Geometry

The control circuit system stiffness is included in the formulation of modal Lagrangian equation as an external load path. The load path is modelled as a set of linear and rotational springs which give rise to additional strain energy. Consider there are N_s such load paths attached to the blade (main load path) via massless rigid arms at $\underline{r}=\underline{r}_s$ $(s=1,..,N_s)$ as shown in the schematic diagram below,

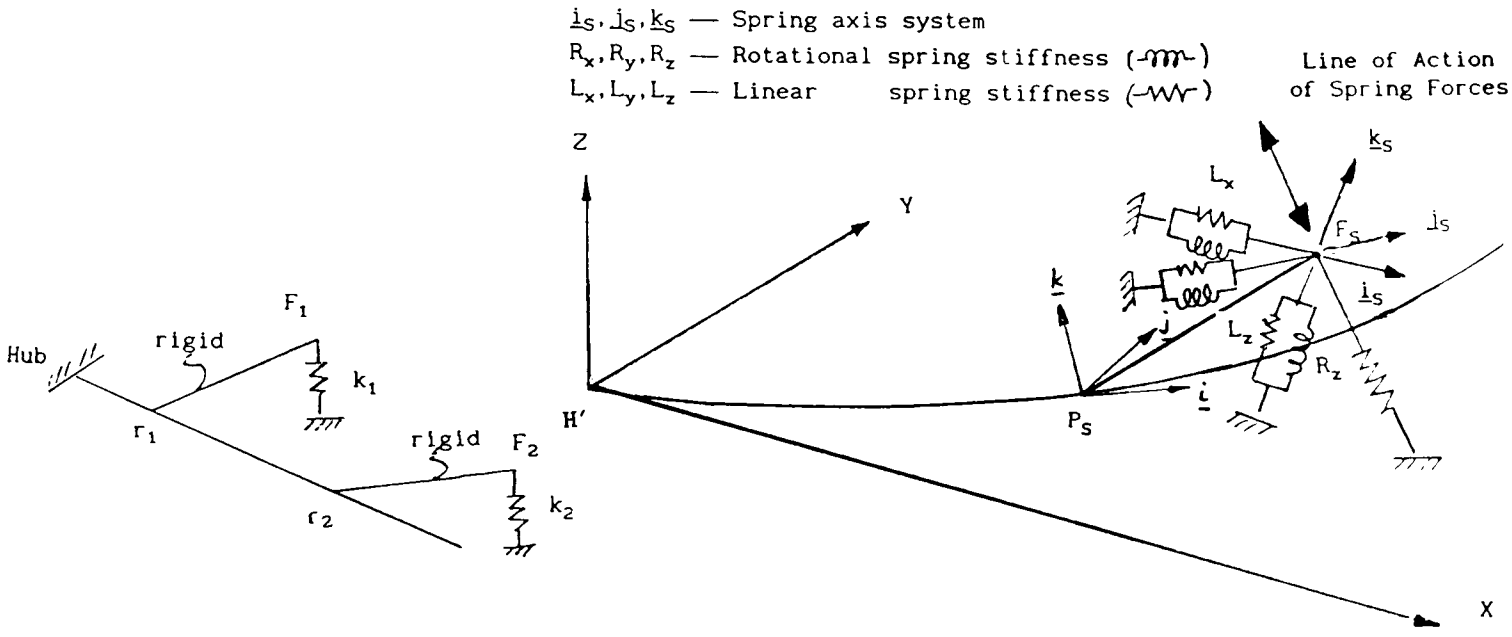

where $\underline{i}_s, \underline{j}_s, \underline{k}_s$ are the unit vectors in the spring axis system;

L_X, L_y, L_Z are the linear spring rates; and

R_X, R_y, R_Z are the rotational spring rates.

Let $\underline{r}_{F_s}=\{l_{r_s}, l_{\eta_s}, l_{\zeta_s}\}^T$ be the position vector of the fixed end F_s of the s'th load path relative to the local axis system with the origin at the attachment point P_s. If ϑ_m is the pitch angle applied in the modes analysis, the position vector of F_s in the rotating blade axis system then becomes

$$\underline{r}_{F_{s_m}} = T_{\vartheta_m}\, \underline{r}_{F_s}$$

or

$$\begin{Bmatrix} l_{u_m} \\ l_{v_m} \\ l_{w_m} \end{Bmatrix} = \begin{bmatrix} 1 & 0 & 0 \\ 0 & \cos\vartheta_m & -\sin\vartheta_m \\ 0 & \sin\vartheta_m & \cos\vartheta_m \end{bmatrix} \cdot \begin{Bmatrix} l_{r_s} \\ l_{\eta_s} \\ l_{\zeta_s} \end{Bmatrix}$$

where $l_{r_s}, l_{\eta_s}, l_{\zeta_s}$ are $O(\varepsilon)$ quantities.

In order to determine the additional strain energy contribution from the control circuit springs, the linear and rotational deformations of the spring attachment point F_s are needed.

B.2 Linear Deformation of Spring Attachment Point

The coordinates of the root-end F_s in the rotating blade axis system are, after deformation,

$$\underline{S}_{F_1} = \begin{Bmatrix} U_p \\ V_p \\ W_p \end{Bmatrix} + P \left\{ \begin{Bmatrix} u \\ v \\ w \end{Bmatrix} + T_\zeta T_\beta \underbrace{T_\phi T_\vartheta}_{T_{\bar{\vartheta}}} \begin{Bmatrix} l_{r_s} \\ l_{\eta_s} \\ l_{\zeta_s} \end{Bmatrix} \right\} \quad \text{at } \underline{r} = \underline{r}_s$$

and before deformation,

$$\underline{S}_{F_0} = \underline{S}_{F_1} \Big|_{u=v=w=\phi=\beta=\zeta=0}$$

$$= \begin{Bmatrix} U_p \\ V_p \\ W_p \end{Bmatrix} + P T_\vartheta \begin{Bmatrix} l_{r_s} \\ l_{\eta_s} \\ l_{\zeta_s} \end{Bmatrix}$$

Hence, the linear displacement of F_s is given by

$$\delta\underline{S}_F = \underline{S}_{F_1} - \underline{S}_{F_0}$$

$$= P \left\{ \begin{Bmatrix} u \\ v \\ w \end{Bmatrix} + (T_\zeta T_\beta T_\phi - I) T_\vartheta \begin{Bmatrix} l_{r_s} \\ l_{\eta_s} \\ l_{\zeta_s} \end{Bmatrix} \right\}$$

where I is a unit matrix of order 3. For small ζ, β, ϕ, and to $O(\varepsilon)$ accuracy,

$$T_\zeta T_\beta T_\phi - I = \begin{bmatrix} 0 & -\zeta & -\beta \\ \zeta & 0 & -\phi \\ \beta & \phi & 0 \end{bmatrix} + O(\varepsilon^2)$$

$$\therefore \delta\underline{S}_F = P \left\{ \begin{Bmatrix} u \\ v \\ w \end{Bmatrix} + \begin{bmatrix} 0 & -\zeta & -\beta \\ \zeta & 0 & -\phi \\ \beta & \phi & 0 \end{bmatrix} \begin{bmatrix} 1 & 0 & 0 \\ 0 & \cos\vartheta & -\sin\vartheta \\ 0 & \sin\vartheta & \cos\vartheta \end{bmatrix} \begin{Bmatrix} l_{r_s} \\ l_{\eta_s} \\ l_{\zeta_s} \end{Bmatrix} \right\} + O(\varepsilon^3)$$

$$= P \left\{ \begin{Bmatrix} u \\ v \\ w \end{Bmatrix} + \begin{bmatrix} 0 & -\zeta & -\beta \\ \zeta & 0 & -\phi \\ \beta & \phi & 0 \end{bmatrix} \begin{Bmatrix} l_{r_s} \\ l_{\eta_s}\cos\vartheta - l_{\zeta_s}\sin\vartheta \\ l_{\eta_s}\sin\vartheta + l_{\zeta_s}\cos\vartheta \end{Bmatrix} \right\} + O(\varepsilon^3)$$

$$= P \left\{ \begin{Bmatrix} u \\ v \\ w \end{Bmatrix} + \begin{bmatrix} 0 & -\zeta & -\beta \\ \zeta & 0 & -\phi \\ \beta & \phi & 0 \end{bmatrix} \begin{Bmatrix} l_u \\ l_v \\ l_w \end{Bmatrix} \right\} + O(\varepsilon^3)$$

$$= P \begin{Bmatrix} u-\zeta l_v-\beta l_w \\ v+\zeta l_u-\phi l_w \\ w+\beta l_u+\phi l_v \end{Bmatrix} + O(\varepsilon^3)$$

where $\begin{Bmatrix} l_u \\ l_v \\ l_w \end{Bmatrix} = \begin{Bmatrix} l r_s \\ l\eta_s \cos\vartheta - l\zeta_s \sin\vartheta \\ l\eta_s \sin\vartheta + l\zeta_s \cos\vartheta \end{Bmatrix}$ are the coordinates of the rigid rod attachment F_s in the local blade axis system.

B.3 Rotational Deformation of Spring Attachment Point

For the rotational deformation at F_s, we proceed in a similar manner. Consider the final position of F_s is achieved via ordered rotations, $\zeta, -\beta, \phi$. The rotational displacements of F_s in the rotating blade axis-system are, after deformation,

$$\underline{\vartheta}_{F_1} = P \left\{ T_\zeta T_\beta \begin{Bmatrix} \phi \\ 0 \\ 0 \end{Bmatrix} + T_\zeta \begin{Bmatrix} 0 \\ -\beta \\ 0 \end{Bmatrix} + \begin{Bmatrix} 0 \\ 0 \\ \zeta \end{Bmatrix} \right\}$$

and before deformation,

$$\underline{\vartheta}_{F_0} = \underline{\vartheta}_{F_1}\Big|_{\zeta=\beta=\phi=0}$$

$$= \underline{0}$$

Hence the rotational displacement of F_s is given by

$$\delta\underline{\vartheta}_F = \underline{\vartheta}_{F_1} - \underline{\vartheta}_{F_0}$$

$$= P \left\{ T_\zeta T_\beta \begin{Bmatrix} \phi \\ 0 \\ 0 \end{Bmatrix} + T_\zeta \begin{Bmatrix} 0 \\ -\beta \\ 0 \end{Bmatrix} + \begin{Bmatrix} 0 \\ 0 \\ \zeta \end{Bmatrix} \right\}$$

$$= P \begin{Bmatrix} \phi\cos\zeta\cos\beta+\beta\sin\zeta \\ \phi\sin\zeta\cos\beta-\beta\cos\zeta \\ \phi\sin\beta+\zeta \end{Bmatrix}$$

For small ζ, β, ϕ and to $O(\varepsilon^2)$ accuracy,

$$\delta\underline{\vartheta}_F = = P \begin{Bmatrix} \phi+\zeta\beta \\ -\beta+\phi\zeta \\ \zeta+\phi\beta \end{Bmatrix} + O(\varepsilon^3)$$

B.4 Spring Orientation

Now consider the spring orientation. Suppose the root-end of the rigid arm is earthed via a system of springs, both linear and rotational types. In general, the line of action of the force will not be parallel to the displacement, *ie.* the cross-impedance of the attachment system is non-zero and the same would apply to the rotations.

Assume that there exists a set of mutually orthogonal directions relative to the rotating axis system for which both the translational and rotational cross-impedances are zero. Let these orientations be achieved by successive rotations $t_z, -t_y, t_x$ about the respective axes, then the transformation matrix, S, from the spring axes to the blade axes is therefore defined as

$$\begin{Bmatrix} \underline{i} \\ \underline{j} \\ \underline{k} \end{Bmatrix} = T_{t_z} T_{t_y} T_{t_x} \begin{Bmatrix} \underline{i}_s \\ \underline{j}_s \\ \underline{k}_s \end{Bmatrix} = S \cdot \begin{Bmatrix} \underline{i}_s \\ \underline{j}_s \\ \underline{k}_s \end{Bmatrix}$$

$$\text{where } S = T_{t_z} T_{t_y} T_{t_x} = \begin{bmatrix} ct_z & -st_z & 0 \\ st_z & ct_z & 0 \\ 0 & 0 & 1 \end{bmatrix} \begin{bmatrix} ct_y & 0 & -st_y \\ 0 & 1 & 0 \\ st_y & 0 & ct_y \end{bmatrix} \begin{bmatrix} 1 & 0 & 0 \\ 0 & ct_x & -st_x \\ 0 & st_x & ct_x \end{bmatrix}$$

$$= \begin{bmatrix} ct_z ct_y & -st_z ct_x - ct_z st_y st_x & st_z st_x - ct_z st_y ct_x \\ st_z ct_y & ct_z ct_x - st_z st_y st_x & -ct_z st_x - st_z st_y ct_x \\ st_y & ct_y st_x & ct_y ct_x \end{bmatrix}$$

with the notations $ct_z = \cos t_z, st_z = \sin t_z$, *etc.* used. Let the linear and rotational spring rates in the (orthogonal) spring axis system be given by $K_{L_s} = \text{Diag}(L_X, L_Y, L_Z)$ and $K_{R_s} = \text{Diag}(R_X, R_Y, R_Z)$. Therefore, the spring forces and moments in the spring axes $F_s X_s Y_s Z_s$, origin at F_s, are

$$\begin{Bmatrix} F_x \\ F_y \\ F_z \end{Bmatrix} = K_{L_s} S^T \, \delta \underline{S}_F = \begin{bmatrix} L_X & 0 & 0 \\ 0 & L_y & 0 \\ 0 & 0 & L_Z \end{bmatrix} S^T P \begin{Bmatrix} u - \zeta l_v - \beta l_w \\ v + \zeta l_u - \phi l_w \\ w + \beta l_u + \phi l_v \end{Bmatrix} + O(\varepsilon^3)$$

$$\begin{Bmatrix} M_x \\ M_y \\ M_z \end{Bmatrix} = K_{R_s} S^T \, \delta \underline{\vartheta}_F = \begin{bmatrix} R_X & 0 & 0 \\ 0 & R_y & 0 \\ 0 & 0 & R_Z \end{bmatrix} S^T P \begin{Bmatrix} \phi + \zeta\beta \\ -\beta + \phi\zeta \\ \zeta + \phi\beta \end{Bmatrix} + O(\varepsilon^3)$$

where L_X, L_Y, L_Z and R_X, R_Y, R_Z are O(1) quantities.

B.5 Strain Energy Contribution from the Control Circuit System

The total strain energy contribution from all N_s load paths is then obtained by summing,

$$U_s = \frac{1}{2} \int_{0}^{R} \sum_{s=1}^{N_s} \delta(r_s)$$

$$\left\{ \{u - \zeta l_v - \beta l_w,\ v + \zeta l_u - \phi l_w,\ w + \beta l_u - \phi l_w\} P^T S \begin{bmatrix} L_X & 0 & 0 \\ 0 & L_y & 0 \\ 0 & 0 & L_Z \end{bmatrix} S^T P \begin{Bmatrix} u - \zeta l_v - \beta l_w \\ v + \zeta l_u - \phi l_w \\ w + \beta l_u + \phi l_v \end{Bmatrix} \right.$$

$$\left. + \{\phi + \zeta\beta, -\beta + \phi\zeta, \zeta + \phi\beta\} P^T S \begin{bmatrix} R_X & 0 & 0 \\ 0 & R_y & 0 \\ 0 & 0 & R_Z \end{bmatrix} S^T P \begin{Bmatrix} \phi + \zeta\beta \\ -\beta + \phi\zeta \\ \zeta + \phi\beta \end{Bmatrix} \right\} dr + O(\varepsilon^4)$$

Let $\left[L\right] = P^T S \begin{pmatrix} L_x & 0 & 0 \\ 0 & L_y & 0 \\ 0 & 0 & L_z \end{pmatrix} S^T P$ and $\left[R\right] = P^T S \begin{pmatrix} R_x & 0 & 0 \\ 0 & R_y & 0 \\ 0 & 0 & R_z \end{pmatrix} S^T P$, then

$$U_s = \frac{1}{2} \int_{0}^{R} \sum_{s=1}^{N_s} \delta(r_s) \Bigg\{ \{u-\zeta l_v-\beta l_w,\ v+\zeta l_u-\phi l_w,\ w+\beta l_u-\phi l_v\} \left[L\right] \begin{Bmatrix} u-\zeta l_v-\beta l_w \\ v+\zeta l_u-\phi l_w \\ w+\beta l_u+\phi l_v \end{Bmatrix}$$

$$\{\phi+\zeta\beta,\ -\beta+\phi\zeta,\ \zeta+\phi\beta\} \left[R\right] \begin{Bmatrix} \phi+\zeta\beta \\ -\beta+\phi\zeta \\ \zeta+\phi\beta \end{Bmatrix} \Bigg\}\ dr\ + O(\varepsilon^4)$$

For zero shear flexibility, $\beta=w'+O(\varepsilon^4)$, $\zeta=v'+O(\varepsilon^4)$, then

$$U_s = \frac{1}{2} \int_{0}^{R} \sum_{s=1}^{N_s} \delta(r_s) \Bigg\{ \{u-v' l_v-w' l_w,\ v+v' l_u-\phi l_w,\ w+w' l_u-\phi l_v\} \left[L\right] \begin{Bmatrix} u-v' l_v-w' l_w \\ v+v' l_u-\phi l_w \\ w+w' l_u+\phi l_v \end{Bmatrix}$$

$$\{\phi+v'w',\ -w'+\phi v',\ v'+\phi w'\} \left[R\right] \begin{Bmatrix} \phi+v'w' \\ -w'+\phi v' \\ v'+\phi w' \end{Bmatrix} \Bigg\}\ dr\ + O(\varepsilon^4)$$

Appendix C - Treatment and Representation of Axial Degree of Freedom

C1 - Treatment of Axial Modes

Consider a straight blade with coincidental section axes. Assume it has undergone elastic axial and flap deformations only, *ie.* no lag or torsion, and the modes are calculated in vacuum with zero collective pitch *ie.* $\vartheta_m=0$. Also assume the axial and flap modes are uncoupled such that the bending moment and radial shear at radius r for the i'th mode, are conveniently given by

$$-M_{y_i} = EIw_i'' = \int_r^R (V_{z_i}-V_x w_i')\, dr = \int_r^R \left\{ -\int_r^R (m\omega_i^2 w_i - V_x w_i')dr \right\} dr \qquad (C1)$$

$$V_{x_i} = EAu_i' = \int_r^R m(\Omega^2+\omega_i^2)\, u_i\, dr \qquad (C2)$$

where ω_i is the natural frequency. From *Eqn.*C2,

$$V_{x_i} = EAu_i' \qquad (C3)$$

$$V_{x_i}' = -m(\Omega^2+\omega_i^2)u_i \qquad (C4)$$

Multiply *Eqn.*C3 by u_j' and *Eqn.*C4 by u_j and integrate with respect to r to give,

$$\int_0^R V_{x_i}u_j'\, dr = \int_0^R EAu_i'u_j'\, dr \qquad (C5)$$

$$\int_0^R V_{x_i}'u_j\, dr = -(\Omega^2+\omega_i^2)\int_0^R mu_iu_j\, dr \qquad (C6)$$

Integrate the LHS of *Eqn.*C5 by parts and apply the boundary conditions

$$\Rightarrow \int_0^R V_{x_i}u_j'\, dr = \left[V_{x_i}u_j\right]_0^R - \int_0^R V_{x_i}'u_j\, dr = -\int_0^R V_{x_i}'u_j\, dr$$

Add to *Eqn.*C6 leads to

$$\int_0^R EAu_i'u_j'\, dr = (\Omega^2+\omega_i^2)\int_0^R mu_iu_j\, dr \qquad (C7)$$

Since the modes are orthogonal such that the inertia orthogonality relationship for the uncoupled axial modes is

$$\int_0^R mu_iu_j\, dr = 0 \qquad \text{for all } i\neq j$$

$$= I_i \qquad \text{for all } i=j. \qquad (C8)$$

From *Eqn.*C7, the stiffness orthogonality follows,

$$\int_0^R EAu_i'u_j'\,dr = 0 \qquad \text{for all } i\neq j$$

$$= (\Omega^2+\omega_i^2)I_i \qquad \text{for all } i=j \tag{C9}$$

Now consider the simplified modal response equation,

$$\ddot{q}_i + \lambda_i^2 q_i = \frac{1}{\Omega^2 I_i}\int_0^R \left\{ \frac{dL}{dr}w_i - EA\sum_{j=1}^{\infty} q_j\left[(u_j'+\frac{w'w_j'}{2})w'w_i' + \frac{w'w_j'}{2}\,u_i'\right]\right\} dr$$

where $\lambda_i (=\frac{\omega_i}{\Omega})$ is the normalised natural frequency. Since u_i and w_i are uncoupled, then for the axial mode only, it reduces to

$$\ddot{q}_i + \lambda_i^2 q_i = \frac{-1}{\Omega^2 I_i}\int_0^R EA\,\frac{w'^2}{2}\,u_i'\,dr \tag{C10}$$

Let the fore-shortening effect be represented by

$$\int_r^R \frac{w'^2}{2}\,dr = \sum_{j=1}^{\infty}\alpha_j u_j$$

$$\therefore \quad \frac{-w'^2}{2} = \sum_{j=1}^{\infty}\alpha_j u_j' \tag{C11}$$

Then *Eqn.*C10 becomes

$$\ddot{q}_i + \lambda_i^2 q_i = \frac{1}{\Omega^2 I_i}\int_0^R EA\sum_{j=1}^{\infty}\alpha_j u_j' u_i'\,dr \tag{C12}$$

and apply the stiffness orthogonality (*Eqn.*C9), it reduces to

$$= \frac{\alpha_i(\Omega^2+\omega_i^2)}{\Omega^2}$$

$$= (1 + \lambda_i^2)\,\alpha_i \tag{C13}$$

Therefore, the n'th harmonic of q_i in *Eqn.*C12 becomes

$$q_{i_{(n)}} = \left(\frac{1 + \lambda_i^2}{\lambda_i^2 - n^2}\right)\alpha_i \tag{C14}$$

Since for the axial modes, λ_i is high, typically 30R (1R≡once per rev), then for $n \ll \lambda_i$ and $1 \ll \lambda_i$, $q_i \simeq \alpha_i$

$$\therefore \sum_{i=1}^{\infty} q_i u_i' \simeq \sum_{i=1}^{\infty}\alpha_i u_i' = \frac{-w'^2}{2} \tag{C15}$$

Hence if there is no pure axial mode defined within the frequency range of interest, upto 12R typically, then u_i=0 for all modes considered and therefore $\sum q_i u_i'$=0. Thus the fore-shortening effect is not represented. Consequently, the axial freedom must be eliminated from the equation by expressing it as fore-shortening terms. This can however lead to problems using Modal Summation to calculate structural loads and correction terms are needed. For example, the radial loads due to axial motion can be mis-constructed as flap shears. Further work is required in this area, but these problems should not arise if structural loads are computed using Force Integration (*Appendix* G) instead of Modal Summation.

C2 - Representation of Axial Degree of Freedom

From *Eqn.*G24 of *Appendix* G that the radial shear is defined as $V_x = \frac{\partial f}{\partial u'}$.

To O(ε) accuracy and with zero shear flexibility,

$$V_x = (EI_{11}+EI_{22})\vartheta'\phi' + EA\left[\, u' - vV_p'' - wW_p'' + \frac{1}{2}(v'^2+w'^2)\,\right]$$
$$+ EB_1[\, v''\sin\vartheta - w''\cos\vartheta + \phi(v''+V_p'')\cos\vartheta + \phi(w''+W_p'')\cos\vartheta\,]$$
$$+ EB_2[-v''\cos\vartheta - w''\sin\vartheta + \phi(v''+V_p'')\sin\vartheta - \phi(w''+W_p'')\cos\vartheta\,]$$
$$+ GB_1\phi'[v'\cos\vartheta + w'\sin\vartheta] + GB_2\phi'[v'\sin\vartheta - w'\cos\vartheta] + O(\varepsilon^2)$$

where $EI_{22}=\iint_{\eta\xi} E\eta^2 d\eta d\xi$; $EI_{11}=\iint_{\eta\xi} E\xi^2 d\eta d\xi$; $EB_1=\iint_{\eta\xi} E\xi d\eta d\xi$; $EB_2=\iint_{\eta\xi} E\eta d\eta d\xi$;

$EA=\iint_{\eta\xi} E d\eta d\xi$; $GB_1=\iint_{\eta\xi} G\xi d\eta d\xi$; $GB_2=\iint_{\eta\xi} G\eta d\eta d\xi$.

To O(ε^2) accuracy, the u′ eliminant is defined as

$$u' = \frac{V_x}{EA} - k_A^2\vartheta'\phi' + vV_p'' + wW_p'' - \frac{1}{2}(v'^2+w'^2)$$
$$+ v''(e_{A2}\cos\vartheta - e_{A1}\sin\vartheta) + w''(e_{A2}\sin\vartheta + e_{A1}\cos\vartheta) + O(\varepsilon^3)$$

where $e_{A1}=\frac{EB_1}{EA}$, $e_{A2}=\frac{EB_2}{EA}$, $k_A^2=\frac{EI_{22}+EI_{11}}{EA}$. Hence

$$u = \int_o^r \Big\{ \frac{V_x}{EA} - k_A^2\vartheta'\phi' + \underline{\underline{vV_p''}} + \underline{\underline{wW_p''}} - \frac{1}{2}(v'^2+w'^2)$$
$$+ v''(e_{A2}\cos\vartheta - e_{A1}\sin\vartheta) + w''(e_{A2}\sin\vartheta + e_{A1}\cos\vartheta) \Big\} dr + O(\varepsilon^3)$$

Integrate the underlined term by parts,

$$\therefore u = vV_p' + wW_p' + \int_o^r \Big\{ \frac{V_x}{EA} - k_A^2\vartheta'\phi' - v'V_p' - w'W_p' - \frac{1}{2}(v'^2+w'^2)$$
$$+ v''(e_{A2}\cos\vartheta - e_{A1}\sin\vartheta) + w''(e_{A2}\sin\vartheta + e_{A1}\cos\vartheta) \Big\} dr + O(\varepsilon^3)$$

Appendix D: Proof of the Generalised Orthogonality Relationship - Bi-orthogonality

D.1 Eigenvalue Problem

Consider the basic set of linear equations of order n for a dynamical system,

$$m\ddot{\underline{x}} + c\dot{\underline{x}} + k\underline{x} = \underline{f} \qquad \text{(D1)}$$

where the coefficient matrices are not necessarily all real and with at least one being unsymmetrical. The system is generally referred to as a linear non-self-adjoint[1*] system. The dynamic characteristics are obtained by solving the homogeneous equation, *ie.* when $\underline{f}=\underline{0}$,

$$m\ddot{\underline{x}} + c\dot{\underline{x}} + k\underline{x} = \underline{0} \qquad \text{(D2)}$$

Assume a solution of the form $\underline{x}=\underline{\phi}e^{\lambda t}$ where $\underline{\phi}$ is a complex eigenvector, then *Eqn.*D2 becomes

$$(\lambda^2 m + \lambda c + k)\,\underline{\phi} = \underline{0} \qquad \text{(D3)}$$

This gives a characteristic equation of order 2n in λ, and subsequently 2n $\underline{\phi}$, such that the roots λ can be real or complex. If the roots are real, they can be either negative which correspond to a damped system with an aperiodic decaying motion or positive for which the system is divergent. If the roots are complex, they appear in conjugate complex pairs with corresponding eigenvector pairs.

Assuming that all the roots are distinct, a constituent solution of the homogeneous equation is

$$\underline{x} = \underline{\phi}_r k_r e^{\lambda_r t} \qquad r = 1,2,..,2n$$
$$= [\phi]\,\{k_r e^{\lambda_r t}\}$$

where k_r are arbitrary constants which may be real or pairs of conjugate complex numbers. $[\phi]$ is the rectangular (nx2n) modal matrix consisting of columns of eigenvectors $\underline{\phi}_r$. It is noted immediately that $[\phi]$ cannot be used as a transformation matrix of the form

$$\underline{x} = [\phi]\underline{\eta}(t) \qquad \text{(D4)}$$

1*

Consider an eigenvalue problem $A\underline{u}=\lambda\underline{u}$, the adjoint eigenvalue problem is defined as $A^T\underline{v}=\lambda\underline{v}$. Since the eigenvalues of A and A^T are the same and the eigen-functions corresponding to distinct eigenvalues are orthogonal *ie.* $\underline{v}_s^T\underline{u}_r=0$ if $\lambda_r\neq\lambda_s$. The system is said to be self-adjoint if $\underline{v}_r=\underline{u}_r$ (r=1,2,...n) *ie.* when A is symmetric.

to obtain a solution of the non-homogeneous problem since there are 2n $\underline{\phi}_r$'s and consequently 2n coordinates of $\eta_r(t)$ but there are only n coordinates of $\underline{x}$. The normal approach is to introduce $\dot{\underline{x}}$ as a vector of auxiliary coordinates. This leads to a set of 2n first order differential equations however it should be noted that the solution will not be affected by the form of the system equation.

Eqn. D1 can be re-cast into the first order form in a number of ways of which we quote

$$I\dot{\underline{z}} - S\underline{z} = \underline{g} \tag{D5}$$

where

$$I = \begin{bmatrix} I & 0 \\ 0 & I \end{bmatrix}; \quad S = \begin{bmatrix} -m^{-1}c & -m^{-1}k \\ I & 0 \end{bmatrix}; \quad \underline{g} = \begin{Bmatrix} m^{-1}\underline{f} \\ \underline{0} \end{Bmatrix}; \quad \underline{z} = \begin{Bmatrix} \dot{\underline{x}} \\ \underline{x} \end{Bmatrix}$$

The homogeneous form of *Eqn.* D5 is a standard eigenvalue problem,

$$S\underline{z} = \lambda\underline{z} \tag{D6}$$

in comparison with the generalised eigenvalue problem of the form $A\underline{z}=\lambda B\underline{z}$ where $S=B^{-1}A$ is the system matrix. The proof of generalised orthogonality (bi-orthogonality) relationship now involves the use of both the right-hand (RH) and the left-hand (LH) eigenvectors, which are defined below.

D.2 Definition of Left-Hand Eigenvectors

Consider a particular solution to the standard eigenvalue problem,

$$S\underline{z}_r = \lambda_r\underline{z}_r \tag{D7}$$

where λ_r is the eigenvalue and $\underline{z}_r$ is the RH-eigenvector of the system matrix S, where the nomenclature of the RH portion is usually ignored. For each of $\underline{z}_r$, there is a corresponding vector $\underline{y}_r$ such that it satisfies

$$\underline{y}_r^H S = \underline{y}^H\lambda_r \quad \text{or} \quad S^H\underline{y}_r=\lambda_r^*\underline{y}_r \tag{D8}$$

where $\underline{y}_r$ is known as the LH-eigenvector of S and that the Hermitian notation is used here, where $S^H=S^{*T}$ *ie.* the conjugate transpose. It is noted that if λ_r is one of the eigenvalues of the S, then λ^* is the corresponding eigenvalue of S^H [D1]. The bi-orthogonality relationship follows.

D.3 Bi-orthogonality Relationship

Consider a typical solution of the standard eigenvalue problem by letting

$$\underline{z} = \begin{Bmatrix} \dot{\underline{x}} \\ \underline{x} \end{Bmatrix} = \underline{\Phi} e^{\lambda t} = \begin{Bmatrix} \lambda \underline{\phi} \\ \underline{\phi} \end{Bmatrix} e^{\lambda t} \tag{D9}$$

Note that $\underline{\Phi}$ is a 2nx1 vector and $\underline{\phi}$ is a nx1 vector. The r'th RH eigen-solution of *Eqn.*D9 satisfies

$$(S - \lambda_r I)\underline{\Phi}_r = \underline{0} \qquad \text{where } \underline{\Phi}_r = \begin{Bmatrix} \lambda_r \underline{\phi}_r \\ \underline{\phi}_r \end{Bmatrix} \tag{D10}$$

The s'th LH eigen-solution of *Eqn.*D10 is defined as

$$\underline{\Gamma}_s^H (S - \lambda_s I) = \underline{0}^H \qquad \text{where } \underline{\Gamma}_s = \begin{Bmatrix} \lambda_s \underline{\gamma}_s \\ \underline{\gamma}_s \end{Bmatrix} \tag{D11}$$

Pre-multiply *Eqn.*D10 by $\underline{\Gamma}_s^H$ and post-multiply *Eqn.*D11 by $\underline{\Phi}_r$ and subtract, one obtains

$$(\lambda_s - \lambda_r)\ \underline{\Gamma}_s^H I \underline{\Phi}_r = 0 \qquad \text{for all r,s} \tag{D12}$$

and from which the following relationships are obtained,

$$\left.\begin{aligned} \Gamma^H \Phi &= \mathrm{Diag}(C_r) \\ \Gamma^H S \Phi &= \mathrm{Diag}(\lambda_r C_r) \end{aligned}\right\} \tag{D13}$$

where C_r is a complex constant, which may be normalised to unity by scaling the rows of Γ^H and columns of Φ. *Eqns.*D13 state the bi-orthogonality (or sometimes known as the bi-normal orthogonality) relationship. The modal matrix $[\Gamma]$, composed of the LH-eigenvectors, $\underline{\Gamma}_r = \begin{Bmatrix} \lambda_r \underline{\gamma}_r \\ \underline{\gamma}_r \end{Bmatrix}$, are just those needed with $[\Phi]$, composed of the RH-eigenvectors, $\underline{\Phi}_r = \begin{Bmatrix} \lambda_r \underline{\phi}_r \\ \underline{\phi}_r \end{Bmatrix}$, (r=1,..,2n) to diagonalise the system matrix S. This bi-orthogonality relationship is general and is valid for *any* physical linear dynamical system.

D.4 Similarity Transformation

In *Section* D3, it is shown that it is possible to diagonalise the system matrix S using both the RH and LH-eigenvectors. However, should we not be able to obtain the LH-eigenvectors, we can proceed the following manner [D2]. Consider *Eqn.*D6,

$$S\underline{z} = \lambda\underline{z}$$

$$\Rightarrow \quad S\Phi = \Phi\Lambda \tag{D14}$$

where $\Lambda=\text{diag}(\lambda_r)$. Pre-multiply *Eqn.*D14 by Φ^{-1},

$$\Phi^{-1}S\Phi - \Phi^{-1}\Phi\Lambda = 0$$

$$\Phi^{-1}S\Phi = \Lambda \tag{D15}$$

ie. $\Phi^{-1}(\equiv\Gamma^H)$ is just needed, together with Φ, to diagonalise the system matrix $S=B^{-1}A$. This process is known as the similarity transformation and is used extensively as an iterative procedure in eigen-solution [D3]. However, the drawback is that *all* the RH-eigenvectors are required and cannot be used if only a sub-set of the eigenvectors is determined.

D.5 Application of Bi-orthogonality Relationship to System Response

Let us examine how the bi-orthogonality relationship is used in the system response analysis. Assume a transformation of variables in *Eqn.*D5,

$$\underline{z} = \Phi\ \underline{\eta}(t) \tag{D16}$$

where Φ is the 2nx2n modal matrix consisting of columns of $\underline{\Phi}_r$ and $\underline{\eta}(t)$ is the 2nx1 vector of unknown generalised coordinates η_r. Pre-multiply *Eqn.*D5 by $\underline{\Gamma}_s^H$ leads to

$$\Gamma^H\Phi\dot{\underline{\eta}}(t) - \Gamma^HS\Phi\underline{\eta}(t) = [\Gamma]^Hg \tag{D17}$$

Using the bi-orthogonality relationship (*Eqn.*D13), *Eqn.*D17 reduces to 2n uncoupled first order equations in η_r,

$$\dot{\eta}_r(t) - \lambda_r\eta_r(t) = \frac{\underline{\Gamma}_r^Hg}{C_r} \qquad r= 1,2,\ldots,2n \tag{D21}$$

where $C_r=\Gamma_r^H\Phi_r$ is the normalising factor for the dynamical system.

References

D1. Noble B "Applied Linear Algebra" - Chapter 9
Prentice Hall, 1969

D2. Simpson A Private Correspondence dated: 26-04-93.

D3. Wilkinson "The Algebraic Eigenvalue Problem" *pp.*3-4
Oxford University Press, 1965

Appendix E: Relationship of Blade Absolute and Relative Displacements

Consider a straight (k'th) blade occupying azimuthal position ψ_k. Assume that a point P on the blade elastic axis, distance r from the hub, has undergone deformation described by $\underline{U}=\{u,v,w,R_x,R_y,R_z\}^T$ relative to the moving hub and the hub itself has also undergone elastic deformation described by $\underline{H}=\{x_H,y_H,z_H,\phi_H,\vartheta_H,\psi_H\}^T$ as follows;

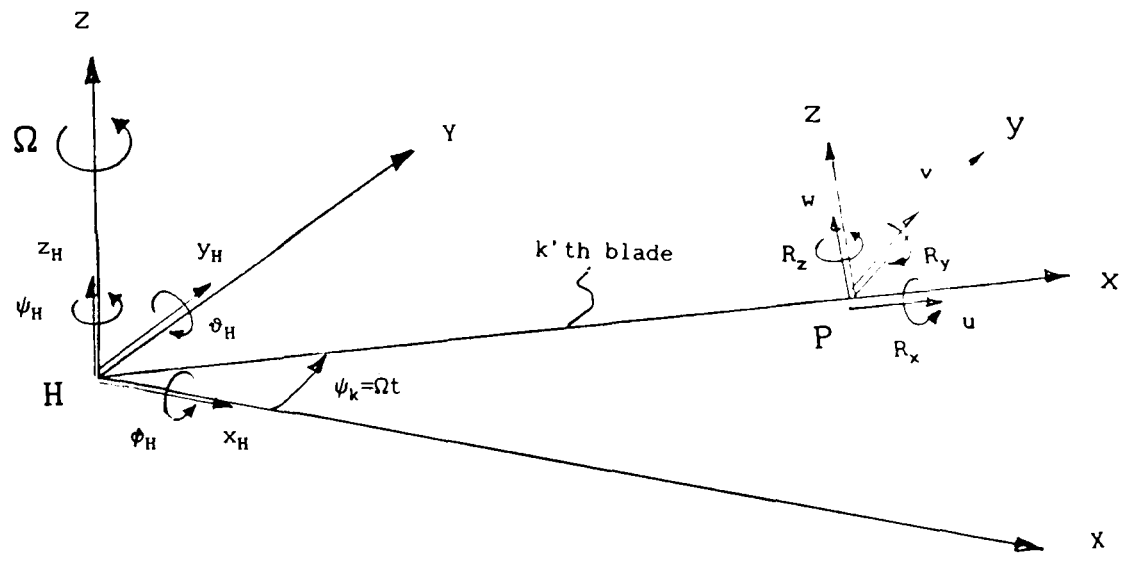

From simple kinematic consideration, the components of total displacement at point P can be shown to be related to the blade and hub displacements as

$$
\begin{aligned}
u_T &= u_k + x_H\cos\psi_k + y_H\sin\psi_k \\
v_T &= v_k - x_H\sin\psi_k + y_H\cos\psi_k + r\psi_H \\
w_T &= w_k + z_H + r(\phi_H\sin\psi_k - \vartheta_H\cos\psi_k) \\
R_{x_T} &= R_{x_k} + \phi_H\cos\psi_k + \vartheta_H\sin\psi_k \\
R_{y_T} &= R_{y_k} - \phi_H\sin\psi_k + \vartheta_H\cos\psi_k \\
R_{z_T} &= R_{z_k} + \psi_H
\end{aligned}
$$

where suffix T refers to the total (absolute) value. Apply the multi-blade coordinate transformation to the blade displacements, one gets

$$
\begin{Bmatrix} u \\ v \\ w \\ R_x \\ R_y \\ R_z \end{Bmatrix}_T = \begin{Bmatrix} u_0 \\ v_0+r\psi_H \\ w_0+z_H \\ R_{x_0} \\ R_{y_0} \\ R_{z_0}+\psi_H \end{Bmatrix} + \cos\psi_k \begin{Bmatrix} u_C+x_H \\ v_C+y_H \\ w_C-r\vartheta_H \\ R_{x_C}+\phi_H \\ R_{y_C}+\vartheta_H \\ R_{z_C} \end{Bmatrix} + \sin\psi_k \begin{Bmatrix} u_S+y_H \\ v_S-x_H \\ w_S+r\phi_H \\ R_{x_S}+\vartheta_H \\ R_{y_S}-\phi_H \\ R_{z_S} \end{Bmatrix}
$$

$$= \begin{Bmatrix} u_O \\ v_O \\ w_O \\ R_{x_O} \\ R_{y_O} \\ R_{z_O} \end{Bmatrix}_R + \begin{bmatrix} 0&0&0&0&0&0 \\ 0&0&0&0&0&r \\ 0&0&1&0&0&0 \\ 0&0&0&0&0&0 \\ 0&0&0&0&0&0 \\ 0&0&0&0&0&1 \end{bmatrix} \begin{Bmatrix} x_H \\ y_H \\ z_H \\ \phi_H \\ \vartheta_H \\ \psi_H \end{Bmatrix} + \cos\psi_k \left\{ \begin{Bmatrix} u_C \\ v_C \\ w_C \\ R_{x_C} \\ R_{y_C} \\ R_{z_C} \end{Bmatrix}_R + \begin{bmatrix} 1&0&0&0&0&0 \\ 0&1&0&0&0&0 \\ 0&0&0&0&-r&0 \\ 0&0&0&1&0&0 \\ 0&0&0&0&1&0 \\ 0&0&0&0&0&0 \end{bmatrix} \begin{Bmatrix} x_H \\ y_H \\ z_H \\ \phi_H \\ \vartheta_H \\ \psi_H \end{Bmatrix} \right\}$$

$$+ \sin\psi_k \left\{ \begin{Bmatrix} u_S \\ v_S \\ w_S \\ R_{x_S} \\ R_{y_S} \\ R_{z_S} \end{Bmatrix}_R + \begin{bmatrix} 0&1&0&0&0&0 \\ -1&0&0&0&0&0 \\ 0&0&0&r&0&0 \\ 0&0&0&0&1&0 \\ 0&0&0&-1&0&0 \\ 0&0&0&0&0&0 \end{bmatrix} \begin{Bmatrix} x_H \\ y_H \\ z_H \\ \phi_H \\ \vartheta_H \\ \psi_H \end{Bmatrix} \right\}$$

or

$$\underline{U}_T = \underbrace{\underline{U}_{O_R} + [HO]\underline{H}}_{\underline{U}_{O_T}} + \cos\psi_k \underbrace{\{\underline{U}_{C_R} + [HC]\underline{H}\}}_{\underline{U}_{C_T}} + \sin\psi_k \underbrace{\{\underline{U}_{S_R} + [HS]\underline{H}\}}_{\underline{U}_{S_T}}$$

where suffix R refers to the relative blade value and $\underline{U}_{O_T}$, $\underline{U}_{C_T}$ and $\underline{U}_{S_T}$ are the total blade displacements in terms of the coupled coordinates. Noting that the hub matrices [HO], [HC], [HS] are independent of time and by equating the harmonics, one gets

$$\begin{Bmatrix} \underline{U}_O \\ \underline{U}_C \\ \underline{U}_S \end{Bmatrix}_T = \begin{Bmatrix} \underline{U}_O \\ \underline{U}_C \\ \underline{U}_S \end{Bmatrix}_R + \begin{bmatrix} [HO] \\ [HC] \\ [HS] \end{bmatrix} \underline{H}$$

or

$$\underline{U}_{\mathbb{C}_T} = \underline{U}_{\mathbb{C}_R} + [HM]\,\underline{H}$$

Matrix Products

The matrix products defined in *Eqn.* 3.85 are

$$P_1 = \begin{bmatrix} B & 0 & 0 \\ 0 & B & 0 \\ 0 & 0 & B \\ C & 0 & 0 \\ 0 & C+\Omega^2 B_4 & -\Omega B_3 \\ 0 & \Omega B_3 & C+\Omega^2 B_4 \end{bmatrix} \begin{bmatrix} [HO] \\ [HC] \\ [HS] \end{bmatrix} \underline{H} = \begin{bmatrix} B[HO] \\ B[HC] \\ B[HS] \\ C[HO] \\ (C+\Omega^2 B_4)[HC] - \Omega B_3[HS] \\ (C+\Omega^2 B_4)[HS] + \Omega B_3[HC] \end{bmatrix} \underline{H}$$

$$P_2 = \begin{bmatrix} 0 & 0 & 0 \\ 0 & 0 & 0 \\ 0 & 0 & 0 \\ -B_3 & 0 & 0 \\ 0 & -B_3 & -2\Omega B_4 \\ 0 & 2\Omega B_4 & -B_3 \end{bmatrix} \begin{bmatrix} [HO] \\ [HC] \\ [HS] \end{bmatrix} \dot{\underline{H}} = \begin{bmatrix} 0 \\ 0 \\ 0 \\ -B_3[HO] \\ -B_3[HC] - 2\Omega B_4[HS] \\ -B_3[HS] + 2\Omega B_4[HC] \end{bmatrix} \dot{\underline{H}}$$

$$P_3 = \begin{bmatrix} 0 & 0 & 0 \\ 0 & 0 & 0 \\ 0 & 0 & 0 \\ -B_4 & 0 & 0 \\ 0 & -B_4 & 0 \\ 0 & 0 & -B_4 \end{bmatrix} \begin{bmatrix} [HO] \\ [HC] \\ [HS] \end{bmatrix} \ddot{\underline{H}} = \begin{bmatrix} 0 \\ 0 \\ 0 \\ -B_4[HO] \\ -B_4[HC] \\ -B_4[HS] \end{bmatrix} \ddot{\underline{H}}$$

where

$$B_4 = m\begin{bmatrix} -1 & 0 & 0 & 0 & 0 & 0 \\ 0 & -1 & 0 & 0 & 0 & 0 \\ 0 & 0 & -1 & 0 & 0 & 0 \\ 0 & 0 & 0 & -(k_{zz}+k_y) & 0 & 0 \\ 0 & 0 & 0 & 0 & -k_{zz} & 0 \\ 0 & 0 & 0 & 0 & 0 & -k_{yy} \end{bmatrix}; \quad B_3 = 2m\Omega\begin{bmatrix} 0 & 1 & 0 & 0 & 0 & 0 \\ -1 & 0 & 0 & 0 & 0 & 0 \\ 0 & 0 & 0 & 0 & 0 & 0 \\ 0 & 0 & 0 & 0 & k_{zz} & 0 \\ 0 & 0 & 0 & -k_{zz} & 0 & 0 \\ 0 & 0 & 0 & 0 & 0 & 0 \end{bmatrix};$$

$$[HO] = \begin{bmatrix} 0 & 0 & 0 & 0 & 0 & 0 \\ 0 & 0 & 0 & 0 & 0 & r \\ 0 & 0 & 1 & 0 & 0 & 0 \\ 0 & 0 & 0 & 0 & 0 & 0 \\ 0 & 0 & 0 & 0 & 0 & 0 \\ 0 & 0 & 0 & 0 & 0 & 1 \end{bmatrix}; \quad [HC] = \begin{bmatrix} 1 & 0 & 0 & 0 & 0 & 0 \\ 0 & 1 & 0 & 0 & 0 & 0 \\ 0 & 0 & 0 & 0 & -r & 0 \\ 0 & 0 & 0 & 1 & 0 & 0 \\ 0 & 0 & 0 & 0 & 1 & 0 \\ 0 & 0 & 0 & 0 & 0 & 0 \end{bmatrix}; \quad [HS] = \begin{bmatrix} 0 & 1 & 0 & 0 & 0 & 0 \\ -1 & 0 & 0 & 0 & 0 & 0 \\ 0 & 0 & 0 & r & 0 & 0 \\ 0 & 0 & 0 & 0 & 1 & 0 \\ 0 & 0 & 0 & -1 & 0 & 0 \\ 0 & 0 & 0 & 0 & 0 & 0 \end{bmatrix}$$

Then,

$$-B_3[HO] = -2m\Omega\begin{bmatrix} 0 & 0 & 0 & 0 & 0 & r \\ 0 & 0 & 0 & 0 & 0 & 0 \\ 0 & 0 & 0 & 0 & 0 & 0 \\ 0 & 0 & 0 & 0 & 0 & 0 \\ 0 & 0 & 0 & 0 & 0 & 0 \\ 0 & 0 & 0 & 0 & 0 & 0 \end{bmatrix}$$

$$-B_3[HC] - 2\Omega B_4[HS] = -2m\Omega\begin{bmatrix} 0 & 0 & 0 & 0 & 0 & 0 \\ 0 & 0 & 0 & 0 & 0 & 0 \\ 0 & 0 & 0 & -r & 0 & 0 \\ 0 & 0 & 0 & 0 & -k_{yy} & 0 \\ 0 & 0 & 0 & 0 & 0 & 0 \\ 0 & 0 & 0 & 0 & 0 & 0 \end{bmatrix}$$

$$-B_3[HS] + 2\Omega B_4[HC] = +2m\Omega\begin{bmatrix} 0 & 0 & 0 & 0 & 0 & 0 \\ 0 & 0 & 0 & 0 & 0 & 0 \\ 0 & 0 & 0 & 0 & r & 0 \\ 0 & 0 & 0 & -k_{yy} & 0 & 0 \\ 0 & 0 & 0 & 0 & 0 & 0 \\ 0 & 0 & 0 & 0 & 0 & 0 \end{bmatrix}$$

and

$$-B_4[HO] = -m\begin{bmatrix} 0 & 0 & 0 & 0 & 0 & 0 \\ 0 & 0 & 0 & 0 & 0 & -r \\ 0 & 0 & -1 & 0 & 0 & 0 \\ 0 & 0 & 0 & 0 & 0 & 0 \\ 0 & 0 & 0 & 0 & 0 & 0 \\ 0 & 0 & 0 & 0 & 0 & -k_{yy} \end{bmatrix}$$

$$-B_4[HC] = -m\begin{bmatrix} -1 & 0 & 0 & 0 & 0 & 0 \\ 0 & -1 & 0 & 0 & 0 & 0 \\ 0 & 0 & 0 & 0 & r & 0 \\ 0 & 0 & 0 & -(k_{zz}+k_{yy}) & 0 & 0 \\ 0 & 0 & 0 & 0 & -k_{zz} & 0 \\ 0 & 0 & 0 & 0 & 0 & 0 \end{bmatrix}$$

$$-B_4[HS] = -m\begin{bmatrix} 0 & -1 & 0 & 0 & 0 & 0 \\ 1 & 0 & 0 & 0 & 0 & 0 \\ 0 & 0 & 0 & -r & 0 & 0 \\ 0 & 0 & 0 & 0 & -(k_{zz}+k_{yy}) & 0 \\ 0 & 0 & 0 & k_{zz} & & 0 \\ 0 & 0 & 0 & 0 & 0 & 0 \end{bmatrix}$$

The B_5 and B_6 matrices for a straight blade with coincidental axes are

$$B_{50} = 2m\Omega\begin{bmatrix} 0 & 0 & 0 & 0 & 0 & r \\ 0 & 0 & 0 & 0 & 0 & 0 \\ 0 & 0 & 0 & 0 & 0 & 0 \\ 0 & 0 & 0 & 0 & 0 & 0 \\ 0 & 0 & 0 & 0 & 0 & 0 \\ 0 & 0 & 0 & 0 & 0 & 0 \end{bmatrix}; \quad B_{5c} = 2m\Omega\begin{bmatrix} 0 & 0 & 0 & 0 & 0 & 0 \\ 0 & 0 & 0 & 0 & 0 & 0 \\ 0 & 0 & 0 & -r & 0 & 0 \\ 0 & 0 & 0 & 0 & 0 & 0 \\ 0 & 0 & 0 & 0 & 0 & 0 \\ 0 & 0 & 0 & 0 & 0 & 0 \end{bmatrix}; \quad B_{5s} = 2m\Omega\begin{bmatrix} 0 & 0 & 0 & 0 & 0 & 0 \\ 0 & 0 & 0 & 0 & 0 & 0 \\ 0 & 0 & 0 & 0 & -r & 0 \\ 0 & 0 & 0 & 0 & 0 & 0 \\ 0 & 0 & 0 & 0 & 0 & 0 \\ 0 & 0 & 0 & 0 & 0 & 0 \end{bmatrix};$$

$$B_{60} = m\begin{bmatrix} 0 & 0 & 0 & 0 & 0 & 0 \\ 0 & 0 & 0 & 0 & 0 & -r \\ 0 & 0 & -1 & 0 & 0 & 0 \\ 0 & 0 & 0 & 0 & 0 & 0 \\ 0 & 0 & 0 & 0 & 0 & 0 \\ 0 & 0 & 0 & 0 & 0 & 0 \end{bmatrix}; \quad B_{6c} = m\begin{bmatrix} -1 & 0 & 0 & 0 & 0 & 0 \\ 0 & -1 & 0 & 0 & 0 & 0 \\ 0 & 0 & 0 & -r & 0 & 0 \\ 0 & 0 & 0 & 0 & 0 & 0 \\ 0 & 0 & 0 & 0 & 0 & 0 \\ 0 & 0 & 0 & 0 & 0 & 0 \end{bmatrix}; \quad B_{6s} = m\begin{bmatrix} 0 & -1 & 0 & 0 & 0 & 0 \\ 1 & 0 & 0 & 0 & 0 & 0 \\ 0 & 0 & 0 & -r & 0 & 0 \\ 0 & 0 & 0 & 0 & 0 & 0 \\ 0 & 0 & 0 & 0 & 0 & 0 \\ 0 & 0 & 0 & 0 & 0 & 0 \end{bmatrix}.$$

By considering the products of B_3, B_4 matrices with those of [HO],[HC],[HS] and the orderings of hub displacement and mk_{zz} terms, we note immediately the following relationship;

$$\begin{aligned} -B_3[HO] &= -B_{50} \\ -B_3[HC] - 2\Omega B_4[HS] &= -B_{5C} \\ -B_3[HS] + 2\Omega B_4[HC] &= -B_{5S} \\ -B_4[HO] &= -B_{60} \\ -B_4[HC] &= -B_{6C} \\ -B_4[HS] &= -B_{6S} \end{aligned}$$

ie. The coefficient matrices B_5's and B_6's are expressible in terms of B_3 and B_4 matrices.

Appendix F - Derivation of Modal Inertia and Stiffness Expressions for the Single Blade Real Modes System

The analytical expressions of the modal inertia and stiffness for the single blade real modes system are derived from the first principle, where the system equation is given by *Eqn.*3.72, with $\dot{\underline{U}}=\underline{0}$ as

$$\left.\begin{aligned} A_0\underline{U}' + A_1\underline{U} - \underline{F} &= \underline{0} \\ \underline{F}' + B_1\underline{U}' + B_2\underline{U} + B_4\ddot{\underline{U}} &= \underline{0} \end{aligned}\right\} \qquad \text{(F1)}$$

where the matrices possess the properties as defined in *Eqn.*3.73 *ie.*

$A_0^T = A_0;\ A_1 = -B_1^T;\ B_2^T = B_2;\ B_4^T = B_4.$

In matrix form, *Eqn.*F1 becomes

$$\begin{Bmatrix} \underline{F} \\ \underline{F}' \end{Bmatrix} = \begin{bmatrix} A_0 & A_1 \\ A_1^T & -B_2 \end{bmatrix} \begin{Bmatrix} \underline{U}' \\ \underline{U} \end{Bmatrix} + \begin{bmatrix} 0 \\ -B_4 \end{bmatrix} \begin{Bmatrix} \ddot{\underline{U}} \end{Bmatrix} \qquad \text{(F2)}$$

where $B_1=-A_1^T$ is used. The j'th solution ($\underline{U}=\underline{U}_j e^{\lambda_j t}$) can be expressed as

$$\begin{Bmatrix} \underline{F}_j \\ \underline{F}'_j \end{Bmatrix} = \begin{bmatrix} A_0 & A_1 \\ A_1^T & -(B_2+\lambda_j^2 B_4) \end{bmatrix} \begin{Bmatrix} \underline{U}'_j \\ \underline{U}_j \end{Bmatrix} \qquad \text{(F3)}$$

Pre-multiply by $\left\{\underline{U}_i'^T, \underline{U}_i^T\right\}$

$$\left\{\underline{U}_i'^T, \underline{U}_i^T\right\} \begin{Bmatrix} \underline{F}_j \\ \underline{F}'_j \end{Bmatrix} = \left\{\underline{U}_i'^T, \underline{U}_i^T\right\} \begin{bmatrix} A_0 & A_1 \\ A_1^T & -(B_2+\lambda^2 B_4) \end{bmatrix} \begin{Bmatrix} \underline{U}'_j \\ \underline{U}_j \end{Bmatrix} \qquad \text{(F4)}$$

or

$$\underline{U}_i'^T\underline{F}_j + \underline{U}_i^T\underline{F}'_j = \underline{U}_i'^T A_0\underline{U}'_j + \underline{U}_i'^T A_1\underline{U}_j + \underline{U}_i^T A_1^T\underline{U}'_j - \underline{U}_i^T B_2\underline{U}_j - \lambda_j^2\underline{U}_i^T B_4\underline{U}_j$$

Integrate from tip to root,

$$\int_0^R (\underline{U}_i'^T\underline{F}_j + \underline{U}_i^T\underline{F}'_j)dr = \int_0^R \left\{ \underline{U}_i'^T A_0\underline{U}'_j + \underline{U}_i'^T A_1\underline{U}_j + \underline{U}_i^T A_1^T\underline{U}'_j - \underline{U}_i^T B_2\underline{U}_j - \lambda_j^2\underline{U}_i^T B_4\underline{U}_j \right\} dr \qquad \text{(F5)}$$

Integrate the second term on the LHS by parts and apply boundary condition,

$$\int_0^R \underline{U}_i^T\underline{F}'_j dr = \left[\underline{U}_i\underline{F}_j\right]_0^R - \int_0^R \underline{U}_i'^T\underline{F}_j dr = -\int_0^R \underline{U}_i'^T\underline{F}_j dr$$

Therefore,

$$\int_0^R (\underline{U}_i'^T\underline{F}_j - \underline{U}_i'^T\underline{F}_j)dr = 0 = \int_0^R \left\{ \underline{U}_i'^T A_0\underline{U}'_j + \underline{U}_i'^T A_1\underline{U}_j + \underline{U}_i^T A_1^T\underline{U}'_j - \underline{U}_i^T B_2\underline{U}_j - \lambda_j^2\underline{U}_i^T B_4\underline{U}_j \right\} dr \qquad \text{(F6)}$$

Interchanging i and j in *Eqn.*F6,

$$0 = \int_0^R \left\{ \underline{U}_j'^T A_0 \underline{U}_i' + \underline{U}_j'^T A_1 \underline{U}_i + \underline{U}_j^T A_1^T \underline{U}_i' - \underline{U}_j^T B_2 \underline{U}_i - \lambda_i^2 \underline{U}_j^T B_4 \underline{U}_i \right\} dr \qquad \text{(F7)}$$

Transpose *Eqn.*F7 and use the matrix properties, leads to

$$0 = \int_0^R \left\{ \underline{U}_i'^T A_0 \underline{U}_j' + \underline{U}_i^T A_1^T \underline{U}_j' + \underline{U}_i'^T A_1 \underline{U}_j - \underline{U}_i^T B_2 \underline{U}_j - \lambda_i^2 \underline{U}_i^T B_4 \underline{U}_j \right\} dr \qquad \text{(F8)}$$

Subtract *Eqn.*F8 from *Eqn.*F6 leads to

$$(\lambda_i^2 - \lambda_j^2) \int_0^R \underline{U}_i^T B_4 \underline{U}_j \, dr = 0 \qquad \text{(F9)}$$

Thus the modal orthogonality relationship is

$$\boxed{\begin{aligned} &\int_0^R \underline{U}_i^T B_4 \underline{U}_j \, dr = 0 \quad \text{for all } i \neq j \\ &\qquad\qquad = I_i \quad \text{for all } i = j \end{aligned}} \qquad \text{(F10)}$$

From *Eqn.*F6, the modal stiffness relationship is obtained as

$$\boxed{\begin{aligned} &\int_0^R \left\{ \underline{U}_i'^T A_0 \underline{U}_j' + \underline{U}_i'^T A_1 \underline{U}_j + \underline{U}_i^T A_1^T \underline{U}_j' - \underline{U}_i^T B_2 \underline{U}_j \right\} dr = 0 \quad \text{for all } i \neq j \\ &\qquad\qquad = \lambda_i^2 I_i \quad \text{for all } i = j \end{aligned}} \qquad \text{(F11)}$$

Appendix G - Formulation of Blade Structural Loads

G.1 Hamilton's Principle

The expressions for the blade structural loads are obtained by the application of Hamilton's Principle,

$$\int_{t_1}^{t_2} [\delta(K-U) + \delta W]\, dt = 0 \qquad (G1)$$

or in terms of the kinetic and energy functions,

$$\delta \int_{t_1}^{t_2} \left[\int_{0}^{r} (g-f)\, dr + \delta W \right] dt = 0 \qquad (G2)$$

By considering the arbitrary variation of the energy functions and virtual work with respect to each of the blade displacements: u,v,w,ϕ,β,ζ, the analytical structural load expressions can be derived.

G.2 Variation of Kinetic Energy

The variation of kinetic energy with respect to each of the generalised variables, defined by the blade elastic deformation, x_k, where $x_k = u,v,w,\phi,\beta,\zeta$, is

$$\delta \int_{t_1}^{t_2} K\, dt = \delta \int_{t_1}^{t_{2r}} \int_{0}^{r} g\, dr\, dt = \int_{t_1}^{t_{2r}} \int_{0}^{r} \left[\frac{\partial g}{\partial x_k}\delta x_k + \frac{\partial g}{\partial \dot{x}_k}\delta \dot{x}_k \right] dr\, dt \qquad (G3)$$

Note that the operators; δ, $\dot{(\,)}=\frac{\partial}{\partial t}$, and the order of integration are commutative such that

$$\delta(\dot{x}_k) = \delta\left(\frac{\partial x_k}{\partial t}\right) = \frac{\partial}{\partial t}(\delta x_k) \quad \text{and} \quad \int_{t_1}^{t_{2r}} \int_{0}^{r} (\,)\, dr\, dt = \int_{0}^{r} \int_{t_1}^{t_2} (\,)\, dt\, dr$$

Integrating the second term of *Eqn.*G3 by parts, yields

$$\int_{t_1}^{t_{2r}} \int_{0}^{r} \frac{\partial g}{\partial \dot{x}_k}\delta \dot{x}_k\, dr\, dt = \int_{0}^{r} \int_{t_1}^{t_2} \frac{\partial g}{\partial \dot{x}_k} \frac{\partial}{\partial t}(\delta x_k)\, dt\, dr$$

$$= \int_{0}^{r} \left[\frac{\partial g}{\partial \dot{x}_k}\delta x_k \right]_{t_1}^{t_2} dr - \int_{0}^{r} \int_{t_1}^{t_2} \left[\frac{d}{dt}\left(\frac{\partial g}{\partial \dot{x}_k}\right)\delta x_k \right] dt\, dr$$

Since by definition, the variation of x_k *ie.* $\delta x_k = 0$ at both $t=t_1$ and t_2, then

$$\therefore \delta \int_{t_1}^{t_2} K\, dt = \int_{t_1}^{t_{2r}} \int_{0}^{r} \left[\frac{\partial g}{\partial x_k} - \frac{d}{dt}\left(\frac{\partial g}{\partial \dot{x}_k}\right) \right]\delta x_k\, dr\, dt \qquad (G4)$$

G.3 Variation of Strain Energy

The variation of strain energy with respect to the blade generalised variables x_k & x'_k then becomes

$$\delta\int_{t_1}^{t_2} U\,dt = \delta\int_{t_1}^{t_{2r}}\int_{0}^{r} f\,dr\,dt = \int_{t_1}^{t_{2r}}\int_{0}^{r}\left[\frac{\partial f}{\partial x_k}\delta x_k + \frac{\partial f}{\partial x'_k}\delta x'_k\right] dr\,dt \qquad (G5)$$

Using the commutation of the operators; δ, $()' = \frac{\partial}{\partial r}$, and the order of integration such that

$$\delta(x'_k) = \delta\left(\frac{\partial x_k}{\partial r}\right) = \frac{\partial}{\partial r}(\delta x_k)$$

Integrating the second term by parts,

$$\int_{t_1}^{t_{2r}}\int_{0}^{r}\frac{\partial f}{\partial x'_k}\,\delta x'_k\,dr\,dt = \int_{t_1}^{t_{2r}}\int_{0}^{r}\frac{\partial f}{\partial x'_k}\,\frac{\partial}{\partial r}(\delta x_k)\,dr\,dt$$

$$= \int_{t_1}^{t_2}\left[\frac{\partial f}{\partial x'_k}\,\delta x_k\right]_0^r dt - \int_{t_1}^{t_{2r}}\int_{0}^{r}\left[\frac{\partial}{\partial r}\left(\frac{\partial f}{\partial x'_k}\right)\delta x_k\right] dr\,dt$$

$$\therefore \delta\int_{t_1}^{t_2} U\,dt = \int_{t_1}^{t_{2r}}\int_{0}^{r}\left[\frac{\partial f}{\partial x_k} - \frac{\partial}{\partial r}\left(\frac{\partial f}{\partial x_k}\right)\right]\delta x_k\,dr\,dt + \int_{t_1}^{t_2}\left[\frac{\partial f}{\partial x'_k}\delta x_k\right]_0^r dt \qquad (G6)$$

G.4 Variation of Additional Strain Energy due to Secondary Load Paths

As discussed in *Section* 3.2.10, the control circuit system stiffness is considered as an external load path, modelled as a set of springs. They will give rise to additional strain energy, U_s, where from *Appendix* B,

$$U_s = \frac{1}{2}\int_0^R \sum_{s=1}^{N_s}\delta(r_s)\Big\{ \{u-\zeta l_v-\beta l_w, v+\zeta l_u-\phi l_w, w+\beta l_u-\phi l_w\}\begin{bmatrix}L\end{bmatrix}\begin{Bmatrix}u-\zeta l_v-\beta l_w\\ v+\zeta l_u-\phi l_w\\ w+\beta l_u+\phi l_v\end{Bmatrix}$$

$$\{\phi+\zeta\beta, -\beta+\phi\zeta, \zeta+\phi\beta\}\begin{bmatrix}R\end{bmatrix}\begin{Bmatrix}\phi+\zeta\beta\\ -\beta+\phi\zeta\\ \zeta+\phi\beta\end{Bmatrix}\Big\} dr + O(\varepsilon^4) \qquad (G7)$$

The partial derivatives of U_s are

$$\frac{\partial U_s}{\partial u} = \int_0^r \sum_{s=1}^{N_s}\delta(r-r_s)\ \{1,0,0\}\ \begin{bmatrix}L\end{bmatrix}\begin{Bmatrix}u-\zeta l_v-\beta l_w\\ v+\zeta l_u-\phi l_w\\ w+\beta l_u+\phi l_v\end{Bmatrix} + O(\varepsilon^2)$$

$$\frac{\partial U_s}{\partial v} = \int_0^r \sum_{s=1}^{N_s}\delta(r-r_s)\ \{0,1,0\}\ \begin{bmatrix}L\end{bmatrix}\begin{Bmatrix}u-\zeta l_v-\beta l_w\\ v+\zeta l_u-\phi l_w\\ w+\beta l_u+\phi l_v\end{Bmatrix} + O(\varepsilon^3)$$

$$\frac{\partial U_s}{\partial w} = \int_0^r \sum_{s=1}^{N_s} \delta(r-r_s)\ \{0,0,1\}\ \left[L\right] \begin{Bmatrix} u-\zeta l_v-\beta l_w \\ v+\zeta l_u-\phi l_w \\ w+\beta l_u+\phi l_v \end{Bmatrix} + O(\varepsilon^3)$$

$$\frac{\partial U_s}{\partial \phi} = \int_0^r \sum_{s=1}^{N_s} \delta(r-r_s)\Big\{\ \{0,-l_w,l_v\}\ \left[L\right] \begin{Bmatrix} u-\zeta l_v-\beta l_w \\ v+\zeta l_u-\phi l_w \\ w+\beta l_u+\phi l_v \end{Bmatrix}$$

$$+\ \{1,\zeta,\beta\}\ \left[R\right] \begin{Bmatrix} \phi+\zeta\beta \\ -\beta+\phi\zeta \\ \zeta+\phi\beta \end{Bmatrix} \Big\}\ dr + O(\varepsilon^3)$$

$$\frac{\partial U_s}{\partial \beta} = \int_0^r \sum_{s=1}^{N_s} \delta(r-r_s)\Big\{\ \{-l_w,0,l_u\}\ \left[L\right] \begin{Bmatrix} u-\zeta l_v-\beta l_w \\ v+\zeta l_u-\phi l_w \\ w+\beta l_u+\phi l_v \end{Bmatrix}$$

$$+\ \{\zeta,-1,\phi\}\ \left[R\right] \begin{Bmatrix} \phi+\zeta\beta \\ -\beta+\phi\zeta \\ \zeta+\phi\beta \end{Bmatrix} \Big\}\ dr + O(\varepsilon^3)$$

$$\frac{\partial U_s}{\partial \zeta} = \int_0^r \sum_{s=1}^{N_s} \delta(r-r_s)\Big\{\ \{-l_v,l_u,0\}\ \left[L\right] \begin{Bmatrix} u-\zeta l_v-\beta l_w \\ v+\zeta l_u-\phi l_w \\ w+\beta l_u+\phi l_v \end{Bmatrix}$$

$$+\ \{\beta,\phi,1\}\ \left[R\right] \begin{Bmatrix} \phi+\zeta\beta \\ -\beta+\phi\zeta \\ \zeta+\phi\beta \end{Bmatrix} \Big\}\ dr + O(\varepsilon^3)$$

and $$\frac{\partial U_s}{\partial u'} = \frac{\partial U_s}{\partial v'} = \frac{\partial U_s}{\partial w'} = \frac{\partial U_s}{\partial \phi'} = \frac{\partial U_s}{\partial \beta'} = \frac{\partial U_s}{\partial \zeta'} = 0. \qquad \text{(G8)}$$

G.5 Virtual Displacement

The virtual work is determined by first defining the virtual displacement of the blade point. The virtual displacement are considered to be made up of two parts: the linear deflection of the blade elastic axis and the rotation of a point on the cross-section.

G.5.1 Virtual Deflection

The position vector of the blade elastic axis in the local blade section Or$\eta\xi$-axis system, after deformation, is simply given by,

$$\underline{R}_e = \begin{Bmatrix} u \\ v \\ w \end{Bmatrix}$$

and the vector of virtual deflections is

$$\delta\underline{R}_e = \begin{Bmatrix} \delta r_x \\ \delta r_y \\ \delta r_z \end{Bmatrix} = \begin{Bmatrix} \delta u \\ \delta v \\ \delta w \end{Bmatrix} \qquad \text{(G9)}$$

G.5.2 Virtual Rotation

The virtual rotation of a point on the blade cross-section is obtained in a similar fashion. Consider the ordered (sequential) rotations $\zeta,-\beta,\phi$ of the blade cross-section, the vector of virtual rotations of the blade cross-section, in the local blade cross-section $Or\eta\xi$-axis system, is then given by

$$\delta\underline{\gamma}_b = \begin{Bmatrix}\delta\gamma_x\\ \delta\gamma_y\\ \delta\gamma_z\end{Bmatrix} = \left\{ T_\zeta T_\beta \begin{Bmatrix}\delta\phi\\ 0\\ 0\end{Bmatrix} + T_\zeta \begin{Bmatrix}0\\ -\delta\beta\\ 0\end{Bmatrix} + \begin{Bmatrix}0\\ 0\\ \delta\zeta\end{Bmatrix} \right\}$$

$$\text{where } T_\zeta = \begin{bmatrix}\cos\zeta & -\sin\zeta & 0\\ \sin\zeta & \cos\zeta & 0\\ 0 & 0 & 1\end{bmatrix}; \quad T_\beta = \begin{bmatrix}\cos\beta & 0 & -\sin\beta\\ 0 & 1 & 0\\ \sin\beta & 0 & \cos\beta\end{bmatrix}.$$

$$\therefore \delta\underline{\gamma}_b = \begin{Bmatrix}\delta\gamma_x\\ \delta\gamma_y\\ \delta\gamma_z\end{Bmatrix} = \begin{Bmatrix}\delta\phi\cos\zeta\cos\beta + \delta\beta\sin\zeta\\ \delta\phi\sin\zeta\cos\beta - \delta\beta\cos\zeta\\ \delta\phi\sin\beta + \delta\zeta\end{Bmatrix} \tag{G10}$$

G.6 Virtual Work

G.6.1 Contribution from Applied Loads

The virtual work due to all external applied loads; aerodynamic lift, drag and moment on the blade is identical to those for the Lagrangian equation and is given by *Eqn.*3.37;

$$\delta W_{AERO} = \int_0^r \left\{ \frac{dA}{dr}\cdot\delta u - \frac{dD}{dr}\cdot\delta v + \frac{dL}{dr}\cdot\delta w + \frac{dM}{dr}\cdot\delta\phi \right\} dr \tag{G11}$$

where $\frac{dA}{dr}$ is the lift and drag loads resolved in the axial direction.

G.6.2 Contribution from Blade Loads

The virtual work due to the internal blade loads; $\underline{F}=\{V_x,V_y,V_z\}^T$ and $\underline{M}=\{M_x,M_y,M_z\}^T$ in the local blade cross-section $Or\eta\xi$-axis system is

$$\delta W_{BLADE} = \underline{F}\cdot\delta\underline{R}_e + \underline{M}\cdot\delta\underline{\gamma}_b$$

$$= \{V_x,V_y,V_z\}\cdot\begin{Bmatrix}\delta r_x\\ \delta r_y\\ \delta r_z\end{Bmatrix} + \{M_x,M_y,M_z\}\cdot\begin{Bmatrix}\delta\gamma_x\\ \delta\gamma_y\\ \delta\gamma_z\end{Bmatrix} \tag{G12}$$

*Eqn.*G12 is valid for all radial positions r and is expressed as coefficients of $\delta u,\delta v,\delta w,\delta\phi,\delta\zeta,\delta\beta$ and becomes

$$\delta W_{BLADE} = V_x\delta u + V_y\delta v + V_z\delta w + \{M_x,M_y,M_Z\}\cdot\left\{ T_\zeta T_\beta \begin{Bmatrix}\delta\phi\\ 0\\ 0\end{Bmatrix} + T_\zeta \begin{Bmatrix}0\\ -\delta\beta\\ 0\end{Bmatrix} + \begin{Bmatrix}0\\ 0\\ \delta\zeta\end{Bmatrix} \right\}$$

$$= V_x\delta u + V_y\delta v + V_z\delta w + (M_x\cos\zeta\cos\beta + M_y\sin\zeta\cos\beta + M_z\sin\beta)\delta\phi$$
$$+ (M_x\sin\zeta - M_y\cos\zeta)\delta\beta + M_z\delta\zeta \tag{G13}$$

G.7 Hamiltonian Equation

Having defined the various components, the Hamiltonian Equation (*Eqn.*G2) can be written in full as

$$\int_{t_1}^{t_2}\Bigg\{\int_0^r\Bigg\{\delta u\Big\{\frac{\partial g}{\partial u}-\frac{d}{dt}\Big(\frac{\partial g}{\partial \dot{u}}\Big)-\frac{\partial(f+U_s)}{\partial u}+\frac{\partial}{\partial r}\Big(\frac{\partial f}{\partial u'}\Big)\Big\}$$

$$+\delta v\Big\{\frac{\partial g}{\partial v}-\frac{d}{dt}\Big(\frac{\partial g}{\partial \dot{v}}\Big)-\frac{\partial(f+U_s)}{\partial v}+\frac{\partial}{\partial r}\Big(\frac{\partial f}{\partial v'}\Big)\Big\}$$

$$+\delta w\Big\{\frac{\partial g}{\partial w}-\frac{d}{dt}\Big(\frac{\partial g}{\partial \dot{w}}\Big)-\frac{\partial(f+U_s)}{\partial w}+\frac{\partial}{\partial r}\Big(\frac{\partial f}{\partial w'}\Big)\Big\}$$

$$+\delta\phi\Big\{\frac{\partial g}{\partial \phi}-\frac{d}{dt}\Big(\frac{\partial g}{\partial \dot{\phi}}\Big)-\frac{\partial(f+U_s)}{\partial \phi}+\frac{\partial}{\partial r}\Big(\frac{\partial f}{\partial \phi'}\Big)\Big\}$$

$$+\delta\beta\Big\{\frac{\partial g}{\partial \beta}-\frac{d}{dt}\Big(\frac{\partial g}{\partial \dot{\beta}}\Big)-\frac{\partial(f+U_s)}{\partial \beta}+\frac{\partial}{\partial r}\Big(\frac{\partial f}{\partial \beta'}\Big)\Big\}$$

$$+\delta\zeta\Big\{\frac{\partial g}{\partial \zeta}-\frac{d}{dt}\Big(\frac{\partial g}{\partial \dot{\zeta}}\Big)-\frac{\partial(f+U_s)}{\partial \zeta}+\frac{\partial}{\partial r}\Big(\frac{\partial f}{\partial \zeta'}\Big)\Big\}\Bigg\}\,dr$$

$$-\Big[\frac{\partial f}{\partial u'}\delta u+\frac{\partial f}{\partial v'}\delta v+\frac{\partial f}{\partial w'}\delta w+\frac{\partial f}{\partial \phi'}\delta\phi+\frac{\partial f}{\partial \beta'}\delta\beta+\frac{\partial f}{\partial \zeta'}\delta\zeta\Big]_0^r$$

$$+\int_0^r\Big\{\frac{dA}{dr}\cdot\delta u-\frac{dD}{dr}\cdot\delta v+\frac{dL}{dr}\cdot\delta w+\frac{dM}{dr}\cdot\delta\phi\Big\}\,dr$$

$$+\Big[V_x\delta u+V_y\delta v+V_z\delta w+(M_x\cos\zeta\cos\beta+M_y\sin\zeta\cos\beta+M_z\sin\beta)\delta\phi$$

$$+(M_x\sin\zeta-M_y\cos\zeta)\delta\beta+M_z\delta\zeta\Big]_0^r\Bigg\}\,dt=0 \qquad (G14)$$

The above expression is true for a single blade.

G.8 Blade Structural Load Equations

The variations in u,v,w,ϕ,β,ζ may be arbitrarily assigned at time t, provided that the boundary conditions are not violated. It is therefore possible to postulate an alternative variation in the range from r_0 to r whilst retaining the same value at both $r=r_0$ and r. Subtracting the two variation equations, the coefficient of δx_k must vanish and the following expressions are thus obtained.

$$\left.\begin{aligned}
&\frac{\partial g}{\partial u} - \frac{d}{dt}\left(\frac{\partial g}{\partial \dot{u}}\right) - \frac{\partial (f+U_s)}{\partial u} + \frac{\partial}{\partial r}\left(\frac{\partial f}{\partial u'}\right) + \frac{dA}{dr} = 0 && \text{(a)}\\
&\frac{\partial g}{\partial v} - \frac{d}{dt}\left(\frac{\partial g}{\partial \dot{v}}\right) - \frac{\partial (f+U_s)}{\partial v} + \frac{\partial}{\partial r}\left(\frac{\partial f}{\partial v'}\right) - \frac{dD}{dr} = 0 && \text{(b)}\\
&\frac{\partial g}{\partial w} - \frac{d}{dt}\left(\frac{\partial g}{\partial \dot{w}}\right) - \frac{\partial (f+U_s)}{\partial w} + \frac{\partial}{\partial r}\left(\frac{\partial f}{\partial w'}\right) + \frac{dL}{dr} = 0 && \text{(c)}\\
&\frac{\partial g}{\partial \phi} - \frac{d}{dt}\left(\frac{\partial g}{\partial \dot{\phi}}\right) - \frac{\partial (f+U_s)}{\partial \phi} + \frac{\partial}{\partial r}\left(\frac{\partial f}{\partial \phi'}\right) + \frac{dM}{dr} = 0 && \text{(d)}\\
&\frac{\partial g}{\partial \beta} - \frac{d}{dt}\left(\frac{\partial g}{\partial \dot{\beta}}\right) - \frac{\partial (f+U_s)}{\partial \beta} + \frac{\partial}{\partial r}\left(\frac{\partial f}{\partial \beta'}\right) = 0 && \text{(e)}\\
&\frac{\partial g}{\partial \zeta} - \frac{d}{dt}\left(\frac{\partial g}{\partial \dot{\zeta}}\right) - \frac{\partial (f+U_s)}{\partial \zeta} + \frac{\partial}{\partial r}\left(\frac{\partial f}{\partial \zeta'}\right) = 0 && \text{(f)}
\end{aligned}\right\} \quad \text{(G15)}$$

And as a by-product, the following boundary conditions are obtained;

$$\left.\begin{aligned}
V_x - \frac{\partial f}{\partial u'} &= 0 && \text{(a)}\\
V_y - \frac{\partial f}{\partial v'} &= 0 && \text{(b)}\\
V_z - \frac{\partial f}{\partial w'} &= 0 && \text{(c)}\\
M_x\cos\zeta\cos\beta + M_y\sin\zeta\cos\beta + M_z\sin\beta - \frac{\partial f}{\partial \phi'} &= 0 && \text{(d)}\\
-M_y\cos\zeta + M_x\sin\zeta - \frac{\partial f}{\partial \beta'} &= 0 && \text{(e)}\\
M_z - \frac{\partial f}{\partial \zeta'} &= 0 && \text{(f)}
\end{aligned}\right\} \quad \text{(G16)}$$

*Eqns.*G15 can be re-arranged to eliminate the derivatives, *eg.* differentiate *Eqn.*G16a and then substitute into *Eqn.*G15a results,

$$\left.\begin{aligned}
V_x' = \frac{d}{dr}\left(\frac{\partial f}{\partial u'}\right) &= \frac{d}{dt}\left(\frac{\partial g}{\partial \dot{u}}\right) - \frac{\partial g}{\partial u} - \frac{\partial (f+U_s)}{\partial u} - \frac{dA}{dr} && \text{(a)}\\
\text{Similarly,}&\\
V_y' &= \frac{d}{dt}\left(\frac{\partial g}{\partial \dot{v}}\right) - \frac{\partial g}{\partial v} - \frac{\partial (f+U_s)}{\partial v} + \frac{dD}{dr} && \text{(b)}\\
V_z' &= \frac{d}{dt}\left(\frac{\partial g}{\partial \dot{w}}\right) - \frac{\partial g}{\partial w} - \frac{\partial (f+U_s)}{\partial w} - \frac{dL}{dr} && \text{(c)}
\end{aligned}\right\} \quad \text{(G17)}$$

Use small angle assumption, *Eqns.*G16d-f become

$$\left.\begin{aligned}
M_x + \zeta M_y + \beta M_z &= \frac{\partial f}{\partial \phi'} + O(\varepsilon^3) && \text{(d)}\\
-M_y + \zeta M_x &= \frac{\partial f}{\partial \beta'} + O(\varepsilon^3) && \text{(e)}\\
M_z &= \frac{\partial f}{\partial \zeta'} && \text{(f)}
\end{aligned}\right\} \quad \text{(G18)}$$

Differentiate *Eqns.*G18d-f with respect to r and substitute into the *Eqns.*G15d-f will lead to,

$$\left.\begin{aligned}
M_x' + (\zeta M_y)' + (\beta M_z)' &= \frac{d}{dt}\left(\frac{\partial g}{\partial \dot{\phi}}\right) - \frac{\partial g}{\partial \phi} + \frac{\partial (f+U_s)}{\partial \phi} - \frac{dM}{dr} + O(\varepsilon^3) \\
-(M_y)' + (\zeta M_x)' &= \frac{d}{dt}\left(\frac{\partial g}{\partial \dot{\beta}}\right) - \frac{\partial g}{\partial \beta} + \frac{\partial (f+U_s)}{\partial \beta} + O(\varepsilon^3) \\
M_z' &= \frac{d}{dt}\left(\frac{\partial g}{\partial \dot{\zeta}}\right) - \frac{\partial g}{\partial \zeta} + \frac{\partial (f+U_s)}{\partial \zeta}
\end{aligned}\right\} \qquad \text{(G19)}$$

Thus, the analytical expressions for the structural loads are

$$\left.\begin{aligned}
V_x' &= \frac{d}{dt}\left(\frac{\partial g}{\partial \dot{u}}\right) - \frac{\partial g}{\partial u} + \frac{\partial (f+U_s)}{\partial u} - \frac{dA}{dr} \\
V_y' &= \frac{d}{dt}\left(\frac{\partial g}{\partial \dot{v}}\right) - \frac{\partial g}{\partial v} + \frac{\partial (f+U_s)}{\partial v} + \frac{dD}{dr} \\
V_z' &= \frac{d}{dt}\left(\frac{\partial g}{\partial \dot{w}}\right) - \frac{\partial g}{\partial w} + \frac{\partial (f+U_s)}{\partial w} - \frac{dL}{dr} \\
\underbrace{M_x' + (\zeta M_y)' + (\beta M_z)'}_{M_{x_{def}}'} &= \frac{d}{dt}\left(\frac{\partial g}{\partial \dot{\phi}}\right) - \frac{\partial g}{\partial \phi} + \frac{\partial (f+U_s)}{\partial \phi} - \frac{dM}{dr} + O(\varepsilon^3) \\
\underbrace{-(M_y)' + (\zeta M_x)'}_{-M_{y_{def}}'} &= \frac{d}{dt}\left(\frac{\partial g}{\partial \dot{\beta}}\right) - \frac{\partial g}{\partial \beta} + \frac{\partial (f+U_s)}{\partial \beta} + O(\varepsilon^3) \\
M_{z_{def}}' &= \frac{d}{dt}\left(\frac{\partial g}{\partial \dot{\zeta}}\right) - \frac{\partial g}{\partial \zeta} + \frac{\partial (f+U_s)}{\partial \zeta}
\end{aligned}\right\} \qquad \text{(G20)}$$

and the corresponding boundary conditions are

$$\left.\begin{aligned}
V_x &= \frac{\partial f}{\partial u'} \\
V_y &= \frac{\partial f}{\partial v'} \\
V_z &= \frac{\partial f}{\partial w'} \\
\underbrace{M_x + \zeta M_y + \beta M_z}_{M_{x_{def}}} &= \frac{\partial f}{\partial \phi'} + O(\varepsilon^3) \\
\underbrace{-M_y + \zeta M_x}_{-M_{y_{def}}} &= \frac{\partial f}{\partial \beta'} + O(\varepsilon^3) \\
M_{z_{def}} &= \frac{\partial f}{\partial \zeta'}
\end{aligned}\right\} \qquad \text{(G21)}$$

The above analytical expressions can be further simplified using the following relationships, by noting that $u'=-\frac{1}{2}(v'^2+w'^2)+O(\varepsilon^3)$ (*Appendix* B), $\beta=w'+O(\varepsilon^4)$, $\zeta=v'+O(\varepsilon^4)$ and manipulating the equations. To $O(\varepsilon^2)$,

$$\left.\begin{aligned} \frac{\partial f}{\partial \beta} &= -\frac{\partial f}{\partial w'} + w'\frac{\partial f}{\partial u'} + O(\varepsilon^3) = -V_z + w'V_x + O(\varepsilon^3) \\ \frac{\partial f}{\partial \zeta} &= -\frac{\partial f}{\partial v'} + v'\frac{\partial f}{\partial u'} + O(\varepsilon^3) = -V_y + v'V_x + O(\varepsilon^3) \end{aligned}\right\} \quad \text{(G22)}$$

Hence *Eqns.*G20 and G21 are simplified respectively as

$$\left.\begin{aligned} V_x' &= \frac{d}{dt}\left(\frac{\partial g}{\partial \dot{u}}\right) - \frac{\partial g}{\partial u} + \frac{\partial (f+U_s)}{\partial u} - \frac{dA}{dr} \\ V_y' &= \frac{d}{dt}\left(\frac{\partial g}{\partial \dot{v}}\right) - \frac{\partial g}{\partial v} + \frac{\partial (f+U_s)}{\partial v} + \frac{dD}{dr} \\ V_z' &= \frac{d}{dt}\left(\frac{\partial g}{\partial \dot{w}}\right) - \frac{\partial g}{\partial w} + \frac{\partial (f+U_s)}{\partial w} - \frac{dL}{dr} \\ M_x' + (\zeta M_y)' + (\beta M_z)' &= \frac{d}{dt}\left(\frac{\partial g}{\partial \dot{\phi}}\right) - \frac{\partial g}{\partial \phi} + \frac{\partial (f+U_s)}{\partial \phi} - \frac{dM}{dr} + O(\varepsilon^3) \\ -M_y' + (\zeta M_x)' &= \frac{d}{dt}\left(\frac{\partial g}{\partial \dot{\beta}}\right) - \frac{\partial g}{\partial \beta} + \frac{\partial U_s}{\partial \beta} - V_z + w'V_x + O(\varepsilon^3) \\ M_z' &= \frac{d}{dt}\left(\frac{\partial g}{\partial \dot{\zeta}}\right) - \frac{\partial g}{\partial \zeta} + \frac{\partial U_s}{\partial \zeta} - V_y + v'V_x + O(\varepsilon^3) \end{aligned}\right\} \quad \text{(G23)}$$

and the boundary conditions are

$$\left.\begin{aligned} V_x &= \frac{\partial f}{\partial u'} \\ V_y &= \frac{\partial f}{\partial v'} \\ V_z &= \frac{\partial f}{\partial w'} \\ M_x + \zeta M_y + \beta M_z &= \frac{\partial f}{\partial \phi'} + O(\varepsilon^3) \\ -M_y + \zeta M_x &= \frac{\partial f}{\partial \beta'} + O(\varepsilon^3) \\ M_z &= \frac{\partial f}{\partial \zeta'} \end{aligned}\right\} \quad \text{(G24)}$$

These expressions can be derived using REDUCE.

Appendix H - Orthogonalisation Process

Appendix H1: Analytical Expressions

- CRFD System Equations *vs* CRFA Structural Loads

CRFD	CRFA
Load Derivatives	
$V_x' = \frac{d}{dt}(\frac{\partial g}{\partial \dot{u}}) - \frac{\partial g}{\partial u} - \frac{dA_0}{dx}$	$V_x' = \frac{d}{dt}(\frac{\partial g}{\partial \dot{u}}) - \frac{\partial g}{\partial u} + \frac{\partial (f+U_s)}{\partial u} - \frac{dA}{dr}$
$V_y' = \frac{d}{dt}(\frac{\partial g}{\partial \dot{v}}) - \frac{\partial g}{\partial v} + \frac{dD_0}{dx}$	$V_y' = \frac{d}{dt}(\frac{\partial g}{\partial \dot{v}}) - \frac{\partial g}{\partial v} + \frac{\partial (f+U_s)}{\partial v} + \frac{dD}{dr}$
$V_z' = \frac{d}{dt}(\frac{\partial g}{\partial \dot{w}}) - \frac{\partial g}{\partial w} - \frac{dL_0}{dx}$	$V_z' = \frac{d}{dt}(\frac{\partial g}{\partial \dot{w}}) - \frac{\partial g}{\partial w} + \frac{\partial (f+U_s)}{\partial w} - \frac{dL}{dr}$
$M_x' = \frac{d}{dt}(\frac{\partial g}{\partial \dot{R}_x}) - \frac{\partial g}{\partial R_x} + \frac{\partial f}{\partial R_x} - \frac{dM_0}{dx}$	$M_x' + (\zeta M_y)' + (\beta M_z)' = \frac{d}{dt}(\frac{\partial g}{\partial \dot{\phi}}) - \frac{\partial g}{\partial \phi} + \frac{\partial (f+U_s)}{\partial \phi} - \frac{dM}{dr} + O(\varepsilon^3)$
$M_y' = \frac{d}{dt}(\frac{\partial g}{\partial \dot{R}_y}) - \frac{\partial g}{\partial R_y} + \frac{\partial f}{\partial R_y}$	$-(M_y)' + (\zeta M_x)' = \frac{d}{dt}(\frac{\partial g}{\partial \dot{\beta}}) - \frac{\partial g}{\partial \beta} + \frac{\partial (f+U_s)}{\partial \beta} + O(\varepsilon^3)$
$M_z' = \frac{d}{dt}(\frac{\partial g}{\partial \dot{R}_z}) - \frac{\partial g}{\partial R_z} + \frac{\partial f}{\partial R_z}$	$M_z' = \frac{d}{dt}(\frac{\partial g}{\partial \dot{\zeta}}) - \frac{\partial g}{\partial \zeta} + \frac{\partial (f+U_s)}{\partial \zeta}$
Boundary Conditions	
$V_x = \frac{\partial f}{\partial u'}$	$V_x = \frac{\partial f}{\partial u'}$
$V_y = \frac{\partial f}{\partial v'}$	$V_y = \frac{\partial f}{\partial v'}$
$V_z = \frac{\partial f}{\partial w'}$	$V_z = \frac{\partial f}{\partial w'}$
$M_x = \frac{\partial f}{\partial R_x'}$	$M_x + \zeta M_y + \beta M_z = \frac{\partial f}{\partial \phi'} + O(\varepsilon^3)$
$M_y = \frac{\partial f}{\partial R_y'}$	$-M_y + \zeta M_x = \frac{\partial f}{\partial \beta'} + O(\varepsilon^3)$
$M_z = \frac{\partial f}{\partial R_z'}$	$M_z = \frac{\partial f}{\partial \zeta'}$

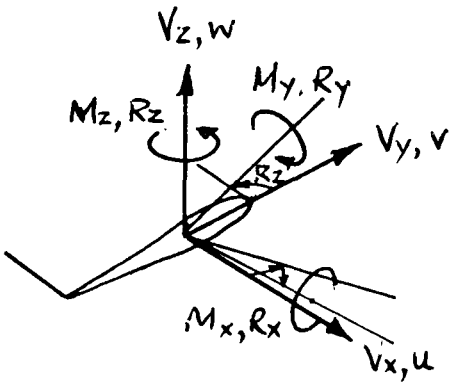

Notations

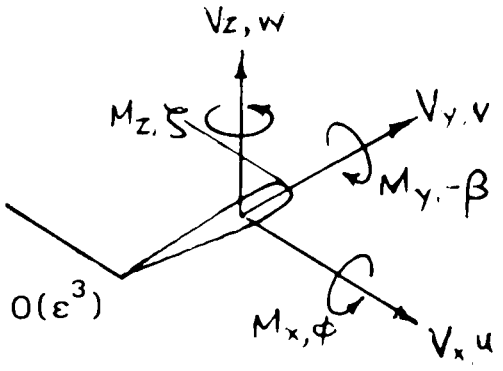

Notations

Notes: In CRFD, a) x is measured along the segment;
b) M_x, M_y, M_z are moments in the sequential axis system;
c) The strain energy function f is independent of u,v,w; and
d) No gravity term is included.

In CRFA, a) r is measured along the blade;
b) M_x, M_y, M_z are moments in the pre-deformed axis system; and
c) f is dependent on u,v,w only if curved blade is assumed.

Appendix H2 - Components of Strain Tensor

CRFA Strain Tensor Components

$$\varepsilon_{11} = (\eta^2+\xi^2)\vartheta'\phi' + u' + \frac{v'^2}{2} + \frac{w'^2}{2} - vV_p'' - wW_p'' + u(v'V_p'' + w'W_p')$$

$$+ 2\eta\vartheta'\{\ \phi(\zeta-v')\cos\vartheta + \phi(\beta-w')\sin\vartheta - u(V_p''\sin\vartheta - W_p''\cos\vartheta) + (\zeta-v')\sin\vartheta - (\beta-w')\cos\vartheta\ \}$$

$$+ 2\xi\vartheta'\{\ -\phi(\zeta-v')\sin\vartheta + \phi(\beta-w')\sin\vartheta - u(V_p''\cos\vartheta - W_p''\sin\vartheta) + (\zeta-v')\cos\vartheta + (\beta-w')\sin\vartheta\ \}$$

$$+ 2\eta\{\ \phi'(\zeta-v')\sin\vartheta - \phi'(\beta-w')\cos\vartheta - \zeta'(\cos\vartheta-\phi\sin\vartheta) - \beta'(\sin\vartheta+\phi\cos\vartheta) + \phi V_p''\sin\vartheta - \phi W_p''\cos\vartheta\ \}$$

$$+ 2\xi\{\ \phi'(\zeta-v')\cos\vartheta + \phi'(\beta-w')\sin\vartheta + \zeta'(\sin\vartheta+\phi\cos\vartheta) - \beta'(\cos\vartheta-\phi\sin\vartheta) + \phi V_p''\cos\vartheta + \phi W_p''\sin\vartheta\ \} + O(\varepsilon^4)$$

$$\varepsilon_{12} = \frac{1}{2}\{\ \xi(-\phi' - \beta\zeta' + \zeta W_p'' - \beta V_p'')$$

$$+ \frac{1}{2}\phi^2(\zeta-v')\cos\vartheta + \frac{1}{2}\phi^2(\beta-w')\sin\vartheta - \phi u(V_p''\sin\vartheta - W_p''\cos\vartheta) + u(V_p''\cos\vartheta + W_p''\sin\vartheta)$$

$$+ \phi(\zeta-v')\sin\vartheta - \phi(\beta-w')\cos\vartheta + \zeta(vV_p'' + wW_p'')\cos\vartheta + \beta(vV_p'' + wW_p'')\sin\vartheta$$
$$- W_p'(wV_p''\cos\vartheta - vV_p''\sin\vartheta) - u'(v'\cos\vartheta + w'\sin\vartheta)$$

$$+ \zeta^2(\zeta-v')\cos\vartheta + \beta^2(\beta-w')\sin\vartheta + \beta\zeta(\zeta-v')\sin\vartheta + \frac{1}{2}\beta^2(\zeta-v')\cos\vartheta - \frac{1}{2}w'\zeta^2\sin\vartheta$$

$$- \frac{1}{3}\zeta^3\cos\vartheta - \frac{1}{3}\beta^3\sin\vartheta - (\zeta-v')\cos\vartheta - (\beta-w')\sin\vartheta\ \} + O(\varepsilon^4)$$

$$\varepsilon_{13} = \frac{1}{2}\{\ \eta(\ \phi' + \beta\zeta' - \zeta W_p'' + \beta V_p'')$$

$$- \frac{1}{2}\phi^2(\zeta-v')\sin\vartheta + \frac{1}{2}\phi^2(\beta-w')\cos\vartheta - \phi u(V_p''\cos\vartheta + W_p''\sin\vartheta) - u(V_p''\sin\vartheta - W_p''\cos\vartheta)$$

$$+ \phi(\zeta-v')\cos\vartheta + \phi(\beta-w')\sin\vartheta - \zeta(vV_p'' + wW_p'')\sin\vartheta + \beta(vV_p'' + wW_p'')\cos\vartheta$$
$$+ W_p'(wV_p''\sin\vartheta - vV_p''\cos\vartheta) + u'(v'\sin\vartheta - w'\cos\vartheta)$$

$$- \zeta^2(\zeta-v')\sin\vartheta - \beta^2(\beta-w')\cos\vartheta + \beta\zeta(\zeta-v')\cos\vartheta - \frac{1}{2}\beta^2(\zeta-v')\sin\vartheta - \frac{1}{2}w'\zeta^2\cos\vartheta$$

$$+ \frac{1}{3}\zeta^3\sin\vartheta - \frac{1}{3}\beta^3\cos\vartheta + (\zeta-v')\sin\vartheta - (\beta-w')\cos\vartheta\ \} + O(\varepsilon^4)$$

CRFD Strain Tensor Components

$$\varepsilon_{11} = (\eta^2+\xi^2)R_p'R_x' + u' + \frac{v'^2}{2} + \frac{w'^2}{2}$$

$$+ 2\eta R_p'\{\ R_x(R_z-v')\cos R_p - R_x(R_y+w')\sin R_p + (R_z-v')\sin R_p + (R_y+w')\cos R_p\ \}$$

$$+ 2\xi R_p'\{\ -R_x(R_z-v')\sin R_p - R_x(R_y+w')\cos R_p + (R_z-v')\cos R_p - (R_y+w')\sin R_p\ \}$$

$$+ 2\eta\{\ R_x'(R_z-v')\sin R_p + R_x'(R_y+w')\cos R_p - R_z'(\cos R_p - R_x\sin R_p) + R_y'(\sin R_p + R_x\cos R_p)\ \}$$

$$+ 2\xi\{\ R_x'(R_z-v')\cos R_p - R_x'(R_y+w')\sin R_p + R_z'(\sin R_p + R_x\cos R_p) + R_y'(\cos R_p - R_x\sin R_p)\ \} + O(\varepsilon^4)$$

$$\varepsilon_{12} = \frac{1}{2}\{\ \xi(-R_x' + R_yR_z')$$

$$+ \frac{1}{2}R_x^2(R_z-v')\cos R_p - \frac{1}{2}R_x^2(R_y+w')\sin R_p$$

$$+ R_x(R_z-v')\sin R_p + R_x(R_y+w')\cos R_p - u'(v'\cos R_p + w'\sin R_p)$$

$$+ R_z^2(R_z-v')\cos R_p - R_y^2(R_y+w')\sin R_p - R_zR_y(R_z-v')\sin R_p + \frac{1}{2}R_y^2(R_z-v')\cos R_p - \frac{1}{2}R_z^2w'\sin R_p$$

$$- \frac{1}{3}R_z^3\cos R_p + \frac{1}{3}R_y^3\sin R_p - (R_z-v')\cos R_p + (R_y+w')\sin R_p\ \} + O(\varepsilon^4)$$

$$\varepsilon_{13} = \frac{1}{2}\{\ \eta(R_x' - R_yR_z')$$

$$- \frac{1}{2}R_x^2(R_z-v')\sin R_p - \frac{1}{2}R_x^2(R_y+w')\cos R_p$$

$$+ R_x(R_z-v')\cos R_p - R_x(R_y+w')\sin R_p + u'(v'\sin R_p - w'\cos R_p)$$

$$- R_z^2(R_z-v')\sin R_p - R_y^2(R_y+w')\cos R_p - R_zR_y(R_z-v')\cos R_p + \frac{1}{2}R_y^2(R_z-v')\sin R_p - \frac{1}{2}R_z^2w'\cos R_p$$

$$+ \frac{1}{3}R_z^3\sin R_p + \frac{1}{3}R_y^3\cos R_p + (R_z-v')\sin R_p + (R_y+w')\cos R_p\ \} + O(\varepsilon^4)$$

Appendix H3 - Curved Segment Consideration

Consider the blade is made up of a number of straight segments, where the position vector of the kink at the root of the d^{th} segment is defined as $\underline{r}_d=\{X_s,Y_s,Z_s\}^T$ in the H'XYZ-axis system. Note that any point on the segment can be defined by $\underline{r}$, measured along the segment from the root as shown below;

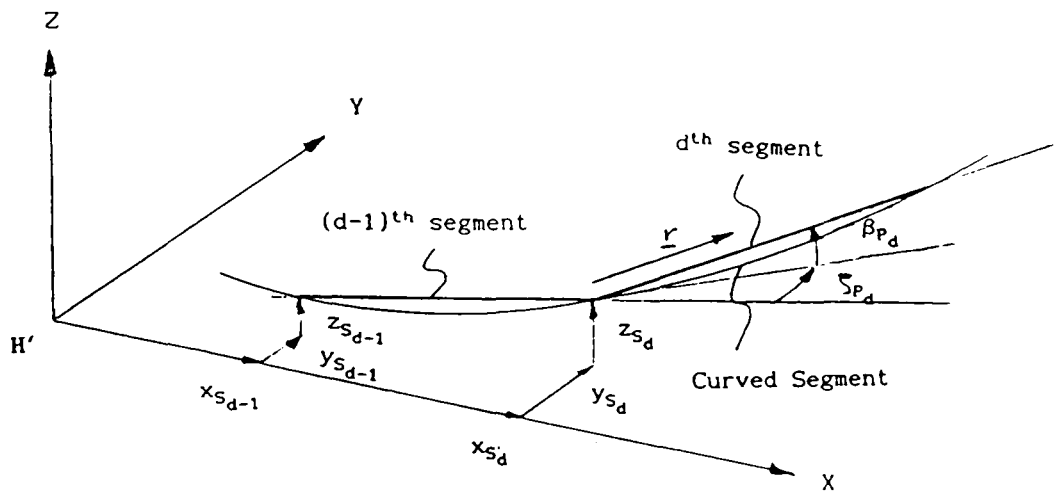

Curved vs Straight Segment

The orientation of the d^{th} straight segment is achieved by sequential rotations, $\zeta_{p_d}, -\beta_{p_d}$ about the local ($(d-1)^{th}$ segment) axis system. The local slopes can be expressed in terms of all the previous transformations using the Heaviside function as a summation series

$$V'_p = \frac{dV_p}{dr} = \zeta_p = \sum_d H(r-r_d)\ \delta\zeta_{p_d}$$

$$W'_p = \frac{dW_p}{dr} = \beta_p = \sum_d H(r-r_d)\ \delta\beta_{p_d}$$

where the Heaviside function is defined as $H(r-r_d)\begin{cases} = 0 & \text{if } r < r_d \\ = 1 & \text{if } r \geq r_d \end{cases}$

Subsequently, the local coordinates and curvatures can be defined by integrating and differentiating the slopes respectively.

For the local coordinates,

$$V_p = \int_0^r V'_p\ dr = \int_0^r \sum_d H(r-r_d)\ \delta\zeta_{p_d}\ dr = \sum_d (r-r_d)\ H(r-r_d)\ \delta\zeta_{p_d}$$

$$W_p = \int_0^r W'_p\ dr = \int_0^r \sum_d H(r-r_d)\ \delta\beta_{p_d}\ dr = \sum_d (r-r_d)\ H(r-r_d)\ \delta\beta_{p_d}$$

and the local curvatures,

$$V''_p = \frac{dV'_p}{dr} = \frac{d}{dr}\left[\sum_d H(r-r_d)\ \delta\zeta_{p_d}\right] = \sum_d \delta(r-r_d)\ \delta\zeta_{p_d}$$

$$W''_p = \frac{dW'_p}{dr} = \frac{d}{dr}\left[\sum_d H(r-r_d)\ \delta\beta_{p_d}\right] = \sum_d \delta(r-r_d)\ \delta\beta_{p_d}$$

where the Delta function is defined as $\delta(r-r_d)=\frac{d}{dr}\left[H(r-r_d)\right]$ $\begin{cases} = 0 \text{ if } r\neq r_d \\ = 1 \text{ if } r=r_d \end{cases}$

Consider a matrix transformation whenever there is a discontinuity in the orientation of the undeformed elastic axis. Let $\underline{r}_{d+}=\{x_{d+}, y_{d+}, z_{d+}\}$ and $\underline{r}_{d-}=\{x_{d-}, y_{d-}, z_{d-}\}$ represent the coordinate of a point being expressed in the d^{th} and $(d-1)^{th}$ segment coordinate respectively. $\underline{r}_{d+}$ and $\underline{r}_{d-}$ are related via

$$\underline{r}_{d-} = T_{\zeta_{p_d}} T_{\beta_{p_d}} \underline{r}_{d+}$$

or

$$\begin{Bmatrix} x_{d-} \\ y_{d-} \\ z_{d-} \end{Bmatrix} = \begin{bmatrix} \cos\zeta_{p_d} & -\sin\zeta_{p_d} & 0 \\ \sin\zeta_{p_d} & \cos\zeta_{p_d} & 0 \\ 0 & 0 & 1 \end{bmatrix} \begin{bmatrix} \cos\beta_{p_d} & 0 & -\sin\beta_{p_d} \\ 0 & 1 & 0 \\ \sin\beta_{p_d} & 0 & \cos\beta_{p_d} \end{bmatrix} \cdot \begin{Bmatrix} x_{d+} \\ y_{d+} \\ z_{d+} \end{Bmatrix}$$

$$= \begin{bmatrix} \cos\zeta_{p_d}\cos\beta_{p_d} & -\sin\zeta_{p_d} & -\cos\zeta_{p_d}\sin\beta_{p_d} \\ \sin\zeta_{p_d}\cos\beta_{p_d} & \cos\zeta_{p_d} & -\sin\zeta_{p_d}\sin\beta_{p_d} \\ \sin\beta_{p_d} & 0 & \cos\beta_{p_d} \end{bmatrix} \cdot \begin{Bmatrix} x_{d+} \\ y_{d+} \\ z_{d+} \end{Bmatrix}$$

To $O(\varepsilon^2)$, for small ζ_{p_d}, β_{p_d},

$$= \begin{bmatrix} 1-\frac{1}{2}(\zeta_{p_d}^2+\beta_{p_d}^2) & -\zeta_{p_d} & -\beta_{p_d} \\ \zeta_{p_d} & 1-\frac{1}{2}\zeta_{p_d}^2 & -\zeta_{p_d}\beta_{p_d} \\ \beta_{p_d} & 0 & 1-\frac{1}{2}\beta_{p_d}^2 \end{bmatrix} \cdot \begin{Bmatrix} x_{d+} \\ y_{d+} \\ z_{d+} \end{Bmatrix} + o(\varepsilon^3)$$

For a continuous curved beam, consider there are finite but large number of straight segments of which the orientation of the d^{th} segment is achieved by ordered rotations, $\delta\zeta_{p_d}, -\delta\beta_{p_d}$ about the $(d-1)^{th}$ axis system such that the above relationship holds for each transformation as follows,

$$\begin{Bmatrix} x_{d-} \\ y_{d-} \\ z_{d-} \end{Bmatrix} = \begin{bmatrix} 1-\frac{1}{2}(\delta\zeta_{p_d}^2+\delta\beta_{p_d}^2) & -\delta\zeta_{p_d} & -\delta\beta_{p_d} \\ \delta\zeta_{p_d} & 1-\frac{1}{2}\delta\zeta_{p_d}^2 & -\delta\zeta_{p_d}\delta\beta_{p_d} \\ \delta\beta_{p_d} & 0 & 1-\frac{1}{2}\delta\beta_{p_d}^2 \end{bmatrix} \cdot \begin{Bmatrix} x_{d+} \\ y_{d+} \\ z_{d+} \end{Bmatrix} + o(\varepsilon^3)$$

$$= \begin{Bmatrix} x_{d+} \\ y_{d+} \\ z_{d+} \end{Bmatrix} - \begin{bmatrix} \frac{1}{2}(\delta\zeta_{p_d}^2+\delta\beta_{p_d}^2) & \delta\zeta_{p_d} & \delta\beta_{p_d} \\ -\delta\zeta_{p_d} & \frac{1}{2}\delta\zeta_{p_d}^2 & \delta\zeta_{p_d}\delta\beta_{p_d} \\ -\delta\beta_{p_d} & 0 & \frac{1}{2}\delta\beta_{p_d}^2 \end{bmatrix} \cdot \begin{Bmatrix} x_{d+} \\ y_{d+} \\ z_{d+} \end{Bmatrix} + o(\varepsilon^3)$$

Then

$$\begin{Bmatrix} x_{d+} \\ y_{d+} \\ z_{d+} \end{Bmatrix} = \begin{Bmatrix} x_{d-} \\ y_{d-} \\ z_{d-} \end{Bmatrix} + [A] \cdot \begin{Bmatrix} x_{d+} \\ y_{d+} \\ z_{d+} \end{Bmatrix} + O(\varepsilon^3)$$

where $[A] = \begin{bmatrix} \frac{1}{2}(\delta\zeta_{p_d}^2+\delta\beta_{p_d}^2) & \delta\zeta_{p_d} & \delta\beta_{p_d} \\ -\delta\zeta_{p_d} & \frac{1}{2}\delta\zeta_{p_d}^2 & \delta\zeta_{p_d}\delta\beta_{p_d} \\ -\delta\beta_{p_d} & 0 & \frac{1}{2}\delta\beta_{p_d}^2 \end{bmatrix}$.

Now consider a point along the blade, of which its position can be determined by integrating from the tip to the root using the all the segment transformations, *ie.* if $\underline{R}=\{X,Y,Z\}^T$ is the position vector of the point defined in the general curved segment notation then,

$$\begin{Bmatrix} X \\ Y \\ Z \end{Bmatrix} = \begin{Bmatrix} x_{d+} \\ y_{d+} \\ z_{d+} \end{Bmatrix} + \int_0^r \begin{Bmatrix} X' \\ Y' \\ Z' \end{Bmatrix} dr$$

$$= \begin{Bmatrix} x_{d-} \\ y_{d-} \\ z_{d-} \end{Bmatrix} + [A] \cdot \begin{Bmatrix} x_{d+} \\ y_{d+} \\ z_{d+} \end{Bmatrix} + \int_0^r \begin{Bmatrix} X' \\ Y' \\ Z' \end{Bmatrix} dr + O(\varepsilon^3)$$

which may be expressed in terms of the Heaviside and Delta functions as

$$= \begin{Bmatrix} x_{(d-1)+} \\ y_{(d-1)+} \\ z_{(d-1)+} \end{Bmatrix} + H(r-r_d)\ [A] \cdot \begin{Bmatrix} x_{d+} \\ y_{d+} \\ z_{d+} \end{Bmatrix} + \int_0^r \begin{Bmatrix} X' \\ Y' \\ Z' \end{Bmatrix} (1-\delta(r-r_d))dr + O(\varepsilon^3)$$

and including all the kinks,

$$= \sum_d H(r-r_d)[A] \cdot \begin{Bmatrix} x_{d+} \\ y_{d+} \\ z_{d+} \end{Bmatrix} + \int_0^r \begin{Bmatrix} X' \\ Y' \\ Z' \end{Bmatrix} \{1-\sum_d \delta(r-r_d)\}dr + O(\varepsilon^3)$$

where the last term, representing the straight segment contribution, is written as

$$\begin{Bmatrix} X_s \\ Y_s \\ Z_s \end{Bmatrix} = \int_0^r \begin{Bmatrix} X' \\ Y' \\ Z' \end{Bmatrix} \{1-\sum_d \delta(r-r_d)\}\ dr$$

Hence,

$$\begin{Bmatrix} X \\ Y \\ Z \end{Bmatrix} = \begin{Bmatrix} X_s \\ Y_s \\ Z_s \end{Bmatrix} + \sum_d H(r-r_d)\ [A] \begin{Bmatrix} x_{d+} \\ y_{d+} \\ z_{d+} \end{Bmatrix} + O(\varepsilon^3)$$

and the corresponding slopes become,

$$\begin{Bmatrix} X' \\ Y' \\ Z' \end{Bmatrix} = \begin{Bmatrix} X'_s \\ Y'_s \\ Z'_s \end{Bmatrix} + \sum_d \delta(r-r_d)\ [A] \begin{Bmatrix} x_{d+} \\ y_{d+} \\ z_{d+} \end{Bmatrix} + O(\varepsilon^3)$$

Since $\sum_d \delta(r-r_d)\frac{1}{2}(\delta\zeta^2_{p_d}) = \frac{1}{\delta r}(\frac{1}{2}V'^2_p)$,

in the limit, $= \frac{1}{\partial r}(\frac{1}{2}V'^2_p)$

$= V'_pV''_p$

etc. Therefore,

$$\begin{Bmatrix} X' \\ Y' \\ Z' \end{Bmatrix} = \begin{Bmatrix} X'_s \\ Y'_s \\ Z'_s \end{Bmatrix} + \begin{bmatrix} V'_pV''_p+W'_pW''_p & V''_p & W''_p \\ -V''_p & V'_pV''_p & V'''_pW''_p \\ -W''_p & 0 & W'_pW''_p \end{bmatrix} \begin{Bmatrix} X \\ Y \\ Z \end{Bmatrix} + O(\varepsilon^3)$$

Using this relationship, the variables valid for the straight segments are related to those of curved segment via

Slopes & Curvatures

$$\begin{Bmatrix} u' \\ v' \\ w' \end{Bmatrix}_s = \begin{Bmatrix} u' \\ v' \\ w' \end{Bmatrix} - \sum_d \delta(r-r_d) \begin{bmatrix} 0 & \delta\zeta_{p_d} & \delta\beta_{p_d} \\ -\delta\zeta_{p_d} & 0 & 0 \\ -\delta\beta_{p_d} & 0 & 0 \end{bmatrix} \cdot \begin{Bmatrix} u \\ v \\ w \end{Bmatrix} + O(\varepsilon^3) = \begin{Bmatrix} u' - vV''_p - wW''_p \\ v' + uV''_p \\ w' + uW''_p \end{Bmatrix} + O(\varepsilon^3)$$

$$\begin{Bmatrix} R'_x \\ R'_y \\ R'_z \end{Bmatrix}_s = \begin{Bmatrix} \phi' \\ -\beta' \\ \zeta' \end{Bmatrix} - \sum_d \delta(r-r_d) \begin{bmatrix} 0 & \delta\zeta_{p_d} & \delta\beta_{p_d} \\ -\delta\zeta_{p_d} & 0 & 0 \\ -\delta\beta_{p_d} & 0 & 0 \end{bmatrix} \cdot \begin{Bmatrix} \phi' \\ -\beta' \\ \zeta' \end{Bmatrix} + O(\varepsilon^3) = \begin{Bmatrix} \phi' + \beta V - \zeta W''_p \\ -\beta' + \phi V''_p \\ \zeta' + \phi W''_p \end{Bmatrix} + O(\varepsilon^3)$$

Shear & Moment Derivatives

$$\begin{Bmatrix} V'_x \\ V'_y \\ V'_z \end{Bmatrix}_s = \begin{Bmatrix} V'_x \\ V'_y \\ V'_z \end{Bmatrix} - \sum_d \delta(r-r_d) \begin{bmatrix} 0 & \delta\zeta_{p_d} & \delta\beta_{p_d} \\ -\delta\zeta_{p_d} & 0 & 0 \\ -\delta\beta_{p_d} & 0 & 0 \end{bmatrix} \cdot \begin{Bmatrix} V_x \\ V_y \\ V_z \end{Bmatrix} + O(\varepsilon^3) = \begin{Bmatrix} V'_x + O(\varepsilon^2) \\ V'_y + V''_pV_x + O(\varepsilon^3) \\ V'_z + W''_pV_x + O(\varepsilon^3) \end{Bmatrix}$$

$$\begin{Bmatrix} M_x \\ M_y \\ M_z \end{Bmatrix}'_s = \begin{Bmatrix} M_x \\ M_y \\ M_z \end{Bmatrix}' - \sum_d \delta(r-r_d) \begin{bmatrix} 0 & \delta\zeta_{p_d} & \delta\beta_{p_d} \\ -\delta\zeta_{p_d} & 0 & 0 \\ -\delta\zeta_{p_d} & 0 & 0 \end{bmatrix} \cdot \begin{Bmatrix} M_x \\ M_y \\ M_z \end{Bmatrix} + O(\varepsilon^3) = \begin{Bmatrix} M'_x - V''_pM_y - W''_pM_z \\ M'_y \\ M'_z \end{Bmatrix} + O(\varepsilon^3)$$

In summary, the deflections and slopes, moments and shears, and their spatial derivatives for the two systems are related viz,

Blade displacements, slopes and curvatures

$$\begin{Bmatrix} u \\ v \\ w \\ R_x \\ R_y \\ R_z \end{Bmatrix}_s = \begin{Bmatrix} u \\ v \\ w \\ \phi \\ -w' \\ v' \end{Bmatrix} + O(\varepsilon^3) \quad \text{and} \quad \begin{Bmatrix} u' \\ v' \\ w' \\ R_x' \\ R_y' \\ R_z' \end{Bmatrix}_s = \begin{Bmatrix} u' - vV_p'' - wW_p'' \\ v' + uV_p'' \\ w' + uW_p'' \\ \phi' + \beta V_p'' - \zeta W_p'' \\ -\beta' + \phi V_p'' \\ \zeta' + \phi W_p'' \end{Bmatrix} + O(\varepsilon^3)$$

Blade forces, moments and derivatives,

$$\begin{Bmatrix} V_x \\ V_y \\ V_z \\ M_x \\ M_y \\ M_z \end{Bmatrix}_s = \begin{Bmatrix} V_x \\ V_y \\ V_z \\ M_x \\ M_y \\ M_z \end{Bmatrix} + O(\varepsilon^3) \quad \text{and} \quad \begin{Bmatrix} V_x' \\ V_y' \\ V_z' \\ M_x' \\ M_y' \\ M_z' \end{Bmatrix}_s = \begin{Bmatrix} V_x' \\ V_y' + V_p'' V_x \\ V_z' + W_p'' V_x \\ M_x' - V_p'' M_y - W_p'' M_z \\ M_y' \\ M_z' \end{Bmatrix} + O(\varepsilon^3)$$

Appendix H4: Equations of Motion for the CRFD System

The information contained in Pages H8 to H20 is commercially confidential and is removed from this dissertation. Any query regarding the content should be referred to the author, Mr W Y F Chan, Box 231, Aerodynamics Department, GKN Westland Helicopters Limited, Yeovil, Somerset, England.

Appendix H6: Coefficients of Generalised Coordinates

The orthogonalisation process described in *Section* 3.5.3 allows the forcing functions for all the system modes to be identified with reduced algebra. It can also be used to obtain the Lagrangian Equation using effectively a reversed Hamiltonian Principle. This is carried out by evaluating all the coefficients, associated with each of the generalised coordinates, which are given by *Eqns.*G14 in *Appendix* G. Because the modes are linearised, the non-linear modal terms will subsequently result on the RHS as forcing functions. In order to gain insight, it is necessary to identify these terms analytically. We adopt the following treatment.

Consider for the real modes system, *eg.* the torsion coefficient (C_ϕ) is defined by the product of torsion forcing (F_ϕ) and the variation of twist $\delta\phi = \sum \delta q_i t_i$ (*Eqn.*G15d), then

$$C_\phi = \int_0^R \left\{ \delta\phi \cdot F_\phi \right\} dr = \sum \delta q_i \int_0^R t_i \cdot \left\{ \underbrace{\frac{\partial g}{\partial \phi} - \frac{d}{dt}\left(\frac{\partial g}{\partial \dot{\phi}}\right) - \frac{\partial (f+U_s)}{\partial \phi} + \frac{dM}{dr}}_{\text{Direct}} + \underbrace{\frac{\partial}{\partial r}\left(\frac{\partial f}{\partial \phi'}\right)}_{\text{Indirect}} \right\} dr$$

ie. F_ϕ consists of both direct (mainly external) F_{ϕ_1} and indirect (internal) $\frac{\partial F_{\phi_2}}{\partial r}$ (*ie.* $F_{\phi_2} = \frac{\partial f}{\partial \phi'}$) terms. By evaluating F_ϕ for the aeroelastic and dynamic (linearised) systems independently, then upon subtraction, all the residual terms can be identified. The identification of the direct terms is normally straightforward but this is not the case for the non-linear terms which appear in both the direct and indirect terms. One can evaluate the indirect term $\frac{\partial}{\partial r}\left(\frac{\partial f}{\partial \phi'}\right)$ as indicated, then they can be treated exactly as those direct terms. Alternatively, we can integrate the indirect term by parts,

$$\int_0^R t_i \cdot \left\{ \frac{\partial}{\partial r}\left(\frac{\partial f}{\partial \phi'}\right) \right\} dr = \left[t_i \cdot \frac{\partial f}{\partial \phi'} \right]_0^R - \int_0^R t_i' \cdot \frac{\partial f}{\partial \phi'} \, dr = - \int_0^R t_i' \cdot \frac{\partial f}{\partial \phi'} \, dr$$

Thus, the torsion coefficient becomes,

$$C_\phi = \sum \delta q_i \int_0^R t_i \cdot F_\phi \, dr = \sum \delta q_i \int_0^R \left\{ t_i \cdot F_{\phi_1} - t_i' \cdot F_{\phi_2} \right\} dr \text{ where} \begin{cases} F_{\phi_1} = \dfrac{\partial g}{\partial \phi} - \dfrac{d}{dt}\left(\dfrac{\partial g}{\partial \dot{\phi}}\right) - \dfrac{\partial (f+U_s)}{\partial \phi} + \dfrac{dM}{dr} \\ F_{\phi_2} = \dfrac{\partial f}{\partial \phi'} \end{cases}$$

$$0 = \sum_i \delta q_i \int_0^R \{u_i, v_i, w_i, t_i, \beta_i, \zeta_i\} \cdot \begin{Bmatrix} F_u \\ F_v \\ F_w \\ F_\phi \\ F_\beta \\ F_\zeta \end{Bmatrix} dr$$

$$= \sum_i \delta q_i \int_0^R \left\{ \{u_i, v_i, w_i, t_i, \beta_i, \zeta_i\} \cdot \begin{Bmatrix} F_{u_1} \\ F_{v_1} \\ F_{w_1} \\ F_{\phi_1} \\ F_{\beta_1} \\ F_{\zeta_1} \end{Bmatrix} - \{u_i', v_i', w_i', t_i', \beta_i', \zeta_i'\} \begin{Bmatrix} F_{u_2} \\ F_{v_2} \\ F_{w_2} \\ F_{\phi_2} \\ F_{\beta_2} \\ F_{\zeta_2} \end{Bmatrix} \right\} dr$$

where $F_{u_1} = \frac{\partial g}{\partial u} - \frac{d}{dt}\left(\frac{\partial g}{\partial \dot{u}}\right) - \frac{\partial (f+U_s)}{\partial u} + \frac{dA}{dr} = -V_x'$; $\qquad F_{u_2} = \frac{\partial f}{\partial u'} = V_x$;

$F_{v_1} = \frac{\partial g}{\partial v} - \frac{d}{dt}\left(\frac{\partial g}{\partial \dot{v}}\right) - \frac{\partial (f+U_s)}{\partial v} - \frac{dD}{dr} = -V_y'$; $\qquad F_{v_2} = \frac{\partial f}{\partial v'} = V_y$;

$F_{w_1} = \frac{\partial g}{\partial w} - \frac{d}{dt}\left(\frac{\partial g}{\partial \dot{w}}\right) - \frac{\partial (f+U_s)}{\partial w} + \frac{dL}{dr} = -V_z'$; $\qquad F_{w_2} = \frac{\partial f}{\partial w'} = V_z$;

$F_{\phi_1} = \frac{\partial g}{\partial \phi} - \frac{d}{dt}\left(\frac{\partial g}{\partial \dot{\phi}}\right) - \frac{\partial (f+U_s)}{\partial \phi} + \frac{dM}{dr} = -\left\{(M_x' + (\zeta M_y)' + (\beta M_z)'\right\}$; $\qquad F_{\phi_2} = \frac{\partial f}{\partial \phi'} = M_x + \zeta M_y + \beta M_z$;

$F_{\beta_1} = \frac{\partial g}{\partial \beta} - \frac{d}{dt}\left(\frac{\partial g}{\partial \dot{\beta}}\right) - \frac{\partial (f+U_s)}{\partial \beta} = -\left\{-M_y' + (\zeta M_x)'\right\}$; $\qquad F_{\beta_2} = \frac{\partial f}{\partial \beta'} = -M_y + \zeta M_x$;

$F_{\zeta_1} = \frac{\partial g}{\partial \zeta} - \frac{d}{dt}\left(\frac{\partial g}{\partial \dot{\zeta}}\right) - \frac{\partial (f+U_s)}{\partial \zeta} = -M_z'$; $\qquad F_{\zeta_2} = \frac{\partial f}{\partial \zeta'} = M_z$;

These expressions are in fact those given in *Appendix* H5 except there is no secondary load path contribution and there is a sign change required for the direct forcing terms.

expressions for the modal inertia (I_1) and modal stiffness (λ_i^2) for the real modes system to be obtained by linearising the dynamic terms. Let us consider the torsion degree of freedom in more detail. For illustrative purposes only, the analysis will be restricted to a symmetrical section blade without centre offset terms or control system springs, we have (with ϕ retained),

$$F_{\phi_1} = \frac{dM}{dr} - m\Omega^2(km_2^2-km_1^2)(\sin\vartheta\cos\vartheta + \phi\cos2\vartheta) - m(km_2^2+km_1^2)(\ddot{\vartheta}+\ddot{\phi}) + (EI_{22}-EI_{11})[(v''^2-w''^2)\sin\vartheta\cos\vartheta - v''w''\cos2\vartheta]$$

$$F'_{\phi_2} = \frac{\partial}{\partial r}\left\{ (EI_{11}+EI_{22})\vartheta'[u'+\frac{1}{2}(v'^2+w'^2)] + GJ(\phi'+w'v'') \right\}$$

$\therefore$ The torsion coefficient $C_\phi = \sum\delta q_i \int_0^R \left\{ t_i \cdot F_{\phi_1} - t_i' \cdot F_{\phi_2} \right\} dr$ for the aeroelastic system from *Appendix* H5 is

$$(C_\phi)_A = \sum\delta q_i \int_0^R \left\{ \frac{dM}{dr}t_i - m\Omega^2(km_2^2-km_1^2)t_i\sin\vartheta\cos\vartheta - m(km_2^2+km_1^2)(\ddot{\vartheta}+\ddot{\phi})t_i + (EI_{22}-EI_{11})[(v''^2-w''^2)\sin\vartheta\cos\vartheta - v''w''\cos2\vartheta]t_i \right.$$
$$\left. - t_i' \cdot \left\{ (EI_{11}+EI_{22})\vartheta'[u'+\frac{1}{2}(v'^2+w'^2)] + GJ(\phi'+w'v'') \right\} \right\} dr$$

Express in terms of the modal components, *ie.* $\phi=\phi_N$ where $\phi_N=\sum q_j t_j$, $v''=v_0''+v_N''$ where $v_N''=\sum q_j v_j''$ *....etc. ie.* $()_N$ contains the modal contribution only, then $(C_\phi)_A$ becomes

$$(C_\phi)_A = \sum\delta q_i \int_0^R \left\{ \frac{dM}{dr}t_i - m\Omega^2(km_2^2-km_1^2)t_i[\sin\vartheta\cos\vartheta + (\phi_0+\phi_N)\cos2\vartheta] - m(km_2^2+km_1^2)(\ddot{\vartheta}+\ddot{\phi}_N)t_i \right.$$
$$+ (EI_{22}-EI_{11})t_i[(v_0''^2-w_0''^2 + 2v_0''v_N''-2w_0''w_N'' + v_N''^2-w_N''^2)\cos\vartheta\sin\vartheta - (v_0''w_0'' + v_0''w_N''+v_N''w_0'' + v_N''w_N'')\cos2\vartheta]$$
$$\left. - t_i' \cdot \left\{ (EI_{11}+EI_{22})\vartheta'[u_0'+\frac{1}{2}(v_0'^2+w_0'^2) + u_N'+2v_0'v_N'+2w_0'w_N' + v_N'^2+w_N'^2] + GJ(\phi_0'+w_0'v_0'' + \phi_N'+w_0'v_N''+w_N'v_0'' + w_N'v_N'') \right\} \right\} dr$$

The corresponding expression for the dynamic system from *Appendix* H4, after linearising, is

$$(C_\phi)_D = \sum\delta q_i \int_0^R \left\{ \frac{dM_0}{dr}t_i - m\Omega^2(km_2^2-km_1^2)t_i[\sin\vartheta_m\cos\vartheta_m + (\phi_0+\phi_N)\cos2\vartheta_m] - m(km_2^2+km_1^2)\ddot{\phi}_N t_i \right.$$
$$+ (EI_{22}-EI_{11})t_i[(v_0''^2-w_0''^2 + 2v_0''v_N''-2w_0''w_N'')\sin\vartheta_m\cos\vartheta_m - (v_0''w_0'' + v_0''w_N''+v_N''w_0'')\cos2\vartheta_m] \Big\}$$
$$\left. - t_i' \cdot \left\{ (EI_{11}+EI_{22})\vartheta'[u_0'+\frac{1}{2}(v_0'^2+w_0'^2) + u_N'+2v_0'v_N'+2w_0'w_N'] + GJ(\phi_0'+w_0'v_0'' + \phi_N'+w_0'v_N''+w_N'v_0'') \right\} \right\} dr$$

$$(C_\phi)_A-(C_\phi)_D = \sum\delta q_i \cdot f_{\phi_i}$$

$$= \sum\delta q_i \int_0^R \Big\{ \underbrace{\left(\frac{dM}{dr}-\frac{dM_0}{dr}\right)t_i}_{\text{Applied}} - \underbrace{m(km_2^2+km_1^2)\ddot{\vartheta}t_i}_{\text{Cyclic inertia}} + \underbrace{(EI_{22}-EI_{11})[(v_N''^2-w_N''^2)\cos\vartheta_m\sin\vartheta_m - v_N''w_N''\cos2\vartheta_m]t_i}_{\text{Non-linear (1)}}$$

$$- \underbrace{t_i' \cdot \Big\{ (EI_{11}+EI_{22})\vartheta' \frac{1}{2}(v_N'^2+w_N'^2) + GJw_N'v_N'' \Big\}}_{\text{Non-linear (2)}}$$

$$- \underbrace{\Big[m\Omega^2(km_2^2-km_1^2)t_i[\sin\vartheta\cos\vartheta + \phi\cos2\vartheta] + (EI_{22}-EI_{11})t_i[(v''^2-w''^2)\cos\vartheta\sin\vartheta + v''w''\cos2\vartheta] \Big]_{\vartheta_m}^{\vartheta}}_{\text{Pitch Perturbation}} \Big\}\, dr$$

Thus the residual term f_{ϕ_i}, containing typically the applied, cyclic inertia, non-linear correction and pitch perturbatic terms, remains on the RHS as modal forcings for the particular (i^{th}) mode. We could also employ $(F_\phi)_A$ to obtain the moda inertia and modal stiffness expressions as below;

$$(C_\phi)_A = (C_\phi)_D + \sum\delta q_i f_{\phi_i}$$

$$= \sum\delta q_i \Big\{ (C_\phi)_{ss} - \sum\ddot{q}_j I_{\phi_{ij}} - \sum q_j S_{\phi_{ij}} + f_{\phi_i} \Big\}$$

where

$$(C_\phi)_{ss} = \int_0^R \Big\{ \frac{dM_0}{dr}t_i - m\Omega^2(km_2^2-km_1^2)t_i(\sin\vartheta_m\cos\vartheta_m+\phi_0\cos2\vartheta_m) + (EI_{22}-EI_{11})t_i[(v_0''^2-w_0''^2)\sin\vartheta_m\cos\vartheta_m - v_0''w_0''\cos2\vartheta_m]$$

$$- t_i' \cdot \Big\{ (EI_{11}+EI_{22})\vartheta_m'[u_0'+\frac{1}{2}(v_0'^2+w_0'^2)] + GJ(\phi_0'+w_0'v_0'') \Big\}\, dr$$

$$I_{\phi_{ij}} = \int_0^R m(km_2^2+km_1^2)t_j t_i\, dr$$

$$S_{\phi_{ij}} = \int_0 \Big\{ -m\Omega^2(km_2^2-km_1^2)t_i t_j \cos 2\vartheta_m + (EI_{22}-EI_{11})t_i[(2v_0''v_j''-2w_0''w_j'')\sin\vartheta_m\cos\vartheta_m - (v_0''w_j''+v_j''w_0'')\cos 2\vartheta_m]t_i$$
$$- t_i' \cdot \Big\{ (EI_{11}+EI_{22})\vartheta'(u_j'+2v_0'v_j'+2w_0'w_j') + GJ(t_j'+w_0'v_j''+w_j'v_0'') \Big\} \Big\} dr$$

where $(C_\phi)_{ss}$ is the expression for the steady state condition given in the modes with $(C_\phi)_{ss}=0$ *ie.* the equilibri condition; $I_{\phi_{ij}}$ is the modal inertia; and $S_{\phi_{ij}}$ is the modal stiffness from torsion consideration only, which fr orthogonality,

$$I_{\phi_{ij}} = 0 \;\; ; \quad S_{\phi_{ij}} = 0 \qquad \text{if } i \neq j$$
$$= I_{\phi_i}; \qquad = \lambda_{\phi_i}^2 I_{\phi_i} \quad \text{if } i=j \quad \text{where } \lambda_{\phi_i} \text{ is the torsion frequency.}$$

By summing <u>all</u> the degrees of freedom *ie. Eqn.*G14, the total coefficient of the generalised coordinates becomes

$$0 = \sum \delta q_i \Big\{ - \sum \ddot{q}_j I_{ij} - \sum q_j S_{ij} + f_i \Big\}$$

$$\therefore \boxed{I_{ij}\ddot{q}_j + S_{ij}q_j = f_i} \qquad \text{for all } \delta q_i.$$

where $I_{ij} = 0 \;\; ; \quad S_{ij} = 0 \qquad \text{if } i \neq j$
$$= I_i \; ; \qquad = \lambda_i^2 I_i \quad \text{if } i=j$$

and $I_i, S_i (=\lambda_i^2 I_i)$ are the modal inertia and stiffness for the system mode concerned, provided by CRFD. The modal forcin f_i, consistent with CRFA assumption, is defined in *Appendix* I.

Appendix I: RHS Forcing Vector for The CRFA System

The information contained in Pages I1 to I5 is commercially confidential and is removed from this dissertation. Any query regarding the content should be referred to the author, Mr W Y F Chan, Box 231, Aerodynamics Department, GKN Westland Helicopters Limited, Yeovil, Somerset, England.

Appendix J: Blade Structural Load Equations for The CRFA System

The information contained in Pages J1 to J10 is commercially confidential and is removed from this dissertation. Any query regarding the content should be referred to the author, Mr W Y F Chan, Box 231, Aerodynamics Department, GKN Westland Helicopters Limited, Yeovil, Somerset, England.

Appendix K - Chebyshev Polynomial Integration Technique

K1 - Formulation of Hinge Bending Moment using Modal Summation and Force Integration Methods

Consider first that the mode response coefficient q_i is determined by solving the response equation which, for a pure flapping blade in the absence of structural damping, is given by:-

$$\ddot{q}_i + \lambda_i^2 q_i = \frac{1}{\Omega^2 I_i} \int_e^{R_G} \frac{dL}{dr} w_i \, dr \qquad (K1)$$

where $(\dot{}) = \frac{\partial}{\partial \psi}$ and $\int_e^{R_G} ()dr$ denotes the trapezoidal integration is to be carried out from the blade root e to the tip using the aerodynamic radial stations, R_G. The interval, typically 25, is defined from the blade root cut-out to the tip with zero aerodynamic loading inboard of the root cut-out.

The boundary condition, characterised by the hinge bending moment, for an articulated rotor is derived as follows depending on the type of formulation. Consider only the primary forces: applied, inertia and centrifugal forces, acting on the blade,

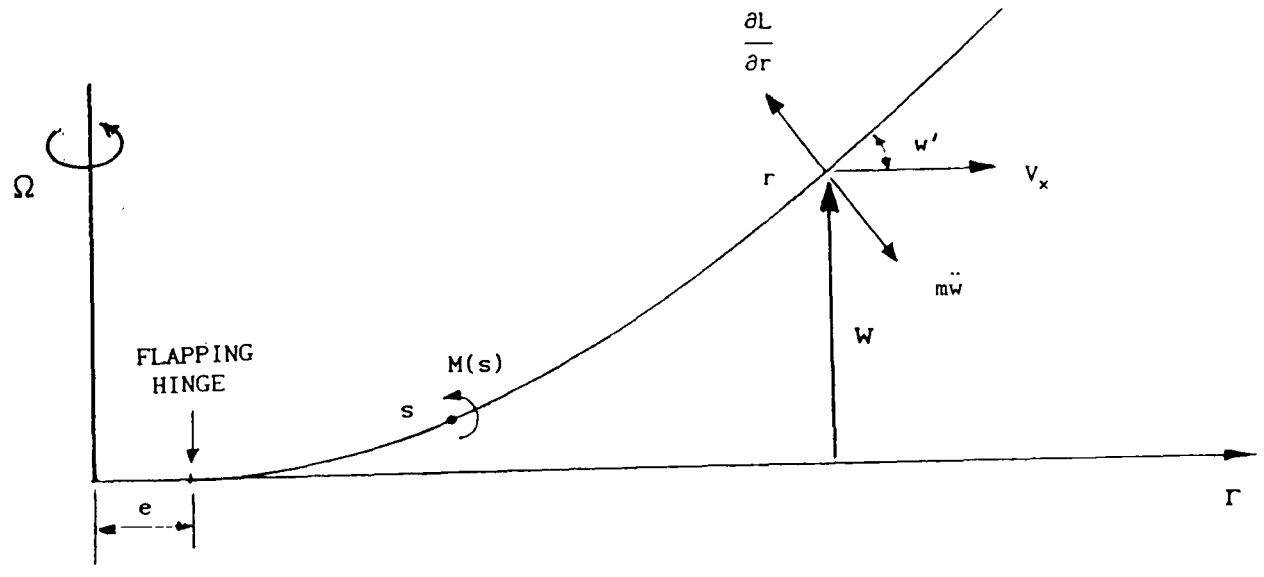

Primary Blade Forces

Then the formulation,

(1) By Force Integration Method

The hinge bending moment based on Force Integration is obtained by directly integrating all the loadings acting on the blade, *ie*

$$M_{FI}(e) = \int_e^{R_F} \left\{ F - I - w' V_x \right\} dr \qquad (K2)$$

where R_F is the dynamic output radial interval defined from the blade root to tip, and the integrated applied (F), inertia (I) and centrifugal (V_x) forces at radius r are defined as

$$F = \int_r^{R_F} \frac{dL}{dr}\, dr; \qquad I = \int_r^{R_F} m\Omega^2 \ddot{w}\, dr; \qquad V_x = \int_r^{R_F} m\Omega^2 r\, dr$$

$$\therefore M_{FI}(e) = \int_e^{R_F}\int_r^{R_F} \frac{dL}{dr}\, drdr - \int_e^{R_F}\int_r^{R_F} m\Omega^2 \ddot{w}\, drdr - \int_e^{R_F} w' \int_r^{R_F} m\Omega^2 r\, drdr \qquad \text{(K3)}$$

Let the flap deflection be expressed in modal summation

$$w(\psi, r) = \sum_{i=1}^{N} q_i(\psi) w_i(r)$$

$$\therefore \ddot{w}(\psi, r) = \sum_{i=1}^{N} \ddot{q}_i(\psi) w_i(r) \qquad w'(\psi, r) = \sum_{i=1}^{N} q_i(\psi)\, w_i'(r)$$

and *Eqn.*K3 becomes

$$M_{FI}(e) = \int_e^{R_F}\int_r^{R_F} \frac{dL}{dr}\, drdr - \Omega^2 \sum_{i=1}^{N} \ddot{q}_i \int_e^{R_F}\int_r^{R_F} m w_i\, drdr - \Omega^2 \sum_{i=1}^{N} q_i \int_e^{R_F} w_i' \int_r^{R_F} mr\, drdr$$

Integrating by parts and applying the boundary condition,

$$= \int_e^{R_F} \left\{ \left(\frac{dL}{dr} - m\Omega^2 \sum_{i=1}^{N} \ddot{q}_i w_i \right)(r-e) - m\Omega^2 r \sum_{i=1}^{N} q_i w_i \right\} dr \qquad \text{(K4)}$$

Substituting $\ddot{q}_i$ from *Eqn.*K1,

$$M_{FI}(e) = \int_e^{R_F} \left\{ \left(\frac{dL}{dr} - m\Omega^2 \sum_{i=1}^{N} w_i \left\{ \frac{\int_e^{R_G} \frac{dL}{dr}\, w_i dr}{\Omega^2 I_i} - \lambda_i^2 q_i \right\} \right)(r-e) - m\Omega^2 r \sum_{i=1}^{N} q_i w_i \right\} dr$$

$$= \int_e^{R_F} \left\{ \left(\frac{dL}{dr} - m\Omega^2 \frac{\sum_{i=1}^{N} w_i \int_e^{R_G} \frac{dL}{dr}\, w_i dr}{\Omega^2 I_i} \right)(r-e) + m\Omega^2 \sum_{i=1}^{N} q_i \left[\lambda_i^2 (r-e) - r \right] w_i \right\} dr \qquad \text{(K5)}$$

(2) By Modal Summation Method

The hinge bending moment based on Modal Summation is obtained by summing the products of modal bending moment M_i output directly from CRFD with the modal responses calculated using *Eqn.*K1,

$$M_{MS}(e) = \sum_{i=1}^{N} q_i M_i(e) = \sum_{i=1}^{N} q_i \int_e^{R_M} m\Omega^2 [\lambda_i^2 (r-e) - r] w_i\, dr \qquad \text{(K6)}$$

where R_M is the dynamic integrated radial interval, typically 500. It is noted from *Eqns.*K5 and K6 that $M_{FI}(e)$ and $M_{MS}(e)$ are related via

$$M_{FI}(e) = M_{MS}(e) + \left\{ \int_e^{R_F} - \int_e^{R_M} \right\} m\Omega^2 \sum_{i=1}^{N} q_i \left[\lambda_i^2(r-e)-r\right] w_i \, dr$$

$$+ \int_e^{R_F} \left(\frac{dL}{dr} - m\Omega^2 \frac{\sum_{i=1}^{N} w_i \int_e^{R_G} \frac{dL}{dr} w_i dr}{\Omega^2 I_i} \right)(r-e)\, dr \qquad \text{(K7)}$$

Now define $\frac{dL}{dr} = m\Omega^2 \sum_{i=1}^{N} \alpha_i w_i$ where $\alpha_i = \frac{\int_e^{R_G} \frac{dL}{dr} w_i dr}{\Omega^2 I_i}$ in *Eqn.*K7, then the second integrand vanishes only if $\int_e^{R_G} m w_i w_j dr = 0$ for all $i \neq j$ *ie.* the inertia orthogonality is valid over the R_G stations. In general, this can be true only if $R_G = R_M$. On the proviso that $R_G = R_M$, *Eqn.*K7 becomes:-

$$M_{FI}(e) = M_{MS}(e) + \left\{ \int_e^{R_F} - \int_e^{R_M} \right\} m\Omega^2 \sum_{i=1}^{N} q_i \left[\lambda_i^2(r-e)-r\right] w_i \, dr \qquad \text{(K8)}$$

Even in this case, $M_{FI}(e)=0$, if and only if,

either $\int_e^{R_F} m\Omega^2 \sum_{i=1}^{N} q_i \left[\lambda_i^2(r-e)-r\right] w_i \, dr = 0$, since by definition, $\int_e^{R_M} (..)dr = 0$

or $R_F = R_M$.

In general, the hinge boundary conditions can only be satisfied if $R_G = R_F = R_M$. Since R_M is by far the largest array of spanwise integration points, it has been shown analytically that correct boundary conditions can be assured only if all integrations are evaluated over R_M stations.

K2 - Treatment of Non-Linear Torsion-Flap-Lag Forcing Terms for the C.P.I. Technique [3.49]

Re-expression of Torsion-Flap-Lag Forcing Terms

The response equation for a single blade, in the absence of damping, but with the torsion-flap-lag forcing is defined as

$$\ddot{q}_i + \lambda_i^2 q_i = \frac{1}{\Omega^2 I_i} \int_0^R \left\{ F_i - (EI_2 - EI_1) t_i \left[v_N'' w_N'' \cos 2\vartheta_m + (w_N''^2 - v_N''^2) \sin\vartheta_m \cos\vartheta_m \right] \right\} dr \qquad \text{(K9)}$$

where F_i represents all other modal forcings and $w''_N=\sum q_j w''_j$ and $v''_N=\sum q_j v''_j$. Based on simplified theory and symmetrical section, the coupled flap and lag modal moment expressions are given by, to $O(\varepsilon)$ accuracy,

$$M_{z_m}=EI_2\cos\vartheta_m(v''_N\cos\vartheta_m+w''_N\sin\vartheta_m) - EI_1\sin\vartheta_m(w''_N\cos\vartheta_m-v''_N\sin\vartheta_m) +O(\varepsilon^2) \quad (K10)$$

$$M_{y_m}=EI_2\sin\vartheta_m(v''_N\cos\vartheta_m+w''_N\sin\vartheta_m) + EI_1\cos\vartheta_m(w''_N\cos\vartheta_m-v''_N\sin\vartheta_m) +O(\varepsilon^2) \quad (K11)$$

Therefore,

$$M_{z_m}w''_N-M_{y_m}v''_N =(EI_2-EI_1)\left[v''_Nw''_N\cos2\vartheta_m + (w''^2_N-v''^2_N)\sin\vartheta_m\cos\vartheta_m\right] +O(\varepsilon^3) \quad (K12)$$

Substituting into *Eqn.*K11 yields

$$\ddot{q}_i+\lambda_i^2q_i = \frac{1}{\Omega^2I_i}\int_0^R \left\{F_i- t_i[M_{z_m}w''_N + M_{y_m}v''_N] \right\} dr \quad (K13)$$

From *Eqns.*K10 & K11,

$$w''_N = M_{z_m}\left(\frac{1}{EI_2} - \frac{1}{EI_1}\right)\sin\vartheta_m\cos\vartheta_m - \frac{M_{y_m}}{EI_1EI_2}(EI_2\cos^2\vartheta_m+EI_1\sin^2\vartheta_m)$$

$$v''_N = M_{y_m}\left(\frac{1}{EI_2} - \frac{1}{EI_1}\right)\sin\vartheta_m\cos\vartheta_m + \frac{M_{z_m}}{EI_1EI_2}(EI_2\sin^2\vartheta_m+EI_1\cos^2\vartheta_m)$$

$$\therefore -(M_{z_m}w''_N+M_{y_m}v''_N) = -\left(\frac{1}{EI_2}-\frac{1}{EI_1}\right)\left(-M_{y_m}\sin\vartheta_m+M_{z_m}\cos\vartheta_m\right)\left(-M_{y_m}\cos\vartheta_m-M_{z_m}\sin\vartheta_m\right)$$

$$\therefore \ddot{q}_i + \lambda_i^2q_i$$

$$= \frac{1}{\Omega^2I_i}\int_e^R\left\{ F_i+t_i\left(\frac{1}{EI_2}-\frac{1}{EI_1}\right)\left(-M_{y_m}\sin\vartheta_m+M_{z_m}\cos\vartheta_m\right)\left(-M_{y_m}\cos\vartheta_m-M_{z_m}\sin\vartheta_m\right) \right\}dr$$

$$= \frac{1}{\Omega^2I_i}\int_e^R\left\{ F_i+t_i\left(\frac{1}{EI_2}-\frac{1}{EI_1}\right)M_1M_2 \right\} dr \quad (K14)$$

where *Eqn.*K14 is the well-known torsion equation given by, for example, [K1]. The torsion moment expression,

$$M'_{x_{def}} = - \frac{dM}{dr} + w''M_z + v''M_y + m\Omega^2\left((km_1^2+km_2^2)\ddot{\bar{\vartheta}} + (km_2^2-km_1^2)\bar{\vartheta}\right)$$

$$\therefore M_{x_{def}} = \int_r^R \frac{dM}{dr}dr - \int_r^R\left(w''M_z + v''M_y\right)dr + \int_r^R m\Omega^2\left((km_1^2+km_2^2)\ddot{\bar{\vartheta}} + (km_2^2-km_1^2)\bar{\vartheta}\right) dr$$

$$= \int_r^R \frac{dM}{dr}dr - \underline{\int_r^R\left(\frac{1}{EI_2}-\frac{1}{EI_1}\right)\left(-M_y\sin\bar{\vartheta} + M_z\cos\bar{\vartheta}\right)\left(M_y\cos\bar{\vartheta} - M_z\sin\bar{\vartheta}\right) dr}$$

$$+ \int_r^R m\Omega^2\left((km_1^2+km_2^2)\ddot{\bar{\vartheta}} + (km_2^2-km_1^2)\bar{\vartheta}\right) dr$$

where the underlined terms are due to torsion-flap-lag coupling.

Application of the CPI technique

The relevant non-linear term in the modal response equation is;

$$M_{NL} = \int_r^R t_i \left(\frac{1}{EI_2}-\frac{1}{EI_1}\right)\left(-M_{y_m}\sin\vartheta_m+M_{z_m}\cos\vartheta_m\right)\left(-M_{y_m}\cos\vartheta_m-M_{z_m}\sin\vartheta_m\right) dr \qquad (K15)$$

where EI_1, EI_2 and ϑ_m are discontinuous and t_i, M_{y_m} and M_{z_m} are continuous functions. Therefore, re-arranging *Eqn.*K15 into products of discontinuous and continuous functions, one gets

$$M_{NL}= \int_r^R t_i M_{y_m}^2 \left[(\frac{1}{EI_2} - \frac{1}{EI_1})\sin\vartheta_m\cos\vartheta_m\right]dr - \int_r^R t_i M_{z_m}^2\left[(\frac{1}{EI_2} - \frac{1}{EI_1})\sin\vartheta_m\cos\vartheta_m\right]dr$$

$$- \int_r^R t_i M_{y_m} M_{z_m} \left[(\frac{1}{EI_2} - \frac{1}{EI_1})(\cos^2\vartheta_m - \sin^2\vartheta_m)\right] dr \qquad (K16)$$

and the structural loads can be treated in the same way.

Reference

K1. Hansford R E & Simons I A
"Torsion-Flap-Lag Coupling on Helicopter Rotor Blades"
Journal of AHS, Vol.18, No.4, October 1973